UNIVERSITY OF SOUTHAMPTON

FACULTY OF MEDICINE, HEALTH & LIFE SCIENCES

School of Biological Sciences

Ligand Binding to Pentraxins

By

Halina Mikolajek

A thesis submitted for the degree of
Doctor of Philosophy

Biochemistry

January 2008

UNIVERITY OF SOUTHAMPTON

ABSTRACT

FACULTY OF MEDICINE, HEALTH & LIFE SCIENCES
SCHOOL OF BIOLOGICAL SCIENCES

Doctor of Philosophy

LIGAND BINDING TO PENTRAXINS

by Halina Mikolajek

The human pentraxin proteins, serum amyloid P component (SAP) and C-reactive protein (CRP) have emerged as potentially important targets in the treatment of amyloidosis and cardiovascular diseases respectively, although their normal physiological functions are unclear. Structurally highly conserved homologous proteins are present in common experimental animals such as the rat, mouse, rabbit and hamster but there are major differences from the human pentraxins in their normal behaviour as acute phase proteins, fine ligand specificity and capacity to activate the complement system.

SAP binds to amyloid fibrils of all types and may contribute to their formation, stabilisation and persistence. In order to extend our current knowledge of ligand recognition by SAP, the crystal structures of SAP complexed to two ligands, Methylmalonic acid and Phosphatidylethanolamine, have been solved to 1.6 Å and 1.4 Å resolution respectively.

Since important biological functions of proteins are often conserved among species, the structural differences between the rat and human pentraxins were investigated. The crystal structure of rat SAP was solved to 2.2 Å resolution by molecular replacement. This pentameric structure displayed subtle differences in the electrostatic properties. It remains to be determined whether this has an effect on avid binding of SAP to DNA, a functional property of human SAP still poorly understood.

CRP, a pentraxin traditionally defined by its binding affinity for PC, was studied in complex with PE. The crystal structure of the CRP-PE complex at 2.7 Å resolution revealed that the nitrogen end of PE dips further downwards into the hydrophobic pocket of CRP than PC.

CRP-mediated complement activation can exacerbate ischemic tissue injury in the heart as well as in the brain. Therefore, knowledge of the exact stoichiometry and the protein-protein interactions between CRP and C1q may aid the development of small molecules capable of disrupting such protein-protein interactions. Purification of C1q has been achieved by ion-exchange chromatography and gel filtration from BPL paste. Crystallisation trials have been performed, however no crystals have been observed that contain the protein-protein complex.

Contents

List of Figures

Chapter 6 **Summary and Conclusion**

List of Tables

Acknowledgements

First of all I would like to thank Professor Steve Wood for providing me with a laboratory to work in and for giving me guidance and support throughout my studies. I am also very grateful for his knowledge in X-ray crystallography, ideas and help during the years and reading of this thesis.

I am very thankful to the British Heart Foundation Charity for funding me during the duration of this PhD.

I would also like to thank more people:

My second supervisor, Professor Mark Pepys, in London for assisting me with these projects and for supplying me with vast amounts of pentraxin proteins. Thank you also very much for letting me visit your lab in London.

People in the Southampton lab: Professor Jon Cooper and Dr Peter Erskine for all their help with the theory and practice of protein crystallography and for their company during various train trips to the ESRF. Thank you also for a constant supply of biscuits and herbal tea to fuel some evenings. Dr Gill, Dr Alun Coker and Dr Simon Kolstoe for their help. Alex (Boyer), for always being a positive person, friend and for putting up with me in the graphics suite. Mohinder, whom might remember me mostly for the person constantly staring at a computer screen and Jeab.

Former PhD students in the lab: Michelle for help with crystallography and for introducing me to the pub culture in England and long discussions about everything and anything really.

Former postdocs, especially Fiyaz, the first one to look after me when I first arrived in the lab as a summer student back then in the summer of 2003 and who taught me various things in the area of protein expression and purification as well as crystallography. Sorry for calling you late night to check on the FPLC... Darren, for being helpful and for providing useful comments and discussions.

Friends in various other labs, especially Clare and Andrea, whom I had loads of fun with and whom I enjoyed vast amounts of cups of tea with. Andy for being a friend and for various discussions.

My friends, especially Pili for always being there when I needed, being down to earth and carrying. Rachel R., for teaching me artistic skills and being a friend.

Meiner Familie: Vielen Dank liebe Mama, lieber Papa und Jadwiga für Eure Liebe, Unterstützung und Geduld während meiner Jahre als Studentin.

My Fiancé's family: Midge, Peter, Hannah and Ben for their constant support and encouragement.

My fiancé, Alexander Bainbridge, for always being there for me.

Abbreviations

Å	Angstrom (1×10^{-10}m)
AA	Amyloid fibrils derived from serum amyloid A
a,b,c	Unit cell dimensions
α,β,γ	Unit cell angles or Eulerian angles
Aβ	Alzheimer's disease β-protein peptide
AL	Amyloid fibrils derived from monoclonal immunoglobulin light chain
AH	Amyloid fibrils derived from monoclonal immunoglobulin heavy chain
ATP	Adenosine 5'-triphosphate
ATTR	Amyloid fibrils derived from transthyretin
ADP	Adenosine diphosphate
apoE	Apolipoprotein
AP	Amyloid P component
B-factor	Temperature factor
β_2-m	β_2-microglobulin
Bis(PC)-H	1,6-bis(phosphocholine)-hexane
BPL	Bio Products Laboratory
°C	Degree Celsius
CC	Correlation coefficient
CCD	Charge-coupled device
CCP4	Collaborative Computational Project Number 4
CE	Cholesterol esters
C1INH	C1 inhibitor
C4BP	C4b-binding protein
CLR	Collagen-like region
CNS	Crystallography & NMR systems
CPHPC	R-1-[6-R-2-carboxy-pyrrolidin-1-yl]-6-oxo-hexanoyl]pyrrolindine-2-carboxylic acid
CPN	Carboxypeptidase N
CPS	Pneumococcal C-polysaccharide
CRP	C-reactive protein
CRPtg	C-reactive protein transgenic

Da	Dalton
dAMP	2'deoxyadenosine-5'-monophosphate
DNA	Deoxyribose nucleic acid
EDTA	Ethylene-diamine-tetraacetic acid
EM	Electron microscopy
eNOS	endothelial nitric oxide synthase
ESRF	European Synchrotron Radiation Facility
FcγR	Fcγ receptors
FP	Hamster female protein
GABA	γ-aminobutyric acid
GAG	glycosaminoglycan
gC1q	C1q globular head region
HDL	High density lipoprotein
h,k,l	Reciprocal space coordinates
(h,k,l)	Miller indices for lattice planes within real space
Ig	Immunoglobulin
IC_{50}	half-maximal inhibitory concentration
ICAM	intercellular adhesion molecule
iNOS	inducible nitric oxide synthase
IL	Interleukin
ITC	Isothermal Titration Calorimetry
K	Degree Kelvin
K_d	Dissociation constant
kDa	Kilo-Dalton
λ	wavelength
LDL	Low density lipoprotein
LLG	log-likelihood-gain
LPS	lipopolysaccharide
MASP's	MBL-associated serine proteases
MBL	Mannan-binding lectin
MIR	Multiple isomorphous replacement
mM	millimollar
MM	Methylmalonic acid
MOβDG	methyl 4,6-O-(1-carboxyethylidine)-β-galactopyranoside

MR	Molecular replacement
mRNA	Messenger Ribonucleic Acid
NCS	Non-crystallographic symmetry
NMR	Nuclear magnetic resonance
NPI	Neuronal pentraxin I
PAMPs	pathogen-associated molecular patterns
PC	Phosphocholine
PE	Phosphoethanolamine
PEG	Polyethylene glycol
PEG MME	Polyethylene glycol monomethyl ether
pH	-log10 [hydrogen ion concentration]
PLA2	Phospholipase A2
PnC	pneumococcal C-polysaccharide
R-factor	Residual index factor
Rms	Root mean square
SAP	Serum amyloid P component
SDS-PAGE	Sodium dodecyl sulfate polyacrylamide gel electrophoresis
SLE	Systematic lupus erythematous
snRNPs	Small nuclear ribonucleoprotein particles
SM	Sphingomyelin
TG	Triglyceride
TNF	Tumour necrosis factor
TRIS	Tris (hydroxymethyl)aminomethane
TSG-14	TNF-stimulated gene 14
TTR	Transthyretin
UC	unesterified cholesterol
VCAM	Vascular cell adhesion molecule
Z-score	number of standard deviations above the mean
x,y,z	Unit cell coordinates (real space)

Chapter 1

Introduction

1.1 Introduction to Pentraxins

The pentraxins are a superfamily of evolutionary conserved proteins, which were originally named for their distinct structural organisation of five identical subunits arranged non-covalently in pentameric radial symmetry (Osmand *et al.*, 1977). The superfamily shares the so-called "pentraxin family signature" of HxCxS/TWxS (x = any amino acid) and may be divided into two distinct structural subfamilies depending on their size: the classical 'short' (~ 25 kDa) pentraxins and the 'long' (~ 50 kDa) pentraxins (Goodman *et al.*, 1996).

The long pentraxins have only been discovered recently and the subfamily consists currently of five members. The first member of the long pentraxin subfamily was described in 1993 (Lee *et al.*, 1993; Alles *et al.*, 1994) and is termed TNF-stimulated gene 14 (TSG-14/PTX3). The other long pentraxin members are the sperm-egg fusion protein (Apexin/p50), the rat neuronal pentraxin I (NPI), the human neuronal pentraxin II (NPII) and the XL-PXN1. All long pentraxins share similarities with the classical short pentraxins in their C-terminal domain but differ for the presence of an additional, unrelated long N-terminal domain (Mantovani *et al.*, 2003).

The classical short pentraxins were the earliest described pentraxins, of which there are currently two members: C-reactive protein (CRP) and Serum amyloid P component (SAP). These members are phylogenically conserved plasma proteins with homologs present in man, most vertebrates and certain invertebrates.

CRP and SAP are characterised by their calcium-dependent ligand binding specificities for phosphocholine (PC) and phosphoethanolamine (PE) respectively (Schwalbe *et al.*, 1992), although CRP also binds PE. Based on these specific binding properties, CRP-like and SAP-like pentraxins have been isolated from many different species. These homologs share substantial sequence homology (Figure 1.1), but there are major differences between species with respect to baseline plasma concentrations, behaviour as acute phase protein, ligand binding specificity and capacity to activate complement.

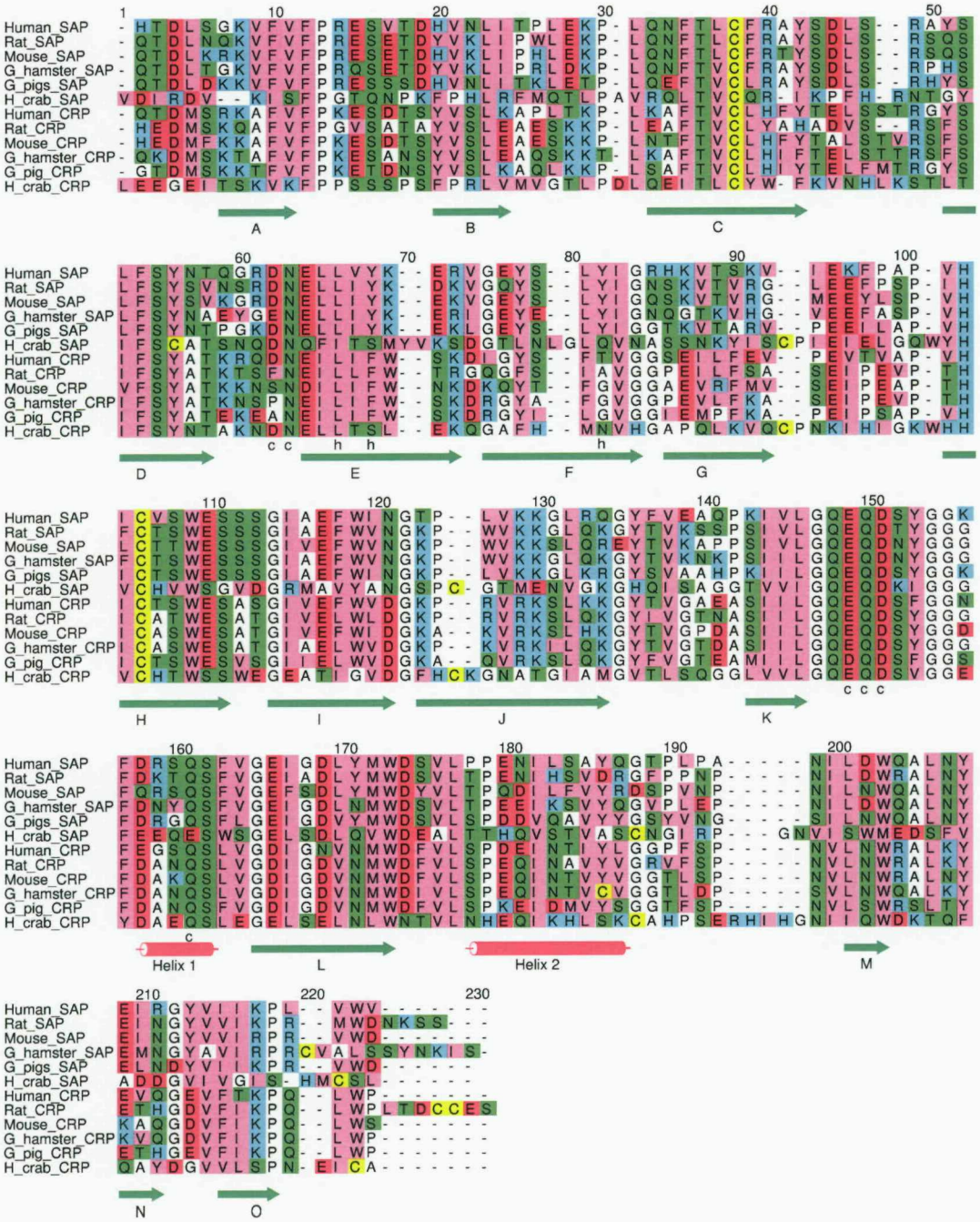

Figure 1.1 A sequence alignment of CRP and SAP from several different species. The alignment was performed using Malign 4.0. The amino acids are coloured according to the scheme: cyan = basic; red = acidic; green = neutral-polar; pink = bulky hydrophobic; white = Gly, Ala and Pro; and yellow = Cys. The secondary structure elements of human SAP as well as the calcium binding residues (c) are indicated below the alignment.

Although the normal physiological roles of the short pentraxins are unclear, their involvement pathologically in diseases such as amyloidosis and cardiovascular disease is beginning to emerge. SAP is universally associated with amyloid deposits, whilst CRP is found associated with all myocardial infarcts and in some atherosclerotic plaques.

This report focuses on the short pentraxins and investigates the structural basis of ligand binding specificity. It is hoped that this will provide an insight into the underlying physiological and pathophysiological roles of the pentraxins, improve relevant animal models and inform pentraxin inhibitor design.

1.2 Physiological Roles of Short Pentraxins

The sequence homology and evolutionary conservation together with the absence of any known polymorphism or deficiency suggests that short pentraxins have an important physiological role.

Both CRP and SAP are present in most mammals with one or the other responding as an acute phase reactant that increases by up to a thousand fold in concentration during an acute phase response. The acute phase response is a non-specific physiological and biochemical response of the body to most forms of tissue injury, inflammation or infection (Pepys & Hirschfield, 2003). It is characterised by a multitude of biosynthetic and metabolic alterations, among which is a dramatic change in the concentration of many plasma proteins, designated acute-phase reactants (Kushner, 1982). These changes are species-specific and vary in direction, magnitude and kinetics (Goldberger *et al.*, 1987). For example, during the acute phase response in humans, concentrations of specific plasma proteins decrease (e.g. albumin, transthyretin and properdin), while (α_1-antitrypsin, α_1-anti-chymotrypsin, fibrinogen, prothrombin, CRP, Cls, C3, C4 and α_1-acid glycoprotein) increase (Goldberger *et al.*, 1987).

CRP was the first protein to be discovered that behaves as an acute phase protein and is considered to be the prototypic acute phase protein in humans and rabbits because its concentration can increase by more than one-thousand fold during the acute phase response (Pepys & Baltz, 1983). These concentrations decrease rapidly following cessation of the stimulus for increased production.

The increased production is regulated mainly at the transcriptional level by the cytokine interleukins-6 (IL-6) and occurs predominantly in hepatocytes. However, other sites of local CRP synthesis and possibly secretion have been suggested. The plasma half-life of human CRP is about 19 hours and is constant under all conditions of health and disease (Pepys & Hirschfield, 2003). Thus, the sole determinant of the dramatic increase in circulating concentrations observed during an acute phase response is the synthesis rate, which therefore reflects the intensity of the pathological process stimulating CRP synthesis (Vigushin *et al.*, 1993).

Unlike its human counterpart, mouse CRP is synthesised only in trace amounts and is not an acute phase protein (Bodmer & Siboo, 1977; Siboo & Kulisek, 1978; Pepys *et al.*, 1979). However, mouse SAP is a major acute phase reactant, increasing from resting levels of around 60 mg/l to peak concentrations of several hundred mg/l during the acute phase response (Pepys *et al.*, 1979). This contrasts human SAP, which is constitutively present at 30 mg/l and remains constant during all forms of infection and tissue injury.

In rats CRP does not appear to be the major acute phase reactant. However, in contrast to humans, rats have a much higher plasma CRP concentrations under basal conditions, i.e. about 300-500 mg/l, which is a 100 times higher than the concentration in humans (Nunomura *et al.*, 1994).

Structurally highly homologous proteins are also present in other experimental animals such as the guinea pig and the Syrian hamster. Syrian hamster SAP, originally termed female protein (FP), is unique because expression of the gene is modulated by sex steroids as well as by mediators of inflammation (Coe, 1977; Coe & Ross, 1985). In addition, the direction of the alteration of serum concentration of SAP (FP) is divergent between sexes in response to inflammatory stimuli. Following inflammation, serum SAP (FP) levels, which are high in the resting state in female hamsters, decrease, while in males the concentration, which are ordinarily low, increase (Rudnick & Dowton, 1993). Although a gene and mRNA transcription product homologous to CRP genes and mRNAs from other species has been identified (Dowton & Holden, 1991), not much is known about the Syrian hamster CRP. Both SAP and CRP have been isolated from guinea pig serum, however, neither pentraxin behave as a major acute phase protein (Rubio *et al.*, 1993).

In the invertebrate Limulus Polyphemus (horseshoe crab), SAP- and CRP-like pentraxins have been identified and characterised. Limulin, the CRP of this species, is constitutively expressed and represents a major component of the horseshoe crab's hemolymph at a concentration of 5 mg/ml (Robey & Liu, 1981). It is, however, not yet clear whether these levels elevate during an acute phase response. As invertebrates do not appear to have immunoglobulins, it has been suggested that

CRP might be serving a primitive form of immunoglobulin (Robey & Liu, 1981). To date, sequences for three Limulus CRP variants have been published (Nguyen *et al.*, 1986a, b). The amount of Limulus SAP has been reported to vary from animal to animal with values of 8-19 % of the total pentraxins in Limulus hemolymph (Shrive *et al.*, 1999).

1.3 Functional Properties of Short Pentraxins

An insight into the physiological roles of CRP and SAP has been provided by the identification of the ligands and effector molecules with which they interact. There are, however, considerable variations in ligand binding specificity between CRPs and SAPs from different species.

1.3.1 CRP Ligands and Effector Molecules

1.3.1.1 Phosphocholine

The principal ligand of CRP was first described in 1930 by Tillett and Francis, who discovered that the addition of acute phase sera of patients with various infections and inflammatory diseases to a solution of pneumococcal C-polysaccharide caused precipitation of a then unknown protein, CRP. Subsequently, the substance in the cell wall C-polysaccharide of pneumococci to which CRP bound, termed fraction C, was identified to contain nitrogen, carbohydrate and phosphorus, but remained uncharacterised until 1968. In 1968, Fraction C was described as a ribitol teichoic acid containing PC (Brundish & Baddiley, 1968). Shortly later, Kaplin and Volanakis (1974) identified the precise identity of the major reacting site for CRP in the cell wall C-polysaccharide as PC. Subsequently, it was shown that human CRP binds to PC residues with high affinity (K_d = 1-2 x 10^{-5} M) (Anderson *et al.*, 1978).

PC has also been demonstrated to be recognised by mouse CRP (Oliveira *et al.*, 1980), rabbit CRP (Oliveira *et al.*, 1980) and Limulin (Robey & Liu, 1981). Rat CRP showed hybrid specificity by binding to both PC and PE (de Beer *et al.*, 1982;

Schwalbe *et al.*, 1992). Interestingly, rat SAP and Syrian hamster SAP (FP), which aligns most closely with SAP, bind also PC (Coe *et al.*, 1981).

PC is increasingly becoming recognised as a structural component of a wide variety of prokaryotic and eukaryotic pathogens. Its presence has now been reported in *Haemophilius influenzae* (Weiser *et al.*, 1997), *Pseudomonas auruginosa*, *Neisseria meningitides* and *Neisseria gonorrhoeae* (Serino & Virji, 2000) and *Aspergillus fumigatus* (Pepys & Longbottom, 1971) as well as a variety of pathogenic protozoa, fungi, nematodes, and other intestinal parasites (Hirschfield, 2003).

Studies with genetically modified mice have shown that the administration of human CRP increases survival of mice infected with *Streptococcus pneumoniae*, an effect likely to be mediated by the strong reaction of CRP towards the PC moiety present on the cell wall of these bacteria (Szalai *et al.*, 1995). According to these authors, CRP transgenic (CRPtg) mice infected with *Streptococcus pneumoniae* are resistant to infections, showing longer survival time and lower mortality than their control littermates. Protection against bacterial infection is not restricted to *S. Pneumoniae*, as recent experiments demonstrated that CRP administration protects also against *Haemophilus influenza*, a pathogen expressing PC (Weiser *et al.*, 1998; Lysenko *et al.*, 2000). Finally, CRPtg animals are resistant to infections with the gram negative pathogen *Salmonella enterica*, even in the absence of CRP binding (Szalai *et al.*, 2000). The greater resistance of hCRPtg mice could be attributed to significantly enhanced early blood clearance and decreased numbers of bacteria in liver and spleen (Szalai *et al.*, 2000).

CRP also binds to PC-containing phospholipids on disrupted cell membranes. Initial evidence for binding of CRP to cell membranes was provided by experiments demonstrating that at sites of inflammation and tissue necrosis CRP is associated with cell membranes of damaged and necrotic cells, but not normal cells (Kushner & Kaplan, 1961). Subsequent studies showed that binding of CRP to the PC polar head group of lecithin in lipid layers required the addition of submicellar concentrations of lysolecithin (Volanakis, 1979). In agreement with these observations, CRP was shown to bind to erythrocytes only after addition of

lysolecithin or treatment with snake phospholipase A_2 (PLA_2) (Narkates & Volanakis, 1982). PLA_2 is an enzyme that hydrolyses the fatty acid ester bond in position 2 of lecithin and other sn-3-phospoglycerides, producing free fatty acids and lysophospholipids, including lysolecithin (Glaser *et al.*, 1993).

In humans, lysophospholipids are generated by human secretory phospholipase A_2 ($sPLA_2$), an enzyme secreted by the liver as an acute phase protein (Glaser *et al.*, 1993). However, $sPLA_2$ is only able to hydrolyse phospholipids of the outer membrane leaflet of normal cells if they show flip-flop exchange between the outer and inner leaflets (Fourcade *et al.*, 1995). Flip-flop exchange usually occurs in damaged cells and cells undergoing apoptosis, resulting in enrichment of the outer leaflet in phosphatidylserine and phosphatidylethanolamine, which are normally present in the inner leaflet (Zachowski, 1993; Martin *et al.*, 1995). As a consequence of their redistribution, phospholipids become susceptible to hydrolysis by $sPLA_2$. The presence of lysolecithin within the outer leaflet allows binding of CRP to the PC polar head group on the cells surface (Hack *et al.*, 1997) (Figure 1.2).

Ligand-complexed human CRP is thought to bind C1q, the first component of the classical pathway of complement and activate the classical pathway of the complement system.

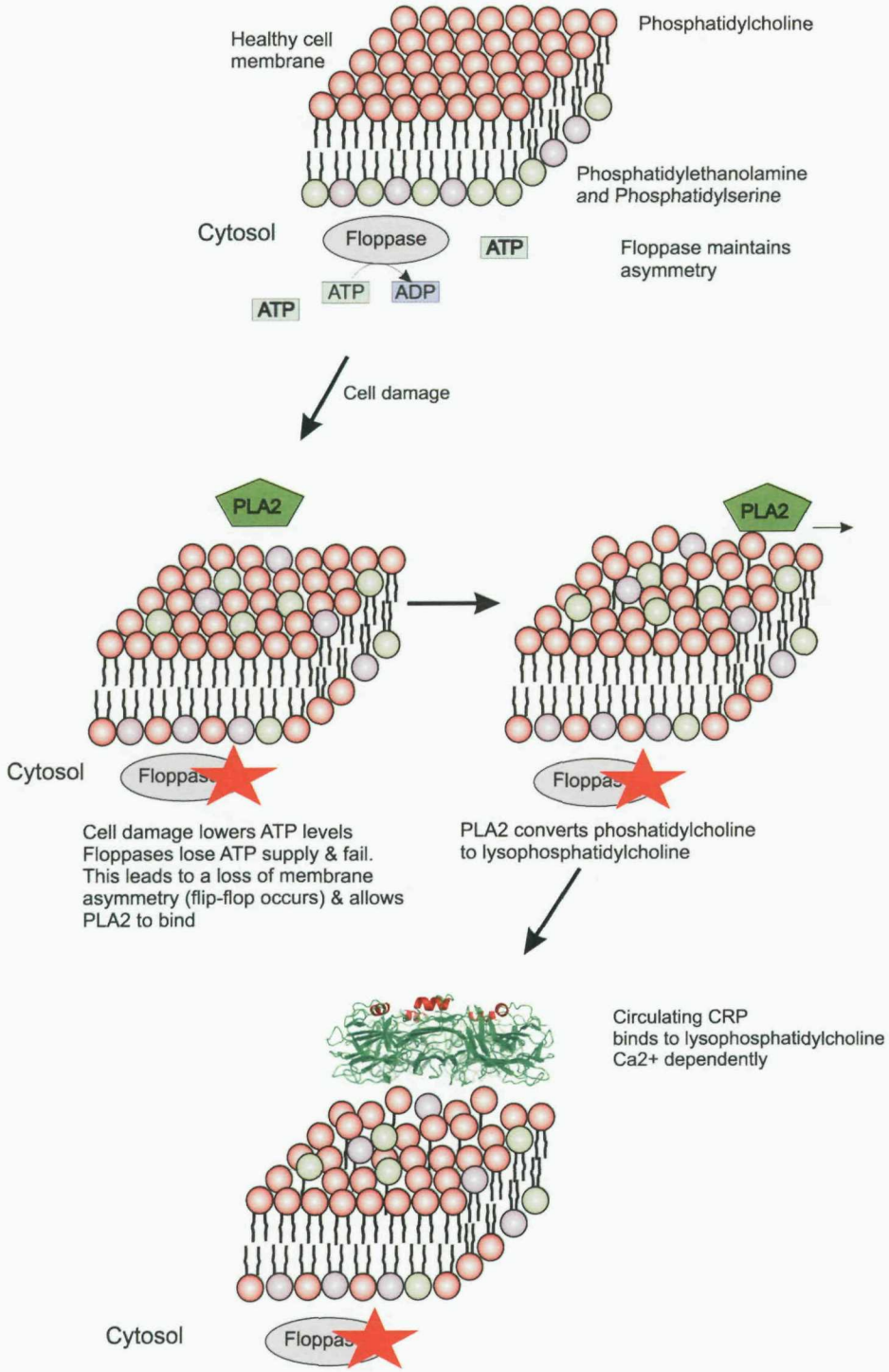

Figure 1.2 A proposed mechanism for the binding of CRP to membrane bilayers. Membranes have an asymmetric distribution of phospholipids: phosphatidylserine (green) & phosphatidylethanolamine (lilac) in the inner leaflet and phosphatidylcholine (red) in the outer leaflet. Floppases maintain this asymmetry by an energy-dependent process, requiring ATP. Cell damage lowers ATP levels and as a result floppases fail, leading to a loss of membrane asymmetry due to membrane flip-flop. The flip-flopped membrane is now susceptible to hydrolysis by PLA_2. CRP is able to bind to lysophosphatidylcholine, which is generated by PLA_2 (amended model from Hack *et al.*, 1997).

1.3.1.2 The Complement System

The complement system is a major effector system of the immune response. As part of the innate immunity it provides the first line of defence against invading pathogens, but it also plays an important role in developing and modulating the adaptive immune response as well (Gal *et al.*, 2007). The complement system comprises more than 35 proteins including soluble plasma proteins and cell-surface-complement receptors, which are involved in a wide range of functions including direct cell lysis, cell adhesion, chemotaxis and the enhancement of B and T cell responses (Walport, 2001). Three different pathways through which the complement system can be activated exist: the classical, lectin and alternative pathways (Figure 1.3).

All three pathways share the common step of activating the central component C3, but they differ according to the nature of recognition (Carroll, 2004). The classical pathway was the first studied; it is activated when the first complement component C1q binds to an immune complex of antigen and IgG or IgM antibody. However, activation can also be mediated by the interaction of C1q with pentraxins, lipopolysaccharides, viral particles, apoptotic cells as well as some other pathogen-associated molecular patterns (PAMPs).

Activation of the lectin pathway is initiated through recognition of PAMPs on pathogens by lectin proteins. To date, three members of this pathway have been identified: Mannan-binding lectin (MBL)(Reid & Turner, 1994), ficolin H and ficolin L (Fujita *et al.*, 2004). MBL is a C-lectin and a member of the collectin family (Carroll, 2004). It includes both collagen and globular regions and is structurally and functionally similar to C1q. However, the six globular heads of MBL form carbohydrate-recognition domains and bind N-acetyl glucosamine and mannose, located on the surface of many microbes (Carroll, 2004).

The alternative pathway contrasts with both classical and lectin pathways, in that it is "on" all the time, though at a low and constant pace due to spontaneous activation of C3 (Carroll, 2004; Lutz *et al.*, 2007).

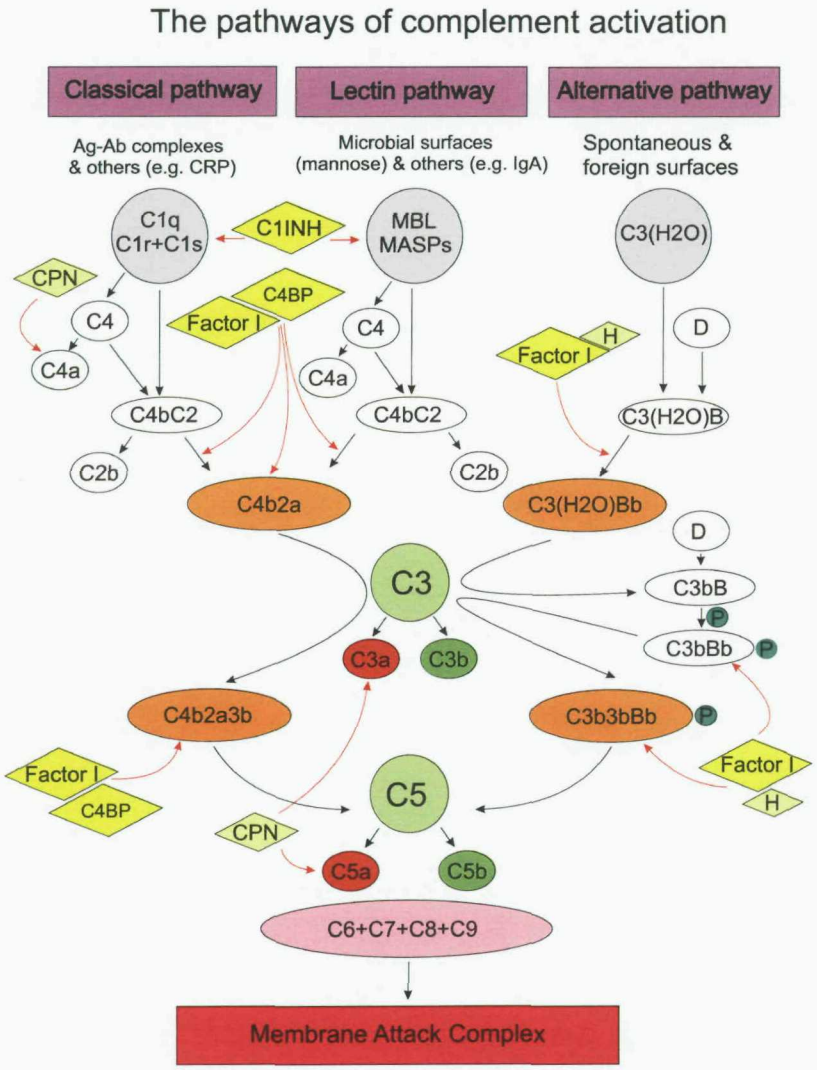

Figure 1.3 Overview of the complement activation pathways. The classical pathway is initiated when C1 binds to antigen-antibody complexes (Ag-Ab). C1q activates the serine proteases C1r & C1s, the later cleaving C4 to C4b, which exposes a specific binding site for C2. Then, C1s cleaves C2, and the resulting C3 convertase, C4b2a, cleaves C3 to C3b to form the C5 convertase C4b2a3b. The last enzymatic step in the cascade is the splitting of C5 into the highly potent anaphylatoxin C5a & the C6-binding fragment C5b. Activation of the lectin pathway is initiated by mannose-binding lectin (MBL) recognising mannose on bacteria. MBL activates the MBL-associated serine proteases (MASPs). Downstream activation of the lectin pathway is virtually identical to classical pathway activation. The alternative pathway activation mechanisms differ from those of the classical & lectin pathways. Under normal physiological conditions, the C3 molecule undergoes spontaneous hydrolysis of its internal thiol-ester and, thereby binds factor B, which is cleaved by factor D to form the C3 convertase C3(H2O)Bb. Then the complex cleaves C3 to C3a and C3b. The latter binds factor B, which is cleaved by factor D to form the second convertaseC3bBb. Properdin (P), the only regulator of complement that amplifies activation, binds to C3bBb, which then cleaves C3 and binds C3b to form the C5 convertase C3b3BbP. This cleaves C5 in the same fashion as the C5 convertase of the classical and lectin pathways. Complement activation is regulated by inhibitory molecules: C1 inhibitor (C1INH) controls C1r, C1s & MASPs, whereas carboxypeptidase N (CPN) inactivates the anaphylatoxins C5a, C3a & C4a. Factor I cleaves and inactivates C4b & C3b, using C4b-binding protein (C4BP) as the cofactor in the classical & lectin pathways and factor H in the alternate pathway (amended from Mollnes *et al.*, 2002).

C3 is the convergence point of all three pathways of complement activation. Proteolytic cleavage of mature C3 is mediated by enzyme complexes (convertases), and generates the anaphylotoxin C3a (9 kDa) and the major fragment C3b (177 kDa) (Bokisch *et al.*, 1969). The anaphylotoxin C3a binds to receptors on mast cells and induces degranulation by releasing histamine, causing increased vascular permeability (Ember *et al.*, 1992). C3b is able to bind covalently to cells and other target surfaces via an exposed thioester (Law *et al.*, 1979). Surface-bound C3b and its breakdown product iC3b act as opsonins for phagocytes (Sim *et al.*, 2004). C3b can also bind covalently to the C4b portion of the C3 convertase, C4b2a, to form a C5 convertase (C4b2a3b). Here C3b acts as a binding site for the substrate C5, allowing the protease to cleave C5 as well as C3.

The C5 convertase initiates the assembly of the membrane attack complex, consisting of complement components C5-C9, which forms a large channel through the membrane of the target cell, enabling ions and small molecules to diffuse freely across the membrane (Chakraborti *et al.*, 2000). This inability to regulate the flow of water and electrolytes leads to cell lysis.

1.3.1.2.1 The Classical Pathway of Complement

The classical pathway of complement is recognised as a major element of anti-bacterial host defence due to its ability to bind and eliminate invading pathogens (Arlaud *et al.*, 2002). Besides this protective action against infection, the classical pathway of complement also plays a role in immune tolerance through its ability to recognise and induce clearance of apoptotic cells (Fishelson *et al.*, 2001). This pathway is initiated by the C1 complex, a multi-molecular protease comprising one recognition protein, C1q, and two modular serine proteases (C1r and C1s) associated as a calcium-dependent tetramer (C1s-C1r-C1r-C1s) (Arlaud, 2001) (Figure 1.4).

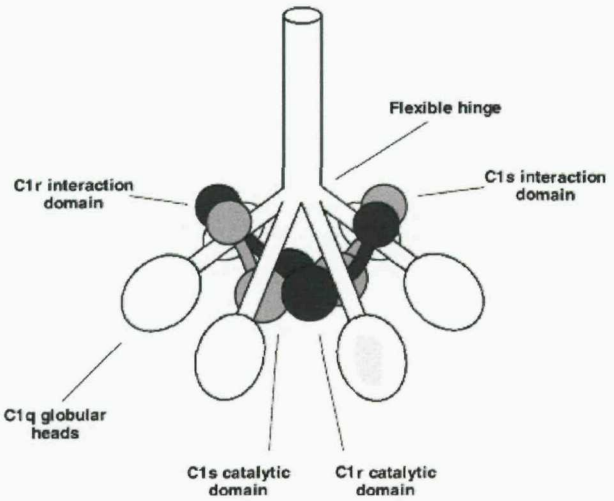

Figure 1.4 Macroscopic model of the C1 complex (Arlaud *et al.*, 2002).

All activators of the classical pathway are recognised and bound by the C1q moiety of C1, a process considered to induce a conformational change in the collagen domain. This conformational change leads to the auto-activation of C1r, which in turn activates C1s (Arlaud *et al.*, 2002). The activated C1s molecule cleaves C4 and C2, the protein substrates of C1 (Arlaud *et al.*, 2002). The function of C1 is regulated by the C1 inhibitor, which can bind and inactivate the activated proteases resulting in dissociation of the complex (Arlaud *et al.*, 2001).

1.3.1.2.2 The Structure and Function of C1q

C1q has a molecular weight of 460 kDa (Reid & Thompson, 1983) and is a hexameric molecule that appears as a bouquet-of-tulip-like structure on electron microscopic micrographs (Figure 1.5). It is assembled from 18 polypeptide chains of three different types: six A (A = 223 residues), six B (B = 226 residues) and six C (C = 217 residues) (Reid, 1983; Kishore & Reid, 2000). Each chain consists of a short N-terminal region (~ 3-9 residues) that is involved in the formation of A-B and C-C interchain disulphide bonds (Figure 1.6). This region is followed by a collagen-like sequence (~ 81 residues), which contains the characteristic repeating collagen sequence of Gly-X-Y (X = Proline, Y = 4-hydroxyproline or 5-hydroxylysine). This collagen-like region gives rise to six collagen-like triple helices, each containing one A, one B and one C chain. This part is referred to as the C1q collagen-like region (C1qCLR) and makes up the stalk. Approximately half way along the collagen-like triple helical region interruptions in the repeating sequence motif Gly-X-Y cause the stalk to diverge into six individual stems. Each stem terminates in a C-terminal globular head region (~ 135 residues) (Sellar *et al.*, 1991), which is referred to as the C1q globular head domain (gC1q).

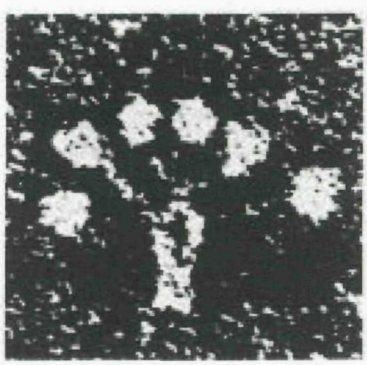

Figure 1.5 An electron micrograph of C1q (Knobel *et al.*, 1974).

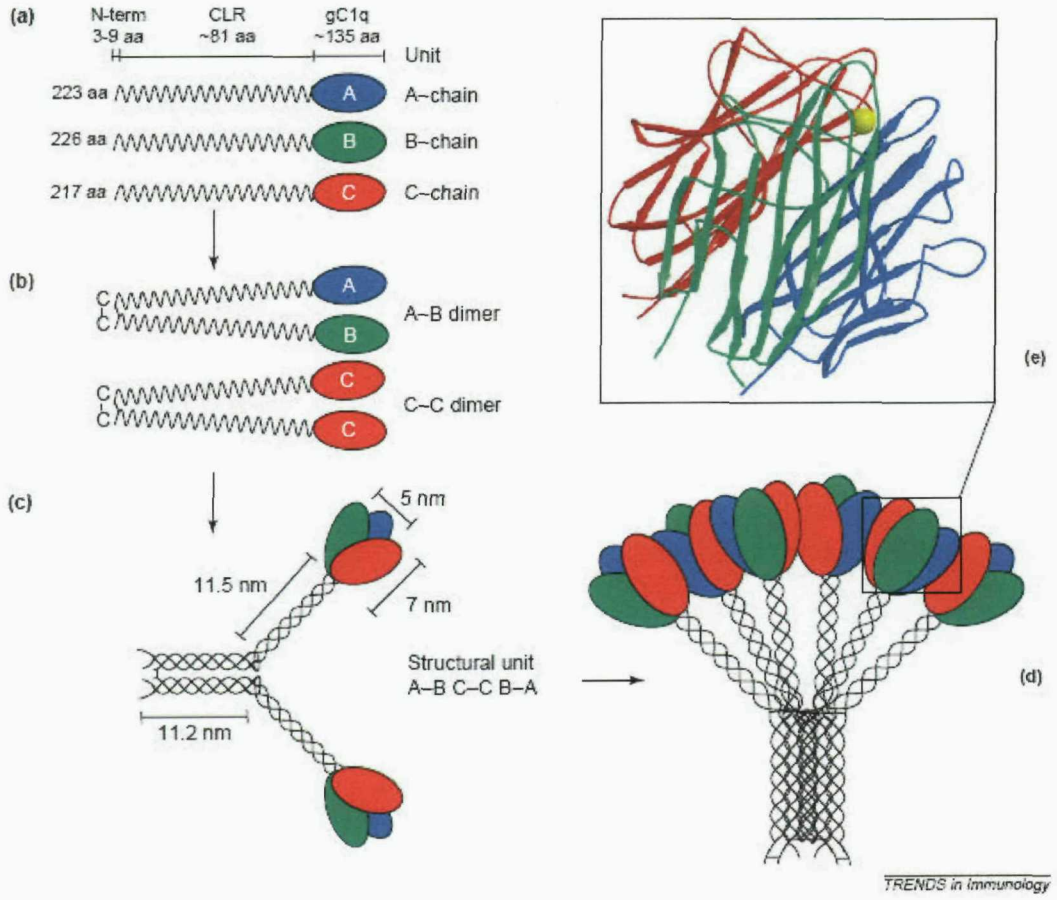

Figure 1.6 Structural organisation of the C1q molecule. C1q is composed of 18 polypeptide chains (6A, 6B, 6C). a) The A, B and C chains each have a short N-terminal region (containing a half cysteine residues involved in interchain disulphide bind formation), followed by a collagen region (CLR) of 81 residues and a C-terminal globular head region of ~ 135 residues. b) The inter chain disulphide bonding yields 6A-B dimmer subunits and 3 C-C dimmer subunits. The triple-helical collagen region in the A and B chains of an A-B subunit, together with one of the C chains present in a C-C subunit, form a structural unit (ABC-CBA), which is held together by both covalent and non-covalent bonds c). Three of these structural units associate via strong non-covalent bonds in the fibril-like central portion to yield the hexameric C1q molecule that has a tulip-like structure d). The crystal structure of the gC1q domain of human C1q (Protein Data bank code 1PK6, depicted as a ribbon diagram of ghA in blue, ghB in green, ghC in red, with the calcium ion shown as a yellow ball), has revealed a compact, spherical, heterotrimeric assembly, held together predominantly by non-polar interactions, with non-crystallographic pseudo-threefold symmetry e) Figure taken from Kishore *et al.*, 2004.

Although the crystal structure of complete intact C1q remains to be determined, the globular head domain of C1q has recently been solved to 1.9 Å by Garboriaud *et al.* (2003). The structure reveals a tight heterotrimeric assembly with non-crystallographic pseudo-three-fold symmetry (Figure 1.7). The assembly exhibits a globular, spherical structure with a diameter of approximately 50 Å and has a single calcium ion bound to the apical centre of the trimer (Gaboriaud *et al.*, 2003).

The subunit structure reveals a 10-stranded β-sandwich with a jellyroll topology homologous to the one described initially for the tumor necrosis factor, consisting of two five-stranded anti-parallel β-sheets (A', A, H, C, F) and (B', B, G, D, E) (Gaboriaud *et al.*, 2003). The beta sheet formed by the B', B, G, D and E strands and A-A' loop form the exterior of the trimer, while the second beta sheet (A', A, H, C, F), loops E-F and G-H are essentially buried and together with the C-terminal half of strand E, account for most of the interfaces between the three modules.

The calcium ion is coordinated by six oxygen ligands contributed by one of the side-chain oxygens of AspB172, the side-chain carbonyls of GlnA177 and GlnB179, the main chain carbonyl of TyrB173, and two water molecules, with an average bond distance of 2.58 Å (Gaboriaud *et al.*, 2003)(Figure 1.8).

The calcium binding site is therefore asymmetrical relative to the trimer, since calcium bridges strand F of module A to strands E and F of module B but is not connected to module C (Gaboriaud *et al.*, 2003). Due to the accessibility of the calcium ion to the solvent, it is possible that some of the charged targets recognised by C1q may interact directly with the calcium ion by displacing one or both of the water molecules.

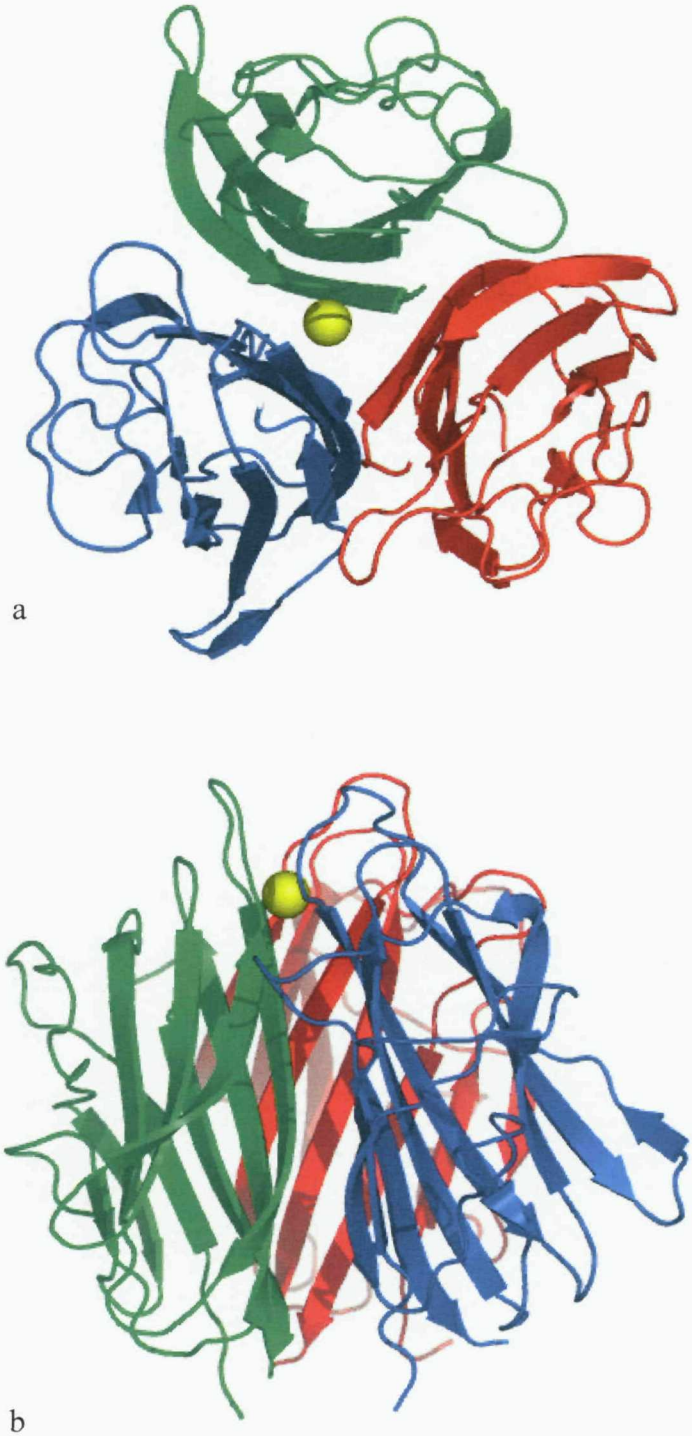

Figure 1.7 The structure of the heterotrimeric C1q globular domain. A ribbon representation of the assembly seen from the top (a) and side (b). Modules A, B and C are shown in blue, green and red, respectively. The calcium ion is shown in yellow (Figure produced from 1PK6.pdb using Pymol and similar pictures).

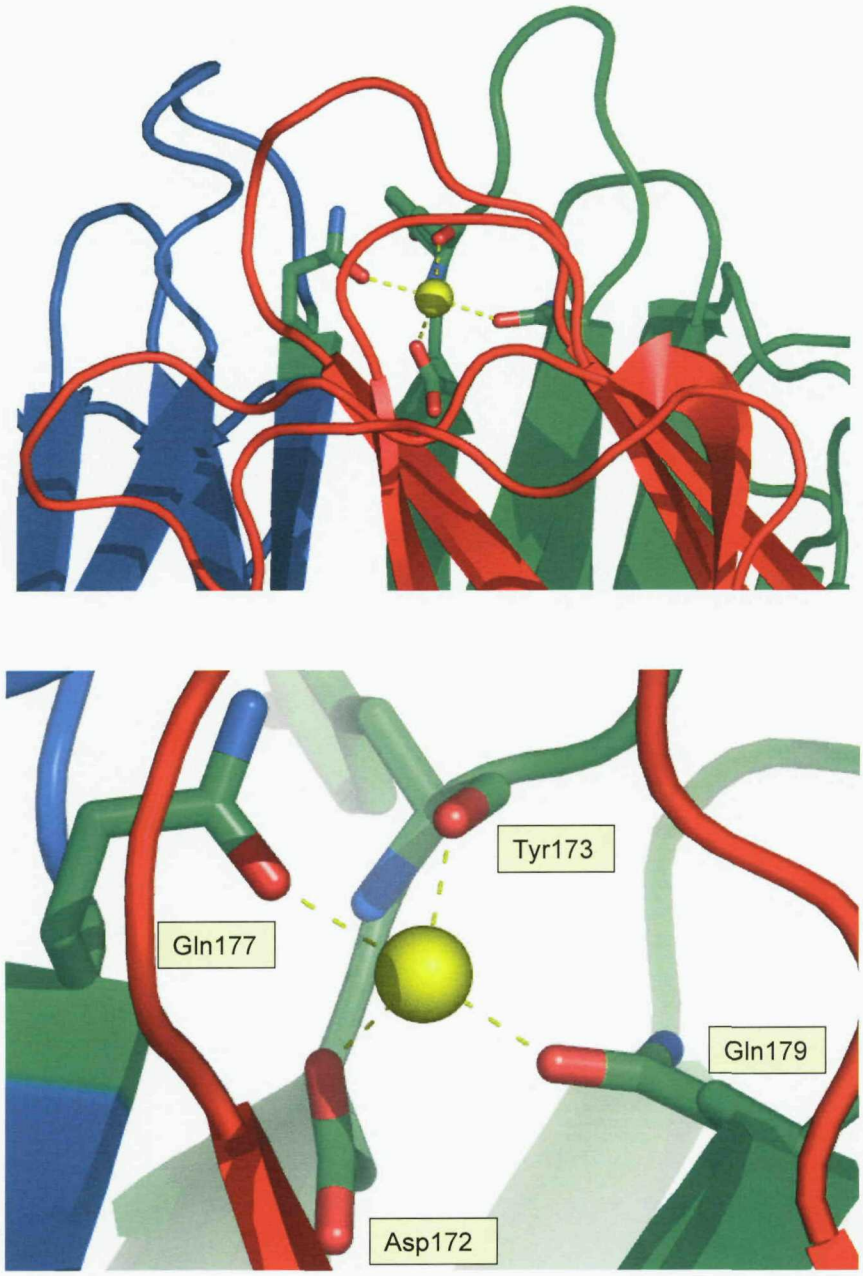

Figure 1.8 The calcium binding site of C1q. The calcium ion is coordinated by the side-chain of AspB172, GlnA177, GlnB179, the main chain carbonyl of TyrB173 and two water molecules (not shown).

Given the heterotrimeric organisation of the C1q globular domain, it has been debated whether the C-terminal globular head region of the human C1q A, B and C chains are functionally autonomous modules or whether the ability of C1q to bind its ligands is dependent upon a combined, globular structure (Kishore *et al.*, 2002; 2003). It appears from studies using recombinant forms of ghA, ghB and ghC that each module within the C1q globular domain has a certain degree of functional independence in binding ligands (Kishore *et al.*, 2003; Kojouharova *et al.*, 2003). This notion has been reaffirmed by the crystal structure of gC1q, which shows that each module of the three subunits exhibits different surface charge patterns (Garboriaud *et al.*, 2003).

The crystal structure also confirms the proposed presence of a calcium ion in the heterotrimeric assembly of the globular domain (Villiers *et al.*, 1980). Although the function of this calcium ion remains to be determined, Garboriaud *et al.* (2003) proposed that the calcium ion contributes to the stability of the heterotrimeric assembly. In addition, the observation that the calcium ion is fully accessible to the solvent has opened the possibility that the calcium ion directly participates in the recognition of ligands (Garboriaud *et al.*, 2003).

Further investigations into the role of calcium using both theoretical and experimental approaches suggest that calcium primarily influences the target recognition properties of C1q toward IgG, IgM, CRP and PTX3 (Roumenina *et al.*, 2005). In addition, a mechanism for the target recognition and classical complement activation by C1q has been proposed, which consists of: (a) initial target recognition of negatively charged molecules by the C1q apex. This is facilitated by the exposed Ca^{2+} ion, which directs its molecular electrical moment towards the top of the gC1q heterotrimer. (b) removal of Ca^{2+} by the bound target due to its negative field followed by reorientation of the electric moment. This generates mechanical stress and a structural change within the CLR domain, which leads to the activation of C1r (Roumenina *et al.*, 2005; 2007).

1.3.1.2.3 CRP-mediated Complement Activation

Activation of the classical complement pathway by CRP was first described in 1974 by Kaplan and Volanakis using pneumococcal C-polysaccharide (PnC) and phospholipids ligands and by Siegel *et al.* (1974) using CRP-protamine complexes. Kaplan and Volanakis reported that the addition of PnC to CRP-containing acute phase sera resulted in the consumption of the complement components: C1, C4, C2 and C3-9 independent of antibody. This indicated that complement activation by CRP complexes proceeded through the classical pathway. They also demonstrated that an effective C3-convertase was formed and that C3 and C1q bound to CRP-PnC complexes reacted with normal serum. Moreover, they found that phosphocholine, which had previously been identified as a major reacting ligand of CRP, completely inhibited the reaction. This led to the testing of CRP with lipid emulsions consisting of cholesterol and either phosphatidylcholine or spingomyelin, which also efficiently activated the classical pathway. Subsequently, they showed that the consumption of guinea pig complement by CRP complexes required participation of human C1q, and that these complexes do not interact with guinea pig C1q. This finding is reminiscent of a similar incompatibility observed in rats. Rat CRP activates neither rat C1q nor human C1q, while human CRP activates both (DeBeer *et al.*, 1982).

Although CRP has been found to initiate complement-mediated lysis of erythrocytes and liposomes (Richards *et al.*, 1977), examination of individual complement components suggests that CRP-mediated complement activation is limited to the initial stage of complement activation involving C1-C4, with little activation of the late complement proteins C5-C9 (Mold *et al.*, 1999). This may be due to the ability of CRP to interact with factor H, leading to inhibition of the pathways that result in formation of the C5 convertases (Mold *et al.*, 1999). As a result, the strong inflammatory responses typically associated with C5a and C5-C9 membrane attack complex are limited.

For many years the location of the CRP binding site on C1q was thought to be within the CLR region (Jiang *et al.*, 1991). In particular, the sequences involving the amino acid residues 14-26 and 76-92 within the CLR of the A chain were

thought to be important for the interaction with CRP (Jiang *et al.*, 1991). This view changed following the recent elucidation of the crystal structure of the globular domain of C1q (Gaboriaud *et al.*, 2003), which strongly supports the C1q-CRP interaction occurring via the gC1q domain. This study suggests that the top of gC1q, which is predominantly basic, fits into the central pore of the CRP pentamer. Moreover the residues Asp112 and Tyr175 of CRP, which were experimentally shown to be critical for C1q binding, would be the contact residues (Agrawal *et al.*, 2001).

1.3.1.3 Nuclear Constituents and Apoptotic Cells

In 1977 Gitlin *et al.* reported the presence of CRP in the nuclei of synoviocytes and histiocytes in the patients with rheumatoid arthritis. This led to the finding that CRP binds to nuclear materials such as histones (Du Clos *et al.*, 1988) and small nuclear ribonucleoproteins (Du Clos *et al.*, 1989). In addition, CRP has been shown to bind to a short cationic sequence of Sm-D protein, which occurs in many nuclear proteins. These autoantigens are often the target of autoantibodies (Jewel *et al.*, 1993).

Potential sources for these autoantigens include cells that are undergoing apoptosis (Casciola-Rosen *et al.*, 1994). Apoptosis (or programmed cell death) is recognised as a highly regulated process essential during development and in the maintenance of normal tissue homeostasis. The process occurs without inflammation and is characterised by the translocation of potentially auto-antigenic molecules from the nucleus to the cell surface where they are displayed to the extracellular environment as membranous blebs/apoptotic bodies (Casciola-Rosen *et al.*, 1994). In addition, changes during the apoptotic process occur also on the outer surface of cells due to the flip-flop exchange of phospholipids from the inner to the outer membrane. This allows CRP binding to the surface of the apoptotic cells (Gershov *et al.*, 2000). Bound CRP augments the classical pathway of complement activation by promoting the binding of C1q and C3b (Gershov *et al.*, 2000). Although, CRP protected the cells from assembly of the terminal membrane attack complex, opsonisation and phagocytosis of apoptotic cells by macrophages was enhanced.

Enhanced phagocytosis of apoptotic cells opsonised with CRP has also been shown to proceed in the absence of complement. This suggests that the mechanism of CRP-induced clearance of apoptotic cells can also be mediated by specific receptors for CRP on phagocytic cells. It has been proposed that Fc receptors for IgG (FcγRs) might serve as pentraxin receptors on phagocytic cells. Several groups have shown binding of CRP to FcγRI (Marnell *et al.*, 1995; Bodman-Smith *et al.*, 2002) and FcγRII (Bharadwaj *et al.*, 1999). However some investigators have voiced doubts about CRP binding to FcγRs (Hundt *et al.*, 2001; Saeland *et al.*, 2001), suggesting that the binding of CRP to Fcγ receptors results from either an interaction of the Fc portion of the anti-CRP antibody with FcγRIIa itself and/or CRP contamination with IgG.

The diverse and conflicting data about the interaction of CRP with the FcγRs was recently reassessed using the technique of ultrasensitive confocal fluorescent microscopy (Manolov *et al.*, 2004) and site-directed mutagenesis (Bang *et al.*, 2005). Manolov et al. (2004) provides quantitative evidence of CRP binding to FcγIIa and demonstrates that the use of anti-CRP antibodies affects CRP binding and leads to false-positive results. This might explain and settle the diverse and conflicting data presented in the literature. The site-directed mutagenesis study of CRP (Bang *et al.*, 2005) identifies residues important to CRP binding to FcγRI and FcγRII further supporting CRP binding to FcγR. These results indicate that the binding sites on CRP for FcγRI and FcγRII overlap.

In summary, the ability of CRP to recognise a wide range of pathogens and damaged host cells; and mediate their elimination by recruiting and activating the complement system as well as phagocytic cells suggests that the main physiological role of CRP is in host defence.

1.3.2 SAP Ligands and Effector Molecules

1.3.2.1 DNA and Chromatin

Like CRP, SAP binds to nuclear components. However, unlike CRP or any other serum protein, SAP has been reported to undergo calcium-dependent binding to DNA and chromatin in physiological conditions (Pepys & Butler *et al.*, 1987). Moreover, the avid binding of SAP to native long chromatin selectively displaced histone H-1, thereby rendering the chromatin soluble (Butler *et al.*, 1990). Furthermore, SAP was reported to bind to extracellular chromatin *in vivo* (Breathnach *et al.*, 1989).

Recently, further insight into the physiological role of SAP was gained from SAP-deficient mice (Bickerstaff *et al.*, 1999). The majority of these SAP-deficient mice appeared to develop antinuclear antibodies, which was interpreted as evidence that SAP is controlling the degradation of chromatin *in vivo* and prevents antinuclear autoimmunity. Moreover, it was postulated that SAP binds to apoptotic cells via chromatin fragments exposed on the blebs of these cells. These chromatin-bearing blebs on apoptotic cells are formed in the late stage of apoptosis. However, it has also been demonstrated that SAP can bind to cells in the early stage of apoptosis independent of chromatin (Familian *et al.*, 2001). In this study, it is hypothesised that binding of SAP to these early apoptotic cells occurs via PE, which is translocated to the outer leaflet of the cell membrane during membrane flip-flop, one of the earliest events during apoptosis.

These findings indicate that SAP is important in reducing the immunogenicity of chromatin and DNA and preventing autoimmunity, however, the mechanism and molecules involved remain to be established. Some reports claim that SAP mediates the clearance of nuclear material through a process independent of the classical pathway as the rate of SAP-mediated chromatin degradation was unaffected in C1q knockout mice (Bickerstaff *et al.*, 1999), while others do not want to exclude the possibility that apoptotic cells may also be cleared via opsonisation with complement (Botto *et al.*, 1998; Familian *et al.*, 2001).

1.3.2.2 Complement

Evidence for the binding of SAP to the complement component C1q was first reported in 1986 by Bristow & Boackle. Subsequently, it was shown that supra-physiological concentrations of SAP (Butler *et al.*, 1990) and solid-phase histones complexed with SAP (Hicks *et al.*, 1992) activate complement via the classical pathway. This was followed by a study of chemically cross-linked SAP oligomers (Jiang *et al.*, 1993). They report that SAP oligomers bind to C1q via the collagen-like region of C1q, at sites located within residues 14-26 and/or 76-92 of the C1q chain A. Since CRP has been shown recently to bind to the globular head region of C1q, it seems unlikely that the two pentraxins would bind different locations on the C1q molecule.

SAP has also been reported to bind to C4b-binding protein (C4BP) (Schwalbe *et al.*, 1990; Garcia de Fruto *et al.*, 1995). While some investigators have found that this binding does not influence the function of C4BP (Schwalbe *et al.*, 1990; Sorensen *et al.*, 1996), others have shown that SAP activates the classical complement pathway by inhibiting the ability of C4BP to function as a cofactor for factor I in the degradation of C4b (Garcia de Fruto & Dahlback, 1994). This led to the speculation that SAP has a regulatory role in the activation of the classical complement pathway *in vivo*.

1.3.2.3 Bacteria/LPS

SAP has been shown to bind to various bacteria including *Klebsiella rhinoscleromatitis* (Hind *et al.*, 1985), *Streptococcus pyrogens* (Hind *et al.*, 1985), *E. coli* (De Haas *et al.*, 2000; Noursadeghi *et al.*, 2000), *Xanthomonas campestris* (Hind *et al.*, 1985), *Salmonella enterica* (De Haas *et al.*, 2000), *Haemophilus influenzae* (De Haas *et al.*, 2000) and *Neisseria meningitides* (Noursadeghi *et al.*, 2000). Binding of SAP to these organisms occurs either through the specific recognition of the carbohydrate ligand 4, 6 cyclic pyruvate acetal of galactose or through LPS on the cell wall of the bacteria.

Recent studies have shown that binding of SAP to gram-negative bacteria via LPS prevents LPS-mediated classical pathway complement activation and results in a clear inhibition of complement component C3 deposition on the bacteria (DeHass *et al.*, 2000). This inhibition of the classical complement pathway has been hypothesised to be due to a competition between SAP and C1q for binding to LPS. As a result, complement-mediated lysis as well as phagocytosis of the bacteria is reduced. This suggests that SAP is not opsonic.

These findings have also been supported by studies of bacterial infection in SAP-deficient mice. These studies demonstrate that for certain organisms to which SAP binds, such as *Streptococcus pyrogens*, *E. coli* and *Neisseria meningitides*, SAP has a strong anti-opsonic effect by inhibiting phagocytosis, resulting in enhanced virulence of the infectious agent (Noursadeghi *et al.*, 2000). This is reflected in the markedly enhanced resistance of SAP deficient mice to otherwise lethal infection with such organisms (Noursadeghi *et al.*, 2000).

However, SAP evidently contributes to survival during infections with organisms to which it does not bind, suggesting that SAP also has some host defence function (Noursadeghi *et al.*, 2000).

1.4 CRP: Its Role in Disease

Although an understanding of the physiological role of CRP remains elusive, CRP has been suggested to play an important role in cardiovascular disease. Cardiovascular disease includes three distinct pathological processes:
(a) atherosclerosis, the disease caused by low-density lipoprotein (LDL), cholesterol and other risk factors that affects most adults in developed countries;
(b) atherothrombosis, the catastrophic event that occludes arterial blood supply and
(c) ischemic infarction that results from arterial occlusion.

A role for CRP in cardiovascular disease was first suggested by the discovery that aggregated human CRP specifically binds LDL and VLDL (DeBeer *et al.*, 1982; Rowe *et al.*, 1984). This finding was later confirmed by Rowe *et al.* (1985) using rat and rabbit CRP and recently by others using various modified and non-modified LDL molecules (Bhakdi *et al.*, 1999; Chang *et al.*, 2002; Taskinen *et al.*, 2005). However, in 1985 scientific interest diminish due to the publication of an immunohistochemical study that reported no deposition of CRP or apolipoprotein B in inflammatory arterial lesions (Rowe *et al.*, 1985). Interest returned with the reports of a prognostic association between CRP levels and future coronary events in patients with known coronary heart disease (Liuzzo *et al.*, 1994; Thompson *et al.*, 1995; Haverkate *et al.*, 1997). Interest was further heightened by epidemiological studies. These studies were enabled due to the availability of routine high-sensitivity assays for CRP and demonstrated an association between baseline CRP values in the general population and future cardiovascular events (Kuller *et al.*, 1996; Ridker *et al.*, 1997; Koenig *et al.*, 1999). As a result, CRP was declared to be a cardiovascular risk factor and marker for cardiovascular diseases.

Although CRP has been shown to have the capacity to activate the complement system (Kaplan & Volanakis, 1974; Siegel *et al.*, 1974), it has taken 20 years to find complement-activating molecules in human atherosclerotic lesions. In 1998, Torzewski *et al.* demonstrated that CRP is present in all stages of human atherosclerosis and that it co-localises with activated complement fragments. In addition, investigators also demonstrated co-localisation of CRP and activated complement fragments within all myocardial infarcts (Lagrand *et al.*, 1997).

Compelling experimental evidence now suggests that CRP-mediated complement activation leads to increased inflammation and exacerbation of tissue injury in myocardial infarction and stroke (Griselli *et al.*, 1999; Gill *et al.*, 2004). All together, these findings suggest that CRP may have an important role in the pathogenesis of atherosclerosis and myocardial infarction/stoke.

1.4.1 Atherosclerosis

Atherosclerosis, the main underlying cause of cardiovascular disease, is a progressive disease characterised by the accumulation of lipids and fibrous elements in the large arteries (Lusis, 2000). It is now clear that arterial inflammation is a key feature of atherosclerosis development, progression and thrombotic complications.

The atherosclerotic process starts as a response to injury to the endothelium and smooth muscle cells of the vessel wall. This injury is initially caused by mechanical shear at specific arterial sites such as branches and curvatures. At these sites, the permeability to macromolecules such as low-density lipoprotein (LDL) particles (Figure 1.9) is increased. Over time, LDL accumulates in the sub-endothelial matrix and can undergo modification by oxidation, glycation (in diabetes) or aggregation. Modified LDL, hypertension, free radicals generated by smoking, diabetes mellitus, hyperhomocysteinemia and certain infections can cause endothelial dysfunction (Epstein, 1999).

A dysfunctional endothelium promotes the recruitment of a variety of inflammatory cells such as monocytes and lymphocytes into the arterial intima through a series of steps regulated by cytokines and adhesion molecules, such as intercellular adhesion molecule -1 (ICAM-1) and vascular cell adhesion molecule -1 (VCAM-1) (Pober *et al.*, 1990). After transmigration of monocytes, they become macrophages and take up lipids (oxidised LDL) via scavenger receptors, forming foam cells (Ablij *et al.*, 2002). These foam cells together with T cells form the fatty streak (Figure 1.10).

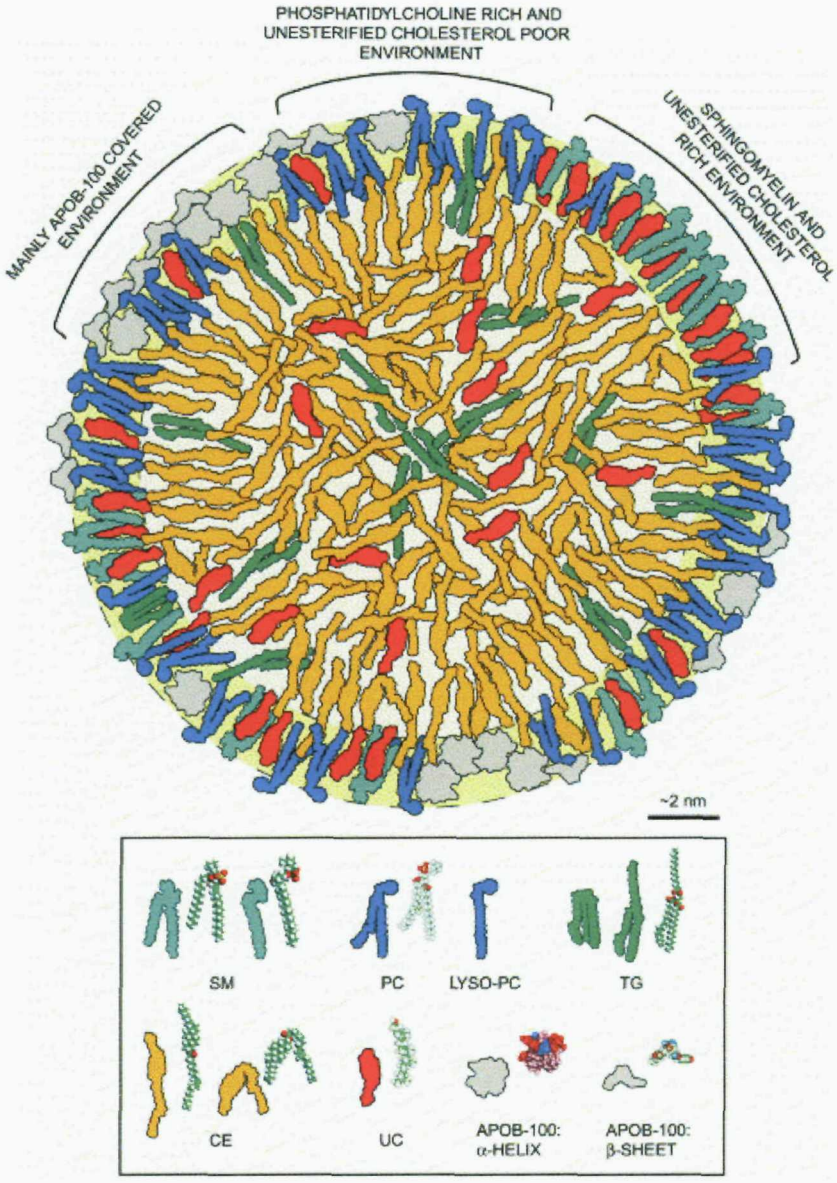

Figure 1.9 Schematic molecular model of an LDL particle. The depicted particle has a diameter of 20 nm and an average composition of 20 % protein (APOB-100), 20 % phospholipids (phosphocholine = PC, sphingomyelin = SM, lysophosphatidylcholine = lyso-PC, phosphatidylethanolamine = PE), 40 % cholesterol esters (CE), 10 % unesterified cholesterol (UC) and 5 % triglyceride (TG). (Figure taken from Hevonoja *et al.*, 2000)

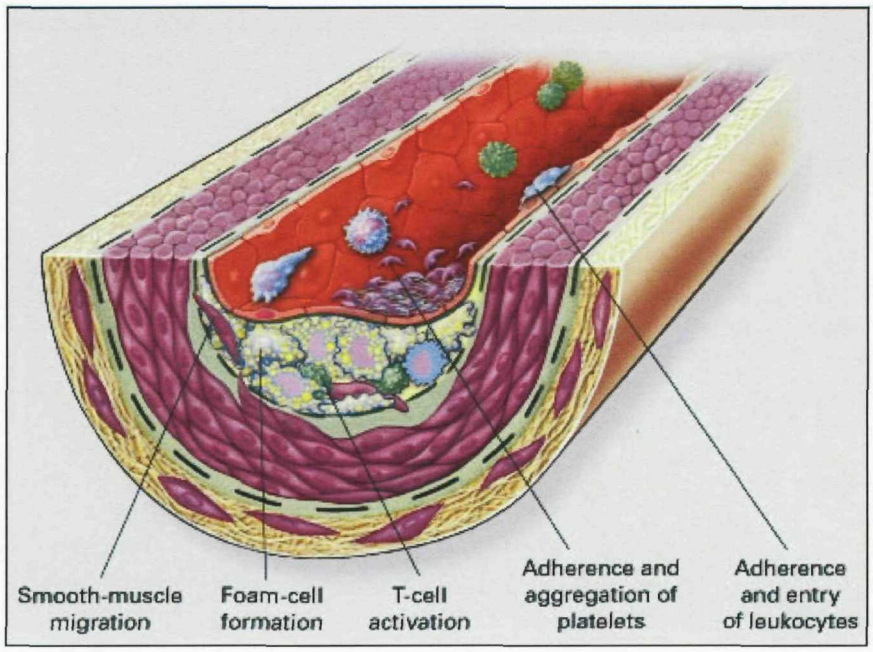

Figure 1.10 Fatty streak formation in atherosclerosis. Fatty streaks consist of lipid-laden macrophages (foam cells) together with T lymphocytes (Figure taken from Ross, 1999).

When foam cells within the fatty streaks die, the cellular debris and lipids form the constituents of the necrotic pore in the lesion. Subsequently, some fatty streaks accumulate smooth muscle cells that migrate from the medial layer due to the production of different cytokines by the inflammatory cells (Lusis, 2000). The smooth muscle cells secrete fibrous elements, causing the formation of a fibrous cap that separates the lesion from the lumen. Occlusive fibrous plaque develops that can become increasingly complex with calcification and ulceration at the luminal surface (Libby, 2002). Rupture of the fibrous cap or ulceration can rapidly lead to thrombosis and usually occurs at sites of thinning of the fibrous cap (Ross, 1999). Thinning of the fibrous cap is apparently due to the continuing influx and accumulation of macrophages, which release metalloproteinases and other proteolytic enzymes at theses sites (Ross, 1999). These enzymes cause degradation of the matrix, leading to hemorrhage, thrombus formation and occlusion of the artery. Thus, inflammatory processes not only promote initiation and progression of atheroma, but also contribute decisively to precipitating acute thrombotic complications of atheroma (Libby *et al.*, 2002).

1.4.1.1 CRP and Atherosclerosis

The discovery that aggregated, but not native, non-aggregated, CRP selectively bound only LDL and some very low-density lipoprotein (VLDL) from whole serum (de Beer *et al.*, 1982) was the first suggestion of a possible relationship to atherosclerosis. However, native CRP does bind to partly degraded, so called modified LDL, as it is found in atheromatous plaques (Bhakdi *et al.*, 1999) and oxidised LDL (Chang, 2002). Binding of CRP to these lipoproteins was proposed to occur through recognition of a phosphocholine moiety that becomes exposed in the modified/oxidised LDL. Recently, CRP was also shown to bind to cholesterol in LDL particles (Taskinen *et al.*, 2002; 2005).

The co-localisation of oxidised LDL, CRP and complement fragments in early atherosclerotic lesions (Lagrand *et al.*, 1997; Torzewski *et al.*, 1998) have led to the hypothesis that oxidised LDL bound to CRP could promote complement activation and thus inflammation in the plaques. This hypothesis has been supported by Bhadkdi *et al.* (1999) using complement activation assays of CRP with enzymatically digested LDL. Subsequently, CRP was reported to opsonise native LDL for macrophages, thereby causing foam cell formation (Zwaka *et al.*, 2001), which is a typical feature of atherosclerosis. The authors claim that the enhanced uptake of CRP/LDL by macrophages is mediated via the cellular FcγII receptor. This report not only contrasts the major hypothesis on foam cell formation in atherosclerosis, but has also been brought into question by several groups. For example, Chang *et al.* (2002) showed recently in a study that CRP promotes the uptake of oxidised but not native LDL because of certain unexposed phosphocholine epitopes on oxidised low-density lipoprotein. Shortly later, Fu and Borensztajn (2002) reported that the uptake of the CRP/LDL complex by macrophages is not mediated by the FcγII receptor and hypothesised that the CRP present in the arterial wall may contribute to the formation of foam cells primarily by its ability to aggregate LDL particles in the presence of calcium.

Further to these previously contradictory *in vitro* studies, numerous *in vitro* studies have tried to address the mechanism by which CRP may promote atherosclerosis. The authors of these studies used commercially available recombinant CRP on

cultured endothelial cells, smooth muscle cells and moncytes/macrophages and suggest that CRP has pro-inflammatory effects. Reported effects of CRP on endothelial cells include: increased production of adhesion molecules (Pasceri *et al.*, 2000; 2001) known to promote adhesion of monocytes to the endothelial cells during the earliest stages of atherosclerosis; decreased expression of endothelial nitric oxide synthase (eNOS) (Venugopal *et al.*, 2002) and prostacyclin (Venugopal *et al.*, 2003) and increased production of endothelin-1 (Verma *et al.*, 2002), all of which are critical regulators of arterial vasodilation. Effects of exogenous CRP on smooth muscle cells include: upregulated expression of angiotensin I receptors, thereby increasing reactive oxygen species and proliferation (Wang *et al.*, 2003); upregulated production of inducible nitric oxide synthase (iNOS) and certain cell signal transduction pathways (Hattori *et al.*, 2003). Similarly, data was also obtained on the effects of CRP on monocytes/macrophages, which showed an increased secretion of monocyte tissue factor, potentially stimulating cell migration and adhesion to endothelial cells (Torzewski *et al.*, 2000). These *in vitro* studies using commercially available recombinant CRP preparations have been criticized for the lack of robust controls performed to assess whether the effects observed were due to contaminants such as azide and LPS in the preparation (Hirschfield & Pepys, 2003; Pepys & Hirschfield, 2003). Shortly later, it was shown that almost all of the published pro-inflammatory effects of CRP were due to contamination of CRP preparations with azide and LPS (Taylor *et al.*, 2005; Lafuente *et al.*, 2005; Pepys *et al.*, 2005).

All of these *in vitro* studies have been supplemented by recent *in vivo* studies, which have been equally controversial and inconclusive. For instance, Paul *et al.* (2004) reported that transgenic human CRP accelerates atherosclerotic lesion development in male but not female apolipoprotein E (apoE) knockout mice. They concluded that CRP is atherogenic. In contrast, two other studies of apoE knockout mice concluded that transgenic human CRP is not pro-atherogenic (Hirschfield *et al.*, 2005; Trion *et al.*, 2005). This finding was supported by a study by Reifenberg *et al.* (2005), which used transgenic rabbit CRP apoE knockout mice. These mice were, however, shown to lack a fully functional complement system, which was attributed to the presence of inhibitors. One of these inhibitors was mouse

fibronectin, which was found in earlier work to have inhibitory effects (Hitsumoto *et al.*, 1999).

In a subsequent report, human CRP was in fact shown to be anti-atherogenic and slowed atherosclerosis development (Kovacs *et al.*, 2007). This study used an atherosclerosis-prone mouse model (apoB) with human-like hypercholesterolemia. Clearly, the development of these transgenic CRP-overexpressing mouse models to study the development of atherosclerosis has resulted in conflicting observations. These conflicting data are possibly due to several problems with the CRPtg mouse model itself. Human CRP is a foreign antigen in the mouse and the transgenic mice are incapable to mount one of the most fundamental pro-inflammatory effect of CRP i.e. lipoprotein dependent complement activation. Therefore, it has been suggested that the effects of human CRP on atherosclerosis in the mouse model may be completely unrelated to its actions in humans.

This led to the proposal that the rabbit may be a better animal model with which to investigate the role of CRP in atherosclerosis. Rabbits, unlike mice, produce a native CRP that is 70 % homologous to humans, highly inducible and responsive to inflammatory stimuli (Kushner & Feldman, 1978). In addition, they are sensitive to a cholesterol diet and rapidly develop atherosclerosis (Fan & Watanabe, 2003). A study followed investigating the role of CRP in atherosclerosis in a rabbit atherosclerosis model (Sun *et al.*, 2005). The authors of this study elaborated three major results. First, CRP levels were significantly elevated in hypercholesterolemic rabbits. Second, elevated CRP levels were strongly correlated with the extent of atherosclerosis in these animals. Third, CRP was ubiquitously present in atherosclerotic lesions in rabbits and this lesional CRP was derived from the circulation rather then synthesised locally in the arterial wall. Although this does not verify causal involvement of CRP in atherosclerosis, they suggest that the rabbit may be an alternative model to assess inhibitory effects of decreasing the CRP level.

All together, investigations regarding a potential role for CRP in atherosclerosis are evolving rapidly. However, it remains to be demonstrated that CRP has a definitive

causal role in atherosclerosis. Further investigations perhaps with agents that directly inhibit CRP might provide the evidence (Pepys *et al.*, 2006).

1.4.2 Myocardial infarction

Arterial occlusion, a complication of atherosclerosis, is the main underlying cause of myocardial infarction and stroke (Libby, 2002). Despite the successful introduction of statins and thrombolytic therapy in the early stages after infarction, heart disease and stroke remain by far the most common cause of death in developed countries.

Myocardial infarction occurs usually when perfusion of myocardium is reduced severely below its needs for an extended period, causing profound ischemia resulting in permanent loss of function through cell death (Nijmeijer *et al.*, 2001).

It is becoming more evident that necrosis, a rapidly occurring form of cell death that may trigger a significant inflammatory response, leads to a destruction of a large group of cells after myocardial ischemia and reperfusion (Zhao & Vinten-Johanson, 2002). However, the induction of apoptosis in myocardium, triggered during reperfusion may independently contribute to the extension of cell death in a dynamic manner. Although the process of necrosis and apoptosis may differ in a number of ways and may proceed down separate ways, a growing body of evidence suggests that there is overlap or cross-over (switch from apoptosis to necrosis) between these two types of cell death (Zhao & Vinten-Johanson, 2002).

An additional mediator of myocardial injury after an ischemic event appears to be inflammation. This inflammation has been shown to contribute to final infarction size and the outcome of the patient (Mullane & Smith, 1990; Pietela *et al.*, 1993; Entman *et al.*, 1991). Both complement and CRP have been suggested to contribute to ischemic myocardial injury.

1.4.2.1 CRP and Myocardial infarction

Ischemic infarction of myocardial tissue has long been known to be a potent stimulus for the acute phase response, in which a wide range of plasma proteins increase dramatically in concentration (Pepys & Hirschfield, 2003). CRP is of specific interest as its circulating concentration after acute myocardial infarction is always increased, starting within 4-6 hours of the onset of symptoms and reaching a peak after ~ 50 hours (Kuschner *et al.*, 1978; de Beer, 1982). The magnitude of this peak value reflects the extent of myocardial necrosis (deBeer *et al.*, 1982) and significantly predicts the outcome and survival both immediately and for months after the event (Ueda, 1996; Pieteila *et al.*, 1996). Furthermore, CRP has been shown to be deposited together with complement within infracted, but not normal myocardium of patients whom had died from acute myocardial infarction (Lagrand *et al.*, 1997). This finding was further supported by a recent immunohistochemical study that demonstrated the accumulation of CRP as well as CRP-complement complexes in human myocardium (Nijmeijer *et al.*, 2003). These findings strongly suggest that CRP activates complement during human myocardial infarction.

The relevance of these pathological findings is supported by *in vivo* animal studies (Griselli *et al.*, 1999; Gill *et al.*, 2004). The authors of these studies used a rat model to exploit the fact that rat CRP does not activate rat complement, whereas human CRP activates both rat and human complement (deBeer *et al.*, 1982). Griselli *et al.* (1999) demonstrated that injection of human CRP into these rats after ligation of the coronary artery enhanced infarct size by 40 %. This effect was completely abrogated by in vivo complement depletion in the rats using cobra venom factor. It is therefore likely that CRP-mediated complement activation contributes significantly to the extent of damage in acute myocardial infarction.

Similarly, human CRP injection into rat subjected to middle cerebral artery occlusion developed larger cerebral infarcts. However, in this study infarct size was not affected by systemic complement depletion with cobra venom factor. Thus, human CRP can contribute to ischemic tissue damage in the brain by a mechanism independent of complement.

Recently, a small molecule inhibitor 1, 6-bis (phochocholine)-hexane (bis(PC)-H) of CRP has been designed and used to investigate the role of CRP-induced complement activation in the pathogenesis of myocardial infarction (Pepys *et al.*, 2006). The authors demonstrate in a rat model of coronary-artery occlusion that the administration of the inhibitor completely attenuates the increase in infarct size produced by injection of human CRP. This effect is hypothesised to be due to the binding of the inhibitor to circulating CRP, which occludes the ligand binding B face of CRP. This prevents CRP from binding to exposed ligands in damaged myocardial cells, thereby abrogating human CRP-dependent complement activation, which may cause further tissue damage.

In summary, there is no compelling evidence that CRP contributes to the pathogenesis of atherosclerosis. In contrast, there is cumulating evidence that CRP exacerbates the tissue injury of ischemic necrosis in heart attacks by activating the complement system.

1.5 SAP: Its Role in Disease

Although the physiological role of SAP remains elusive, there has been much progress in understanding the role of SAP in the pathogenesis of amyloidosis (Tennent *et al.*, 1995; Botto *et al.*, 1997).

1.5.1 Amyloidosis

Amyloidosis is an acquired or hereditary disorder in which normally soluble proteins are deposited extracellularly in the tissues as abnormally insoluble fibrils (Pepys & Hawkins, 2003). These amyloid fibrils associate with heparin and dermatan sulphated glycosaminoglycans (GAG), proteoglycans and the non-fibrillar normal plasma glycoprotein, SAP, to form amyloid deposits. An accumulation of these amyloid deposits causes structural and functional disruption of tissue and ultimately leads to disease. Once considered a rare disease, it has become apparent that processes involved in amyloid formation are important to many different conditions, some of which are more common. To date about 23 different proteins are known to form amyloid fibrils *in vivo* and each of these proteins is associated with a clinically distinct condition (Table 1.1).

Systemic amyloidosis, where amyloid deposits may be present in the viscera, blood vessel walls and connective tissues, is rare but usually fatal (Pepys, 2006). The two most common forms of systemic amyloidosis are light chain (AL) amyloidosis, causing death in 1 in 1500 people in the UK and reactive amyloidosis due to chronic inflammatory diseases (Hirschfield, 2004). In addition, over one million chronic haemodialysis patients worldwide are at risk of developing β_2-microglobulin (β_2-m) amyloidosis as a complication.

However, there are also various forms of localised amyloidosis in which amyloid deposits are restricted to a specific foci or particular organ or tissue (Pepys, 2001). These amyloid deposits can be clinically silent through to causing major complications. The commonest form of local amyloidosis is caused by foci of otherwise benign monoclonal B cells and plasma cells producing monoclonal

immunoglobulin light chains that are deposited as amyloid, most frequently in the respiratory tract, urogenital tract and skin (Goodman *et al.*, 2005).

Table 1.1 Human amyloid fibril proteins and their precursors (from Merlini & Westermark, 2004)

Amyloid Protein	Precursor	Systemic (S) or localised (L)	Syndrome or involved tissues
AL	Immunoglobulin Light chain	S, L	primary Myeloma associated
AH	Immunolglobulin Heavy chain	S, L	primary Myeloma associated
ATTR	transthyretin	S	familial
		L?	Senile systemic tenosynovium
$A\beta_2$-m	β_2-microglobulin	S	hemodialysis
		L?	joints
AA	(apo) serum AA	S	secondary, reactive
AApoPI	apolipoprotein AI	S	familial
		L	aortic
AApoAII	apolipoprotein AII	S	familial
ALys	lysozyme	S	familial
AFib	fibrinogen a chain	S	familial
ACys	cystatin C	S	familial
ABri british	ABriPP	S	familial dementia,
AApoAIV	apolipoprotein AIV	S	senile
Aβ	Aβ protein Precursor (AβPP)	L	Alzheimer's disease, aging
APrP encephalo-	prion protein	L	spongioform pathies
ACal	(pro)calcitonin	L	C-cell thyroid tumors
AIAPP	islet amyloid poly-Peptide	L	islets of Langerhans insulinomas
AANF	atrial natriuretic factor	L	cardia atria
APro	prolactin	L	aging pituitary prolactinomas
AIns	insulin	L	iatrogenic
AMed	lactadherin	L	senile aortic, media
AKer	kerato-epithelin	L	cornea;familial
ALac	lactoferrin	L	corea; familial

In addition, there are important common diseases associated with local amyloid deposition such as Alzheimer's disease, the prion diseases and type 2 diabetes mellitus (Pepys, 2001). However, unlike systemic amyloidosis, in which the amyloid deposits unequivocally cause tissue damage and disease, it is not clear whether cerebral and islet amyloid deposits cause dementia and diabetes respectively, whether they exacerbate these conditions or are just clinically silent epiphenomena (Pepys, 2006).

Despite intensive research efforts, the mechanism by which amyloid deposits damage tissues and organs remains poorly understood. The initial observation that deposition of large amounts of amyloid fibrils is structurally disruptive and incompatible with normal function led to the view that amyloid deposits exert their pathological effects through their physiological presence. This is certainly true for pronounced deposits, which affect the function of the organ mechanically or influence the exchange of nutrients and other molecules between cells and blood stream. However, investigations of the amyloid deposits show a poor correlation between the amount of amyloid present at a particular site and the resultant organ dysfunction (Hawkins & Pepys, 1995). For instance, it has been observed that similar amount of cardiac amyloid deposits have significantly worse functional and prognostic impact in patients with light chain amyloidosis than in patients with transthyretin amyloidosis (Dubrey *et al.*, 1997). This observation suggests that additional factors, besides the amount of amyloid deposits, play an important role.

Recent *in vitro* studies with cultured cells and a variety of different amyloid-like fibrils indicate that amyloid fibrils and their smaller oligomeric aggregates are cytotoxic by inducing cell death (Lorenzo & Yankner, 1994, Simmons *et al.*, 1994; Janson *et al.*, 1999; Nilsberth *et al.*, 2001; Reixach *et al.*, 2004). Although apoptotic cell death induced by amyloid deposition would be compatible with the usual absence of any inflammatory response, direct evidence for this phenomenon to occur has not been shown *in vivo* yet.

1.5.1.1 Structure of Amyloid Fibrils

Despite the diversity of amino-acid sequence, size and tertiary folds among the amyloidogenic proteins known to form amyloid fibrils *in vivo*, all amyloid fibrils share the following tinctorial, morphological and structural characteristics: (1) They stain with Congo red dye and show green birefringence under cross-polarised light as shown in Figure 1.11 (Puchtler *et al.*, 1962). (2) They are uniform, straight unbranched fibrils, approximately 60-100 Å in diameter and of infinite length upon analysis by electron microscopy (Figure 1.12) (Shirahama & Cohen, 1967). (3) They exhibit a cross-β diffraction pattern by X-ray fibre diffraction that arises from the underlying repeating core structure that consists predominantly of β-sheet structure (Eanes & Glenner, 1968; Sunde *et al.*, 1997). This pattern has two characteristic reflections (Figure 1.13): a strong, sharp 4.7 Å meridional reflection, which is thought to arise from the hydrogen-bonding distance between β-strands in a β-sheet and a diffuse equatorial reflection around 10-12 Å, which likely corresponds to the varying distance between β-sheets (Sunde *et al.*, 1997). These three characteristics are now accepted diagnostic hallmarks of amyloid.

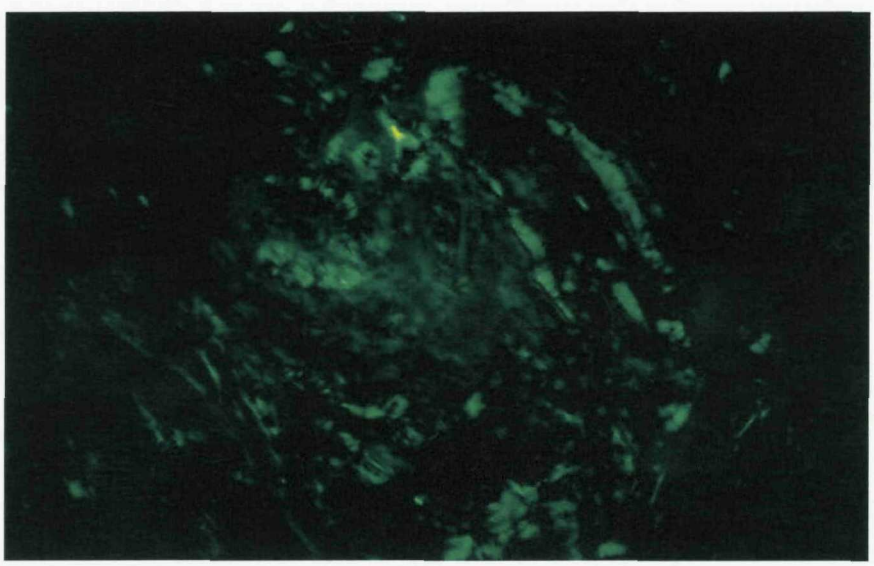

Figure 1.11 Amyloid demonstration apple-green birefringence with polarised light with Congo red dye (Figure taken from Thompson *et al.*, 2002)

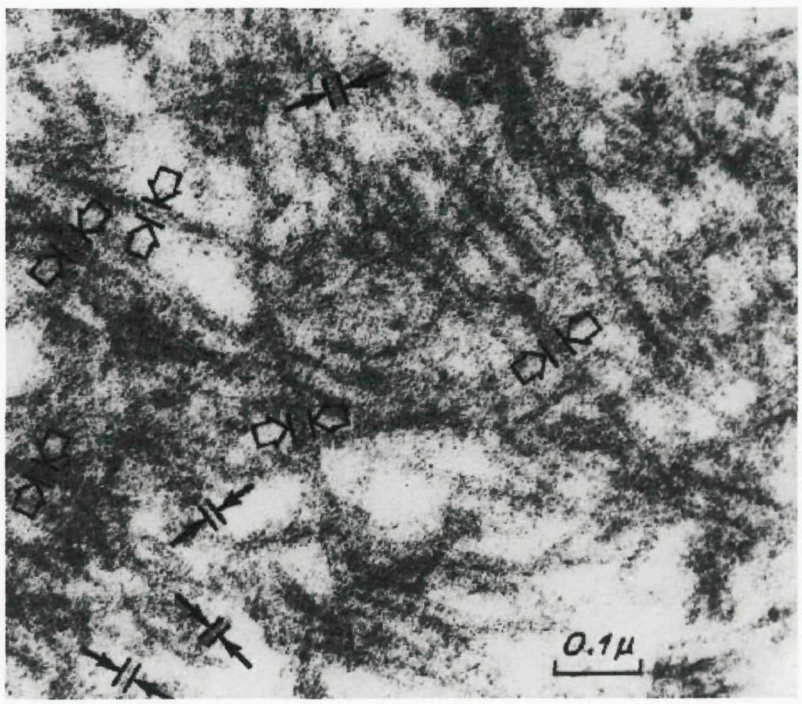

Figure 1.12 An electron micrograph of amyloid fibrils from a section of human amyloidotic spleen. The fibrils are arranged in randon array and are non-branching. The measurements of the width of individual fibrils show moderate variation, with the 100 Å width most common (dark arrows), but also 200-300 Å width observable (open arrows). (Figure taken from Shirahama & Cohen, 1967)

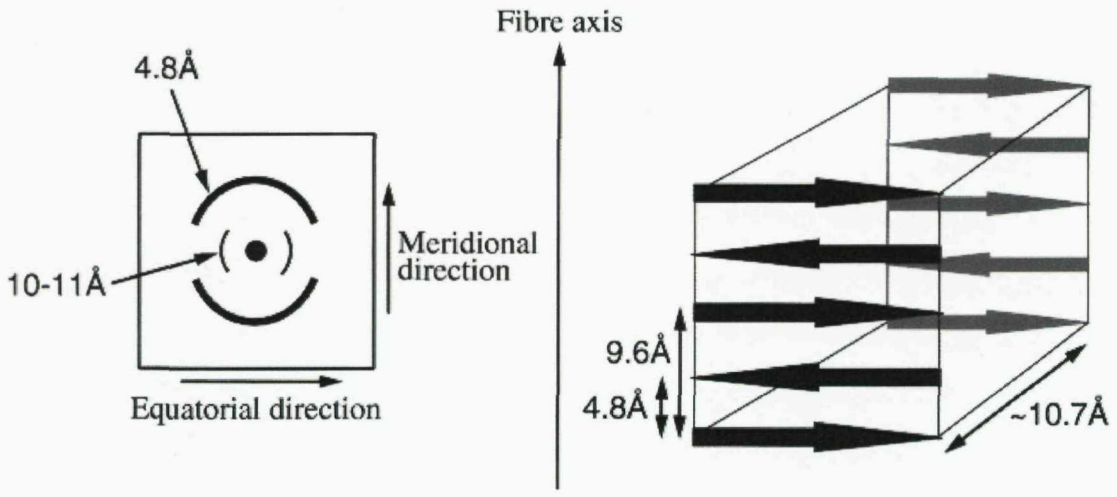

Figure 1.13 The characteristic cross-β spacing from X-ray fibre diffraction from amyloid fibrils and its interpretation. A) A schematic X-ray fibre diffraction pattern, showing the positions of the 4.8 Å meridional and the 10-11 Å equatorial reflections. B) The proposal for the arrangement of two parallel β-sheets. (Serpell *et al.*, 2000)

Although a high-resolution structure of an amyloid fibril has not yet been obtained, a number of three-dimensional models have been put forward to describe the structure of amyloid fibrils. One of the earliest models arose from the analysis of X-ray fibre diffraction patterns from *ex vivo* transthyretin (TTR) Met30 variant amyloid fibrils (Blake & Serpell, 1996). In this model, the TTR amyloid fibril consists of four protofilaments arranged around a hollow centre. Each protofilament is composed of four β-sheets of indefinite length running parallel to the axis of the fibre, with the constitutive β-strands positioned perpendicular to the fibre axis (Figure 1.14). Each β-strand is twisted by 15 ° with respect to its immediate neighbours, thereby generating a novel 115 Å β-helix. This novel helical structure of the protofilament enables the hydrogen bonding between β-strands to be extended over long distances of the amyloid fibril and has been proposed to explain the greater stability of amyloid fibrils (Sunde *et al.*, 1997).

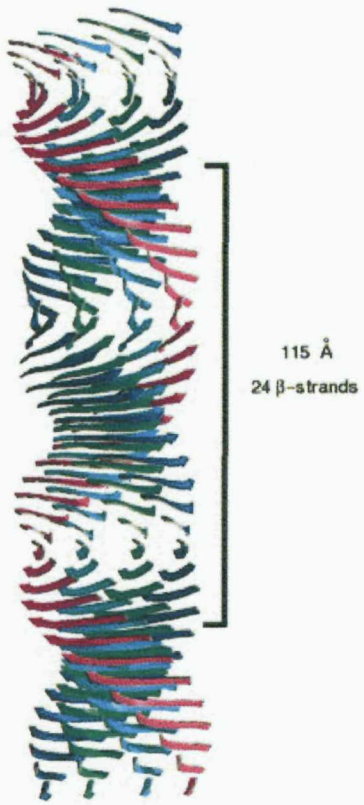

Figure 1.14 Molecular model of the common core protofilament structure of amyloid fibrils. Four β-sheets run parallel to the protofilament axis, with their constituent β-strands perpendicular to the fibril axis. Each β-strand is twisted by 15° with respect to its immediate neighbour, thereby generating a helical twist around a common axis that coincides with the axis of the protofilament. This helical twist generates a helical repeat of 115.5 Å containing 24 β-strands (Figure taken from Sunde *et al.*, 1997).

Although this model has been suggested to represent the core molecular structure of amyloid fibrils, recent data suggest that the arrangement and number of β-sheets in amyloid filaments can vary. For instance, it has been observed that the protofilament of the Aβ fibril formed from residues 34-42 of Aβ adopt an anti-parallel (Lansbury *et al.*, 1995; Balbach *et al.*, 2000; Petkova *et al.*, 2003) rather then a parallel β-sheet structure (Benzinger *et al.*, 1998; Antzutkin *et al.*, 2000; Balbach *et al.*, 2002). This suggests that both β-sheet arrangements are compatible with amyloid fibril structure. In addition, it has been observed that amyloid protofilaments formed from some peptides (Sup35 and HET-s prion) are composed of two β-sheets (Nelson *et al.*, 2005; Ritter *et al.*, 2005) rather then the four β-sheets proposed for the transthyretin amyloid protofilament.

It is now evident that there are also other differences between amyloid fibrils composed of different proteins. These differences appear to be in the number and size of these constituent protofilaments. For example, Aβ, serum amyloid A protein (SAA) and immunoglobulin light chain fibrils have been reported to be composed of five or six protofilaments arranged around a hollow centre as shown in Figure 1.15 (Shirahama & Cohen, 1967; Kirschner *et al.*, 1987; Fraser *et al.*, 1991).

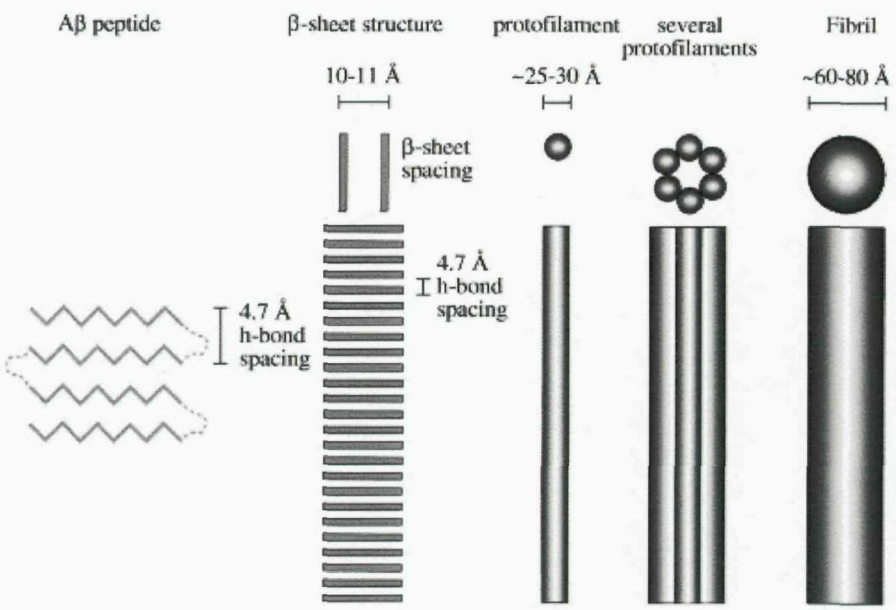

Figure 1.15 Schematic diagram of the hierarchical assembly of structures making up an amyloid fibril from continuous hydrogen bonded β-sheet structure within a protofilament to the organisation of the protofilaments. (Figure taken from Sunde *et al.*, 1997)

1.5.1.2 Amyloid Fibril formation

The mechanism by which proteins form amyloid fibrils (amyloid fibrillogenesis) remains still unclear, however an insight has been provided by studies with proteins known to form amyloid fibrils. These amyloidogenic human proteins have been shown to have unrelated sequences and a wide range of native folds, yet demonstrate the same cross-β structure. For example, transthyretin (Blake *et al.*, 1978; Terry *et al.*, 1993) and β_2-m (Becker & Reeke, 1985) have mainly β-sheet structures, while the amyloidogenic variants of lysozyme (Pepys *et al.*, 1993; Booth *et al.*, 1997) and the prion protein (Riek *et al.*, 1996) have extensive α-helical structures. This suggests that these proteins require a structural conversion when they form amyloid fibrils.

Such a structural conversion has been demonstrated for two amyloidogenic human lysozyme variants and led to the proposal that transient populations of amyloidogenic proteins in an unfolded, molten-globule state are an important feature of the conversion from a soluble to the fibrillar form (Booth *et al.*, 1997). In this proposed mechanism (Figure 1.16), specific amino acid mutations destabilise the native protein and cause partial unfolding of the protein. The partially unfolded, molten globule-like form of the protein self-associates through the exposed regions to initiate fibril formation (Booth *et al.*, 1997). These then act as a template (seed) for further deposition of protein and development of the stable, mainly β-sheet, core structure of the amyloid fibril.

A similar mechanism may also apply to some TTR variants, where mutations destabilise the quaternary structure of the native tetrameric protein (Hammarstrom *et al.*, 2002). Thus for these two proteins, the destabilisation due to the alteration in the amino acid sequence causes an increase in their amyloid propensity. However, changes in the local environment or local concentration of wild-type protein can also result in the onset of amyloid disease. For example, β_2-m and SAA form amyloid only at supra-physiological concentration (Verdone *et al.*, 2002).

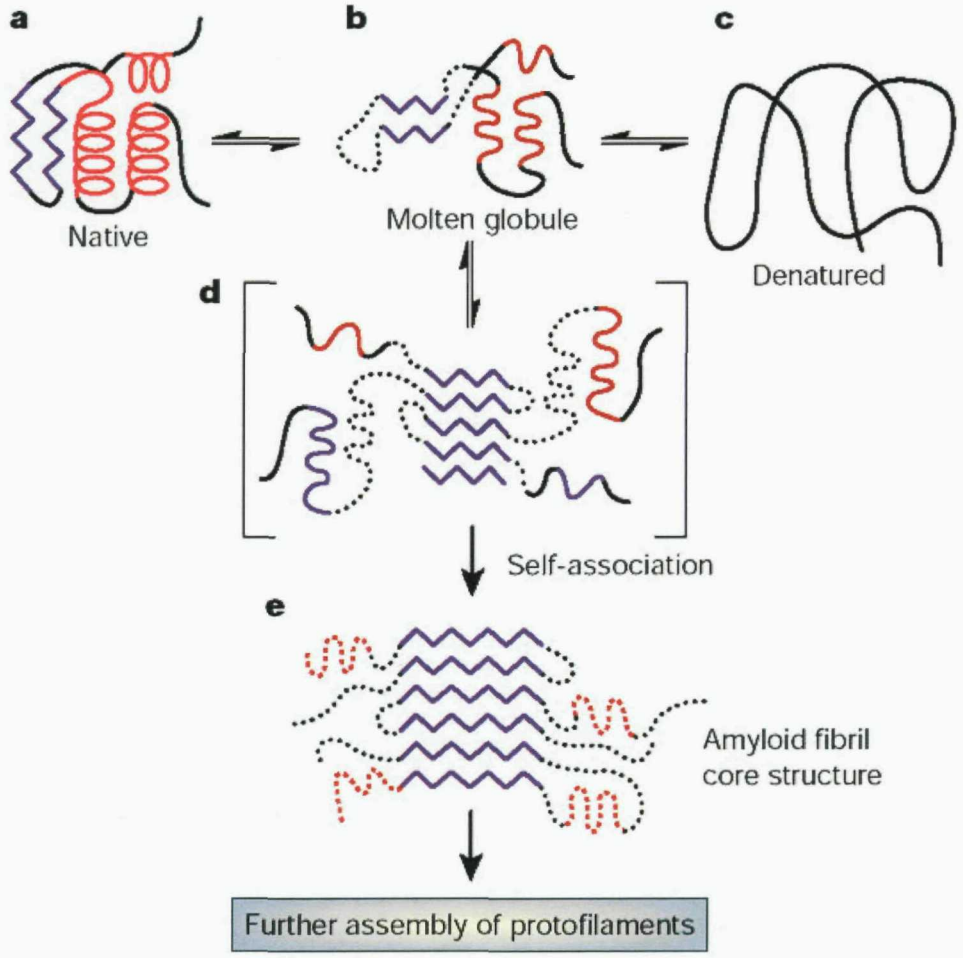

Figure 1.16 The proposed mechanism for lysozyme amyloid fibril formation. A partly folded, molten globule-like form of the protein (b), distinct from the native (a) and denatured (c) states of the protein, self-associates through the β-domain (d) to initiate fibril formation. This provides the template for the further deposition of protein and for the stable, mainly β-sheet, core structure of the protofilaments within the amyloid fibril (e). Purple, β-sheet structure; red, helical structure; dotted lines, undefined structure (Figure taken from Selkoe, 2003)

Amyloid fibril formation has been shown to proceed through a nucleated growth process analogous to crystal growth (Jarrett & Lansbury, 1993; Harper & Lansbury, 1997; Morozova-Roche *et al.*, 2000). This process includes a lag phase, which is the time required for a nucleus (a small number of aggregated molecules) to form; once a nucleus has formed, a fibril growth phase is initiated and proceeds rapidly by further association of either monomers or oligomers with the nucleus.

In addition, a number of studies have demonstrated that proteins that are not amyloidogenic *in vivo* can undergo fibril formation under partially denaturing conditions such as low pH and elevated temperatures (Chiti *et al.*, 1999; Schuler *et al.*, 1999; Damaschun *et al.*, 1999). This led to the idea that the ability to form amyloid fibrils is a generic property of peptides and proteins (Dobson, 1999). The structure of normal globular proteins is dictated primarily by side chain interactions. This contrasts with the core structure of the fibrils, which has been demonstrated to be stabilised by hydrogen bond interactions between the polypeptide main chain (Sunde & Blake, 1997). As the polypeptide main chain is common to all peptides and proteins, this observation explains why fibrils formed from polypeptides of different amino acids sequence are similar in appearance (Dobson, 2004).

It has been suggested that denaturing conditions destabilise the side chain interactions in globular proteins, causing the structures to unfold. These unfolded structures may then self-associate and initiate fibril formation. However, it is not known why only about 23 diverse proteins actually produce amyloid deposits *in vivo*.

1.5.2 SAP and Amyloidosis

SAP, the circulating equivalent of amyloid P, was first discovered immunochemically by Cathcart *et al.* (1965) as a universal constituent of tissue amyloid deposits. Shortly later, electron microscopic studies of amyloid extracts revealed the characteristic pentagonal structure of SAP (Figure 1.17). However, this structure was interpreted as the subunit of aggregated SAP rods, which were believed to be the bulk of amyloid deposits (Bladen *et al.*, 1966). Subsequently, it was shown that amyloid deposits are composed of amyloid fibrils, derived from a range of different precursor proteins in the different forms of the disease, whilst SAP is a minor component associated with the fibrils by virtue of its capacity for calcium-dependent ligand binding to specific determinants shared by all types of amyloid fibrils (Glenner *et al.*, 1980).

It is now well established that circulating SAP binds in a calcium-dependent fashion to all types of amyloid fibril *in vivo* and *in vitro* and that this is the mechanism of accumulation of SAP in amyloid deposits (Pepys *et al.*, 1977; Baltz *et al.*, 1986; Hawkins *et al.*, 1988; 1990; 1995).

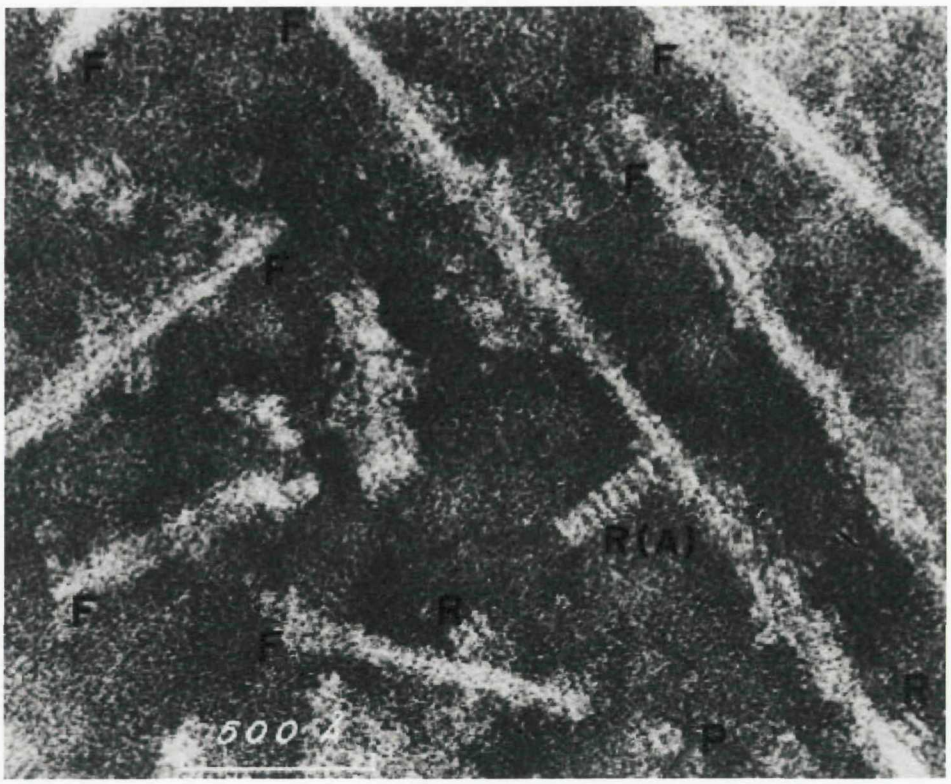

Figure 1.17 An electron micrograph showing amyloid fibrils and the pentagonal structure of SAP (Figure taken from Bladen et al., 1966).

The first suggestion that deposition of SAP in amyloid might be of pathogenic significance, rather then just an epiphenomenon, came from a study which compared mouse strains of varying resistance to experimental, casein induced AA amyloidosis (Baltz *et al.*, 1980). The authors of this study observed that circulating SAP levels correlated with experimental murine AA amyloidosis deposition. This observation was subsequently reconfirmed in the Syrian hamster, in which expression of SAP is under female sex hormone control and females with very high SAP values get AA amyloidosis much more readily than males with low SAP values (Coe & Ross, 1985; 1990; Snel *et al.*, 1989).

Following the characterisation of MOβDG as a low molecular weight ligand for SAP, a number of studies proposed that SAP might contribute to the stability and persistence of amyloid deposits *in vivo* by masking the abnormal fibril structure from recognition by the molecular and cellular mechanisms that should contribute to their clearance and removal (Hind *et al.*, 1984; Pepys *et al.*, 1988). This concept was supported by *in vitro* studies, which showed that binding of SAP to amyloid fibrils protects them from degradation by proteolytic cells and proteolytic enzymes (Tennent *et al.*, 1995).

Prompted by these findings, SAP knockout mice were created by targeted depletion of the SAP gene. These SAP-deficient mice were shown to have delayed and reduced induction of experimental reactive AA amyloidosis (Botto *et al.*, 1997). This observation was confirmed independently by another group (Togashi *et al.*, 1997). It therefore appears that SAP contributes to the pathogenesis of amyloidosis *in vivo*.

In the hope to slow down new amyloid deposition and/or reduce the stability of amyloid deposits, a small molecule inhibitor (R-1-[6-R-2-carboxy-pyrrolidin-1-yl]-6-oxo-hexanoyl]pyrrolindine-2-carboxylic acid) (CPHPC) of SAP was designed and used to investigate the role of SAP in amyloidosis (Pepys *et al.* 2002). The authors of this study demonstrate in a transgenic mouse model expressing the human SAP gene that the administration of this inhibitor induces rapid clearance of circulating SAP, reduces the amount of amyloid associated SAP and lowers the amyloid load in animal where systemic amyloidosis has been induced. They hypothesise that the mechanism by which the inhibitor achieves these effects is due to the dimerisation of human SAP molecules by the inhibitor. This dimerisation not only occludes the binding face of the SAP molecule, but also triggers the clearance of the complexed protein by the liver.

In summary, there is compelling evidence that SAP significantly contributes to the pathogenesis of amyloidosis *in vivo*.

1.6 Structure of Pentraxins

For many years the only structural information about the human pentraxins came from negative-staining electron microscopic studies. These studies revealed that both proteins appeared on micrographs (Figure 1.18) as disc-like objects composed of five subunits arranged with cyclic pentameric symmetry (Pinteric *et al.*, 1976; Pepys *et al.*, 1977; Pepys & Baltz, 1983). Independently, Osmand *et al.* (1977) found that these two proteins had homologous N-terminal amino acid sequences and coined the term pentraxin, derived from the Greek words penta (five) and ragos (berries), for this newly recognised family of plasma proteins.

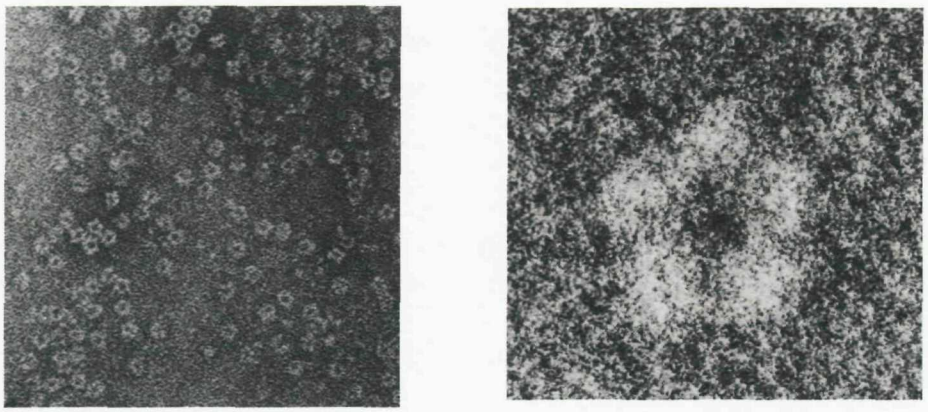

Figure 1.18 An electron micrograph of CRP (Osmand, 1977). A negatively stained electron micrograph (left) showing the typical pentameric disc-like structure face-on and side-on (Magnification x 285,000). Five subunits (right) resolved at a magnification of x 3,000,000.

The determination of the three-dimensional structure of these proteins by X-ray crystallographic studies proved more difficult due to problems in obtaining suitable crystals and structure solution (Shrive *et al.*, 1996). Crystals of human CRP were first reported in 1947 by McCarty. However, it was not until the early 1990's that X-ray diffraction data was collected on crystals of human CRP (De Lucas *et al.*, 1987; Myles *et al.*, 1990) and rat CRP (Hopkins *et al.*, 1994).

The data obtained by Myles *et al.* (1990) was from calcium-depleted human CRP crystals. These crystals were twinned and a structural solution could not be found. Crystals of human SAP were first reported in 1972 by Haupt & Heimburger. However, they named and characterised this protein as a metal-binding 9.5S-α_1-

glycoprotein (CM-Protein III). Later, Wood *et al.* (1988) reported the crystallisation and collection of X-ray diffraction data of a pentameric form of human SAP. This pentameric form contradicted previous X-ray and neutron scattering studies (Perkins & Pepys, 1986), which indicated that under physiological conditions human SAP exists as a decamer with two pentameric discs interacting face to face.

The three-dimensional structure of the human SAP pentamer was finally solved in 1994 by Emsley *et al.* using multiple isomorphous replacement (MIR). This study has provided great insights into the general structure of the protein as well as a detailed description of ligand binding. Subsequently co-crystallisations with other low molecular weight ligands have been reported: MOβDG (Emsley *et al.*, 1994; Thompson *et al.*, 2002), dAMP (Hohenester *et al.*, 1997), PE (Emsley *et al.*, 1994; Pye, 1997), GABA (Pye, 1999), N-Acetyl-D-Proline (Purvis, 2002), N-Acetyl-L-proline and CPHPC (Pepys *et al.*, 2002; Purvis, 2002).

As a result of the determination of the X-ray crystal structure of human SAP (Emsley et al., 1994), the structure of the calcium-bound human CRP could be solved by molecular replacement (Shrive *et al.*, 1996). Shortly later, Thompson *et al.* (1999) solved a higher resolution structure of human CRP in complex with PC.

The three-dimensional structure of the calcium-depleted human CRP was eventually solved by Ramadan *et al.* (2002) using the calcium-bound human CRP structure (Shrive *et al.*, 1996) as a molecular replacement model. The structure reveals a conformational change in a loop involved in calcium binding (residues 138-150).

These structural studies of human CRP have provided a detailed description of the three-dimensional structure of CRP as well as great insight into the basis of calcium and PC binding (Shrive *et al.*, 1996; Thompson *et al.*, 1999). In addition, these structures enabled the design of the potent inhibitor (1, 6-bis (phochocholine-hexane) (bis (PC)-H) of CRP binding (Pepys *et al.*, 2006). This palindromic inhibitor was co-crystallised with human CRP and the crystal structure revealed

multivalent binding of five palindromic drug molecules by two CRP pentamers apposed face to face.

The crystallisation and structure solution of SAP from other species also proved difficult. Myles *et al.* (1990) reported the first crystallisation and collection of X-ray diffraction data of a Limulus pentraxin. These crystals were thought to be Limulus CRP. However, the structure solution of this X-ray diffraction revealed that the crystals themselves were of Limulus SAP data (Shrive *et al.*, 1999). This surprising finding was attributed to the isolations of Limulus pentraxins containing Limulus SAP rather than Limulus CRP.

1.6.1 Pentamer Structure

A single molecule of human CRP and SAP consists of five identical subunits (protomers) assembled into a pentameric structure (Figure 1.19). This pentameric structure is approximately 100 Å in diameter and 35 Å deep, and shows a large 20 Å pore through the centre. In addition, to all five protomers being structurally identical to each other, they also show the same orientation within the pentamer. This creates two distinct faces.

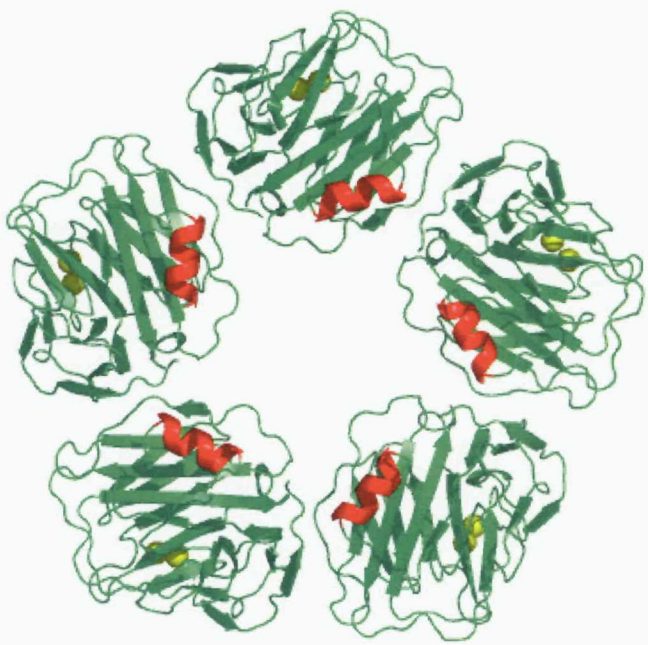

Figure 1.19 The pentameric structure (Figure produced from 1B09.pdb using Pymol).

The general arrangement of the pentameric structures of human CRP and SAP appears at first sight to be identical. However, Thompson *et al.* (1999) showed that with respect to the five fold axis, the protomers forming the human CRP pentamer are rotated towards this axis when compared to those of human SAP. This rotational shift is apparent when the pentamers from both molecules are superimposed and is thought to be responsible for some of the distinct binding properties exhibited by both proteins.

In contrast to the human pentraxins, the limulus pentraxins have been reported to be composed of a different number of protomers. Limulus CRP is believed to be a doubly stacked hexameric ring structure formed from 12 subunits (Tennent *et al.*, 1993), while Limulus SAP (Figure 1.20) is thought to be a doubly stacked octameric ring structure formed from 16 subunits (Shrive *et al.*, 1999). In addition, the relative orientation within the aggregate differs from that in the mammalian pentameric structures, yet both display cyclic circular assemblies (Shrive *et al.*, 1999). Thus, the number and relative orientation of the protomers can differ between species.

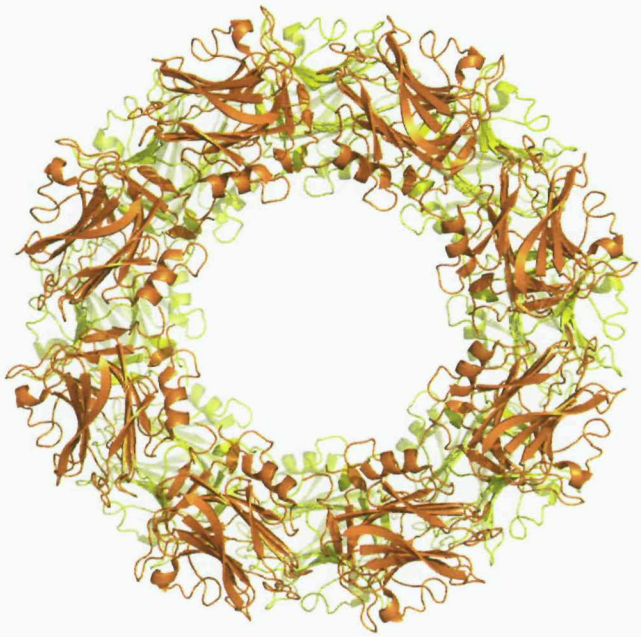

Figure 1.20 The doubly stacked octameric structure of Limulus SAP. Ribbon diagram of Limulus SAP viewed down the molecular 8-fold axis (generated using Pymol from 1QTJ).

1.6.2 Protomer structure

The human CRP and SAP protomers have a diameter of approximately 36 Å and are composed of 206 and 204 amino acid residues respectively. In both proteins the polypeptide chain in each protomer is folded into two anti-parallel β-sheets with a flattened jelly roll topology similar to that of lectins such as concanavalin A (Emsley *et al.*, 1994; Shrive *et al.*, 1996; Thompson *et al.*, 1999). In addition to these β-strands, there is a long α-helix, which lies folded against one of these β-sheets. Situated underneath this α-helix, a disulphide bond is formed between residues Cys36-Cys97 in CRP and Cys36-Cys95 in SAP. This face of the protomer is termed the A or affector face (Figure 1.21), while the opposing face, which displays concave morphology, is termed the B face or binding face (Figure 1.22). This face is formed from the exposed surface of the second β-sheet and contains a double calcium binding site.

This striking similarity between human CRP and SAP protomers is also apparent when superimposing the CRP protomer onto that of the SAP protomer. This superimposition calculation reveals a C_α rms fit of 1.3 Å, which improves to 0.83 Å when three divergent loops (residues 43-48, 68-72, 85-91) are omitted from the calculation (Thompson *et al.*, 1999). These three loops are responsible for the main structural differences between the two protomers and are located in the same region of the protomer, extending into the central pore of the pentamer. This difference is probably due to the insertion of two additional residues (Ser45 and Thr46) into the amino acid sequence of human CRP. These two additional residues form part of a 3_{10} helical turn, which is not present in human SAP. This confirmation in the Leu43-Gly48 loop between strands C and D, together with significant sequence changes in this structural region, imposes severe spatial restrictions and results in the observed displacement of these loop regions (Shrive *et al.*, 1996). As a consequence of this displacement, the protomers of human CRP are all rotated by 22° towards the five-fold axis such that the A face helices are 5 Å closer to the axis while the B face calcium sites are moved away by an equivalent amount (Thompson *et al.*, 1999).

Figure1.21 The A face. The CRP (top) and SAP (bottom) protomer viewed from the affector face. The α-helix is shown in light brown and the β-strands are represented as red and green arrows respectively (Figures generated in Pymol).

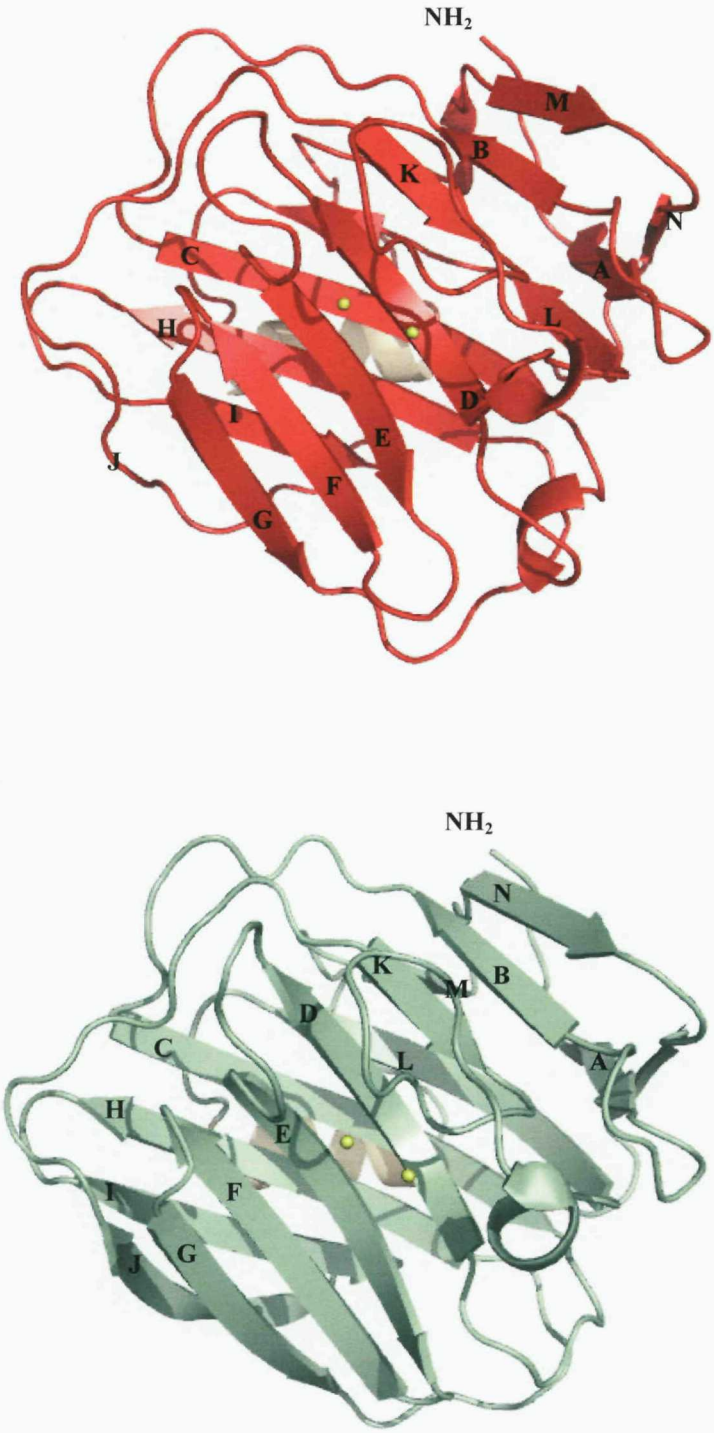

Figure 1.22 The B face. The CRP (top) and SAP (bottom) protomer viewed from the calcium binding site. The β-strands, labelled from A to O from the N- to C-terminus, are arranged in two antiparallel sheets. The calcium ions are represented as yellow spheres.

Another structural difference between the human CRP and SAP protomer is a marked furrow on the A face of the CRP protomer, which is opposite to the calcium-binding site. This furrow starts in a region of positive charge on the surface of the protomer and follows the curvature of the protomer towards the central pore of the pentamer and ends in a region of negative charge half way down the pore (Thompson *et al.*, 1999). The dimensions of this furrow are 24 Å long, 7.5 Å deep and 12.4 Å wide.

The appearance of this furrow is considerably accentuated in human CRP by substitution of some smaller side chains, by reorientation of others and by differences in the pentamer organisation. In human SAP, the residues Tyr160 and Arg38 protrude from what would be the floor of this furrow, while Pro179 and the side chains of Asn186 and other residues contribute to a considerable narrowing to such an extent that the furrow is barely recognisable on the surface of the SAP protomer (Shrive *et al.*, 1996).

Another striking difference between the human CRP and SAP protomers is the presence of a glycosylation site at Asn32 in SAP to which a complex N-linked oligosaccharide chain is attached. This feature is not observed in human CRP. However, interestingly, rat CRP has been shown to have a glycosylation site at Asn128 to which a disialylated biantennary oligosaccharide chain is attached (Sambasivam *et al.*, 1993). In addition, Limulus CRP has also been described as a glycoprotein containing a series of biantennary oligomannose structures (Amatayakul-Chantler *et al.*, 1990). The implications of these changes in these two glycoproteins remain to be determined.

1.6.3 Calcium binding

The calcium binding sites of human CRP and SAP are formed largely by side-chains of polar residues coming from loops located on the concave B face of each of the five protomers. Each calcium binding site contains two calcium ions, which are bound approximately 4 Å apart (Thompson *et al.*, 1999). Calcium ion I in CRP is co-ordinated by the side chains of Asp60, Asn61, Glu138, Asp140 and the main chain carbonyl oxygen of Gln139, giving a total of five coordinating ligands, while

calcium ion II is co-ordinated by Glu138, Asp140, Glu147 and Gln150 giving a total of four coordinating ligands (Thompson *et al.*, 1999) (Figure 1.23). These two calcium ions appear to be bound with equal affinity (Kinoshita *et al.*, 1989).

The equivalent calcium ion I in SAP is coordinated by the side chains of Asp58, Asn59, Glu136, Asp138 and the main chain carbonyl of Gln137. An acetate ion provides the seventh ligand to produce a pentagonal bipyramidal arrangement. A second, less tightly bound calcium ion II is coordinated by the side chains of Glu136, Asp138 and Gln148 as well as the acetate ion and two water molecules (Figure 1.23). This second site is more open due to fewer coordinating groups and has been shown to release its calcium ion easily when washing crystals in calcium-free buffers. This suggests that metals larger than calcium, such as copper or zinc might occupy this site.

The calcium ions in human CRP and SAP appear to be important for the stability of these proteins. The presence of calcium ions in human CRP protects the protein from denaturation induced by high temperatures (Heaton *et al.*, 1999) and by high concentrations of urea (Potempa *et al.*, 1983). However, in the absence of both calcium ions in human CRP, residues 140-150 form a large loop away from the body of the protein (Shrive *et al.*, 1996), exposing an otherwise hidden site of proteolysis. This hidden site was shown to be cleaved by the proteases Nagarse and Pronase, resulting in disruption of the two high-affinity calcium-binding sites (Kinoshita *et al.*, 1989). Similarly, the presence of calcium in human SAP protects the protein from cleavage by chymotrypsin, trypsin, pronase and nagarse (Kinoshita *et al.*, 1992). In the absence of bound metals, SAP is destabilised and readily cleaved at the 144-145 bond, suggesting that the loop carrying these residues is more accessible (Kinoshita *et al.*, 1992).

Residues that provide ligands to the calcium ions are conserved in all SAPs, but although Asp58 is present in hamster SAP, human CRP and Limulus CRP, it varies in other CRPs. Nevertheless, the general arrangement of the site is probably retained.

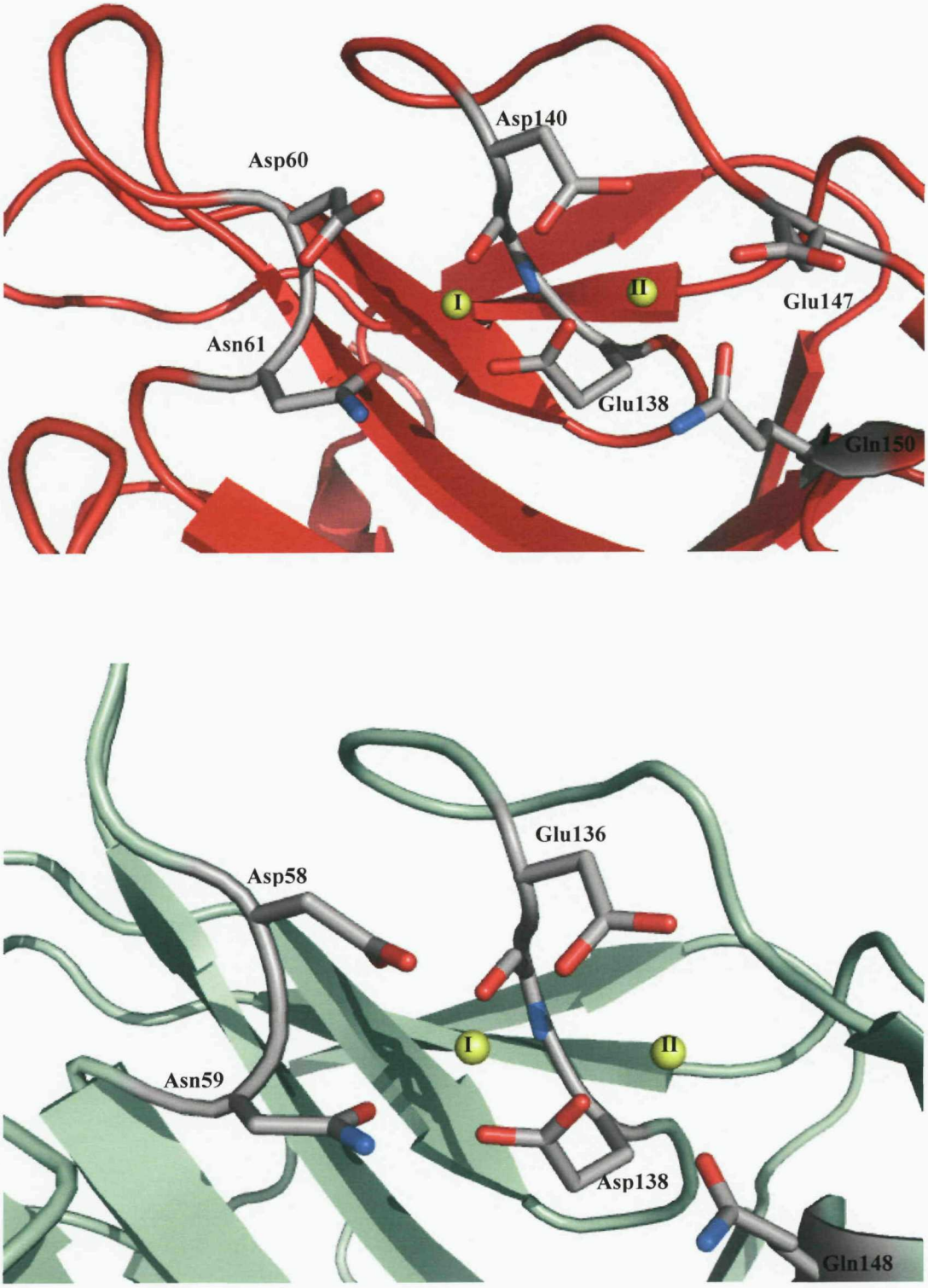

Figure 1.23 The calcium binding site of CRP (top) and SAP (bottom). The two calcium ions (shown as yellow spheres) receive ligands from surrounding protein residues (shown as grey stick models).

1.6.4 Ligand Binding to CRP

1.6.4.1 The Phosphocholine Binding Site

Although PC was described in the 1930s as the principal ligand of CRP, the localisation of the PC binding site was prohibited by the lack of crystallographic data for many years. However, in 1983 Roux *et al.* located the PC binding sites on CRP by immunoelectron microscopy using an anti-PC binding site monoclonal antibody. This antibody binds at or near the PC binding site in the presence of calcium and revealed that the PC binding sites on all CRP protomers are located on one face of the molecule.

Further insight into the PC binding site was gained in 1992 from a site-directed mutagenesis study by Agrawal *et al.* This study demonstrated that the residues Lys57, Arg58 and Trp67 contribute to the structure of the PC binding sites of human CRP. Speculations concerning the PC binding site followed, and centred on whether PC binding is mediated directly by a phosphate-calcium interaction or whether calcium had more of an indirect role as an allosteric effector.

The subsequent elucidation of the crystal structure of human CRP (Shrive *et al.*, 1996) supported the former idea that PC binding is mediated through phosphate binding at the calcium site and a hydrophobic pocket formed by Phe66, Leu64 and Thr76. In addition, they demonstrated that the side chains of Ser68, Ser74 and Glu81 are positioned at the opposite end of this hydrophobic pocket to the calcium ions and a reorientation of the Glu81 side chain would optimise interaction with the choline nitrogen.

Shortly later, the crystal structure of human CRP in complex with PC was reported by Thompson *et al.* (1999). This structure confirmed both the location and mode of PC binding to the B face of the protomer. The two oxygens of the phosphate group of PC interact directly with the two calcium ions, while the remaining third phosphate oxygen is oriented away from the binding site (Thompson *et al.*, 1999). The positively charged quaternary nitrogen of choline interacts with the side chain

of Glu81, while the three choline methyl groups interact with the hydrophobic Phe66.

Further site-directed mutagenesis studies have confirmed the importance of these residues at the PC binding site of CRP. For instance, Agrawal *et al.* (2002) demonstrated that the mutation of the residues Phe66 and Glu81 abolished human CRP binding to PC. This observation was supported by Black *et al.* (2003). The author of this study generated transgenic mice, which expressed a variant of rabbit CRP (F66Y/E81K). This rabbit CRP was demonstrated to dramatically reduce binding of PC. Thus, these observations indicate that these two residues are key determinants in PC binding to CRP.

Interestingly, Phe66 is conserved in human, mouse, rabbit, rat, guinea pig and hamster CRP, while human, mouse, rat, guinea pig and hamster SAP all have Tyr at this position. Similarly, Glu81 is also conserved in CRPs, while being replaced by Lys in SAPs (Gly in the hamster). These substitutions together with various other main chain alterations alter the size and geometry of the hydrophobic pocket and may explain the observed differences in ligand binding specificity and affinity of these proteins for PC and PE.

Unlike human CRP, which is able to bind both PC and PE albeit with lower affinity, human SAP binds to PE but not to PC. The substitution of the residues Tyr66 and Tyr76 in SAP to the residues Phe66 and Thr76 in CRP, coupled with various main chain alterations creates a significantly large hydrophobic pocket in CRP, which as a consequence can accommodate the methyl groups attached to the quaternary nitrogen of PC. In addition, substitution of the residue Lys79 in SAP for the residue Glu81 in CRP favours the interaction with the positively charged quaternary nitrogen of PC. Such an interaction would be much less favourable for Lys79.

However, pentraxins from some species display hybrid binding specificity and bind to both PC and PE (Schwalbe *et al.*, 1992). In particular, hamster SAP and rat CRP showed equal affinity for PC and PE. Interestingly, Tyr74 which would obstruct PC binding by human SAP is retained in hamster SAP, while Glu81 is replaced by

Gly. This substitution may provide enough space and flexibility in the main chain to allow repositioning of the Tyr74 to remove steric limitation on PC binding and may be positioned in such an orientation to allow van der Waals contacts with the PC molecule towards Glu66 (Thompson *et al.*, 1999). Rat CRP does not show any significant substitutions apart from Thr76, which is replaced by Ala.

1.6.4.2 The C1q Binding Site

The discovery that CRP activates the classical pathway of the complement system by binding to C1q led to numerous mutagenesis studies attempting to define the topology and structure of the C1q binding site on CRP. The first study by Agrawal *et al.* (1994) reported that the negatively-charged residue Asp112 of CRP plays a major role in the formation of the C1q binding site as its substitution with Ala resulted in a reduced avidity of ligand-bound CRP to C1q and diminished complement-activating ability. In addition, they demonstrated that the positively charged Lys114 is also implicated in the interaction as its substitution with Ala resulted in significant increased C1q binding and complement activation. Interestingly, a Lys residue is found at that position in all mammalian pentraxins apart from human SAP, which has a Thr at that position.

The subsequent elucidation of the three-dimensional structure of human CRP (Shrive *et al.*, 1996) demonstrated that Asp112 is part of a marked furrow that extends from about the centre of each protomer to its edge at the central pore of the CRP pentamer. This furrow is located on the face of the pentamer opposite the phosphocholine binding sites. It is deep and narrow at its origin, but it becomes wider and shallower towards the pentamer pore. The side walls of this furrow are constructed from Ser5, Arg6, Gln203, Pro206, Trp187, Arg188, Asn160, Gly177, Leu176, Tyr175 and His95, while the bottom is lined by Asn158, His38, Leu37, Val94 and Asp112 (Thompson *et al.*, 1999) (Figure 1.24). The localisation of Asp112 within the relatively open end of this furrow toward the centre of the pentamer led to the proposal that this region of the furrow may be involved in C1q binding.

Shortly later, a site-directed mutagenesis study investigating the residues participating in the formation of this furrow provided further support for this proposal. This study demonstrates that Asp112 and Tyr175 are important contact residues for C1q binding (Agrawal *et al.*, 2001). In addition, Glu88 was shown to influence the conformational change in C1q necessary for complement activation, while Asn158 and His38 were proposed to contribute to the correct geometry of the binding site.

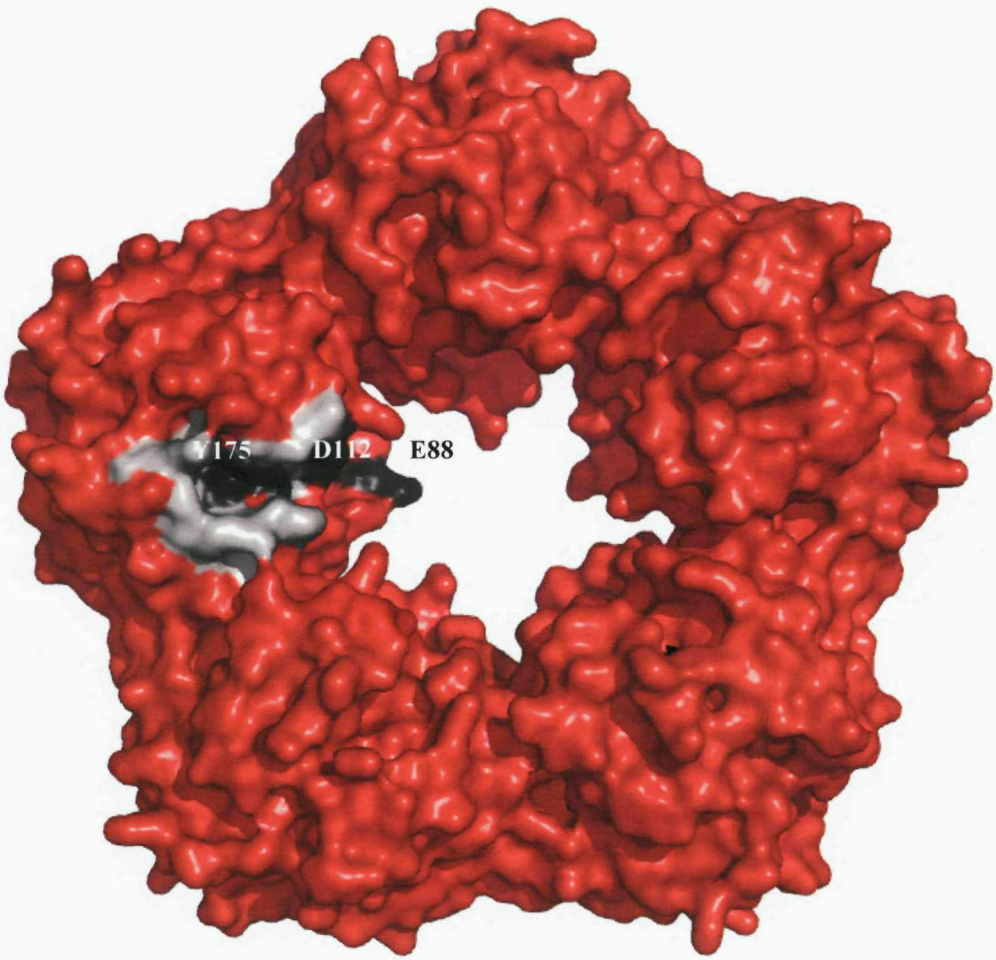

Figure 1.24 The effector face of CRP. Surface representation of the effector face of the CRP pentamer showing residues in the furrow region (grey = residues lining the furrow; black = labelled residues involved in the CRP-C1q interaction). The calcium and PC binding sites are located on the opposite pentameric face.

These consistent observations, together with the crystal structure of CRP led to the hypothesis that the shallow end of this furrow on CRP, and part of an α-helix (residues 169-176) at the C-terminus of CRP are the C1q-binding site on the CRP protomer.

Due to the lack of the three-dimensional structure of the CRP-C1q complex, the exact stoichiometry of CRP-C1q binding remains unclear. However, on the basis of the structural information available on the relative sizes of CRP (102 Å) and the C1q globular head group (50 Å) a plausible model of the interaction has been proposed. In this model only a single globular C1q head from a C1q molecule would bind to a CRP pentamer (Agrawal *et al.*, 2001). Consequently, more then one CRP pentamer in close proximity to each other would be necessary for complement activation, which is an observed requirement for complement activation in vitro.

It is not clear, however, whether there is more than one C1q binding site per CRP pentamer (Agrawal *et al.*, 2001). The C_α of the five Trp175 of the pentamer are positioned on a circle of 38 Å diameter, whilst the C_α of the five Asp112 are arranged in a similar manner (Agrawal *et al.*, 2001). This arrangement suggests that there are five possible C1q binding sites per pentamer. However, it appears that only one of these sites, possibly formed by two adjacent protomers is able to engage (Agrawal *et al.*, 2001).

Thus, an array of CRP molecules bound flat on the surface of a pathogen or damaged cell via PC would present a wide array of possible C1q binding site locations and orientations (Agrawal *et al.*, 2001)(Figure 1.25). This would allow binding of multiple C1q globular heads to multiple pentamers on a one to one basis, without a significant structural rearrangement in either molecule (Agrawal *et al.*, 2001).

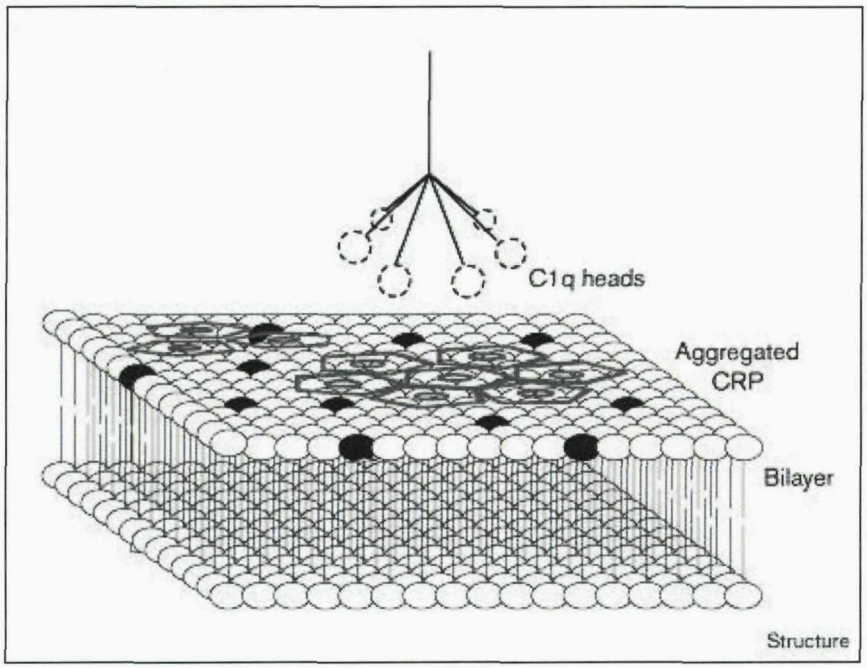

Figure 1.25 A model of C1q binding to CRP on the outer leaflet of a lipid layer (Thompson *et al.*, 1999). This results in the activation of the classical complement pathway.

This model of the CRP-C1q interaction was verified and further defined by molecular modelling studies following the determination of the crystal structure of the C1q globular head (Garboriaud *et al.*, 2003). These studies have revealed that the top of the C1q head structure, predominantly basic, can be accommodated by the negatively charged central pore of the CRP pentamer. In this configuration, there is a striking shape complementarity between CRP and C1q. In addition, the residues Asp112 and Tyr175 from two adjacent protomers are allowed in this model to come into direct contact with appropriate residues from C1q subunits. However, access of the top of the C1q globular head into the pore of CRP structure is under severe steric restraints, implying that optimal C1q binding is accompanied by a slight conformational change in the CRP structure, which has been hypothesised to occur under physiological conditions following ligand binding.

In summary, the proposed models for the CRP-C1q interaction provide a first insight into the structural basis of complement activation by CRP. However, due to the absence of structural data for this complex the precise nature of this interaction remains unclear.

1.6.4.3 Fcγ Receptor Binding Site

CRP has been shown by several groups to trigger some of its physiological effects through binding to Fcγ receptors. Similar to C1q, mutagenesis studies on CRP have provided data to locate the Fcγ receptor binding site on CRP (Marnell *et al.*, 1995; Bang *et al.*, 2005). Marnell *et al.* (1995) identified the residue Leu176 as important to CRP binding to FcγR1 as its substitution with Glu eliminated CRP binding to this receptor. This finding was later confirmed by a second mutagenesis study, which further identified amino acid residues involved in CRP binding to FcγRs. This study showed that residues Lys114, Thr173, Leu176 and Asn186 in CRP are important for FcγR1 binding, whereas Thr173 and Asn186 are important for FcγR2 binding (Bang *et al.*, 2005).

Based on these mutagenesis studies and the data obtained from the crystal structure of CRP, Bang *et al.* proposed that the hydrophobic region formed by the α-helix (Glu169 to Leu176) and the adjacent loop (Gly177 to Asn186) on the A face of CRP provide the major area of contact between CRP and FcγR. This suggests that the binding sites on CRP for FcγR1, FcγR2 and C1q overlap.

1.6.4.4 Binding to the CRP Inhibitor 1, 6-bis (phosphocholine-hexane) (bis(PC)-H)

It has been proposed that CRP-mediated complement activation can exacerbate the tissue injury of ischemic necrosis in heart attacks and strokes (Griselli *et al.*, 1999; Gill *et al.*, 2004). Thus, a potential clinical treatment for cardiovascular diseases could be the administration of a CRP inhibitor, which blocks its functions. Such an inhibitor of CRP binding has been designed on the basis of the crystal structure of the CRP-PC complex and the structure of a potent inhibitor of SAP binding (Pepys *et al.*, 2006).

This inhibitor, 1, 6-bis (phosphocholine-hexane) (bis(PC)-H), is composed of two phosphocholine residues linked by a hexane linker. Its palindromic nature allows it not only to block the ligand binding sites on CRP, but also cross-link CRP pentamers to form B face to B face decamers. A high resolution X-ray crystal

structure of the CRP-bis(PC)-H complex was recently solved to 1.6 Å and confirmed the presence of a CRP decamer cross-linked by five bis(PC)-H molecules (Pepys *et al.*, 2006; Jenvey, 2006). The phosphate groups positioned at the opposing ends of the bis(PC)-H molecule interact directly with the calcium ions. This causes the CRP pentamers to be displaced by a relative rotation of 20° about a common five fold axis.

1.6.5 Ligand Binding to SAP

1.6.5.1 Binding of MOβDG

Ligand binding by SAP was first shown with respect to agarose (Pepys *et al.*, 1977), a marine algae-derived galactan hydrocolloid. However, it was not until 1984 that the specific SAP ligand on agarose was identified (Hind *et al.*, 1984). This ligand of SAP is the pyruvate acetal of galactose, which is a trace constituent of agarose. Further to this finding, Hind *et al.* (1984) synthesised methyl 4, 6-O-(1-carboxyethylidine)-β-D galactopyranoside (MOβDG), the form in which it exists in agarose, and showed that it inhibits and reverses binding of human, mouse and plaice SAP to agarose in vitro.

In order to investigate the interaction between SAP and MOβDG further, co-crystallisation studies were attempted (Emsley *et al.*, 1994; Thompson *et al.*, 2002). These studies identified the ligand binding site in SAP and allowed analysis of the SAP-ligand interactions. The carboxylate group of the pyruvate acetal of MOβDG interacts directly with the two calcium ions of each SAP protomer (2.39 Å to Ca I and 2.45 Å to Ca II) (Thompson *et al.*, 2002).

In addition to this interaction, hydrogen bonds are formed between the oxygens of the carboxyethylidine ring and the side chain amide nitrogens of Asn59 and Gln148 (Emsley *et al.*, 1994). Gln148 is also involved in hydrogen bonds with O3 of the sugar ring, whilst Lys79 hydrogen bonds with the O1 atom (Thompson *et al.*, 2002). Since Gln148 and Asn59 are also involved in calcium binding, it has been proposed that the calcium ions are not only responsible for binding the MOβDG molecule but also for positioning these residues into the correct orientation for

interaction with MOβDG (Thompson *et al.*, 2002). Interestingly, although these two residues are conserved in all mammalian SAPs and CRPs, CRP binds MOβDG only weakly.

The higher affinity of SAP for MOβDG may be explained by the positioning of the methyl group from the pyruvate bridge into a hydrophobic pocket made up by residues Leu62, Tyr64 and Tyr74 (Thompson *et al.*, 2002). This hydrophobic pocket in CRP is altered in size due to the substitution of Tyr64 and Tyr74 in SAP for Phe66 and Thr76 in CRP respectively. In addition to these differences, it has been suggested that the substitution of Lys79 in SAP to Glu81 in CRP would make hydrogen bonding unavailable in the CRP-MOβDG complex.

1.6.5.2 Binding to PE

SAP has been shown to bind with high affinity to PE (Schwalbe *et al.*, 1992), a property which is utilised in the purification protocol of SAP (DeBeer *et al.*, 1982; Hawkins *et al.*, 1991). Subsequently, the determination of the crystal structure of this complex revealed that the interactions between protein and this phosphate ligand are similar to those observed in MOβDG (Emsley *et al.*, 1994; Pye, 1997). However, in contrast to MOβDG, PE binds to the calcium ions via a phosphate group rather than a carboxylate group. Two tyrosine residues similarly to the SAP-MOβDG structure flank the sides of the PE binding region. One of these tyrosine residues, Tyr64, is positioned below the amine group of the PE molecule. This amine group is also held in place by a hydrogen bond via a water molecule to the carboxyl group of Glu66.

1.6.5.3 Binding to dAMP

In the search for a novel SAP ligand, Hohenester *et al.* (1997) identified the mononucleotide 2'-deoxyadenosine-5'-monophosphate (dAMP). This ligand was chosen as it was found to be as effective as an inhibitor of calcium-induced SAP precipitation, but also as a ligand of interest with respect to DNA recognition.

The crystal structure of the SAP-dAMP complex revealed a B-face to B-face SAP decamer. Each subunit in the decamer bound a single dAMP molecule at the calcium binding site, shielding the ligand binding sites in the newly formed interface. Analysis of this interface revealed that the stability of the decamer is mediated by base-stacking of adjacent dAMP ligand molecules in between the two pentamers.

The interactions between SAP and dAMP at the calcium binding site are similar to those involved in ligating MOβDG and PE. An acidic functional group (phosphate group in dAMP) bridges the two calcium ions with calcium-oxygen distances of 2.4 to 2.5 Å (Hohenester *et al.*, 1997). Hydrogen bonds, which are present in the other protein-ligand structures are also formed between SAP and dAMP. These include the hydrogen bond formed between the side chain of Asn59 and one of the phosphate oxygens of dAMP and the hydrogen bonds formed between the side chains of Gln148 and Tyr64 to the 2'deoxyribose ring oxygen atom. However, in the SAP-dAMP complex additional hydrogen bonds are formed between the ligand and the SAP residues Asp145 and Ser147.

Although Hohenester *et al.* (1997) could not provide a structural explanation for the avid binding of SAP to DNA (Butler *et al.*, 1990), they concluded that DNA binding to SAP may involve the basic grooves between protomers in the pentamers rather than the calcium binding site. In addition, they proposed that the concept of the dAMP-induced decamerisation of SAP could prove a viable strategy in drug design as it would abolish the availability of the calcium binding sites for other interactions. Shortly later, this concept was utilised in the development and design of SAP inhibitors.

1.6.5.4 Binding to the SAP inhibitor R-1-[6-[R-2-carboxy-pyrrolidin-1-yl]-6-oxo-hexanoyl]pyrrolidine-2-carboxylic acid (CPHPC)

The findings that SAP binds to amyloid fibrils in all types of amyloid deposits and contributes to the pathogenesis of amyloidosis led to the proposal that inhibition of SAP binding to amyloid fibrils might be a valid therapeutic approach to amyloidosis and amyloid associated diseases (Hind *et al.*, 1984). In an attempt to

identify such an inhibitor, the Roche compound library was screened with a high throughput assay for inhibitors of SAP binding to Alzheimer's disease Aβ amyloid fibrils (Pepys *et al.*, 2002). This screen identified two compounds, one of which was prepared as a dimer to increase affinity. Subsequently, medicinal chemistry and *in vivo* evaluation studies led to the selection of the compound R-1-[6-[R-2-carboxy-pyrrolidin-1-yl]-6-oxo-hexanoyl]pyrrolidine-2-carboxylic acid (CPHPC). This compound is composed of two D-proline residues, which are joined by a four carbon aliphatic linker. This enables the compound not only to block the ligand binding sites on individual protomers, but also to cross-link pairs of pentameric SAP molecules to form B-face to B-face decamers (Pepys *et al.*, 2002).

This CPHPC-mediated decamerisation was confirmed by X-ray crystallographic studies of the SAP-CPHPC complex (Purvis, 2002; Pepys *et al.*, 2002; Jenvey, 2006). These studies revealed that the CPHPC terminal carboxylate groups are bound in the calcium binding sites and that there are no close contacts between the adjacent faces of the two pentameric SAP molecules. Further stabilising interactions are derived from the packing of the pyrrolidine ring of CPHPC into the hydrophobic pocket formed by Leu62, Tyr64 and Tyr74, which is adjacent to the calcium ions. The alkyl chain that links the two proline head groups adopts a kinked rotamer with eclipsed substituents about the C2-C3 bond. Both of the peptide bonds preceding the proline residues were shown to adopt the *cis*-configuration (Jenvey, 2006).

1.7 The aim of the thesis

In the past decades the structure and function of the human pentraxins has been extensively studied. The three-dimensional structures have already been elucidated using X-ray crystallographic methods and the future lies in a more careful investigation of their ligand binding sites. This can provide an insight into the underlying physiological and pathophysiological roles of the pentraxins. In addition, it may be used to improved relevant animal models and lead to the production of new potential pentraxin inhibitors.

To this end, I have used X-ray crystallography as a tool to determine the structures of several human SAP-ligand complexes (Chapter 2) and the structure of rat SAP in complex with PC (Chapter 3). Chapter 4 describes the structure determination of human CRP in complex with PE and discusses the structural differences in the ligand binding site. The final chapter describes an attempt to co-crystallise a CRP-C1q complex.

Chapter 2

Structural Studies of Human Serum Amyloid P Component in Complex with Methylmalonic Acid and Phosphoethanolamine

2.1 Introduction

In the past decade substantial efforts have been directed towards identifying and characterising ligands of low molecular mass that can displace SAP from amyloid deposits. Amyloid deposits can make up as much as 15 % by weight of total amyloid tissue and are thought to be an important contributor to the pathogenesis of a group of diseases called amyloidoses (Pepys & Baltz, 1983). The proposed role of SAP in amyloid pathology is not in the formation of these deposits but in the maintenance of their stability. More specifically the binding of SAP to amyloid fibrils protects amyloid fibrils from degradation by phagocytic cells and proteolytic enzymes (Tennent, Lovat, & Pepys, 1995). Therefore, the design of compounds that displace SAP from amyloid fibrils, which in turn exposes the fibrils to proteolysis and phagocytic clearance mechanisms, comprises a potentially important therapeutic approach for amyloidosis (Hind *et al.*, 1984).

Although the ligand responsible for the interaction between amyloid fibrils and SAP has not yet been identified, a great deal has been learned about ligand binding through the elucidation of the X-ray crystal structure of SAP (Emsley *et al.*, 1994) as well as various SAP-ligand complexes such as MOβDG (Emsley *et al.*, 1994, Thompson et al., 2002), PE (Emsley *et al.*, 1994), dAMP (Hohenester *et al.*, 1997), N-Acetyl-*D*-proline (Purvis, 2002) and N-Acetyl-*L*-proline (Kolstoe, 2005). These crystal structures of SAP-ligand complexes reveal how ligand binding by SAP is mediated by two positively charged calcium ions and a hydrophobic pocket. More specifically, all SAP ligands to date bind to SAP by the coordination of either a negatively charged phosphate or a carboxylate ligand within the calcium binding site, suggesting that binding is driven by charge.

To extend our current understanding of ligand recognition by SAP, high resolution structures of SAP with a phosphate and carboxylate compound were sought. Methylmalonic acid (MM) shares two base elements (a carboxylate and a methyl group) with MOβDG (Figure). Therefore, it was thought that MM, like MOβDG, binds to SAP by the coordination of the methyl group into the protein's hydrophobic pocket as well as the strong electrostatic interactions between the ligand's carboxylate group and the two calcium ions in the protein binding site.

This is of considerable interest, with regards to the geometry of the SAP binding site, as this could answer whether the overall binding of ligands is driven primarily by the association between the highly charged calcium ions and the negatively charged carboxylate oxygens.

The binding of PE to SAP was described previously at medium resolution (2.9 Å) at pH 5.5 by Emsley et al. (1994) and at 1.9 Å by Pye (1999). Emsley et al. reported that the phosphate moiety of the PE molecule bridged the calcium ions and that the amine group of PE hydrogen bonded to the side chain of Tyr74. However, the more recent high resolution data by Pye argues against this hydrogen bond. Crystals of SAP in complex with PE are easily grown and this structure was solved anew to enable detailed analysis of protein ligand binding.

2.2 Methods and Results

2.2.1 Crystallisation of Human SAP-Ligand Complexes

Human SAP was purified from human blood in Professor Mark Pepys's laboratory, UCL, London, as previously described by Hawkins *et al.* (1991). O-Phosphoethanolamine (PE) and Methylmalonic acid (MM) were obtained from Sigma-Aldrich (Product codes P0503 and M54058). Crystallisation of the SAP-MM and SAP-PE complexes was performed at room temperature by the hanging-drop method (Figure 2.1), which is the most common technique used for crystallising proteins.

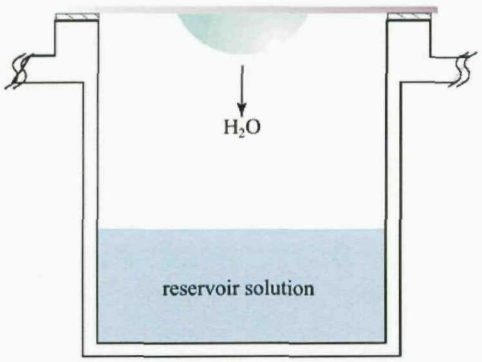

Figure 2.1 A diagram of the hanging-drop vapour diffusion method (amended from http://www.hamptonresearch.com).

In this technique a drop (2 µl) containing pure 14.2 mg/ml SAP and ligand (10 fold excess) is mixed with an equal volume of reservoir solution containing the crystallisation agents (precipitant, salt and buffer) on a siliconised cover slip. The cover slip is inverted onto a greased well containing 1000 µl of reservoir solution, thus producing an enclosed system. The difference in concentration between the drop and the reservoir solution drives the system toward equilibrium by diffusion of water from the drop (via vapour diffusion) to the reservoir. During this process, the concentration of all constituents in the drop slowly increases bringing the protein solution to a supersaturated state, which is ideal for supporting nucleation and subsequent crystal growth (Figure 2.2).

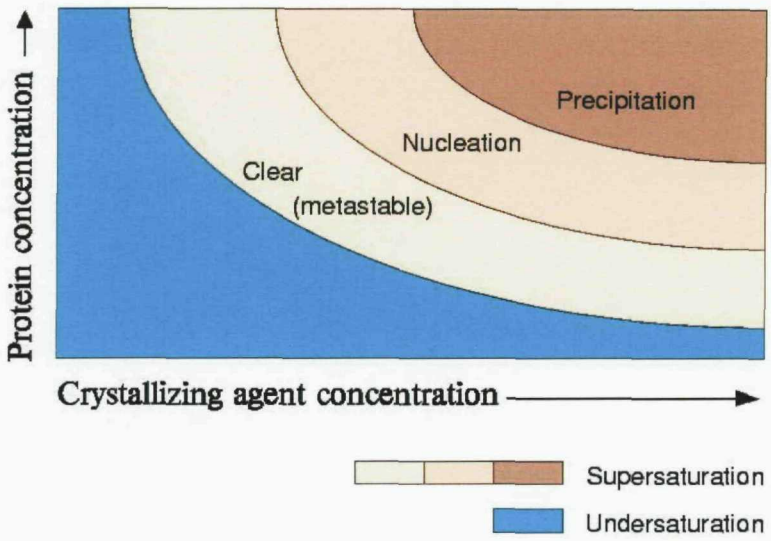

Figure 2.2 A two dimensional solubility diagram illustrating the affect of varying the protein and crystallisation agent solution (from http://www-structmed.cimr.cam.ac.uk/Course/). The blue region represents concentrations of protein and precipitant at which the solution is unsaturated with protein, so neither nucleation nor crystal growth occurs. The supersaturation region supports crystal growth and is subdivided into three distinct zones (Precipitation, Nucleation and Metastable region). The conditions in the nucleation zone support the spontaneous formation and growth of stable nuclei, thereby resulting in the partition of protein from solution into the crystalline state. Further growth of those stable nuclei is supported by conditions in the metastable zone, which does not support nucleation.

There are a large number of factors that influence nucleation and crystal growth (McPherson, 2004). However, the most important of factors include protein purity, protein concentration, precipitant, pH, temperature, the presence of ligand and ionic strength. Hence there are a huge number of parameters that can be varied in a search for conditions that yield crystals. The most popular way of determining the preliminary crystallisation conditions for macromolecules is sampling the chemical composition space for crystallisation using sparse matrix screens (Wooh *et al.*, 2003). This approach is based on a random search for crystallisation conditions and does not take into account any differences between various classes of molecules, which may significantly narrow the search area (Radaev & Sun, 2002). Crystallisation conditions for SAP have previously been summarised by Kolstoe (2005). Therefore, in the case of SAP-ligand complexes, a grid screen was used to refine the known crystallisation condition. In this grid screen, the precipitant concentration, the ligand and the pH of the buffer were varied (Figure 2.3).

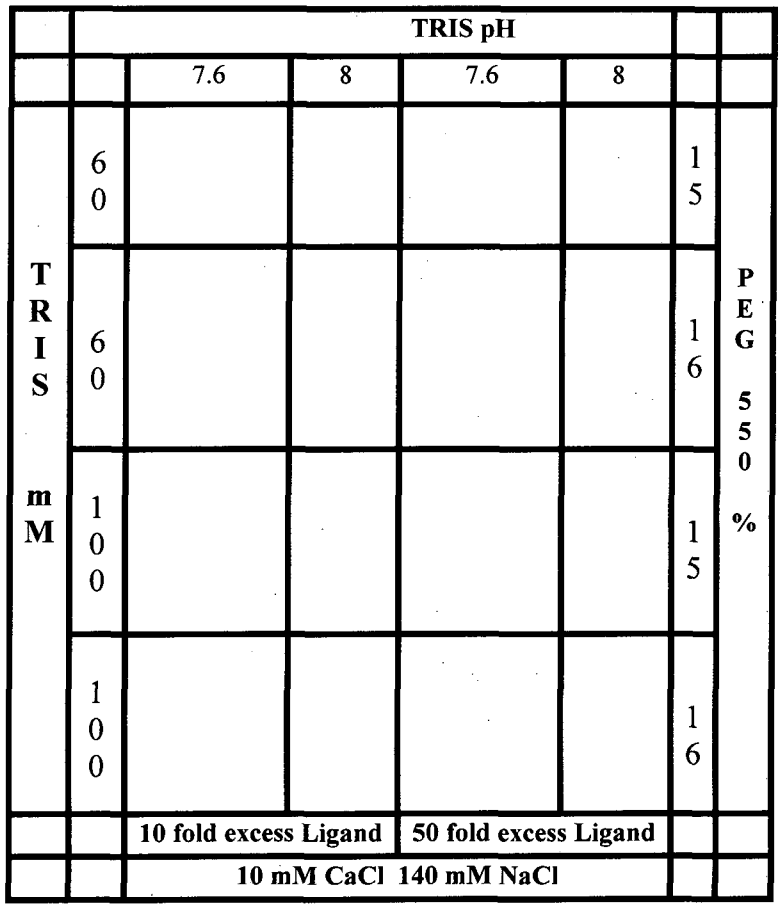

Figure 2.3 Schematic representation of the crystal screening process for SAP-ligand complexes. The pH of the buffer, the concentration of precipitant (PEG 550) and protein: ligand ratios were varied. Hanging drops of approximately 4 µl containing 2 µl well solution and 2 µl protein: ligand solution were used.

Single crystals of the SAP-PE and SAP-MM complex were grown in the crystallisation condition (60 mM Tris-HCl pH 8.0, 140 mM NaCl, 10 mM $CaCl_2$, 16 % PEG MME) (Figures 2.4 & 2.5). These crystals appeared after 5 days and continued to grow for about two weeks to a much larger size (approximate dimensions of 1.5 × 0.4 × 0.4 mm).

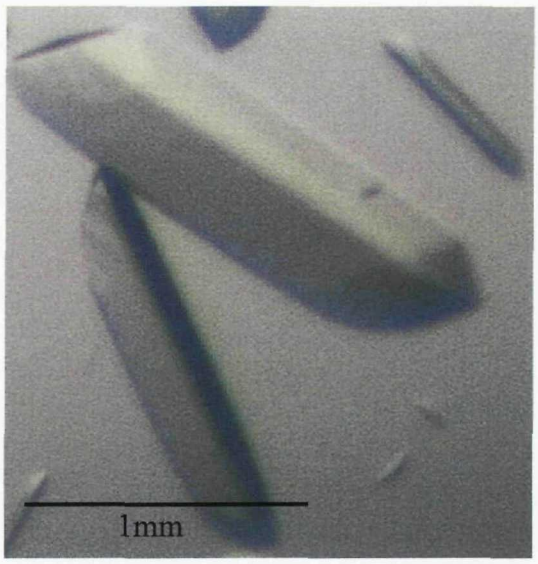

Figure 2.4 SAP crystals grown by the hanging-drop vapour diffusion method in the presence of 20 mM MM (pH 7.8).

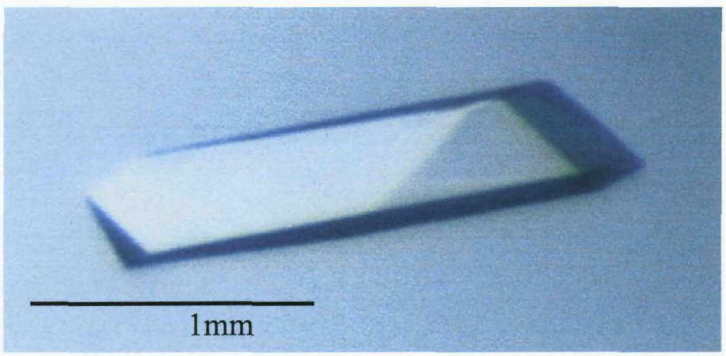

Figure 2.5 A SAP crystal grown by the hanging-drop vapour diffusion method in the presence of 20 mM PE (pH 8).

2.2.2 Data Collection of Human SAP-Ligand Complexes

2.2.2.1 Cryo-Crystallography

Crystals of SAP-ligand complexes were selected with a fibre loop, transferred into mother liquor solutions containing 30 % glycerol and flash cooled to cryogenic temperatures (100 K) by rapid immersion into liquid ethane followed by liquid nitrogen. The use of the cryo-protectant such as glycerol often minimises any disruption of the crystal by ice formation during the cooling procedure, by reducing the crystallisation rates of the water both within the crystal and within the surrounding solvent (Garman *et al.*, 1997). This procedure is essential for collecting data at cryogenic temperatures, as it increases the lifetime of the crystal since free radical damage is reduced at lower temperatures (Garman *et al.*, 1999). Furthermore, due to the lack of crystal degradation during data collection, systematic errors are reduced. The cryo-cooled mounted crystal is then fixed to a goniometer, where the crystal is maintained at cryogenic temperatures by a stream of liquid nitrogen gas for the duration of data collection at an X-ray source.

2.2.2.2 X-ray Sources and Detectors

X-rays are a form of electromagnetic radiation with wavelengths in the range of 0.1 Å to 100 Å, which are able to penetrate protein crystals due to their high energy. Since individual atoms in protein molecules are on average 1.5 Å apart, X-rays can be used to determine three dimensional macromolecular structures to atomic detail as their relatively short wavelength enables them to be diffracted by the electron clouds surrounding the atoms.

X-ray diffraction data from the SAP-ligand crystals were collected at 100 K on the beamline ID 14-2 (λ = 0.98 Å) at the European Synchrotron Radiation Facility (ESRF) in Grenoble, France, with an ADSC Quantum-4 CCD detector (Figure 2.6). This X-ray source is a third generation synchrotron radiation source, which generates X-rays by accelerating electrons in a vacuum to velocities of more than 99 % of the speed of light (Figure 2.7). As the electrons are maintained and accelerated in a circular motion around the synchrotron ring by powerful magnets,

they lose energy in the form of synchrotron light. Accessory devices such as wigglers and undulators give additional bending of the beam, producing higher intensity radiation at shorter wavelengths (Rhodes, 1993). Prior to exposure of the protein crystal to the X-rays, the beam is passed through a monochromator consisting of a single crystal of silicon, germanium or carbon, which selects a single wavelength from the source spectrum.

Diffraction patterns are collected and stored on an electric image plate detector, which operate on the principle of localized light-induced charge accumulation (Figure 2.8).

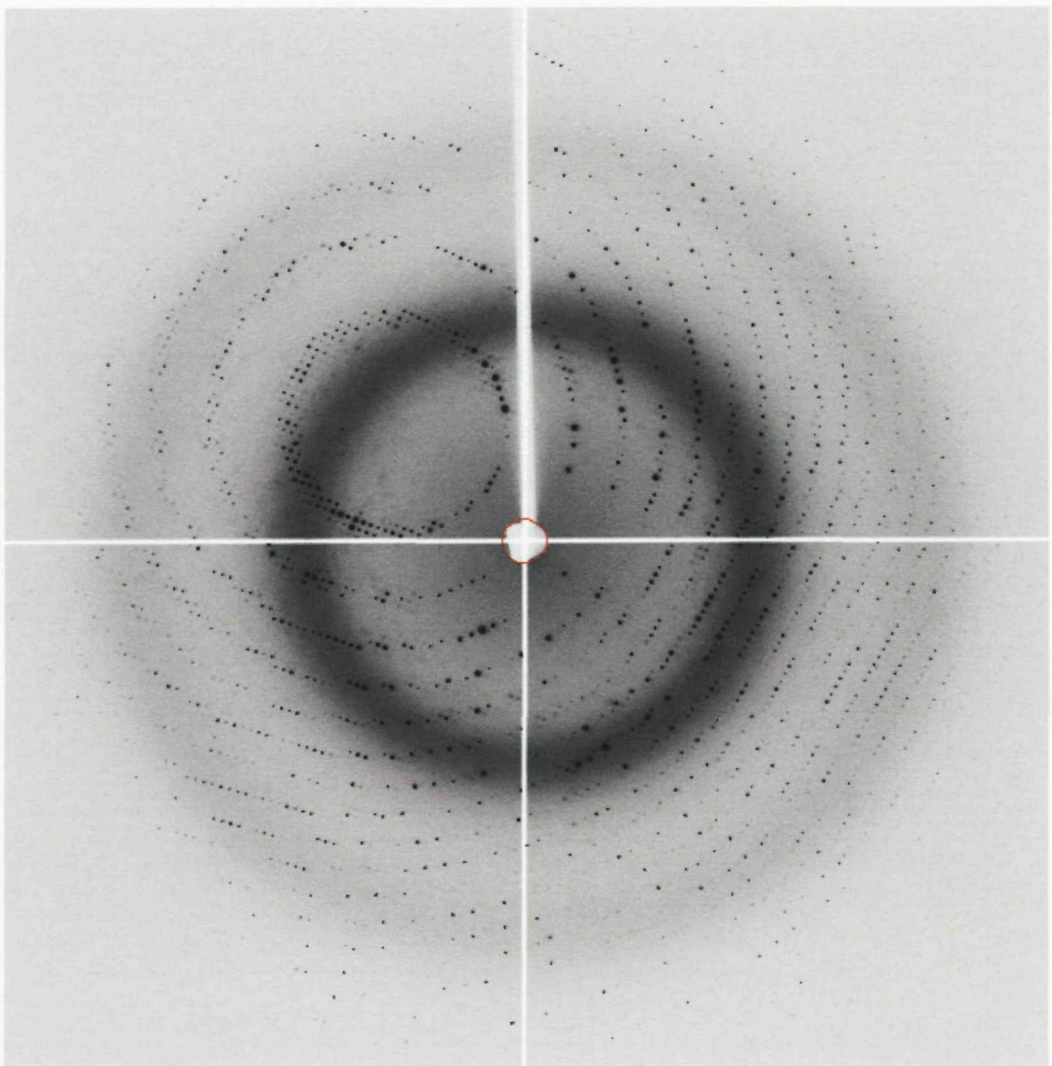

Figure 2.6 A 1° oscillation image collected at the ESRF (Beamline ID 14-2) on a Mar CCD detector from a SAP-PE crystal at cryogenic temperatures, recorded to a maximum resolution of 1.5 Å. For each complex, a data set comprised of a total of 190 images was collected.

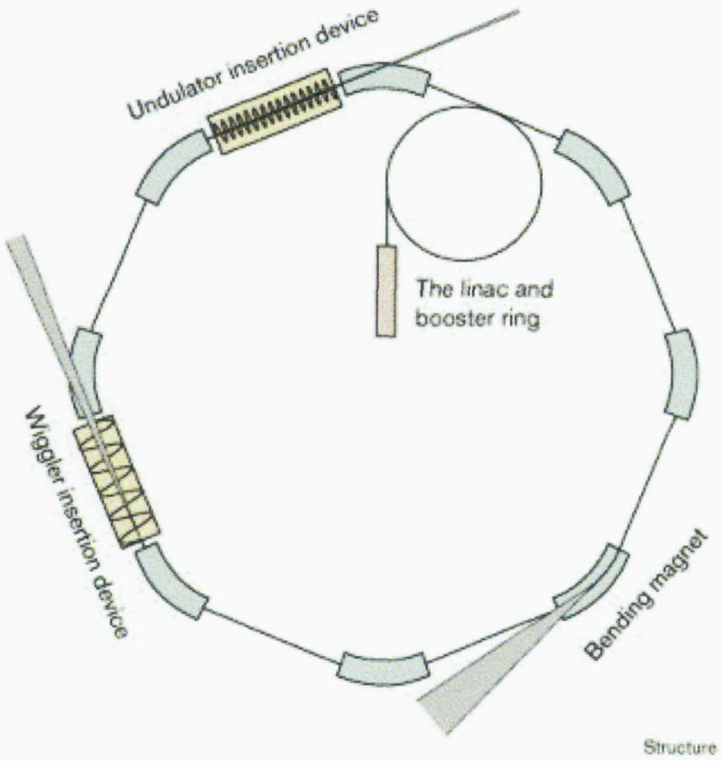

Figure 2.7 Schematic of a synchrotron radiation source showing the linac, booster and storage rings, and the magnetic devices that produce X-ray radiation (Mitchell, 1999).

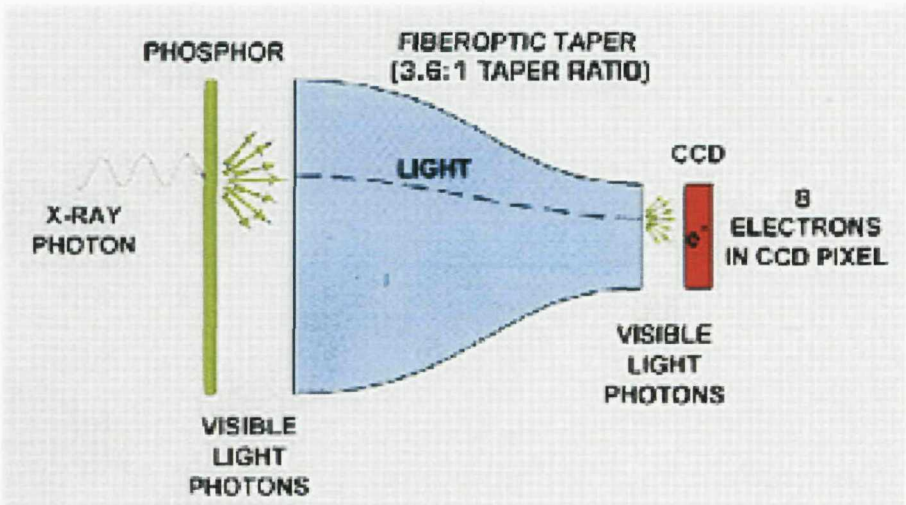

Figure 2.8 The three main components of the Quantum CCD detector are phosphor screen (to convert X-rays to visible light), fiber-optic taper (to demagnify the light image down to the size of the CCD chip), and CCD chip to detect the light image as an electric charge image (from http://www.adsc-xray.com). The electric charge image is read out of the CCD chip and digitized. This is then fed into a computer.

2.2.3 Data Processing of Human SAP-Ligand Complexes

Data processing of the raw image data from the SAP-ligand crystals was carried out to produce a data reflection file (.mtz), which contains the Miller indices (*hkl*) of all reflections recorded together with their intensities and an estimate of their standard error.

The first stage in data processing is called auto-indexing and involves determining the unit cell dimensions and the space group of the crystal. A unit cell is described as the smallest and simplest volume element from which the entire crystal may be constructed by repeated lattice translations. The dimensions of the unit cell are described by the length of three edges (a, b and c) and three angles (α, β, γ). Depending on the values of these dimensions, unit cells can fall into seven crystal systems. Combinations of these seven crystal systems with the four lattice types of centering (*P*, *C*, *F* and *I*) give rise to 14 possible lattice types, the Bravais Lattices. These 14 Bravais lattices only describe how the unit cell can be translated in three dimensions to obtain crystal morphology; the point group provides information on how the asymmetric unit is positioned within the unit cell. An asymmetric unit is the largest aggregate of molecules that possesses no symmetry elements, but which can be juxtaposed onto other identical entities by symmetry operations. The symmetry operations that can be imposed on protein crystals are translations, rotations and screw axes, which are rotations and translations combined. The combination of these available symmetry operations available along with the Bravais lattices leads to a total of 65 space groups relevant to protein crystallography.

There are a number of computer software programs, which can be used to process diffraction data such as DENZO (Otwinowski, 1993), HKL2000, MOSFLM (Leslie, 1992, 1994) and XDS (Kabsch, 1988). Although the user interfaces and the methods employed by each program are subtly different, the basic approach is similar.

Data processing from the SAP-ligand crystals was carried out using the program MOSFLM from the CCP4 (Collaborative computing Project Number 4, 1994)

suite. For the initial auto-indexing procedure, MOSFLM reads the images collected by the CCD detector and selects approximately 200 reflections in the diffraction pattern using a peak search routine. Each reflection in the diffraction pattern is assigned a Miller index notation (*hkl*), whose integers correspond to the lattice planes in the crystal. These reciprocal-lattice coordinates are considered to be vectors between the origin and each of the reflections. The program then calculates the smallest sized triclinic cell with minimal symmetry, which can then be distorted to fit each of the Bravais lattices. The reciprocal-lattice vectors are then compared to those predicted for each space group. The results are presented in the form of a list of possible unit cell dimensions and space groups accompanied by a penalty value. The cell with the highest symmetry but lowest penalty is usually selected. The unit cell is then refined by adjusting a number of parameters such as the detector distance, beam divergence and mosaicity.

Auto-indexing of the diffraction data from the SAP-ligand crystals indicated that the crystals had very similar unit cell dimensions (a = 94.87 Å, b = 69.78 Å, c = 102.24 Å, $\alpha = \gamma = 90.0°$, $\beta = 97°$) (Table 2.1). These unit cell parameters suggested that the crystals belonged to a primitive monoclinic space group of either P2 or $P2_1$.

Penalty	Lattice	a	b	c	α	β	γ	Possible space groups
118	tP	94.87	102.24	69.78	90.1	89.9	97	P4,P41,P42,P43, P422,P4212,P4122 P41212,P422,P42212, P4322,P43212
66	mC	130.72	147.71	69.78	90.1	90.1	85.7	C2
66	oC	130.72	147.71	69.78	90.1	90.1	85.7	C222,C2221
64	mC	147.71	130.72	69.78	89.9	90.1	94.3	C2
54	oP	69.78	94.87	102.24	97	90.1	89.9	P222,P2221,P21212, P212121
53	mP	69.78	94.87	102.24	97	90.1	89.9	P2,P21
53	mP	69.78	102.24	94.87	97	89.9	90.1	P2,P21
2	mP	94.87	69.78	102.24	90.1	97	89.9	P2,P21
0	aP	69.78	94.87	102.24	83	89.9	89.9	P1
0	aP	69.78	94.87	102.24	97	90.1	89.9	P1

Table 2.1 Penalty table for the SAP MM data showing the possible unit cell dimensions and space groups (generated by Mosflm).

As a result, all diffraction images of each data set were integrated in the space group P2. Integration gives each reflection an intensity value by predicting the position in the digitised image of each reflection present on that image (drawing a

box around reflection) and then estimating its intensity (after subtracting the X-ray background) and an error estimate of that intensity.

The program SCALA (Kabsch, 1988) was then used to scale together multiple observations of reflections and merge symmetry related reflections to calculate the R-merge value. The R-merge is a measure of the intensity deviation between all symmetry related reflections, which result from the various symmetry elements in the crystallographic space group. Friedel's law states that these reflections should be identical in intensity if the correct space group was chosen. In addition, the program calculates a scale factor for each image from these symmetry related reflections, which is then applied to the data to create uniformity in intensity across all images.

Each reflection (diffracted X-ray) that is collected by the detector can also be described as a complex three dimensional wave. This wave is the result of the superposition of the waves scattered by the electron density in the unit cell and can be described by the structure factor F_{hkl},

$$F_{hkl} = V \int_0^1 \int_0^1 \int_0^1 \rho(x,y,z) e^{2\pi i(hx+ky+lz)} dxdydz$$

which relates electron density in real space ρ (x, y, z) to the reflections measured in reciprocal space, after correcting for unit cell volume (V). Because F_{hkl} is a periodic function describing a complicated wave, it consists of a frequency, amplitude $|F_{hkl}|$ and phase α_{hkl}:

$$F_{hkl} = |F_{hkl}| \, e^{2\pi i \alpha_{hkl}}$$

Although the amplitude $|F_{hkl}|$ can be obtained directly from the diffraction data as it is directly proportional to the square root of the measured intensity I_{hkl} for the reflection hkl, the phase angle of each reflection is unknown and is the only information a crystallographer needs in order to calculate ρ (x,y,z) and thus obtain atom positions in the protein molecule.

The program used to convert the merged intensities to structure factor amplitudes was TRUNCATE (French & Wilson, 1978).

To confirm that the correct space group was selected, the output from TRUNCATE was entered into the program HKLVIEW (CCP4). HKLVIEW displays zones of reciprocal space as pseudo-precession images, which can be viewed to observe systematic absences in the diffraction pattern. Systematic absences are missing reflections in the diffraction pattern, which arise due to certain symmetry elements in the unit cell.

The resulting pseudo-procession images within the 0, *k*, *l* zone of the processed diffraction data in P2 revealed systematic absences along axis 0, *k*, 0 characteristic of the $P2_1$ space group (Figure 2.9). These observations indicated that the protein-ligand complexes had crystallised in the space group $P2_1$. In this space group, the presence of a screw axis means that not only can the axis rotate the object 180 degrees to generate the 2 fold symmetry, but it also translates half the cell along in the direction of the axis to which the screw is parallel. As a result, both data sets were reprocessed and scaled in the space group $P2_1$.

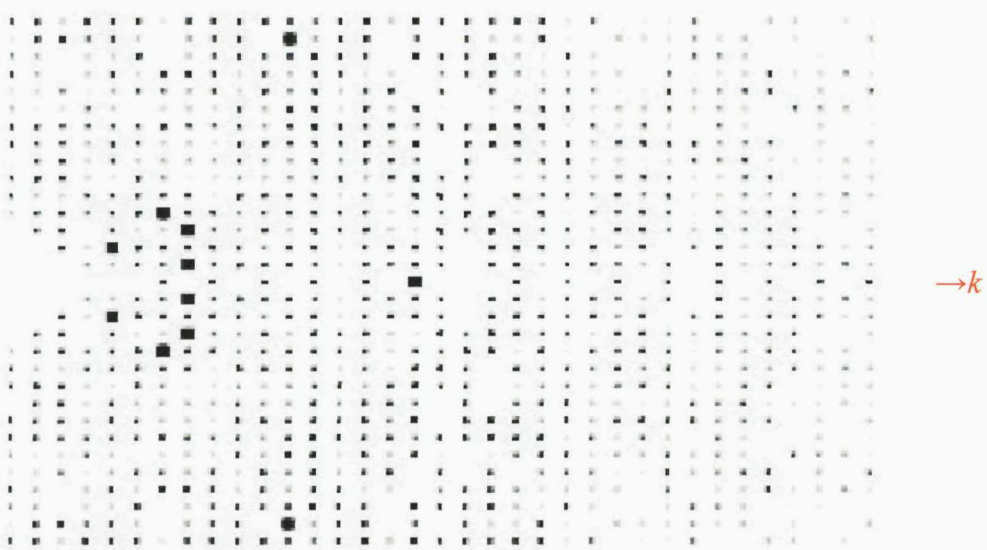

Figure 2.9 A pseudo-precession picture of the processed SAP MM diffraction data in P2. Systematic absences along axis 0, *k*, 0 ($k = 2n$) within the 0, *k*, *l* zone indicate that there is a 2 fold screw axis along the b (prepared using HKLVIEW from the CCP4 suite).

2.2.4 Phase Determination

The diffraction data does not contain phase information for each reflection, which is essential in the calculation of electron density maps and the determination of positions of atoms within the protein molecule. The absence of phase information in the diffraction data has led macromolecular crystallographers to devise methods to overcome the so called "phase problem".

2.2.4.1 Molecular Replacement of Human SAP-Ligand Complexes

The simplest method is molecular replacement, which involves using a previously solved protein structure to determine the orientation (with a rotation function) and position (with a translation function) of the new molecule in the unit cell. The phases calculated from the known protein (in the correct orientation and position) are then used as initial estimates for the unknown protein.

The initial phases for the SAP-ligand complexes were determined with the program MOLREP (Vagin & Teplyakov, 1997) by using the originally derived SAP pentamer (Accession code = 1SAC, Emsley *et al.*, 1994) as the search model with the calcium, ligand and water molecules omitted. However, there are several other program packages for molecular replacement such as AMoRE (Navaza, 1994), X-PLOR/CNS (Brünger, 1990) and PHASER (Read, 2001). Not only do these programs vary in the algorithms they use but also in the methods for performing the rotation and translation function calculations.

The rotation and translation functions are based on the Patterson function, which is the Fourier transform of the experimental intensities and can be expressed as:

$$P_{(u,v,w)} = \frac{1}{V}\sum_{h}\sum_{k}\sum_{l}\left|F_{hkl}\right|^{2} e^{-2\pi i(hu+kv+lw)}$$

The Patterson map that is generated by the function consists of a number of peaks corresponding to inter-atomic vectors (vectors between atoms). As Patterson maps have all phase components set to 0 they can be generated directly from diffraction

data, as well as from coordinates of a previously determined structure (search model).

2.2.4.2 The Rotation Function and Translation Function

The rotation function can be evaluated in real space (Patterson) by rotating one model Patterson with respect to the other Patterson (observed) until they superimpose (utilised in CNS). However, the rotation function can also be computed in reciprocal space with Fourier transforms, if the Pattersons were expressed in terms of spherical harmonics. This method was developed by Crowther (1972) and is used in the program MOLREP, which calculates structure factors for each orientation of the model by the fast Fourier transformation of its electron density.

Having determined the orientation of the new protein molecule in the unit cell based on the rotation search, the position of the search molecule in relation to symmetry elements of the target crystal can be calculated using the translation function. The translation function compares sets of intermolecular vectors (between symmetry related molecules) between the observed target unit cell and those from the search model. Similar to the rotation function, the translation function can be computed by different methods. Some programs determine the translation function in real space by computing two Patterson maps, whereas MOLREP carries out the translation function in reciprocal space using fast Fourier transform (Vagin, 1989).

The accuracy of the rotation and translation function is assessed using a statistic called the Residual index factor (R-factor). The R-factor is calculated by monitoring the correspondence between the calculated structure factor amplitudes from the model ($|F_{calc}|$) and the actual amplitudes derived from the experimentally observed data ($|F_{obs}|$). The R-factor compares the agreement between the two sets of amplitudes as follows:

$$R = \frac{\sum \left| |F_{obs}| - |F_{calc}| \right|}{\sum |F_{obs}|}$$

An alternative to the R-factor is the correlation coefficient, which is used to measure the agreement between observed and calculated structure factors amplitudes. In this case the correct solution should provide the highest correlation coefficient.

For both SAP structures, the cross rotation function yielded five strong cross rotation function solutions (Table 2.2). These five solutions, with a peak height of ~17-18 σ corresponded to the five orientations of a single SAP pentamer in the target asymmetric unit due to its five fold symmetry. This is consistent with the solvent content calculation, which yielded a solvent content of 57 %, suggesting that there is only a single pentamer in the asymmetric unit of the SAP-ligand complex.

The highest peak from the rotation function yielded a translation function peak of ~ 41 σ, which corresponds to the correct position of the SAP pentamer in the target asymmetric unit (table 2.3).

Peak no.	α (°)	β (°)	γ (°)	Rf/σ
1	173.20	72.68	150.72	18.76
2	192.60	36.89	145.31	18.50
3	4.96	35.40	332.87	18.09
4	321.70	0.00	0.00	17.69
5	350.54	71.32	329.27	17.14
6	184.58	20.35	332.02	5.12
7	8.01	52.09	150.20	4.97
8	353.84	88.14	148.51	4.80
9	0.00	16.01	142.18	4.77
10	169.76	56.05	331.84	4.68

Table 2.2 The ten highest cross-rotation function peaks for the SAP-MM data.

Peak no.	X	Y	Z	Rf/σ	Rfac
1	0.254	0	0.259	41.33	0.343
2	0.239	0	0.278	4.68	0.464
3	0.188	0	0.043	4.57	0.462
4	0.279	0	0.267	3.78	0.466
5	0.378	0	0.274	3.53	0.463

Table 2.3 The five highest translation function peaks calculated in space group $P2_1$ using solution 1 (α = 173.20°, β = 72.68°, γ = 150.72°) of the cross rotation function search.

2.2.5 Refinement and Model Building of Human SAP-Ligand Complexes

Once initial phase estimates have been obtained for the measured structure factors by molecular replacement, an initial electron density map can be calculated. This map shows the distribution of electrons and since electrons surround atoms, it is possible to interpret the electron density into build amino acid residues. However, due to errors in the phase estimates used in the initial map calculation, the initial atomic model is considerably inaccurate. To produce a more accurate model, alternate cycles of reciprocal space refinement and manual model building are carried out.

Refinement is the process of improving the agreement between the observed structure factor amplitudes from the diffraction data and those calculated from the atomic model. This method is often referred to as reciprocal space refinement and involves adjusting atomic positions (*x, y, z*), temperature factors and occupancy to values that best fit the observed structure factor amplitudes.

Due to the large number of atoms present in a protein, the ratio of observed data to parameters is poor. This ratio may be changed favourably either by providing additional data (often by the incorporation of stereo-chemical knowledge in the form of restraints) or by reducing the number of parameters (often by constraining features of the structure to specific values). All refinement program packages that have been developed to carry out refinement of macromolecular structures use restraints and constraints to ensure that a reasonable structure ensues during the refinement steps.

The most commonly used refinement programs are SHELXL (Sheldrick &Schneider, 1997), CNS (Brunger *et al.*, 1998) and REFMAC5 (Murshudov *et al.*, 1997). They differ not only in their user interface, but also in their methods. SHELXL uses the method of least squares. In least squares refinement, atom positions are selected that minimise the sums of squares of differences between corresponding calculated and observed structure factor amplitudes. However, the model can get trapped in local minima and this method is not capable of adjusting the atomic coordinates to cross phase barriers. Such errors can be removed in real

space by manual intervention in the form of model building. Progression during refinement is monitored using the R-factor, which is typically below 0.20 for a well-defined protein structure. However, the R-factor can be reduced without improving the quality of the model by including an increased number of parameters. This can be avoided by monitoring the crystallographic R-factor in conjunction with the free R-factor (R-free). The R-free is calculated using 5-10 % of the total reflections, which are not used in the refinement and thus provide an unbiased assessment of each refinement step.

The initial models of the SAP-ligand complexes following molecular replacement were refined using the program SHELXL with a fraction of the reflections (5 %) in the thin resolution shells flagged to calculate the R-free. The resulting model was used to calculate electron density maps, so that the atomic model can be manipulated manually to better fit the electron density. Two types of sigmaA weighted electron density maps (Read *et al.*, 1986), were calculated: a F_o-F_c and a $2F_o$-F_c. These maps were examined and manipulated using the graphics program TURBO-FRODO (Russel *et al.*, 1991). Initially, the side chains of the protein were manually built into the electron density and a round of refinement was performed. During subsequent rounds of model building and refinement calcium atoms, sugar residues and ligand molecules were built into positive electron density (Figure 2.10 a-d). Dictionaries for the ligands were created using the program PRODRG (van Aalten *et al.*, 1996) and a pdb file format was created. After verifying the amino acids and ligands, water molecules were manually built into the positive electron density and refined.

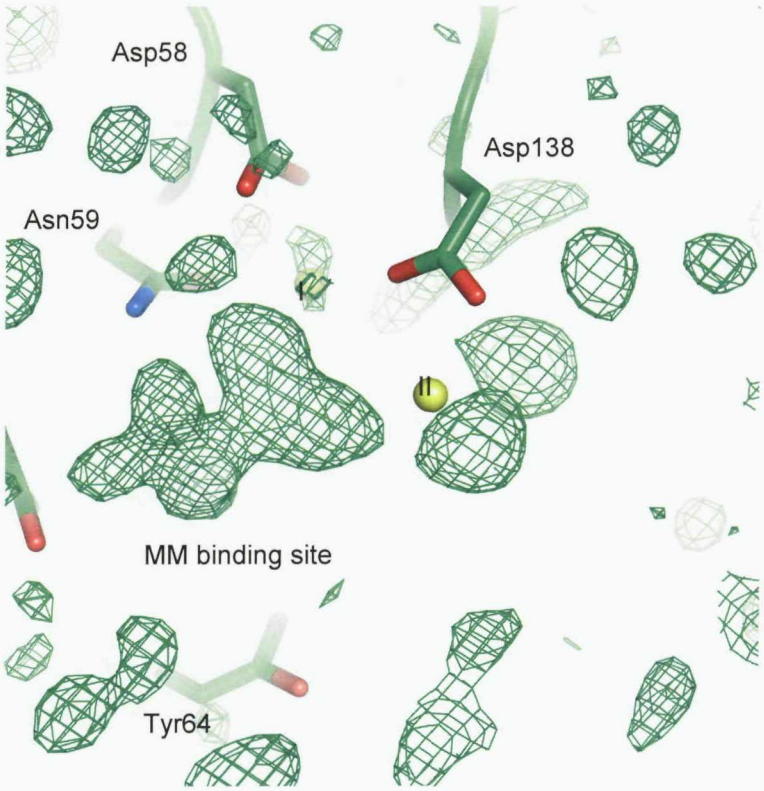

Figure 2.10a F_o-F_c electron density contoured at 2 σ (green) at the calcium binding site before the addition of a MM molecule. The calcium ions (yellow) and amino acid residues (green) of SAP are also shown.

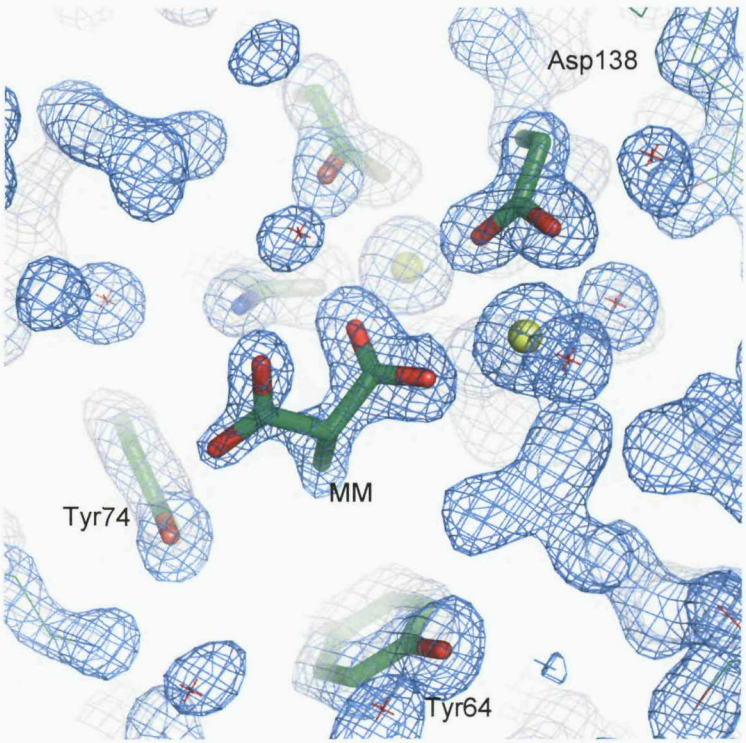

Figure 2.10b $2F_o$-F_c electron density contoured at 1.5 σ (blue) of the fitted MM molecule and surrounding amino acids.

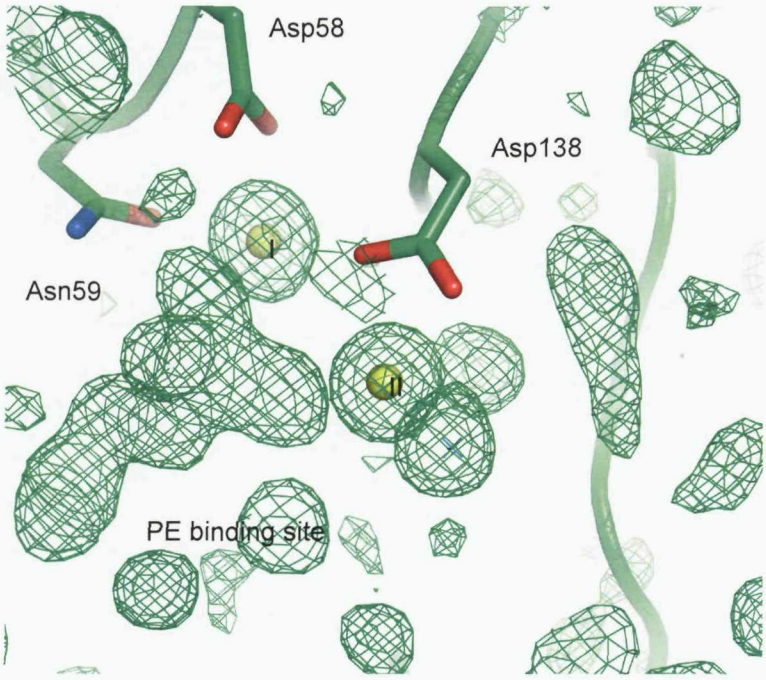

Figure 2.10c F_o-F_c electron density contoured at 2 σ (green) of the calcium binding site before the addition of a PE molecule. The calcium ions (yellow) and amino acid residues (green) of SAP are also shown.

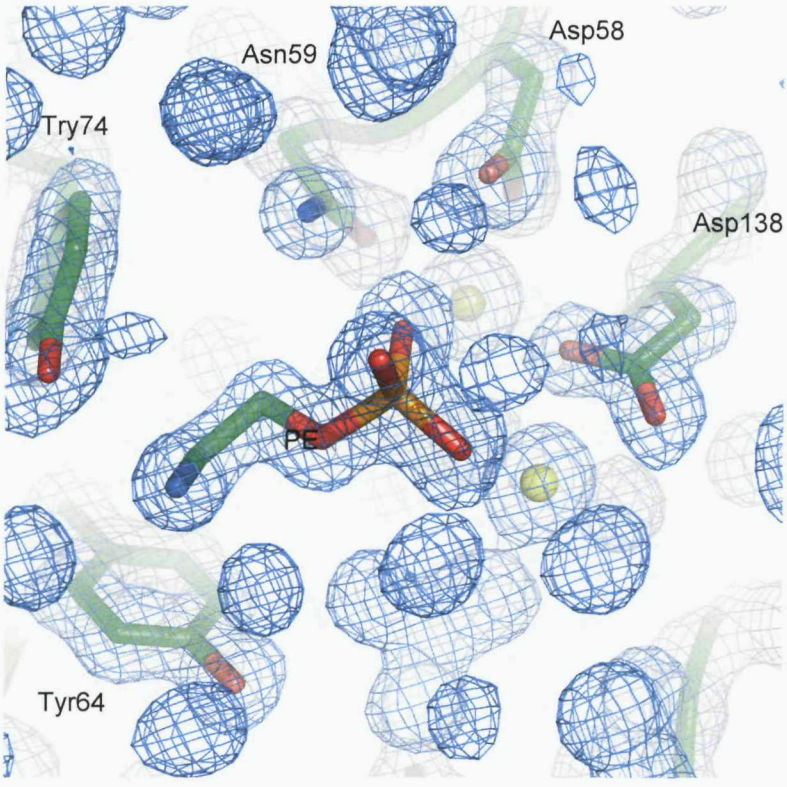

Figure 2.10d 2 F_o-F_c electron density contoured at 1.5 σ (blue) of the fitted PE molecule and surrounding amino acids.

A summary of the R-factor and R-free values during the refinement of each data set are shown in Figure 2.11. The final data processing and refinement statistics for the model are listed in Table 2.4.

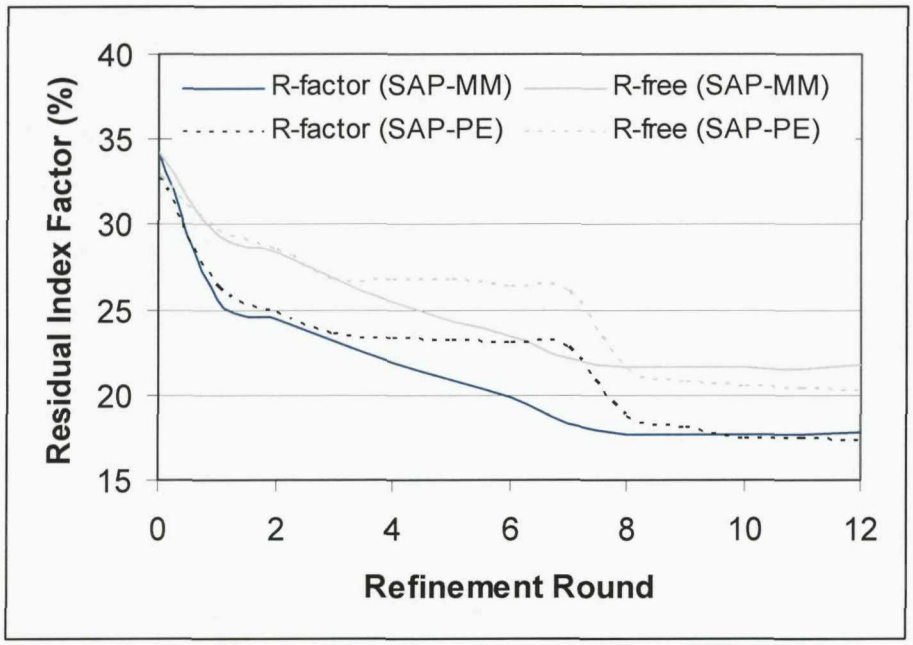

Figure 2.11 Summary of the refinement process for the SAP-ligand structures.

Table 2.4 Summary of the data processing and refinement statistics for the SAP-MM and SAP-PE complex.

	SAP-MM	SAP-PE
Space group	$P2_1$	$P2_1$
Unit cell dimensions (Å)	a = 94.75	a = 94.86
	b = 69.72	b = 69.86
	c = 102.26	c = 102.27
(°)	$\alpha = \gamma = 90.0$	$\alpha = \gamma = 90.0$
	$\beta = 96.9$	$\beta = 96.9$
Resolutions range (Å)	30-1.6 (1.7-1.6)	30-1.5 (1.6-1.5)
No. of reflections	632021 (86780)	789033 (114743)
No. of unique reflections	168819 (23992)	208927 (30159)
Multiplicity	3.7 (3.6)	3.8 (3.8)
Completeness (%)	97.1 (95.1)	98.7 (97.7)
R-merge (%)	9 (50.2)	5 (18)
$(I)/\sigma(I)$ average	10.9 (2.9)	16.8 (6.4)
Model Statistics		
Final resolution (Å)	1.6	1.5
No. of residues	1020	1020
No. of ions	10	10
No. of sugar molecules	5	5
No. of ligand molecules	5	5
No. of water molecules	1103	1103
Rmsd bonds (Å)	0.013	0.010
Rmsd angle distance (Å)	0.026	0.027
R-factor (%)	17.7	17.3
R-free (%)	20.6	20.3

Figures in parentheses apply to data in the highest resolution shell.

2.3 The Structures of SAP in Complex with MM and PE

The overall structure of the protein-ligand complexes is identical to previously described SAP-ligand complexes. However, due to the increase in resolution, the three dimensional structures of SAP in complex with MM and PE provide more detailed information about protein-ligand binding.

The structures of SAP in complex with MM at 1.6 Å and PE at 1.5 Å show good stereo-chemical properties with 99.5 % of residues in the most favoured regions of the Ramachandran plot, 0.5 % in the generously allowed regions and 0 % in the disallowed regions (Figure 2.12). The generously allowed residues consisted of Arg77 from several subunits, located on a type 1 β-turn between strands F and G. Similar conformations have been observed for this residue in previous SAP structures (Purvis, 2002 & Kolstoe, 2005).

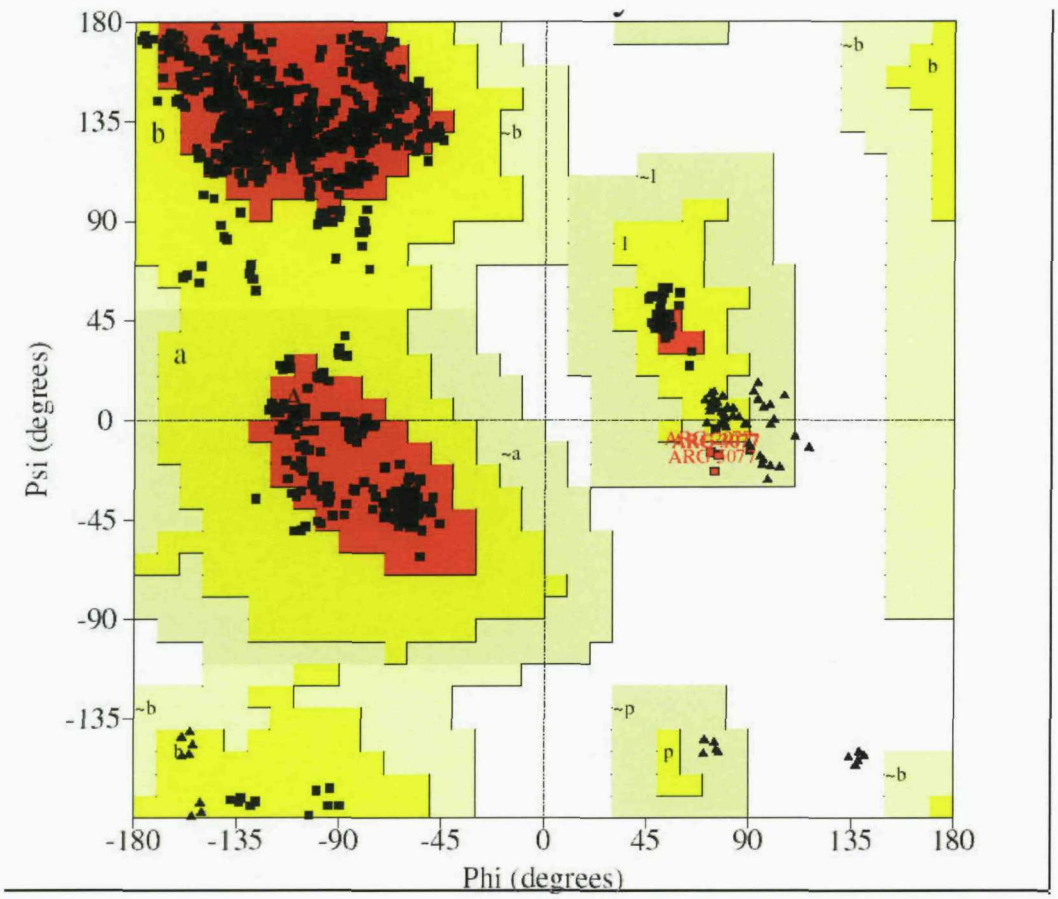

Figure 2.12 Ramachandran plot for the human SAP structure in complex with MM.

Since the two crystals share the same packing structure and almost identical unit cell parameters, the B-factor plots and C_α alignments showed similar features. The overall B-factor value for the human SAP pentamer in complex with MM is 12.67 $Å^2$ (12.10 $Å^2$ for the SAP-PE complex).

An alignment of the temperature factors for the five subunits of the protein-ligand complexes shows increased B-factor values between residues 20 and 30 (Figure 2.13 & 2.14). These residues constitute a flexible loop region, which protrudes from the surface of the protomer. Thus, it would be expected that these regions would have increased B-factor values. Subunit A in both protein-ligand complexes has considerably higher B-factor values between residues 50 - 60 as well as 140 - 150 compared to the other five subunits. In this subunit, these residues are not involved in crystal packing contacts thereby explaining their greater mobility and increased B-factor values.

A comparison of the C_α atom positions between all five SAP subunits of the SAP-MM complex shows high similarity with a C_α rms fit of 0.28 Å (Figure 2.15 & 2.16). The regions in which the largest rms deviation is observed are residues 20 – 30 and 170 - 180, which correlates to the regions with high B-factor values.

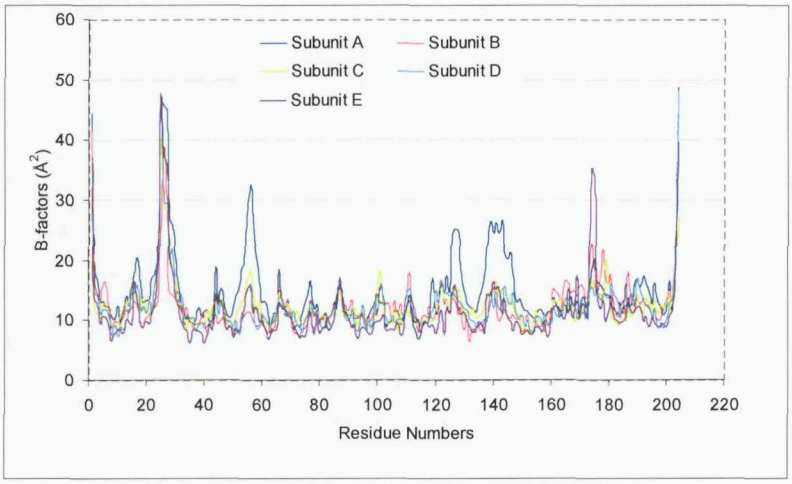

Figure 2.13 Comparison of the average isotropic B-factors for main chain atoms of the five human SAP-MM subunits.

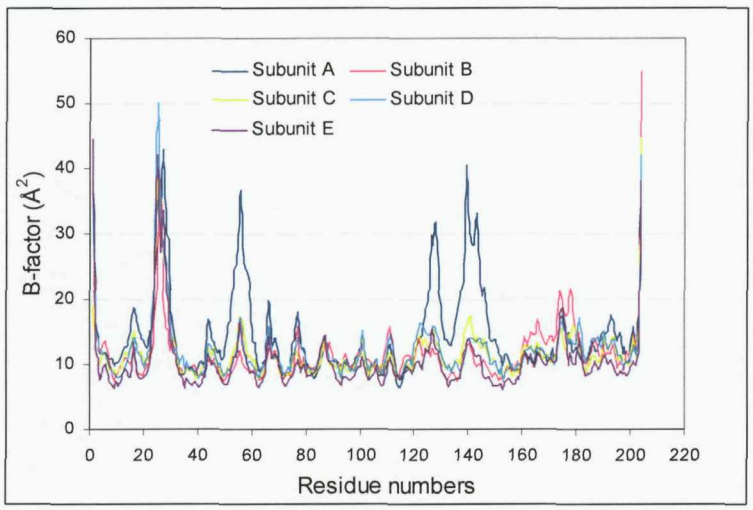

Figure 2.14 Comparison of the average isotropic B-factors for main chain atoms of the five human SAP-PE subunits.

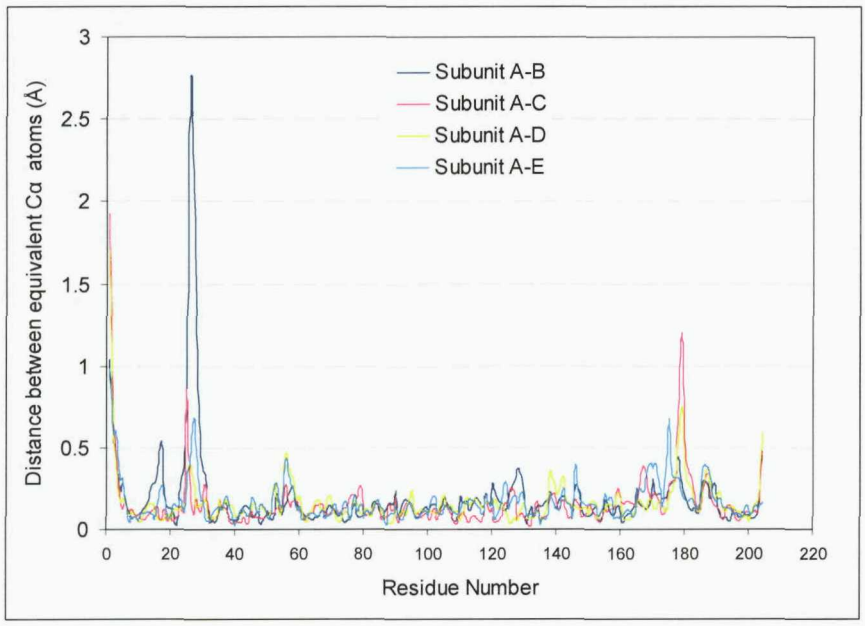

Figure 2.15 A comparison of the root mean squared C_α atom distances between all five human SAP protomers in the human SAP-MM complex.

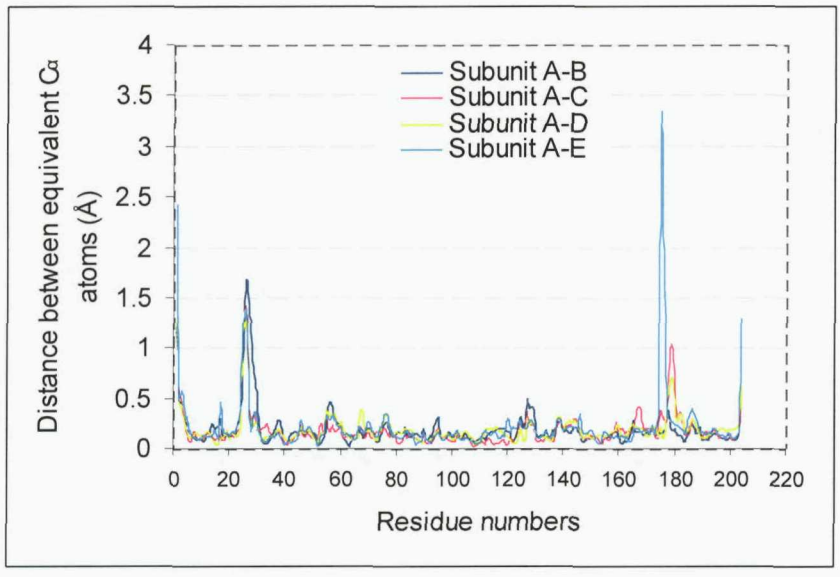

Figure 2.16 A comparison of the root mean squared C_α atom distances between all five SAP protomers in the human SAP-PE complex.

2.4 Discussion

The structure of the SAP-PE complex reported here is the highest resolution structure of SAP to date, enabling a detailed analysis of protein ligand binding. Ligand binding by SAP is dependent on the presence of calcium ions on one face of the SAP pentamer. These two calcium ions along with the hydrophobic pocket form the structural basis for ligand recognition. In all structures described to date (Emsley *et al.*, 1994; Hohenester *et al.*, 1997; Thompson *et al.*, 2002), a negatively charged carboxyl or phosphate group completes the calcium coordination sphere.

Methylmalonic acid was chosen as it has both a carboxyl and methyl group in similar positions to MOβDG. The X-ray crystal structure of SAP-MM complex revealed that the position of the MM at the SAP binding site is reminiscent of the MOβDG binding site (Figure 2.17). Both ligands share the coordination of the carboxyl group with the calcium ions and the interaction of the methyl group with the hydrophobic pocket. However, the position of the methyl group of MM into the hydrophobic pocket made up by Tyr74, Tyr64 and Leu62 causes the second carboxyl group to point away from this pocket (Figure 2.18). As a result, the second carboxyl group of MM forms hydrogen bonding interactions with Tyr74 hydroxyl group (2.7 Å).

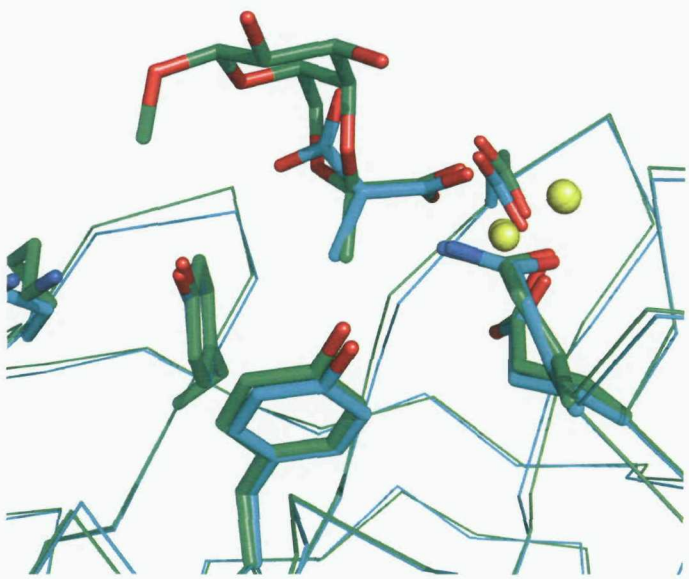

Figure 2.17 Superposition of the 1.6 Å SAP-MM complex (light blue) with the 2.2 Å SAP-MOβDG complex structure (1GYK) (green).

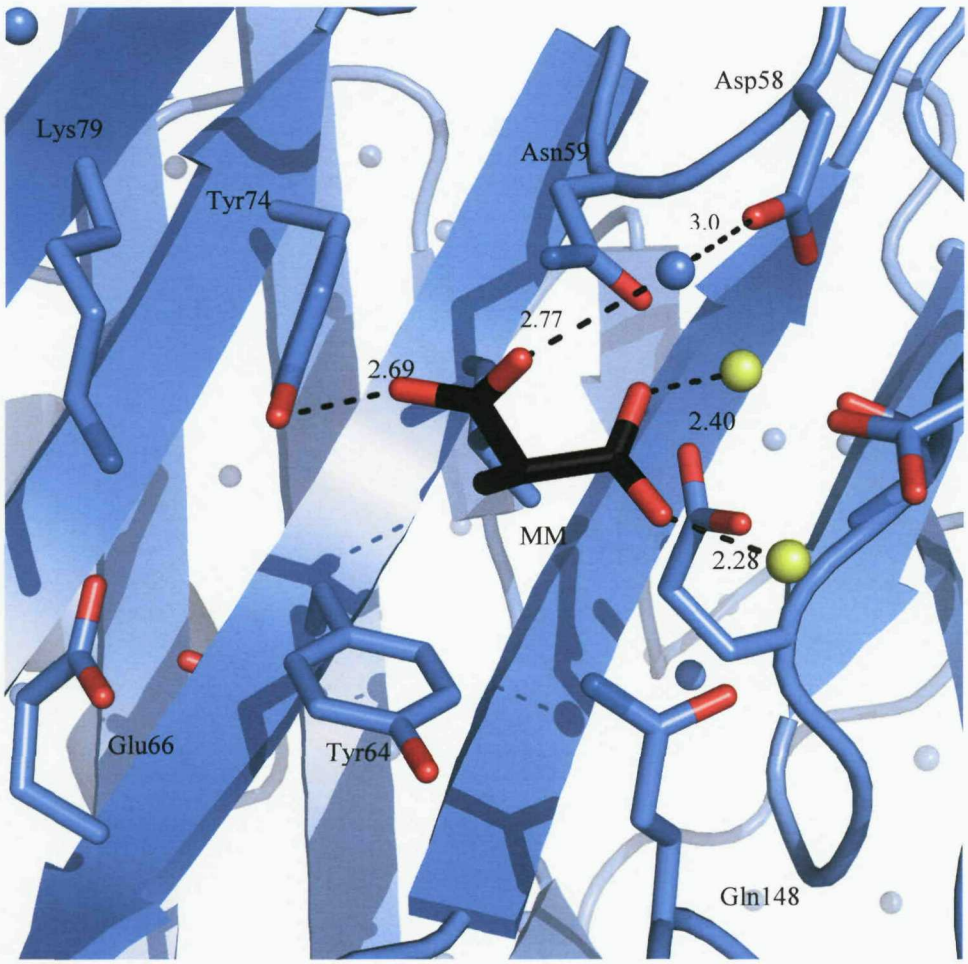

Figure 2.18 Coordination of MM in the SAP binding site. The carboxyl group of MM binds to the two calcium ions (yellow), while the methyl group points into the hydrophobic pocket. Water molecules are in blue. Figure produced in Pymol.

Interestingly, isothermal titration calorimetry data demonstrates a low affinity (Kd >1mM) for the MM/SAP interaction when compared to an affinity of 56 μm for MOβDG/SAP binding. This difference in affinity is also reflected in the ligand occupancy of the crystal form, which contains good density in only 3 out of 5 subunits. As was previously thought, the overall binding of ligands to SAP is driven primarily by the association between the highly charged calcium ions and the negatively carboxylate oxygens as well as the interaction of the methyl group with the hydrophobic pocket. However, these observations indicate that there must be other interactions of importance. The most obvious difference may be the extra hydrogen bond between Gln148 and the carboxyethylidene oxygen of MOβDG.

In the X-ray crystal structure of the SAP-PE complex, PE binds to the calcium ions via a phosphate group rather than a carboxyl group with calcium-oxygen distances of 2.4 - 2.5 Å (Figure 2.19). The amine group of the PE molecule is held in place by a hydrogen bond via a water molecule to the carboxyl group of Glu66. The average distance between the nitrogen atom of the PE molecule to the carboxylate of Glu66 is 5.4 Å, with the distance from the N to the water being 2.84 Å and from the water to the OE being 2.59 Å. Two tyrosine residues similarly to the SAP-MM structure flank the sides of the PE binding region. The amine group of PE is positioned in close proximity to the side chains of Tyr64 and Tyr74, however the distances between the amine group of PE and the hydroxyl groups of either tyrosines are too long for hydrogen bonding interactions (Figure 2.19).

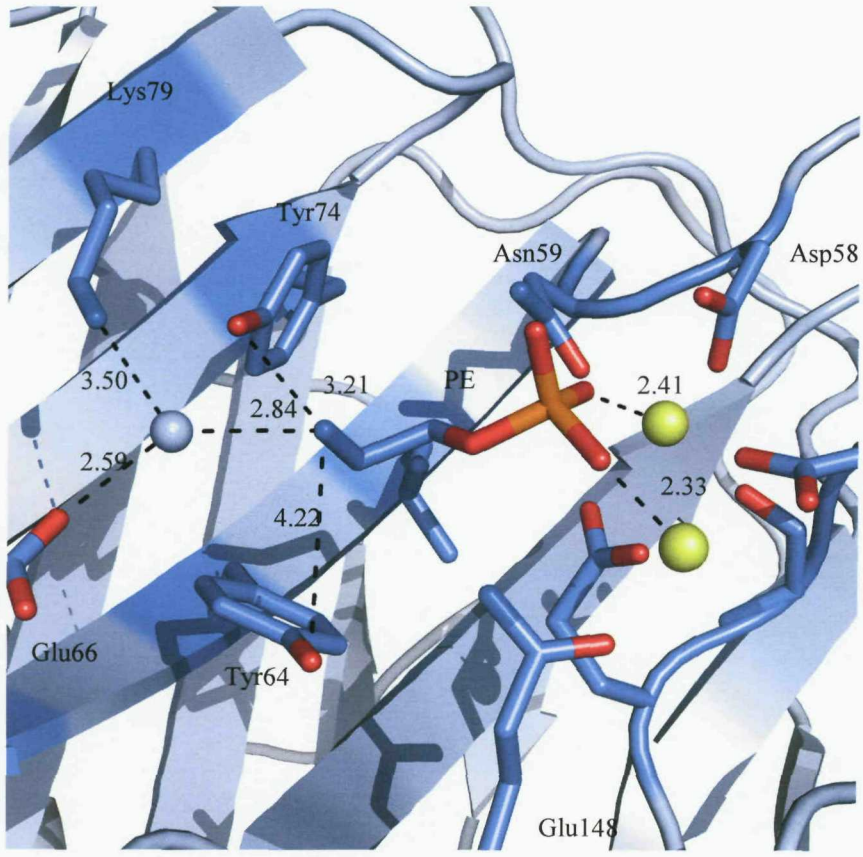

Figure 2.19 Coordination of PE in the SAP binding site. The phosphate group of PE binds to the two calcium ions (yellow), while the amine group is held in position by a hydrogen bond via a water molecule bridging to Glu66.

An α-carbon superposition of the SAP-PE complex structure with the SAP-MM structure shows that there is very little difference in the key residue side-chain positions (Figure 2.20). In the binding sites, the positions of all side chains coordinating the calcium ions is identical, whilst in the hydrophobic pocket the residues (Tyr64 and Tyr74) are shifted by 0.35 Å in the SAP-PE binding site. This movement has provided more space for the nitrogen end of PE molecule, which is held in place by a water molecule. This water molecule is able to hydrogen bond with the surrounding side-chains and appears to provide sufficient stabilisation for the PE molecule. In contrast, the MM molecule forms hydrogen bonding interactions with the hydroxyl group of Tyr74 (2.7 Å) via its second carboxyl group.

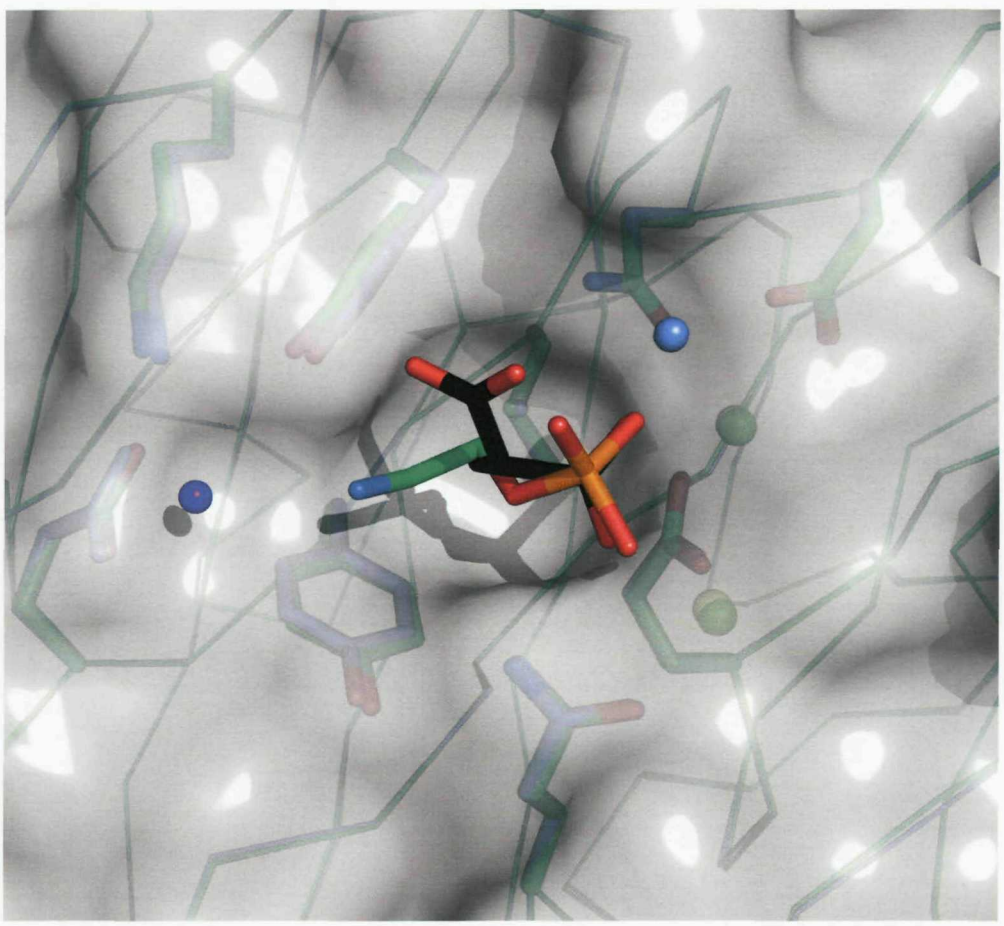

Figure 2.20 Superposition of the 1.6 Å SAP-MM (blue) with the 1.5 Å SAP-PE complex structure (green). MM is shown black and PE in green. Calcium atoms are shown in yellow for the SAP-MM structure and green for the SAP-PE structure. Water molecules are shown as blue space filling spheres.

Chapter 3

Structural Studies of Rat Pentraxins

3.1 Introduction

The two major members of the pentraxin family of plasma proteins, C-reactive protein (CRP) and serum amyloid P component (SAP), are present in the serum of all vertebrates studied to date (Pepys *et al.*, 1978; Baltz *et al.*, 1982). Pentraxin molecules from all these species share the arrangement of subunits with cyclic pentameric symmetry and the property of calcium-dependent specific ligand binding. CRP-like proteins bind to phosphocholine (PC) and pneumococcal C-polysaccharide (PnC) whereas SAP-like proteins bind carbohydrate moieties with high affinity. On the basis of these binding specificities, it has been possible to distinguish and isolate CRP-like and SAP-like pentraxins from serum of many species (Pepys *et al.*, 1978; Baltz *et al.*, 1982; Pepys & Baltz, 1983).

In the early 1980's a substantial effort was directed towards identifying, isolating and characterising the pentraxins from the rat, both because of the inherent interest in the phylogeny of this protein family and because CRP is the classical acute phase reactant in man, whilst SAP is identical with amyloid P component, a universal component of all forms of amyloid deposits. This led to the isolation of a rat serum protein that undergoes calcium-dependent binding to pneumococcal C-polysaccharide and to phosphocholine residues. By virtue of its appearance under the electron microscope, it was variously designated as rat C-reactive protein (De Beer *et al.*, 1982), phosphoryl choline-binding protein (Nagpurkar & Mookerjea, 1981) and rat serum amyloid P component (Pontet *et al.*, 1981). Later, immunochemical and biochemical tests established that the protein isolated by these three laboratories was rat CRP and not rat SAP (Taylor *et al.*, 1984).

Rat CRP, in contrast to other well studied mammalian CRP's, is a glycoprotein containing a single N-linked oligosaccharide at position Asn128 per subunit (Sambasivam *et al.*, 1993). It does not precipitate CPS and its normal serum concentration (about 300 mg/l) is over 300 times greater than that of human CRP (Taylor *et al.*, 1984). Furthermore, cysteine residues Cys208 and Cys209 positioned on an extended C-terminal region unique to rat CRP form two inter-subunit disulphide bridges. Non-reducing SDS-PAGE gels show two bands of 25 and 50 kDa, but the pattern collapses to a single 25 kDa band in reducing

conditions (DeBeer *et al.*, 1982; Rassouli *et al.*, 1992). This raised the possibility that rat CRP is composed of five monomeric subunits, two of which exist as a covalent dimer while the remaining three exist as monomers.

Since important biological functions of proteins are often conserved among species, studies have investigated the capability of rat CRP to activate complement. Remarkably, in contrast to human CRP, rat CRP has been reported to be unable to activate neither human or rat complement (DeBerr *et al.*, 1982; Griselli *et al.*, 1999), despite the fact that human and rat CRP share 70 % sequence identity (Figure 3.1)(Taylor *et al.*, 1994). The significance of these differences remains uncertain because the physiological functions of CRP are unclear and controversial. However, it is of considerable interest to study differences in the phylogeny of this protein family as these differences provide the basis for *in vivo* animal models of the pathogenic role of human CRP in stroke and myocardial infarction.

Although the crystallisation and preliminary X-ray analysis of rat CRP was reported in 1994 by Hopkins *et al.*, the structure remains undetermined.

Rat SAP, like SAP of other species, is a glycoprotein and pentameric. The levels of SAP in rat serum are similar to levels observed in man and it does not behave as an acute phase reactant (De Beer *et al.*, 1982). In this respect, it resembles human SAP but differs from murine SAP, which is a major acute phase reactant (Pepys *et al.*, 1979). Interestingly, it has been noted that rats, unlike mice and man, do not develop amyloidosis (Dunn, 1967; Jakob, 1971; Green, 1974). The presence of SAP in amyloid deposits in all types of amyloidosis suggests a role in the pathogenesis of amyloidosis. In order to increase our understanding of the development, progression and pathogenesis of SAP in amyloidosis, it is of interest to investigate the differences between rat SAP and SAP in these amyloid-susceptible species. The current study describes the determination of the three dimensional structure of rat SAP in complex with PC and compares this data with human SAP.

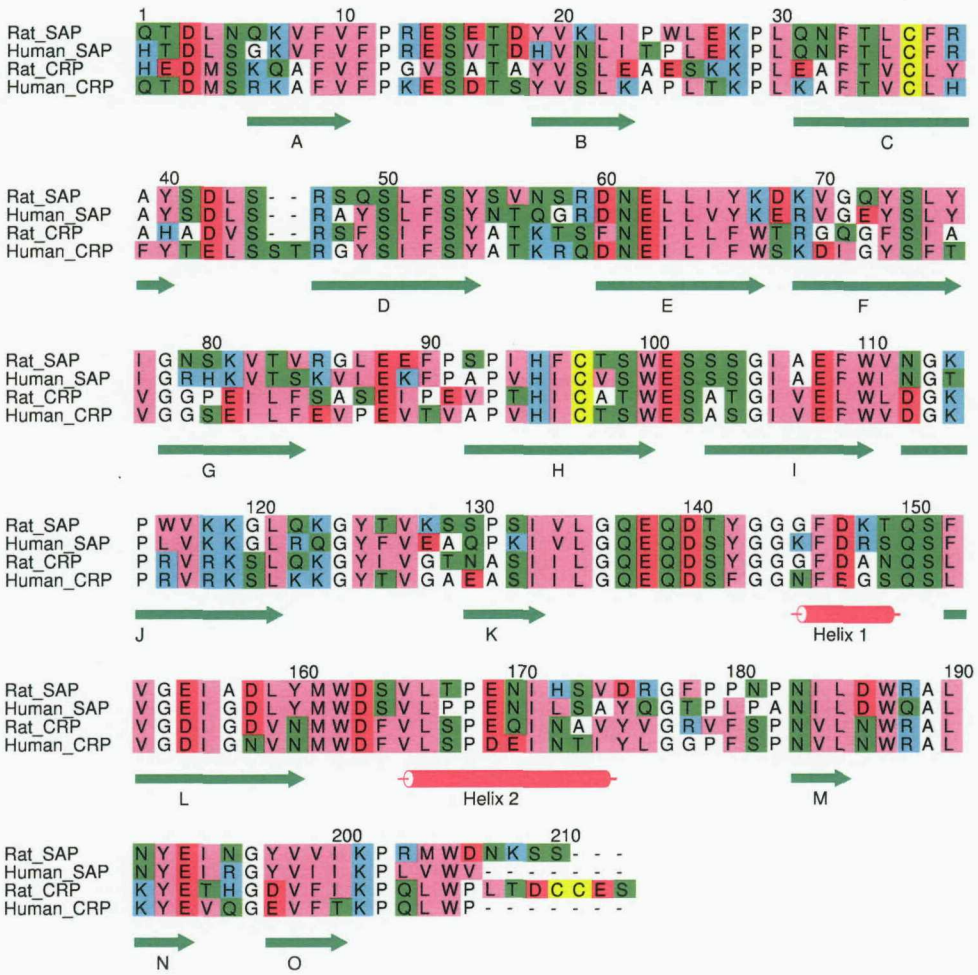

Figure 3.1 Sequence alignment of SAP and CRP from *Rattus norvegicus* (rat) and *Homo sapiens* (human). The rat SAP has 71.1 % sequence identity with human SAP and only 49.5 % identity with human CRP. The amino acids are coloured according to the scheme: cyan=basic; red=acidic; green=neutral-polar; pink=bulky hydrophobic; white=Gly, Ala and Pro; and yellow=Cys. The secondary structure elements of human SAP are indicated below the alignment.

3.2 Methods and Results

3.2.1 Rat CRP

3.2.1.1 Purification and Crystallisation of Rat CRP

Rat CRP was purified in the laboratory of Professor Mark Pepys, UCL, London. A typical preparation of rat CRP from normal rat serum entails calcium-dependent affinity chromatography on PC-Sepharose (Hawkins *et al.*, 1991) equilibrated in TC buffer. The absorbed protein was eluted using TC buffer containing 1 mM PC. HiTrap protein G 5-ml affinity column (GE, Healthcare) was used to remove contaminating rat IgG. The protein was subjected to a second cycle of calcium-dependent binding to PC-Sepharose where TE buffer was used to elute rat CRP (personal communication P. Mangione).

Various attempts to crystallise rat CRP were made using previously determined crystallisation conditions published by Hopkins *et al.*, 1994 (5 % PEG 4000, 100 mM NaCl, 10 mM $CaCl_2$, 25 mM MES pH 6.6) and novel conditions. Crystallisation was performed using the hanging-drop vapour diffusion method at room temperature in 4 µl hanging drops.

Two distinct crystal forms were grown in the presence of calcium and phosphocholine with a protein solution at 31 mg/ml. Crystal form I was grown upon equilibration of protein solution against reservoir buffer containing 100 mM MES pH 6.5, 18 % PEG 4000, 100 mM $CaCl_2$, 140 mM NaCl and 100 fold excess of PC (Figure 3.2). Small crystals (100 x 80 x 80 µm) appeared after 2 months. These crystals had the appearance of small elongated blocks. Crystal form II was grown in 17 % PEG 2000, 100 mM Tris pH 8.2-8.5, 100 mM $CaCl_2$, 100 mM NaCl and 5 % glycerol in the presence of 100 fold excess of PC. These crystals were prismatic in their appearance (Figure 3.3).

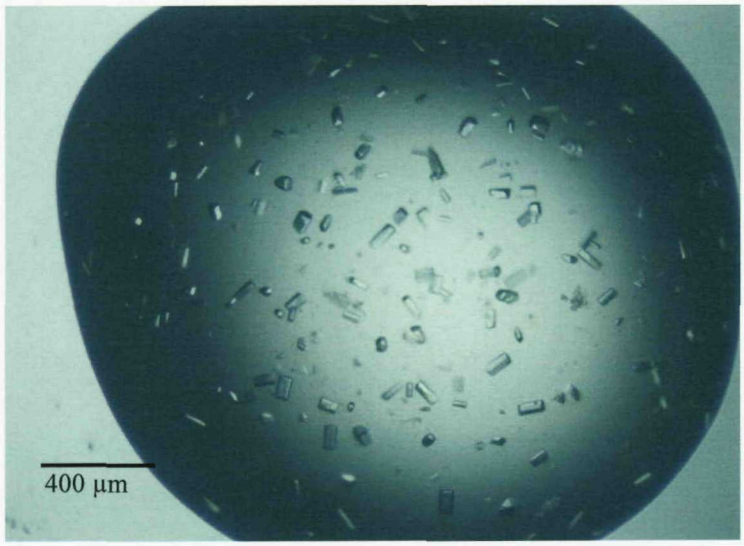

Figure 3.2 Crystals of rat CRP in complex with PC. The crystals were grown in the presence of MES buffer (100 mM MES pH 6.5, 18 % PEG 4000, 100 mM $CaCl_2$, 140 mM NaCl and 100 fold excess PC).

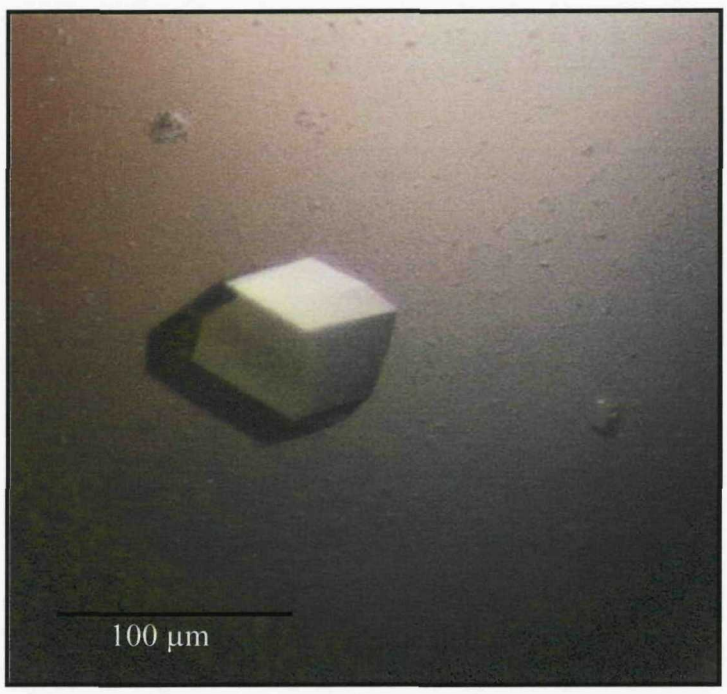

Figure 3.3 A rat CRP crystal in complex with PC. The crystal was grown in Tris buffer (17 % PEG 2000, 100 mM Tris pH 8.2-8.5, 100 mM $CaCl_2$, 100 mM NaCl, 5 % glycerol and 100 fold excess of PC).

3.2.1.2 Cryo-Crystallography and Data Collection from Crystal Form I and II

Several diffraction images were collected from crystals of rat CRP in complex with PC at cryogenic temperatures at the ESRF in Grenoble on an ADSC Quantum–4 CCD detector. The data faded beyond 3.5 Å resolution and was very smeary and quickly deteriorated until no diffraction was observed (Figure 3.4). To date, attempts using different freezing techniques and cryo-protectants have proved unsuccessful.

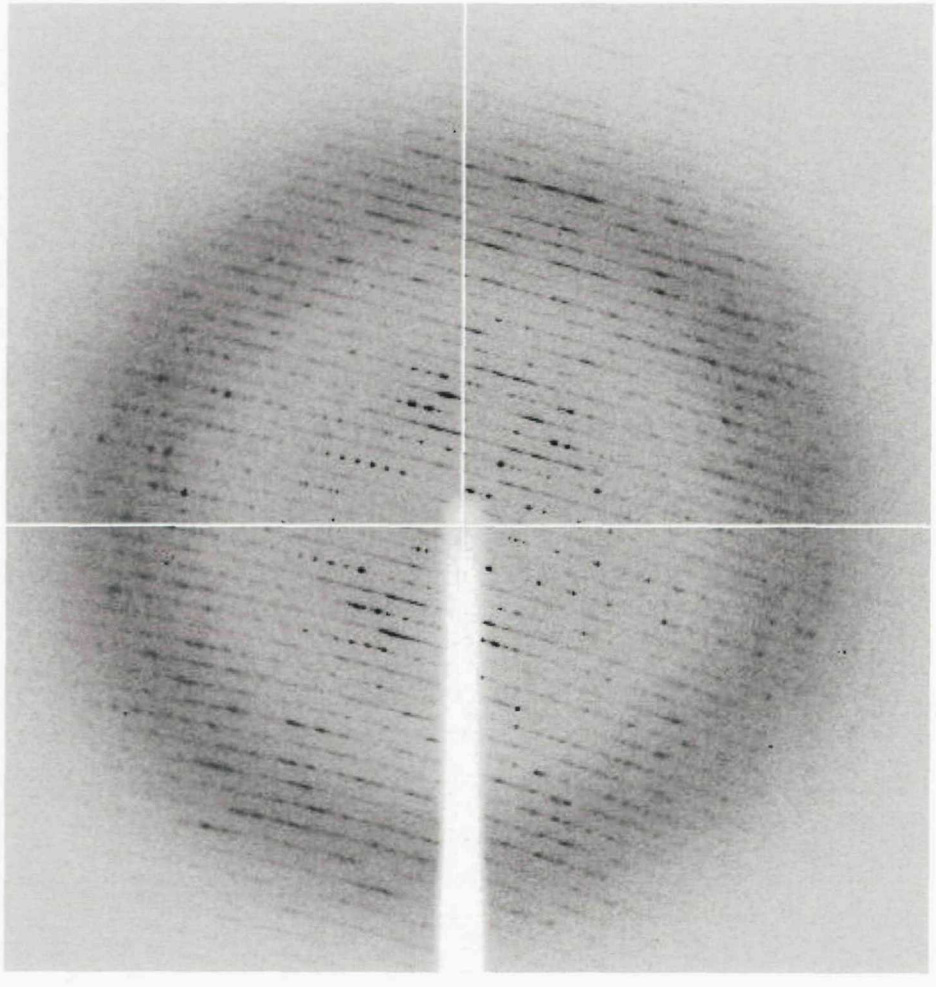

Figure 3.4 A 1° oscillation diffraction image collected from a rat CRP crystal at the ESRF, Grenoble, France.

3.2.2 Rat SAP

3.2.2.1 Purification and Crystallisation of Rat SAP

Rat SAP was purified in Professor Mark Pepys laboratory using a modified version of the purification protocol described by De Beer *et al.* (1982). Rat SAP was isolated from normal rat serum by calcium-dependent affinity chromatography on PE-Sepharose (Hawkins *et al.*, 1991). The TE eluted rat SAP was subjected to further purification including HiTrap protein G 5-ml affinity column (GE, Healthcare) to remove traces of rat IgG and solid-phase immuno-absorption with anti-(rat CRP) antibody to remove rat CRP from the rat SAP preparation. A second cycle of calcium-dependent binding to PE-Sepharose was required to concentrate the rat SAP protein and finally eluted in TE buffer (personal communication P. Mangione).

All SAP structures with the exception of Limulus SAP have been determined from crystals grown in some form of PEG at a pH range 4-8 in the presence of calcium. Therefore, the strategy for crystallising rat SAP involved screening around these conditions. Crystallisation was performed using the hanging-drop vapour diffusion method at room temperature (4 µl drops). Crystals were grown upon equilibration of protein solution (28 mg/ml) against reservoir buffer containing 17 % PEG 550, 60 mM Tris pH 8.0, 140 mM NaCl, 10 mM $CaCl_2$ in the presence of a 100-fold molar excess of phosphocholine (pH adjusted). Crystals appeared after 1 week and grew to dimensions of 0.5 × 0.4 × 0.4 mm after three weeks. These crystals had the appearance of prismatic blocks and were flash cooled in liquid nitrogen without a cryo-protectant prior to data collection (Figure 3.5).

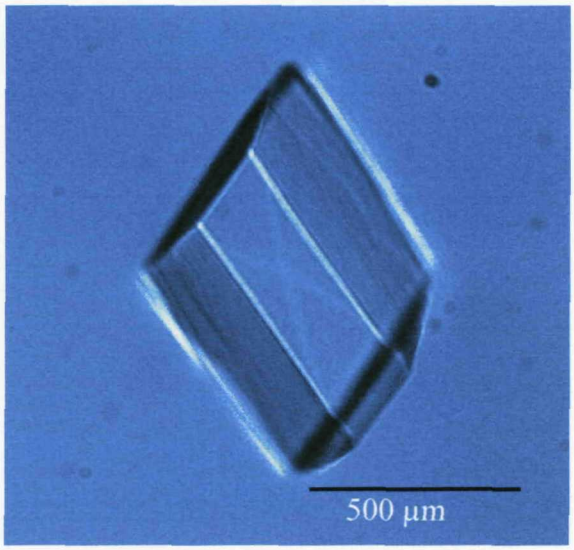

Figure 3.5 Crystal of rat SAP in complex with PC. The crystal was grown in 60 mM Tris pH 8.0, 140 mM NaCl, 10 mM $CaCl_2$, 17 % PEG 550 in the presence of 100-fold molar excess of pH-adjusted PC.

3.2.2.2 Data Collection and Processing of Rat SAP to 2.2 Å

X-ray diffraction data from the rat SAP crystal were collected to 2.2 Å on the beamline ID 14.1 at the ESRF in Grenoble on an ADSC Quantum-4 CCD detector. A data set of 600 0.3° oscillation frames was recorded with an exposure time of 1 second per frame and a crystal to detector distance of 180.93 mm (Figure 3.6).

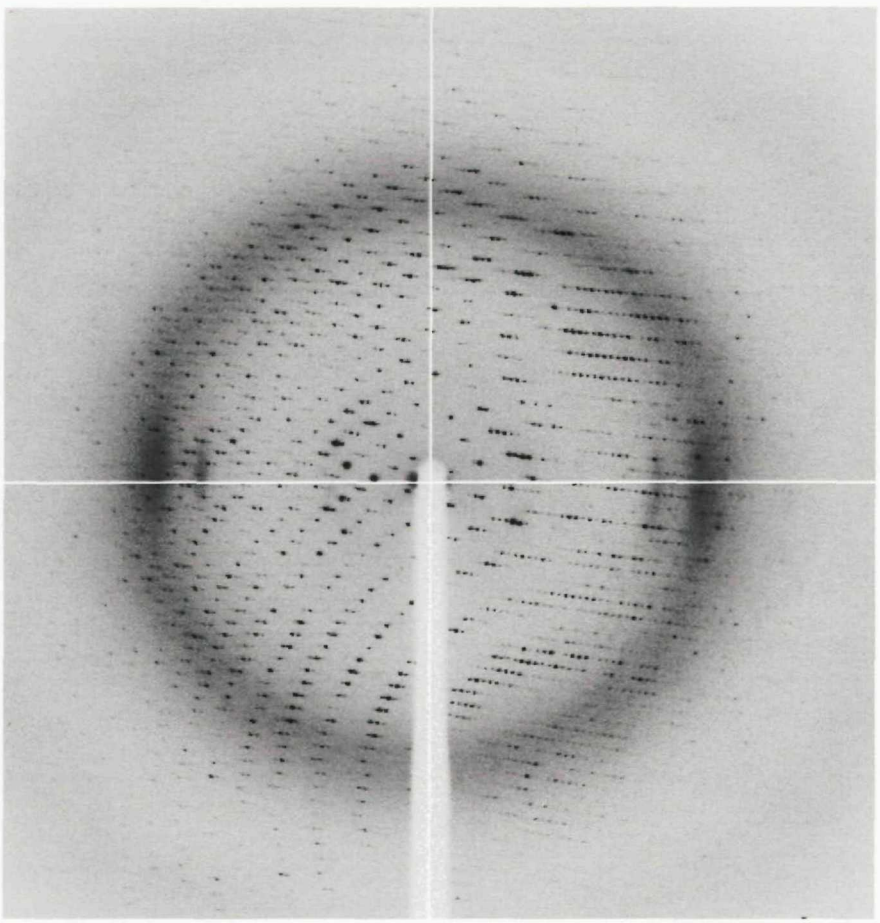

Figure 3.6 A 0.3° oscillation diffraction image collected from the rat SAP crystal at the ESRF, Grenoble, France.

Data processing of the raw data was carried out using MOSFLM. Auto-indexing of the 2.2 Å resolution data from the rat SAP crystal indicated that the crystal has unit cell dimensions of a = 111.2 Å, b = 155.0 Å, c = 144.7 Å, $\alpha = \beta = \gamma = 90°$ and that the crystal belonged to the orthorhombic space group C222 ($C222_1$) or monoclinic space group C2. As a result, diffraction data were processed initially in C222 and C2 space groups (Table 3.1).

Penalty	Lattice	a	b	c	α	β	γ	Possible space groups
87	mP	95.5	95.31	144.79	90	90	108.7	$P2,P2_1$
87	oP	95.31	95.5	144.79	90	90	108.7	$P222,P222_1,P2_12_12$ $P2_12_12_1$
87	mP	95.31	95.5	144.79	90	90	108.7	$P2,P2_1$
1	mC	155.01	111.26	144.79	90	90	90.1	C2
1	oC	111.26	155.01	144.79	90	90	89.9	$C222,C222_1$
1	mC	111.26	155.01	144.79	90	90	89.9	C2
0	mP	95.31	144.79	95.5	90	108.7	90	$P2,P2_1$
0	aP	95.31	95.5	144.79	90	90	71.3	P1
0	aP	95.31	95.5	144.79	90	90	108.7	P1

Table 3.1 Penalty table for the rat SAP data generated by MOSFLM. This table shows the possible unit cell dimensions and space groups for the rat SAP data.

Following post-refinement and integration in MOSFLM, the data was scaled and merged using the program SCALA from the CCP4 suite. The scaled and merged intensities generated from SCALA were converted to structure factor amplitudes using TRUNCATE. However, the final processing statistics for the data (52.88 - 2.2 Å) processed in C222 and C2 were a poor representation of the quality of diffraction with an overall R-merge of 23 %. As a consequence, the data was reprocessed in P2 as previously described. This data reprocessed in the space group P2 gave an R-merge of 9.0 % implying that the crystal belonged to the primitive monoclinic space group. The processed data was displayed as pseudo-procession images using HKLVIEW. The choice of space group was confirmed after analysis of the data on plane 0*kl* revealed the presence of a screw axis along *k*, which is a characteristic of the $P2_1$ space group (Figure 3.7 & Figure 3.8).

Figure 3.7 Pseudo-precession camera image of the rat SAP diffraction data generated using HKLVIEW in P2 (The 0*kl* plane). Systematic absences are observed along the *k* axis indicating the correct space group $P2_1$.

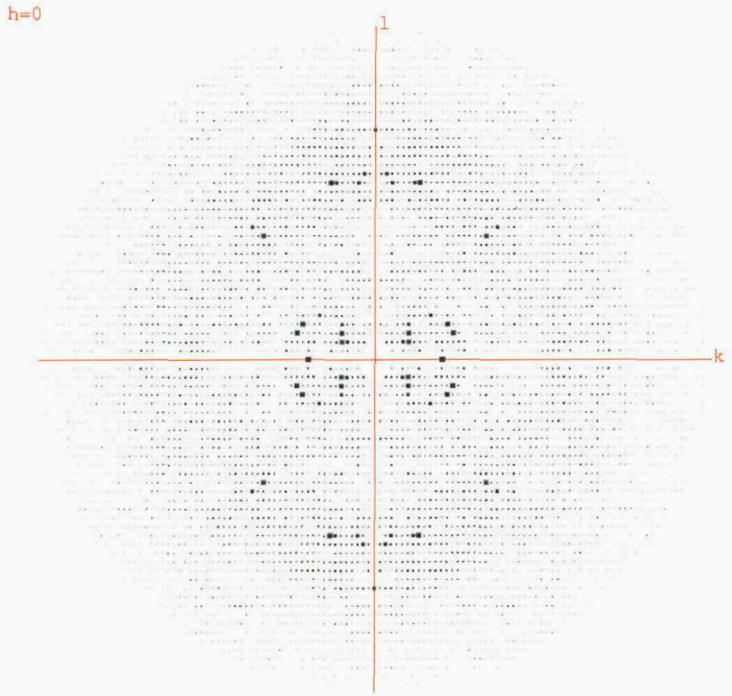

Figure 3.8 Pseudo-precession camera image of the rat SAP diffraction data generated using HKLVIEW in P2 (The 0*kl* plane).

The data was subsequently reprocessed in the space group $P2_1$ with the unit cell dimensions of a = 95.27 Å, b = 144.71 Å, c = 95.49 Å, $\alpha = \gamma = 90°$, $\beta = 108.64°$. The data was scaled, merged and this provided better statistics with an overall R-merge of 7.5 % (Table 3.2).

Space Group	$P2_1$
Unit Cell (Å) (°)	a = 95.27, b = 144.71, c = 95.49 $\alpha = \gamma = 90.0$ $\beta = 108.64$
Resolution range (Å)	52.88 – 2.2 (2.3-2.2)
Measured reflections	363628 (39588)
Unique Reflections	114883 (13712)
Multiplicity	3.2 (2.9)
Completeness (%)	92.9 (76.2)
R-merge (%)	7.5 (31.3)
(I)/sd(I)	12.7 (3.9)

Table 3.2 A summary of the data processing statistics for the rat SAP crystal. Figures in parentheses apply to data in the highest resolution shell.

3.2.2.3 Molecular Replacement of Rat SAP

Initial phases for rat SAP were obtained by molecular replacement using MOLREP. Due to the high sequence identity between human SAP and rat SAP (71 %), a single pentamer from the crystal structure of human SAP (accession code 1SAC; Emsley *et al.*, 1994) with the calcium ions and sugar residues omitted was used as a search model. The solvent content of the unit cell was estimated to be 77 % for a single SAP pentamer in the asymmetric unit and 54 % for two pentamers in the asymmetric unit (Matthews, 1968). As most protein crystals have a solvent content of approximately 50 %, it seemed most likely that the asymmetric unit contained two SAP pentamers.

The cross rotation search was performed using reflections within the resolution range 52.88 to 3.0 Å and yielded 10 significant solutions with a peak height of approximately 10-11 σ (Table 3.3). These ten solutions corresponded to the ten orientations of the rat SAP protomers (2 pentamers) within the target asymmetric unit as implied by the solvent calculations.

Peak no.	α (°)	β (°)	γ (°)	Rf/σ
1	1.87	26.01	153.16	11.03
2	176.47	62.62	151.78	10.98
3	358.20	62.09	145.89	10.83
4	192.93	26.97	140.79	10.76
5	173.80	82.05	332.77	10.70
6	4.93	9.53	319.91	10.64
7	0.00	45.51	334.54	10.55
8	354.91	81.29	327.37	10.49
9	185.90	46.03	326.65	10.43
10	154.75	10.80	350.98	10.22
11	175.79	78.37	150.89	4.50
12	358.20	28.54	337.34	4.45
13	354.87	65.36	328.50	4.44
14	167.39	45.43	336.51	4.40
15	165.84	7.81	158.65	4.40

Table 3.3 Cross-rotation function peaks calculated in MOLREP for the rat SAP data using human SAP as the search model.

The position of each rat SAP pentamer molecule within the asymmetric unit was determined following a translation search calculated in space group $P2_1$ (Table 3.4). The second highest peak from the cross rotation function ($\alpha = 176.47°$, $\beta = 62.62°$, $\gamma = 151.78°$) yielded a translation peak of 11.21 σ (R-factor of 48.3 %). The position of the first molecule corresponded to fractional co-ordinate shifts of X = 0.244, Y = 0.0 and Z = 0.137. The translation search was subsequently repeated with the position of the first molecule fixed, since both molecules within the asymmetric unit must be positioned with respect to the same origin. The position of the second pentamer with respect to the first corresponded to fractional shifts of X = 0.744, Y = 0.261 and Z = 0.254 (peak number 1 from table 3.5, 34.39 σ).

Peak no.	X	Y	Z	Rf/σ	Rfac
1	0.143	0	0.365	12.03	48.8
2	0.244	0	0.254	11.21	48.3
3	0.359	0	0.134	12.17	48.7
4	0.255	0	0.244	11.91	48.8
5	0.861	0	0.137	12.37	48.5
6	0.242	0	0.256	10.46	49.4
7	0.255	0	0.246	10.40	49.7
8	0.244	0	0.257	10.41	49.1
9	0.643	0	0.367	11.81	48.8
10	0.360	0	0.135	11.93	48.6
11	0.360	0	0.171	2.85	53.4
12	0.139	0	0.33	2.47	53.4
13	0.328	0	0.162	2.37	53.4
14	0.167	0	0.237	2.12	53.6
15	0.856	0	0.170	2.84	53.3

Table 3.4 The fifteen highest translation function peaks calculated in space group $P2_1$ using the cross rotation function solutions.

Peak no.	X	Y	Z	Rf/σ	Rfac
1	0.744	0.261	0.254	34.39	42.6
2	0.255	0.760	0.744	33.75	43.1
3	0.744	0.261	0.257	31.55	43.5
4	0.742	0.261	0.256	31.34	44.0
5	0.255	0.760	0.746	31.06	44.3
6	0.644	0.253	0.364	14.13	55.0
7	0.360	0.246	0.635	13.93	55.1
8	0.359	0.246	0.634	14.31	56.3
9	0.643	0.254	0.366	14.00	56.1
10	0.895	0.249	0.009	4.11	51.0

Table 3.5 The ten highest translation function peaks calculated in space group $P2_1$ after fixing the position of the first molecule.

The initial R-factor of the model once the two pentamers had been placed at the correct positions within the unit cell was 42.6 %. In order to check the molecular replacement solution, crystal packing was visualized using Pymol (Delano, 2002).

The diagram demonstrated the feasibility of the present solution and confirmed the presence of two rat SAP pentamers in the asymmetric unit (Figure 3.9). Therefore, it was decided to proceed with refinement after applying the rotation and translational parameters to the model.

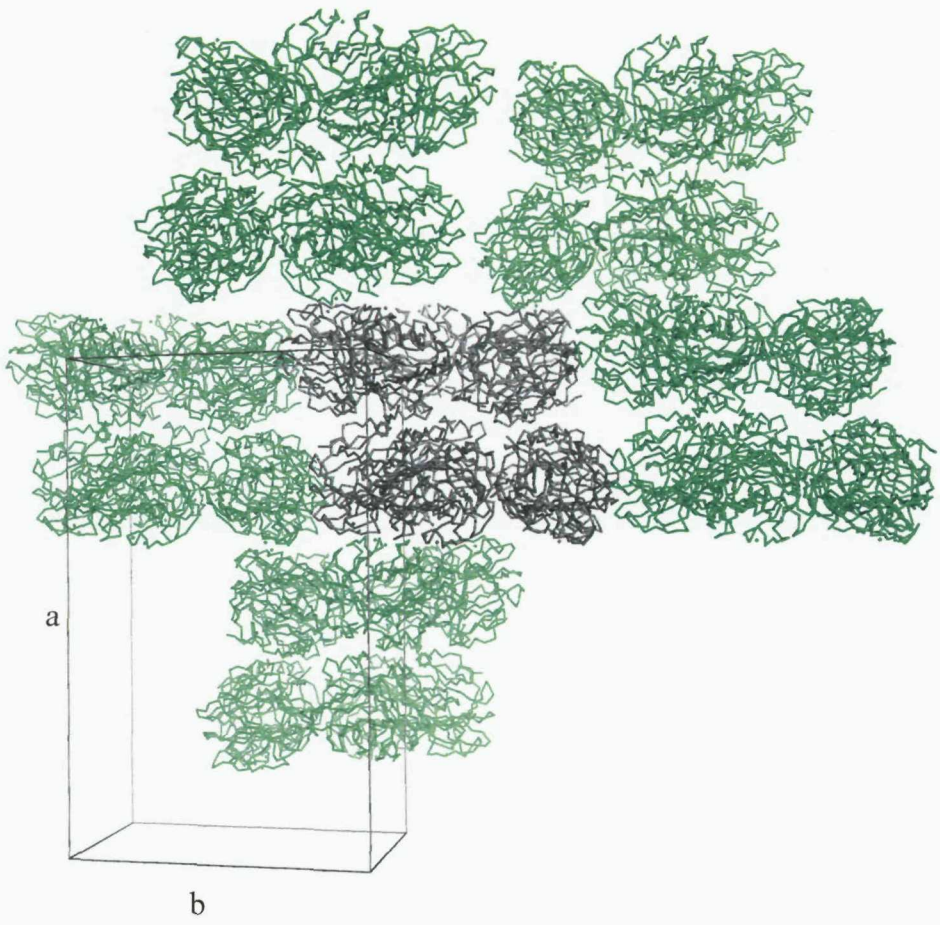

Figure 3.9 Crystal packing of rat SAP in complex with PC (Pymol). The rat SAP PC crystal crystallises in the primitive monoclinic space group $P2_1$ (a = 95.27 Å, b = 144.71 Å, c = 95.49 Å, $\alpha = \gamma = 90°$, $\beta = 108.64°$ with two pentamers in the asymmetric unit (shown in grey). Symmetry related pentamers are shown in green.

3.2.2.4 Refinement and Model Building of Rat SAP at 2.2 Å

The model was refined using the CNS software suite (Crystallography & NMR Systems, Brunger *et al.*, 1998). CNS uses the maximum likelihood function, which is a generalised statistical framework for estimating the parameters of a model on the basis of observations (Bricogne, 1997; Sivia, 1996). This approach differs from least squares in that maximum likelihood can accommodate observations with uncertainties of arbitrary character and model parameters whose values are also expected to have such uncertainties. In addition, the CNS suite provides a simulated annealing protocol, which allows the model to cross energy barriers, thus avoiding the problem of the refinement becoming stuck in a local minimum. Simulated annealing uses either torsion angle (constraints) or Cartesian (restrained) molecular dynamics and involves simulating the heating of all of the protein atoms to cross high barriers separating local minima followed by gradual cooling until all the atoms are in their lowest energy state. The energy of the system can then be minimised using positional refinement and then the B-factors can be refined.

In order to refine the model in CNS, the reflection file was converted into CNS format using the Uppsala software program DATAMAN (Kleywegt & Jones, 1996). An R-free set was selected in thin resolution shells to minimise the bias due to non-crystallographic symmetry. Non-crystallographic symmetry is defined as those symmetry operators occurring between two or more identical subunits within the asymmetric unit. Since there is more than one subunit present in the asymmetric unit, full non-crystallographic symmetry (NCS) restraints were imposed on the ten rat SAP protomers in the first few rounds of refinement, thus improving the observation to parameter ratio. The first round of refinement consisted of rigid body refinement, simulated annealing (slow cool from 5000 to 500 K in 25 K decrements) and grouped B-factor refinement with full NCS restraints.

Rigid body refinement reduced the R-factor from 42.6 to 37.5 % (R-free = 38.2 %). Following simulated annealing and grouped B-factor refinement, the R-factor further was further reduced to 30.4 % (R-free = 33.5 %). After the initial round of

refinement, the resulting model was used to calculate sigmaA weighted $2F_o$-F_c and F_o-F_c electron density maps that were subjected to ten fold symmetry averaging. The maps were calculated within CNS and converted into CCP4 format using the Uppsala software program MAPMAN (Kleywegt & Jones, 1996). The maps generated by MAPMAN were analysed and manipulated using the graphics package COOT (Emsley & Cowtan, 2004). Analysis of the maps indicated well-defined F_o-F_c density for the twenty calcium ions at the binding sites, ten phosphocholine molecules and ten sugar molecules. In addition, difference density was clearly visible for residues corresponding to rat SAP (Figure 3.10), thus validating the molecular replacement solution.

During model building, calcium ions were added and wherever possible rat SAP side chains were built into electron density. This included manually building four additional residues at the C-terminal end of rat SAP.

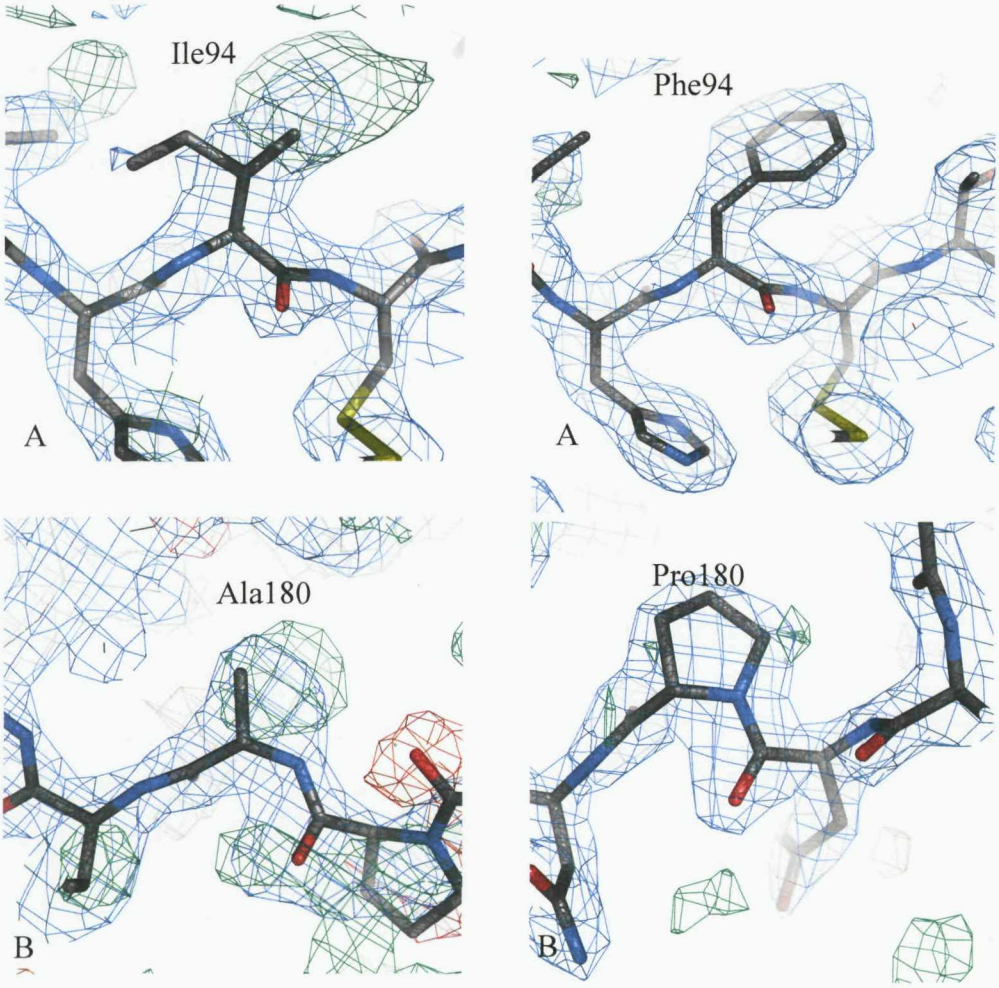

Figure 3.10 F_o-F_c electron density contoured at 1.5 σ showing electron density for rat SAP residues. Diagram (A, left) shows difference density (green) for residue 94, which is phenylalanine in rat SAP but isoleucine in the human SAP search model. Diagram (A, right) shows the phenylalanine residue fitted into electron density. Diagram B (left) shows positive density for residue 180 (green), which is proline in rat SAP but isoleucine in the model. Diagram B (right) shows the proline residue fitted into electron density.

The second round of refinement consisted of simulated annealing (slow cool from 5000 to 500 K in 25 K decrements) and grouped B-factor refinement with full NCS restraints. This reduced the R-factor and R-free to 28.1 % and 29.9 % respectively.

Analysis of the maps revealed good F_o-F_c density for the ten PC molecules, which were built into the structure. During the subsequent round of refinement (minimisation and grouped B factor), NCS restraints were relaxed to a medium value on each of the protein subunits. This further decreased the R-factor to 25.7 % (R-free = 28.5 %). The examination of subsequent maps revealed well defined F_o-F_c density for a sugar molecule attached to Asn32 in each of the ten subunits, which were built into the structure (Figure 3.11).

During consecutive rounds of refinement (minimisation, grouped B factor and individual B factor), NCS restraints were relaxed to the minimal value on each of the protein subunits decreasing the R-factor to 23.1 % (R-free = 26.2 %). During the final stages of model building, water molecules were added to the structure and refined. The R-factor with data to 2.2 Å was 20.7 % (R-free = 25.0 %). The refinement statistics for the model are listed in Table 3.6.

Resolution range (Å)	25 – 2.2
Number of reflections in the working set	111109
Number of reflections in the test set	3465
R-factor (%)	20.7
R-free (%)	25.0
Rms bond length deviation (Å)	0.008
Rms bond angle deviation (°)	1.210

Table 3.6 Refinement statistics for the rat SAP structure in complex with PC.

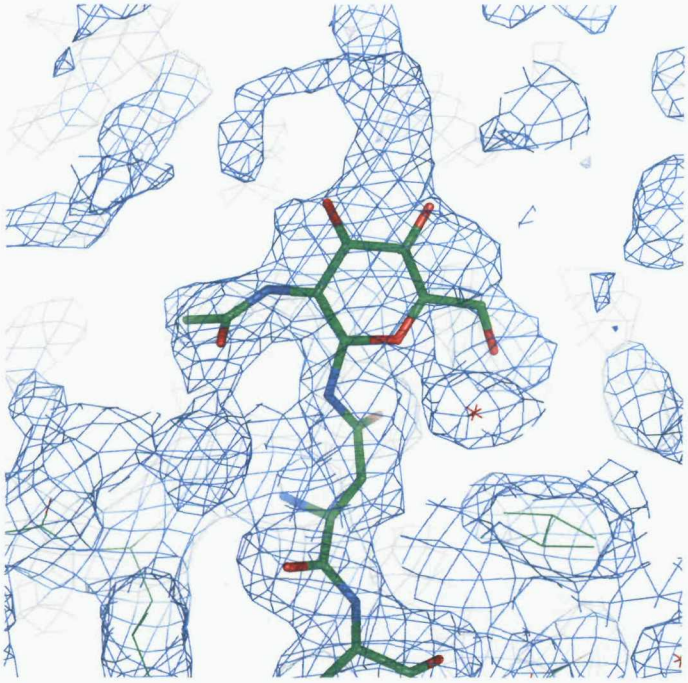

Figure 3.11 $2F_o$-F_c electron density contoured at 1.2 σ for a sugar molecule linked to Asn32.

3.3 Structure of the Rat SAP in Complex with PC

The X-ray crystal structure of the rat SAP-PC complex at 2.2 Å consists of five subunits, which are arranged in pentameric radial symmetry (Figure 3.12). Each subunit is comprised of anti-parallel β strands arranged in two sheets with a jellyroll topology (Figure 3.13). In addition to the β strands, a long α-helix is positioned on the surface of the protomer. All residues involved in the secondary structure elements of rat SAP from the N- to the C- terminus are listed in table 3.7.

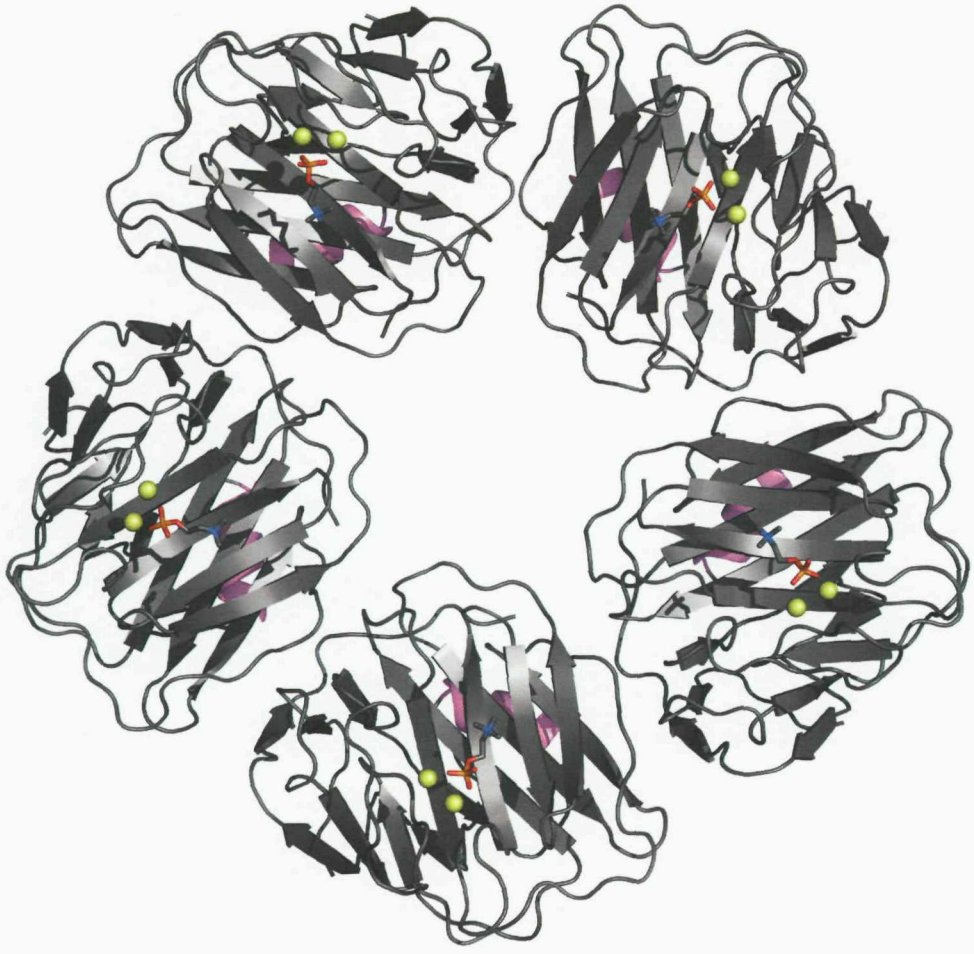

Figure 3.12 Structure of the rat SAP pentamer in complex with PC. Cartoon representation of the pentameric structure of rat SAP viewed down the non-crystallographic five-fold symmetry axis.

The jellyroll is composed of strands ABCDKLMNO and has a β-meander, made up of strands EFGHIJ, added to one end. Strands B, K, D, E, F and G make up the top sheet (Face B), which includes the residues involved in calcium binding. Strands L, C, H and I make up the lower sheet (Face A). It is on this side of the jellyroll, that a short α-helical stretch is located just above the disulphide bridge Cys36 – Cys95. The helix encompasses ten residues (165 – 174) and interacts with the hydrophobic side chains on the surface of the β-pleated sheet with Pro166, Ile169 and Ala172. This leaves Glu167, Ser171 and Glu174 extending into the solvent.

A second α-helix (residues 145-149) forms part of the calcium binding site on the opposite face of the protein. This calcium binding site has two calcium ions bound 4 Å apart and is the site of ligand binding. The remainder of the rat SAP structure is made up of non-repetitive secondary structure and loop regions.

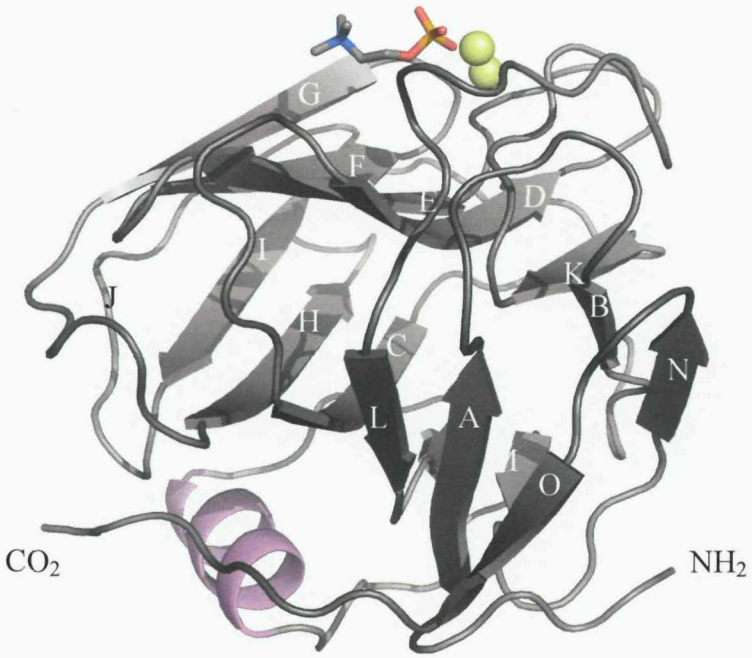

Figure 3.13 Structure of the rat SAP protomer. Cartoon representation of a rat SAP protomer seen from the side. B-strands are labelled according to the jelly roll topology. The α-helix is pink and the two calcium ions are represented as yellow spheres. The PC molecule is represented by sticks (oxygen and nitrogen atoms are shown in red and blue respectively. NH_2 and CO_2 indicate the N- and C- terminal ends of the protomer

Strand/helix	Residues
Strand A	7-11
Strand B	19-22
Strand C	32-40
Strand D	47-54
Strand E	57-67
Strand F	70-75
Strand G	78-83
Strand H	92-99
Strand I	104-109
Strand J	112-118
Strand K	130-134
Alpha helix	145-149
Strand L	153-160
Alpha helix	165-174
Strand M	183-184
Strand N	190-194
Strand O	197-200

Table 3.7 Residues involved in secondary structure elements of rat SAP (listed in order from N- to C-terminus).

The structure of the rat SAP-PC complex at 2.2 Å shows satisfactory stereochemistry with 99.8 % of residues in the most favoured regions of the Ramachandran plot, 0.2 % in the additional allowed regions and 0 % in the disallowed regions (Figure 3.14). The generously allowed residues consist of Asn77 from several subunits, located on a type 1 β-turn between strands F and G. Similar conformations have been observed for the equivalent Arg77 residues in previous SAP structures (Purvis, 2002 & Kolstoe, 2005).

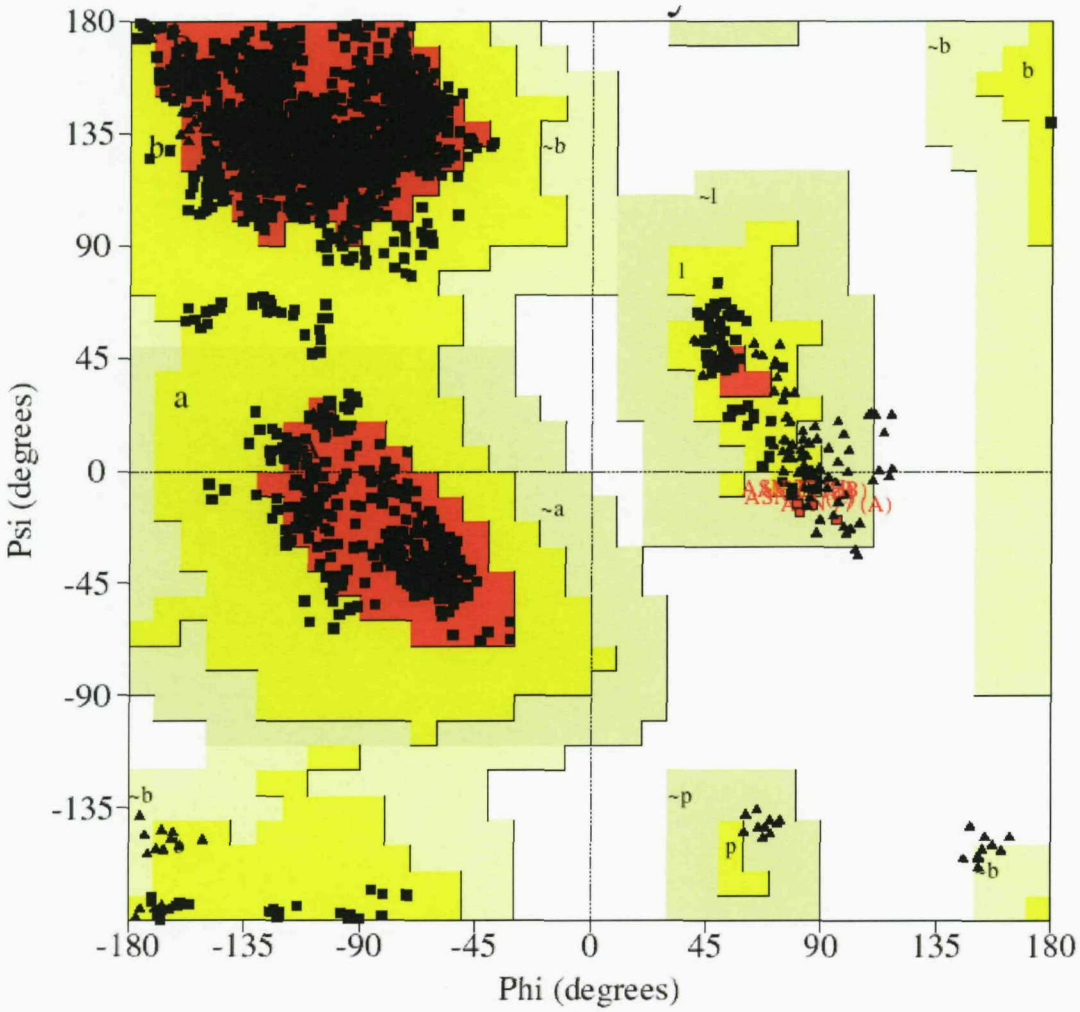

Figure 3.14 Ramachandran plot for the rat SAP structure in complex with PC.

An alignment of the temperature factors for the ten SAP subunits demonstrates a similar B-factor distribution across all subunits (Figure 3.15). The overall B-factor value was 19.22 $Å^2$. The biggest difference in B-factor distribution across the ten pentamers is observed between residues 20–30. Examination of this region reveals

very little electron density surrounding these residues, making model building difficult. These residues constitute a loop region linking β strands B and C, which protrudes from the surface of the protomer. Since this is the most far-reaching of loop regions and is therefore relatively flexible compared to those residues buried in the core of the protomer, increased B-factor values are expected. Subunits D and F have considerably lower B-factor values across this region when compared to the other 8 subunits and this is attributed to crystal packing contacts, stabilising the mobility of the loop region. Subunits A and H have considerably larger B-factor values when compared to the other subunits as they make considerably less crystal contacts thereby explaining their greater mobility and increased B-factor values.

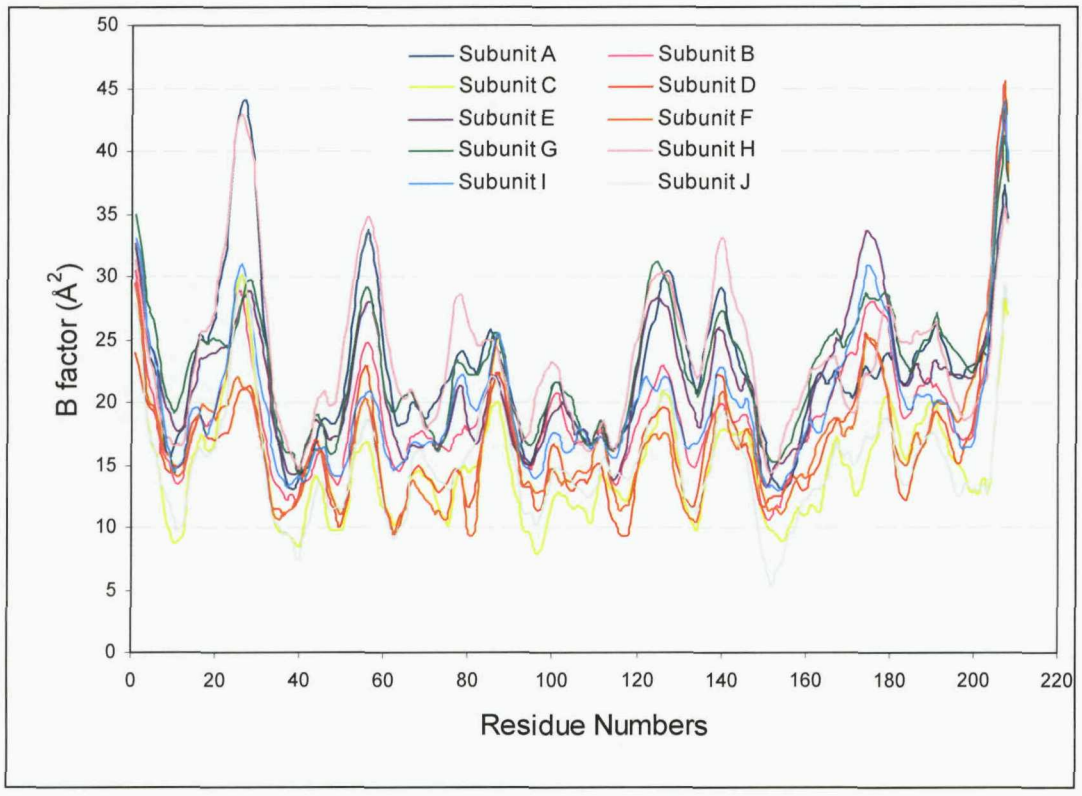

Figure 3.15 Comparison of the average isotropic B-factors for main chain atoms of the ten subunits.

A comparative alignment of the C_α atom positions between all ten SAP protomers reveals remarkable similarity with the C_α rms fit of 0.33 Å (Figure 3.16). The regions in which the largest rms deviation is observed are residues 20-30, which correlates to the regions with high B-factor values. Similar values have been observed in previous SAP structures.

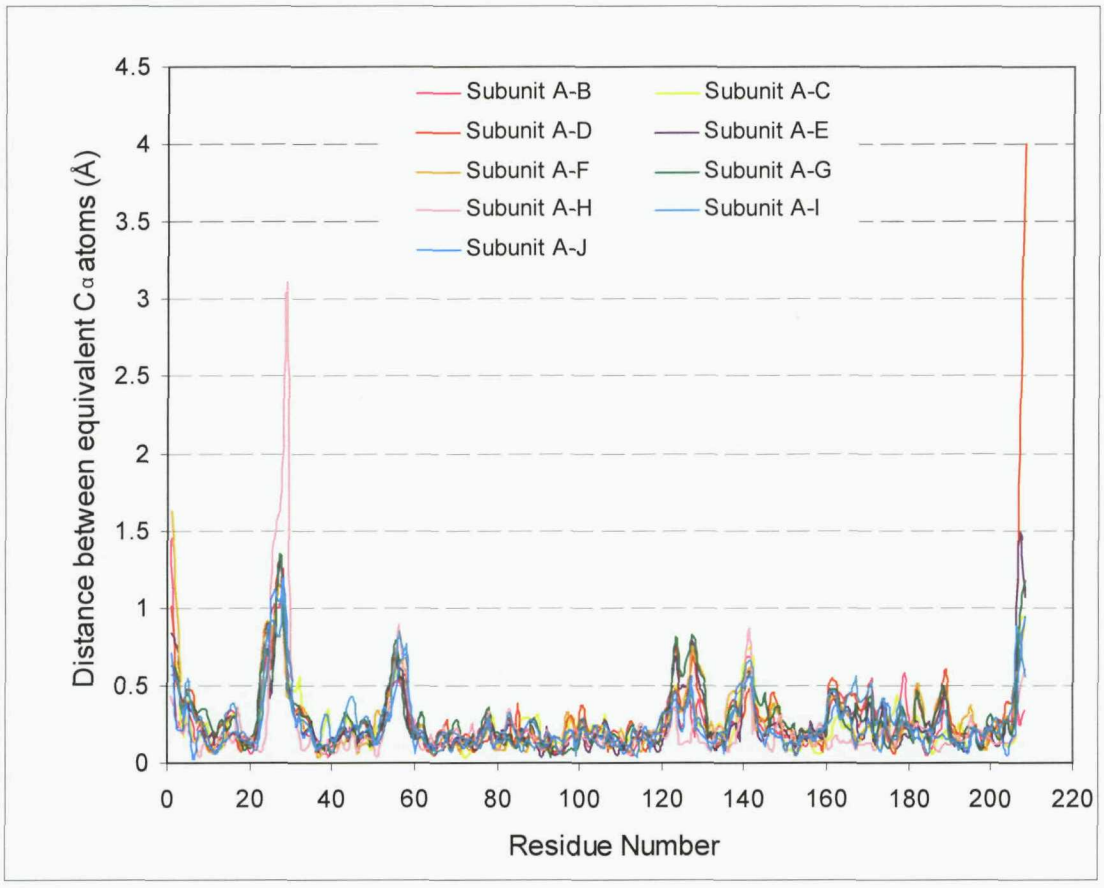

Figure 3.16 A comparison of the root mean squared C_α atom distances between all ten rat SAP protomers in the rat SAP-PC complex.

3.4 Structural Comparison of Rat SAP with Human SAP

As expected, a comparison of the rat SAP pentamer with the human SAP pentamer (1SAC, Emsley *et al.*, 1994) confirms that the structures are similar. Small structural differences in rat SAP occur in four loops linking β-strands (residues 22-28, 53-59, 64-72, 82-87) and following the α-helix (residues 184 – 180). One of these loop regions (22-28) is on the outer surface of the protomer, while the loop regions (174-180 and 84-87) are in the same region of the protomer and extend into the central pore of the pentamer (Figure 3.17 & 3.18 & 3.19). The other loop region (53-59) is involved in calcium binding. These differences are most likely due to sequence variability between the human and rat SAP. However, these regions have poor electron density and high B factor values.

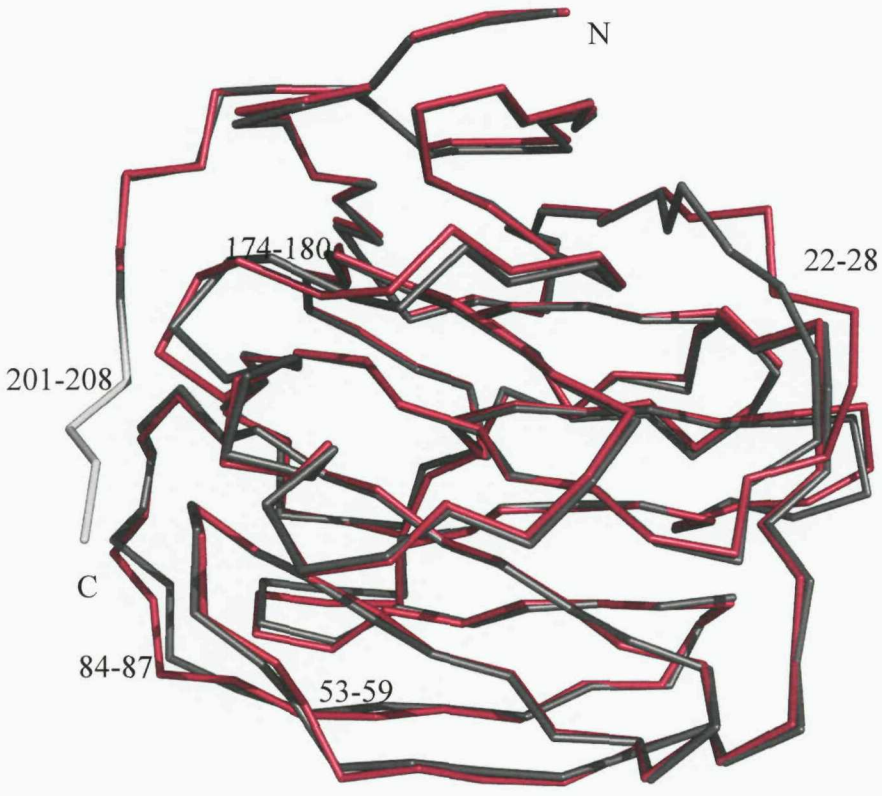

Figure 3.17 Superposition of a rat SAP protomer (light grey) onto human SAP protomer (pink). The regions displaying the largest structural differences have been labelled (Pymol).

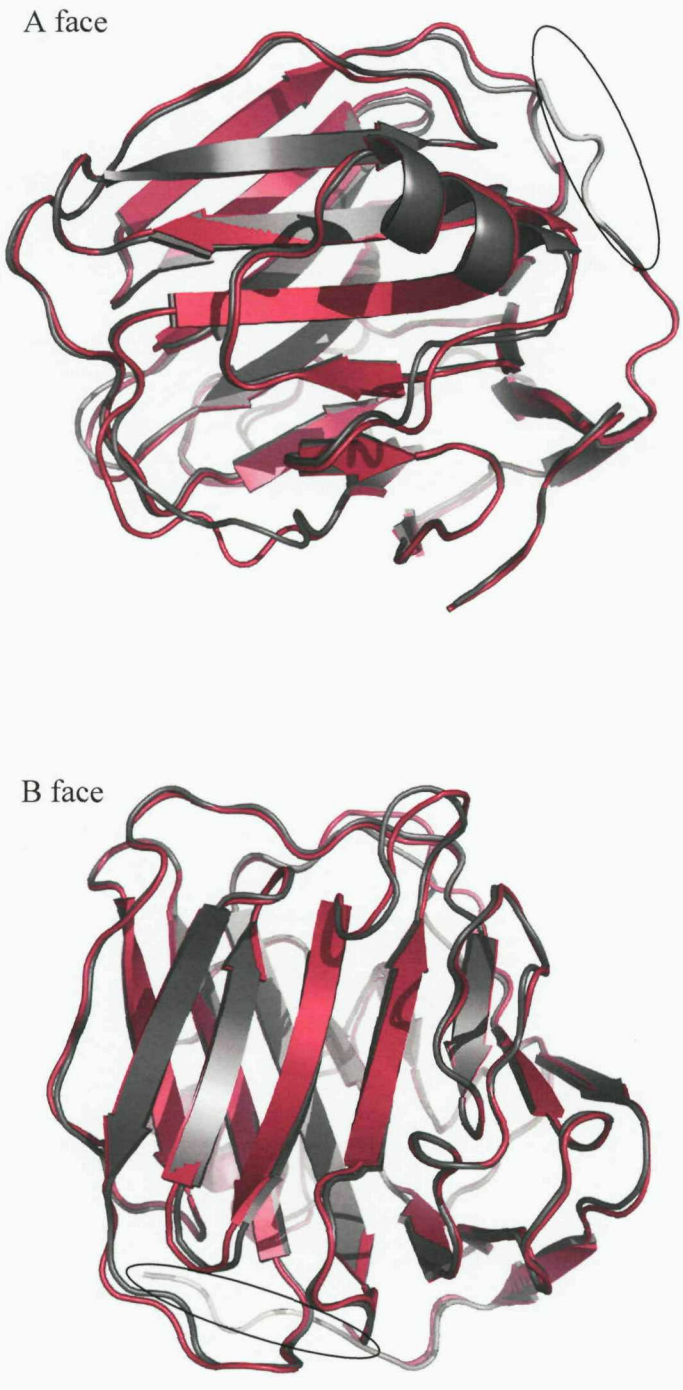

Figure 3.18 Cartoon overlay of a rat SAP protomer (grey) and a human SAP protomer (pink). The white coloured region at the C-terminal end represents the four additional residues in rat SAP.

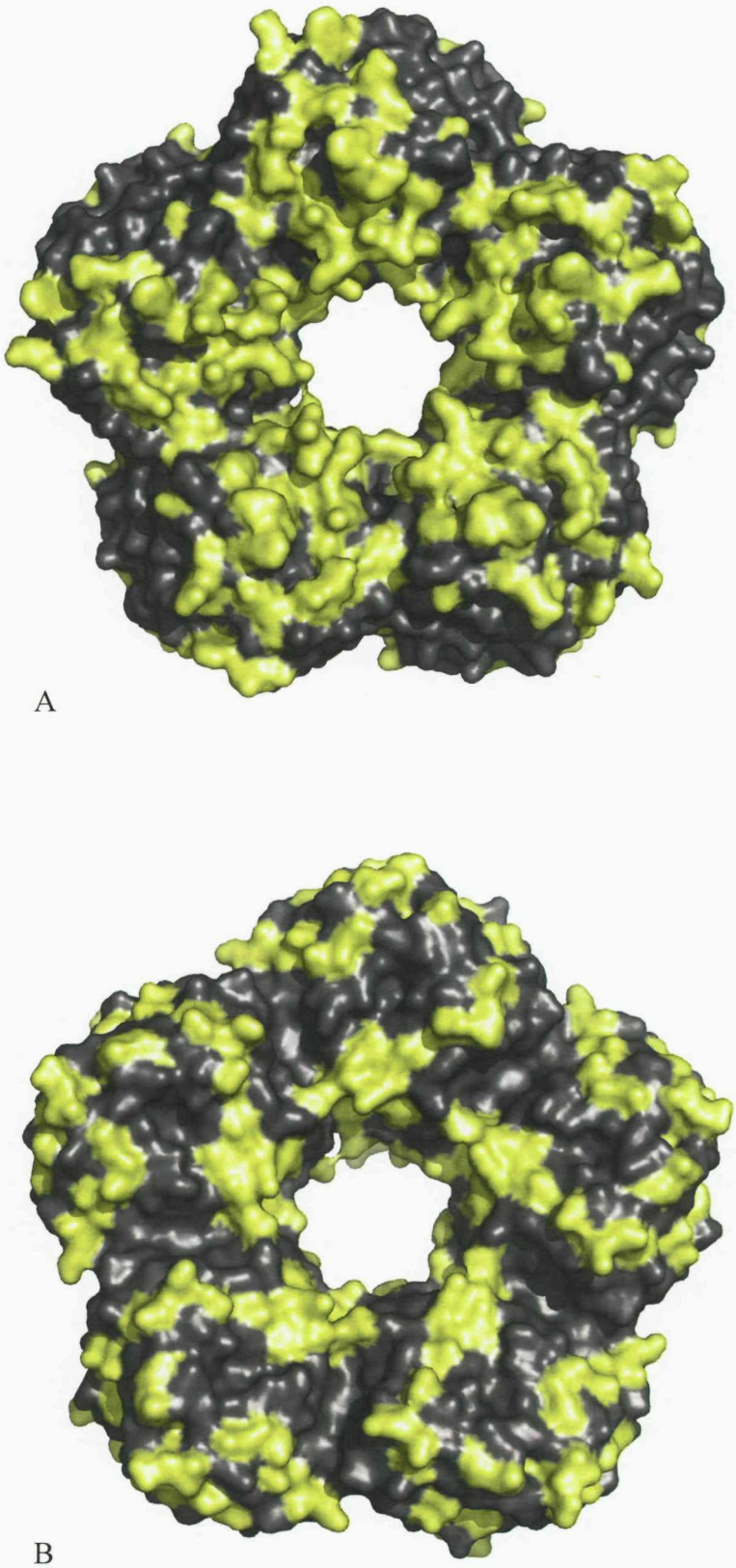

Figure 3.19 Surface representation of a rat SAP pentamer (A = A face, B = B face). The yellow regions indicate the position of residues in rat SAP that differ from the human SAP sequence.

Superposition of the rat SAP structure on human SAP yielded an overall rms deviation of 1.06 Å (Figure 3.20). The regions exhibiting the largest main chain rms deviation are residues 20-30 and 50-60 and are associated with high B-factor values. However, analysis of the average B-factor values for all five subunits between the structures of rat SAP and 1SAC reveals an almost identical distribution of B-factor values across the SAP protomers from the two structures (Figure 3.21). The regions of increased B- factor values are localised to the highly mobile loop regions.

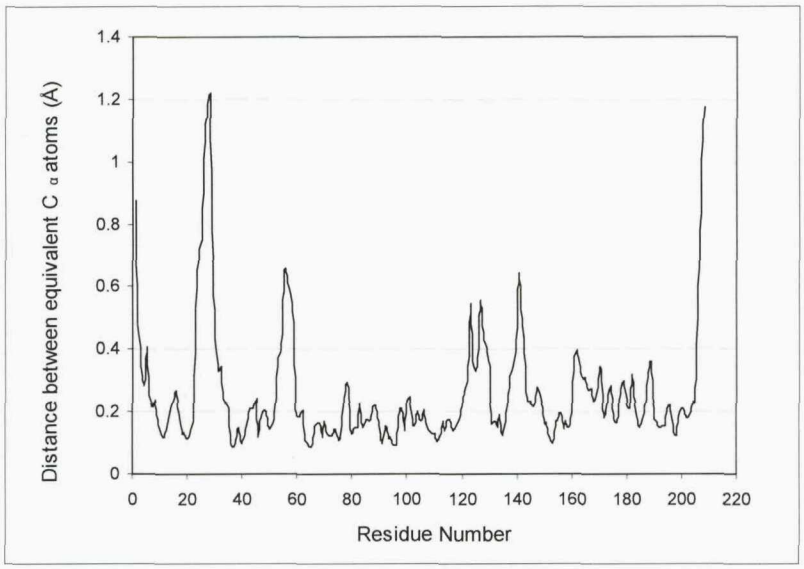

Figure 3.20 Average C_α distance between superimposed subunits of the rat SAP and human SAP (1 SAC) pentamers.

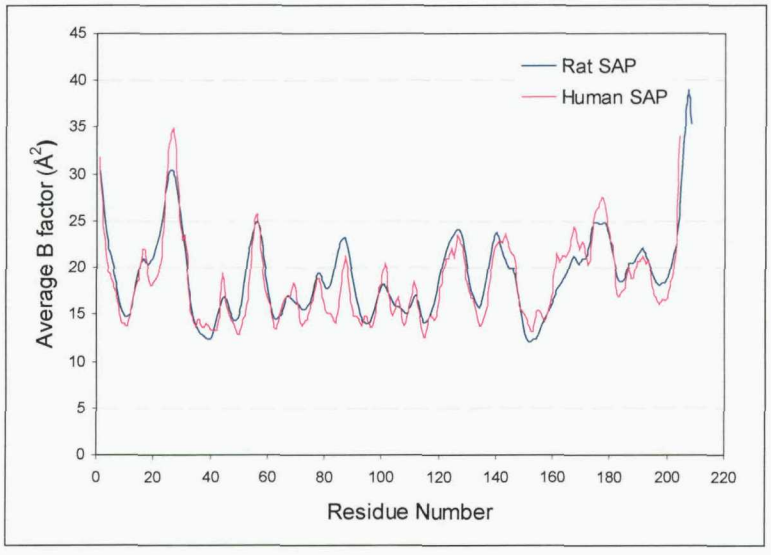

Figure 3.21 A comparison of average isotropic B-factor values for all residues between the rat SAP subunits of the rat SAP-PC complex and human SAP (1SAC).

3.4.1 Protomer-Protomer Contacts of Rat SAP

The buried surface area of a rat SAP protomer is 1478.6 $Å^2$ per subunit, which is similar to that of the human SAP (1463 $Å^2$). Analysis of the inter-protomer contacts in the rat SAP indicate that they are similar to those reported for the human SAP pentamer (Figure 3.22 & Figure 3.23). However, due to sequence differences, there are small changes in the interactions between subunits. For example, residues Val197 and Ile104 form hydrophobic contacts following substitution of Ile197 in human SAP.

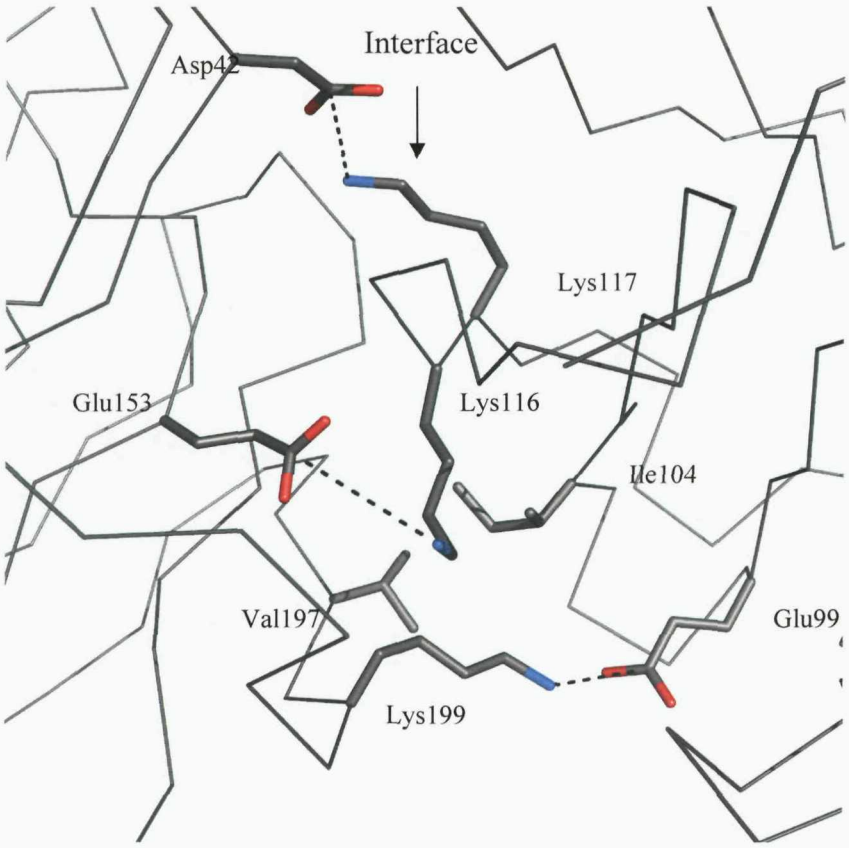

Figure 3.22 Diagram showing the salt bridges formed at the protomer- protomer interface of rat SAP. Salt bridges are formed between Asp42, Glu153, Lys199 of one protomer and Lys117, Lys116 and Glu99 of the adjacent protomer.

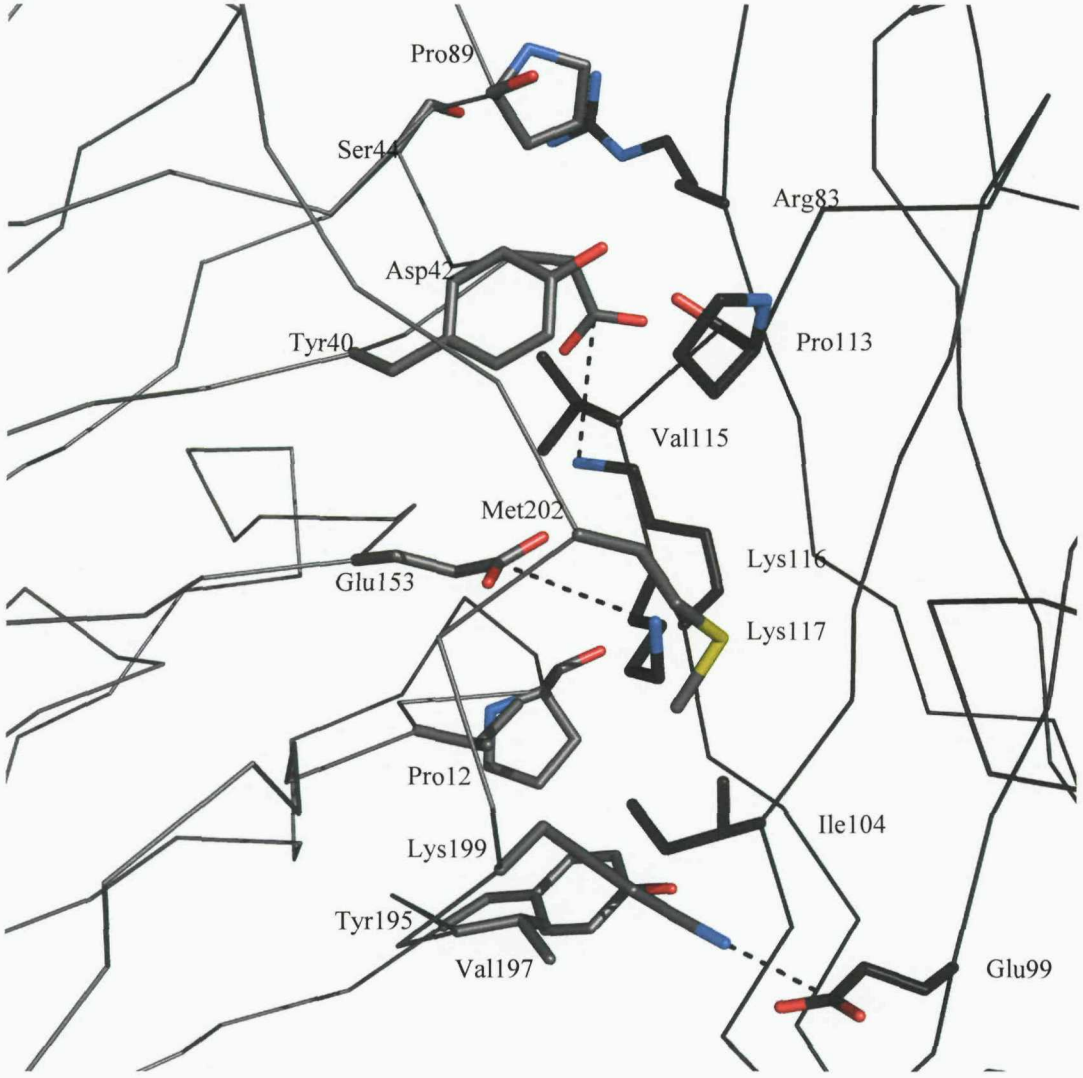

Figure 3.23 Diagram highlighting the residues involved in stabilising the protomer-protomer interface of rat SAP. The two protomers are displayed in light and dark grey. The protomer-protomer interface is stabilised by numerous salt bridges (K199/E99, E153/K117 and D42/K116) and hydrophobic contacts.

3.4.2 Electrostatics of Rat SAP

Analysis of the electrostatic properties of the pentamer reveals that there are some changes in the electrostatic surface of the rat SAP pentamer due to sequence differences. While the human SAP pentamer is a strongly dipolar molecule with a negative A face and a positive B face, the rat SAP pentamer does not seem to be as strongly dipolar (Figure 3.24 & Figure 3.25). A large number of negative residues on the A face of the human SAP pentamer have been substituted for positive or neutral residues in the rat SAP pentamer (Figure 3.26). Changes in the electrostatic surface are also apparent on the B face, which has a cluster of strong negative charge at the centre of the protomer (Figure 3.24). This highly negative region corresponds to the calcium- and ligand-binding region and is accentuated to a wider area in the rat SAP pentamer (Figure 3.24).

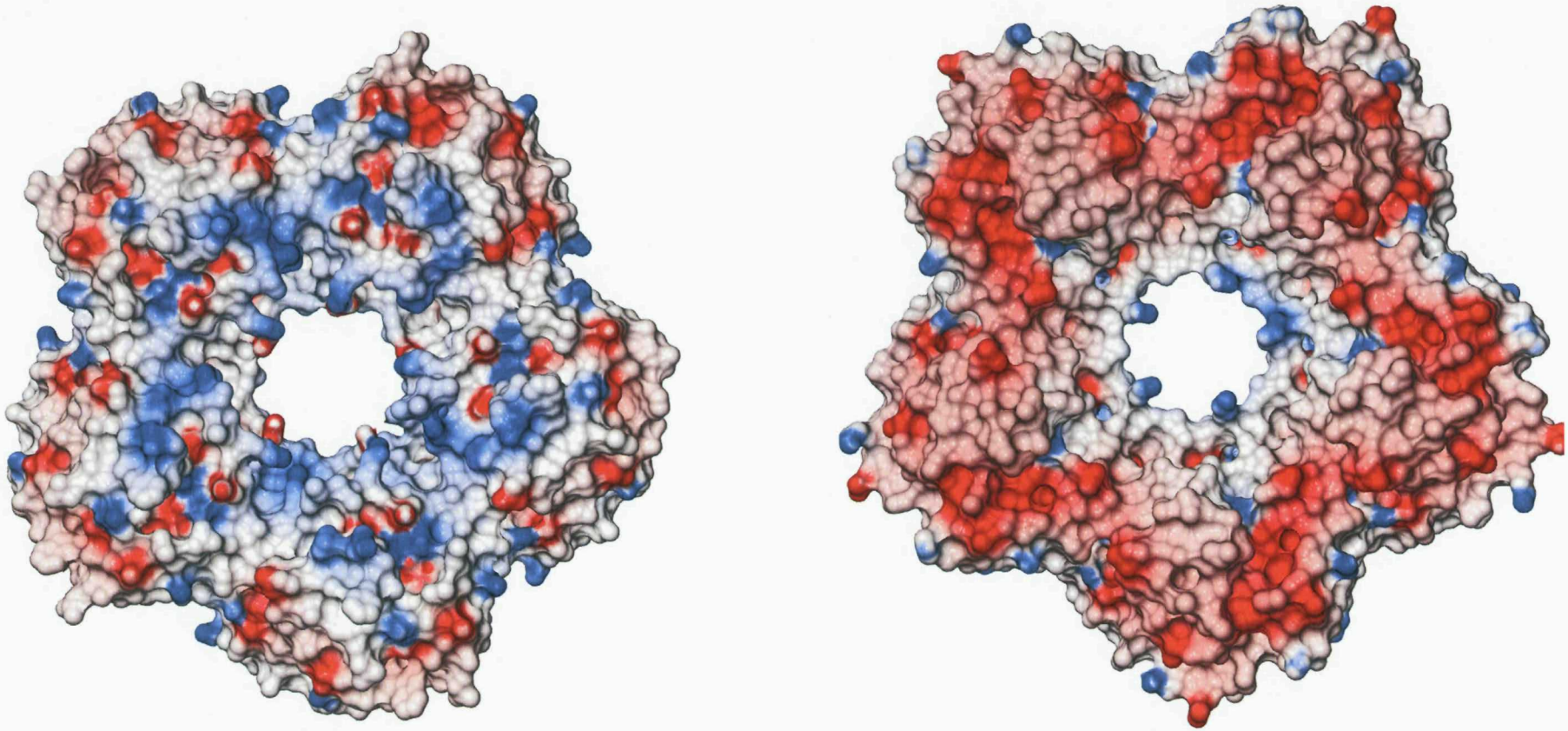

Figure 3.24 Surface charge representation of the A face of the rat SAP pentamer (left) and the human SAP pentamer (right). Negative and positive potential are indicated by red and blue colouring, respectively. The calcium ions and ligands were not included in the calculation. The A face of the rat SAP pentamer is significantly more positive then the A face of the human SAP pentamer. The electrostatic surface potential of the two proteins was calculated using DELPHI and displayed using CueMol & Povray.

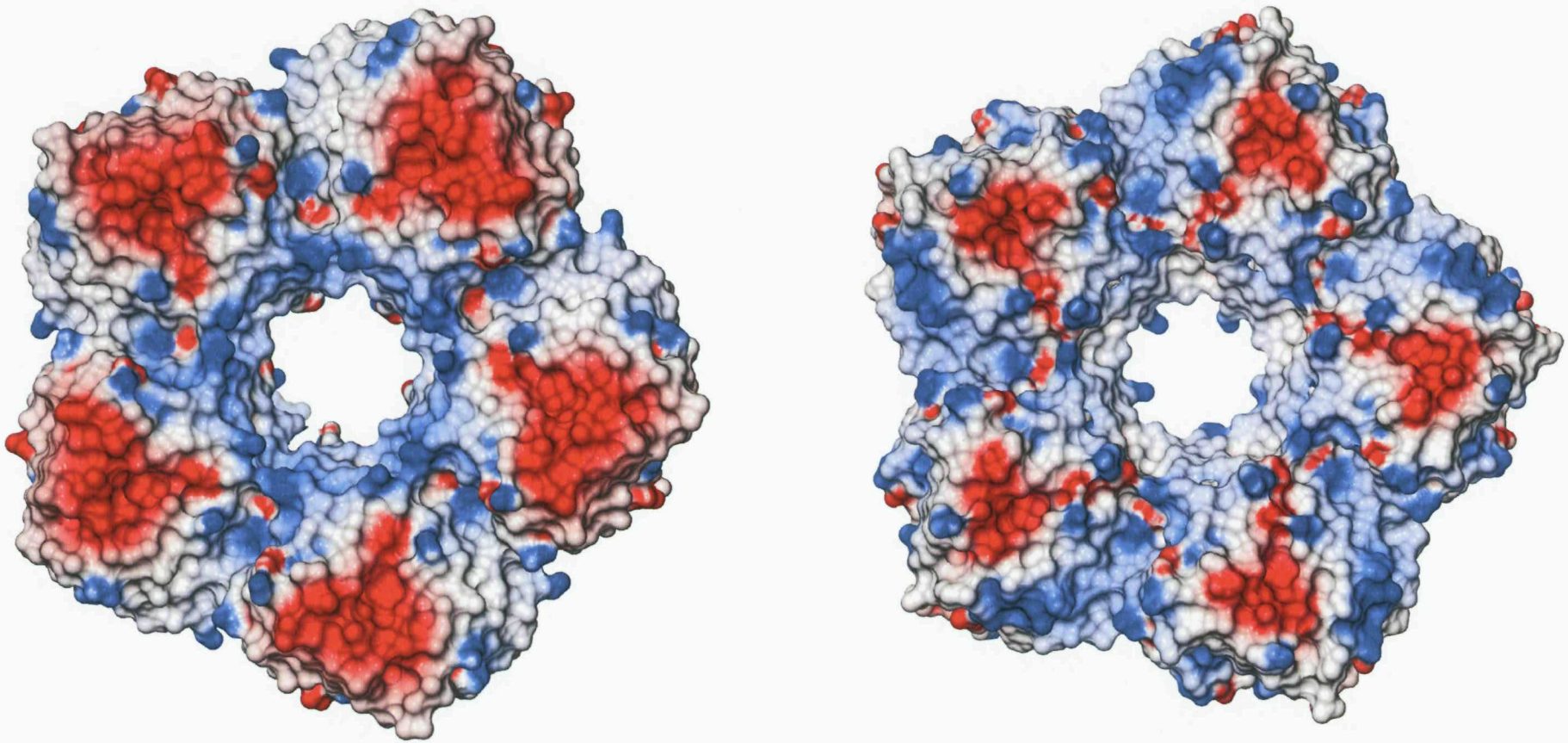

Figure 3.25 Surface charge representation of the B face of the rat SAP pentamer (left) and the human SAP pentamer (right). Negative and positive potential are indicated by red and blue colouring, respectively. The calcium ions and ligands were not included in the calculation. The highly negative region corresponds to the calcium- and ligand-binding region. The electrostatic surface potential of the two proteins was calculated using DELPHI and displayed using CueMol & Povray.

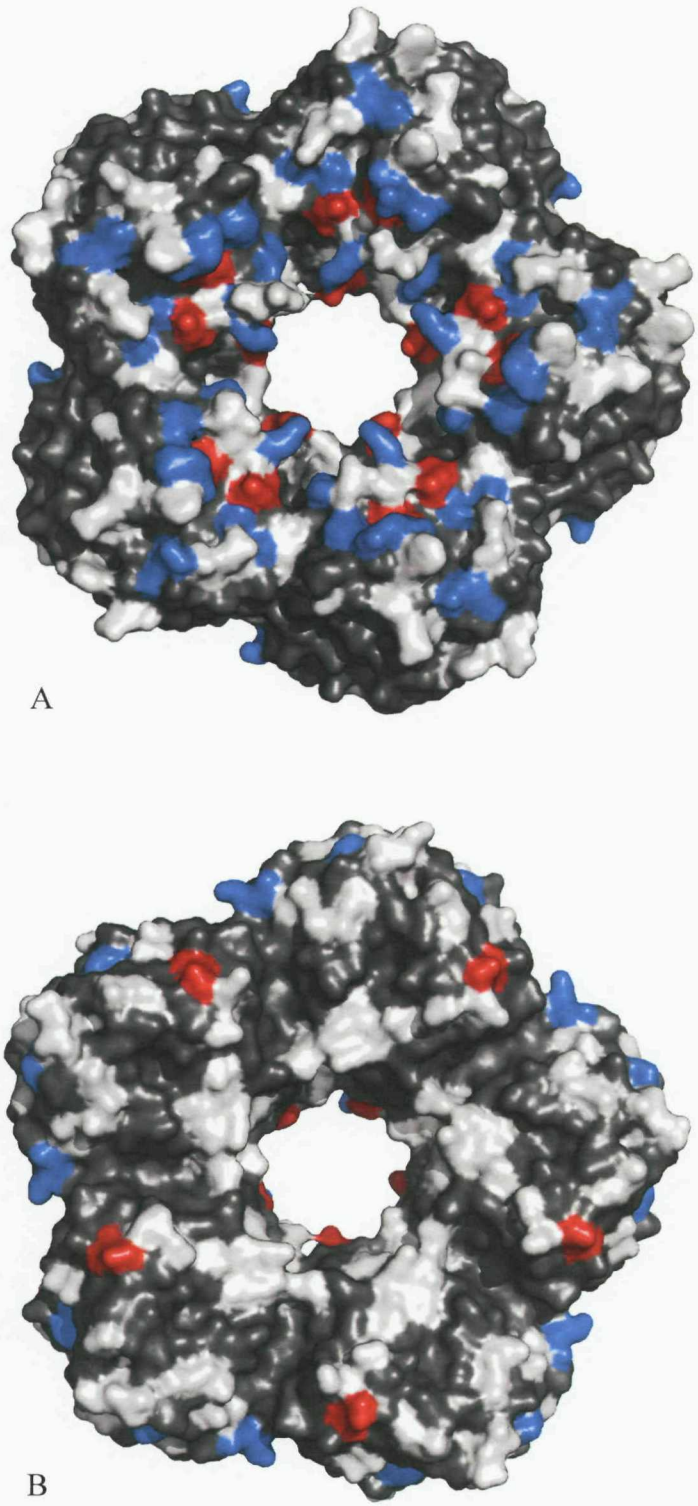

Figure 3.26 Surface properties of the rat SAP pentamer. The diagram shows the residues in rat SAP, that have been substituted for negative (red), positive (blue) or neutral (white) residues. These residues are Glu16, Lys21, Lys112, Lys121 on the A face and Glu87, His170, Asp173, Arg174, Arg186, Arg201, Asp204 and Lys206 on the B face.

3.4.3 The Calcium-Binding Site of Rat SAP

The calcium-binding site in rat SAP is identical to human SAP, situated on the face opposite the α-helix and is formed mainly by polar residues from a long loop. The first calcium ion site (I) is coordinated by the side chains of Asp58, Asn59, Glu136, Asp138 and the main chain carbonyl of Gln137. The second calcium ion site (II), more loosely bound, is coordinated by the side chains of Glu136, Asp138, Gln148 and two water ligands. The bond distances range between 2.3 Å and 2.85 Å as expected for calcium coordination (McPhalen *et al.*, 1991). The two calcium ions are close to each other (3.7 Å) and are bridged by the phosphate group of one PC molecule (Figure 3.27).

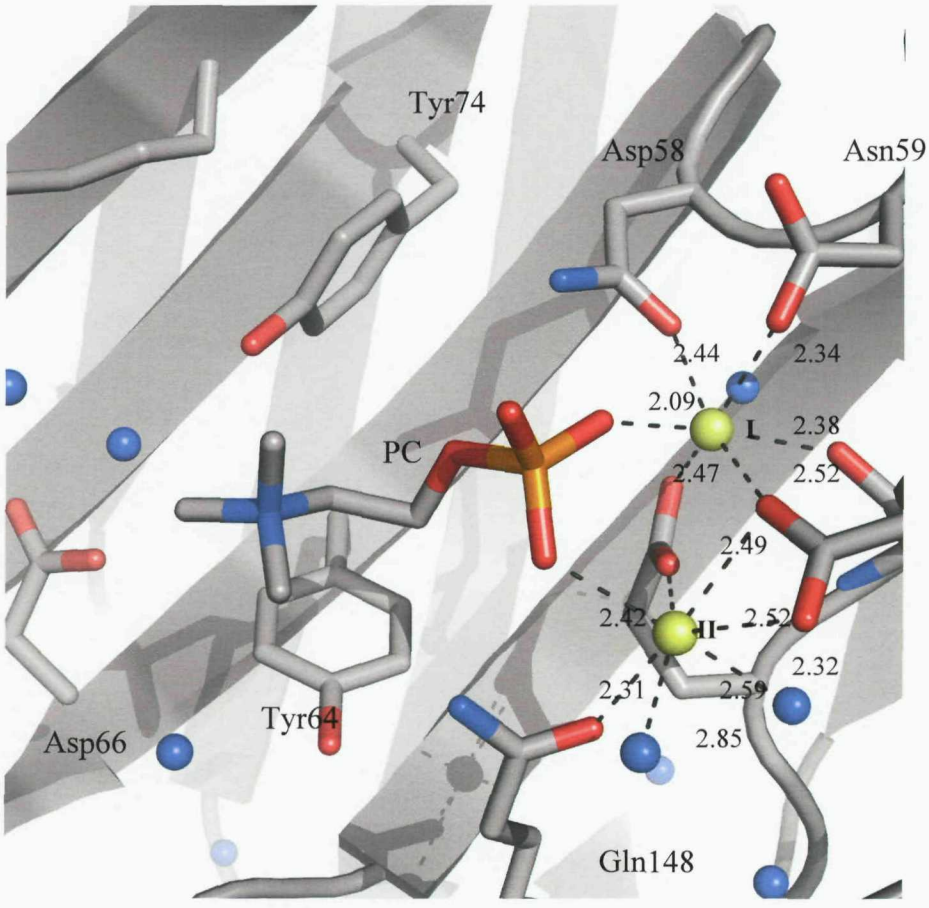

Figure 3.27 The calcium-binding site in rat SAP. Calcium ion I is coordinated by the side chains of Asp58, Asn59, Glu136, Asp138 and the main chain carbonyl of Gln137. The second calcium ion (II) is coordinated by the side chains of Glu136, Asp138, Gln148 and two water ligands.

3.4.4 The Phosphocholine Binding Site of Rat SAP

The phosphocholine binding site in the rat SAP crystal structure is in a similar position to the PE binding site in human SAP. The structures of PE and PC differ only at the nitrogen where three bulky methyl groups are attached in PC (Figure 3.28). In the crystal structure of the human SAP-PE complex, the major interaction between SAP and PE occurs between the phosphate group of PE and the bound calcium ions. Two of the oxygens interact directly with each calcium, leaving the third oxygen pointing away from the binding site and into the solvent. The remaining part of the PE molecule extends from this site into a small hydrophobic pocket, which is lined by two large tyrosine residues (Tyr64 and Tyr74). It was proposed that the bulky side chain of Tyr74 in human SAP would sterically clash with the tri-methyl ammonium group of PC and that the positively charged Lys79 would be introduced to an unfavourable environment due to the presence of the positive charged quaternary nitrogen atom of PC. However, in the rat SAP crystal structure, flexibility in the main chain allows the rearrangement of Tyr74 thus removing the steric clash upon PC binding. In addition Glu66, which interacts with the amine group of PE via a water molecule, is replaced in rat SAP with Asp66. This change may allow the accommodation of the methyl groups of PC (Figure 3.29).

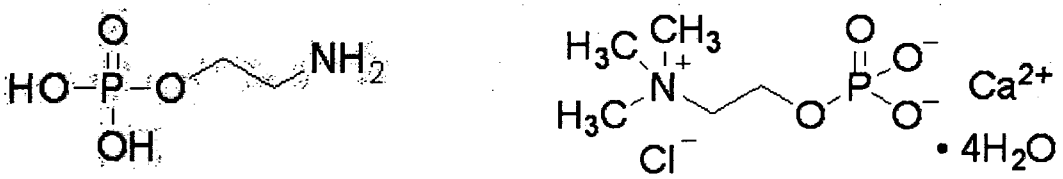

Figure 3.28 The structure of PE (left) and PC (right).

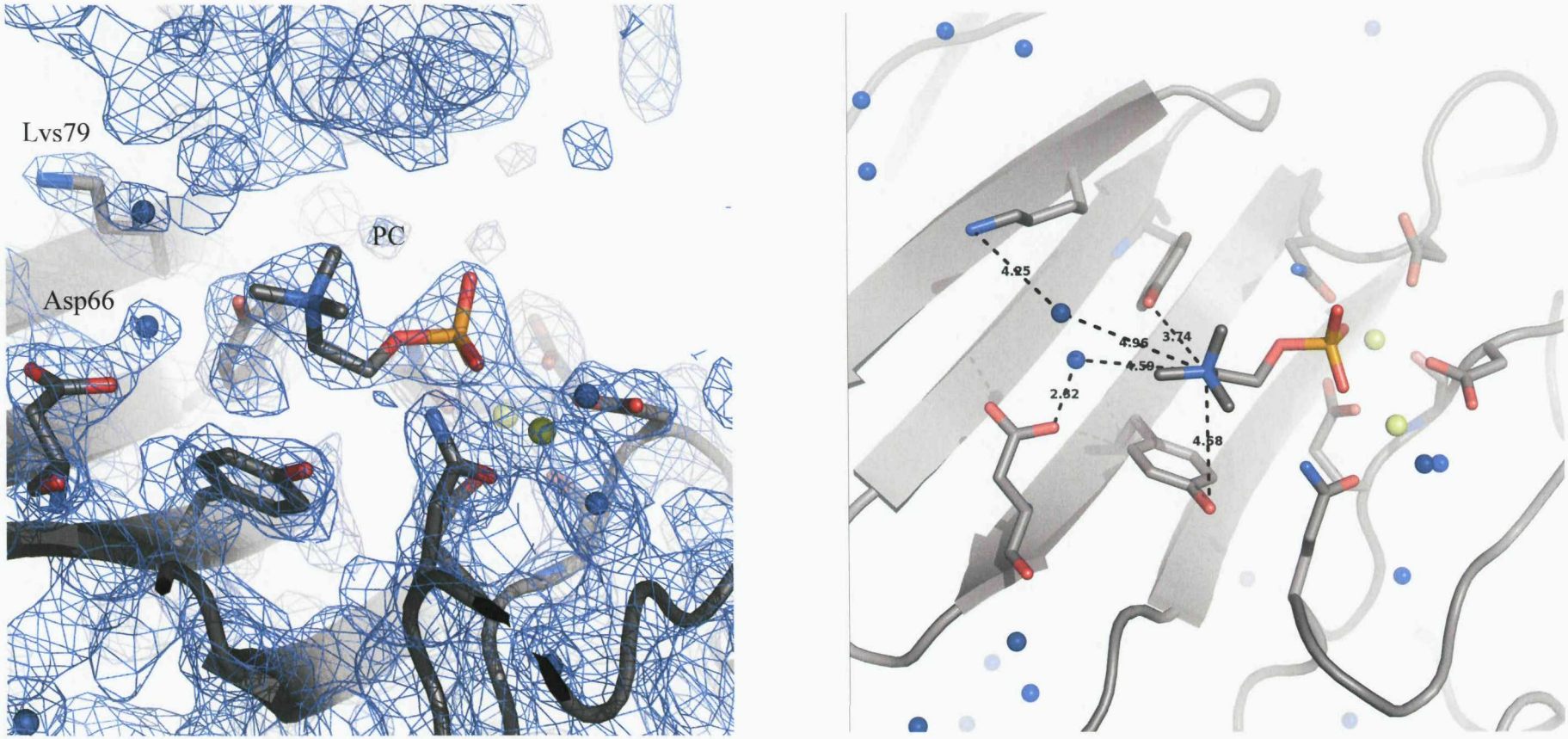

Figure 3.29 $2F_o$-F_c electron density (blue) contoured at 1.5 σ of the Phosphocholine-binding site showing a molecule of PC and the residues in the hydrophobic pocket (left). Diagram on the right shows the coordination of PC into rat SAP. The presence of the bulky tyrosine residues in rat SAP (Tyr64 and Tyr74) forces the tri-methyl ammonium group of PC away from the surface of the protein. Glu66 present in human SAP is replaced by Asp66 in the rat SAP, which holds the quaternary nitrogen of PC in place via a water molecule.

3.5 Discussion

The three-dimensional structure of the rat SAP in complex with PC is the first rat pentraxin to be determined, although preliminary X-ray analysis of rat CRP has been previously published (Hopkins *et al.*, 1994). The amino acid composition of rat SAP is very similar to that of human SAP and thus as expected the pentraxin fold is conserved. However, due to some sequence substitutions in the rat SAP, electrostatic properties of the pentamer are slightly different from that of human SAP, yet both molecules are still bipolar in nature. This observation of subtle changes in the electrostatic properties is of interest as it may be a factor in the resistance of rats to form amyloid. In addition, it remains to be determined whether this has an effect on the avid binding of SAP to DNA, a functional property of human SAP still poorly understood.

Traditionally, human SAP has been described as a protein that does not bind PC (De Beer *et al.*, 1982; Pepys & Baltz, 1983), although it was reported to bind PC in solution with a much lower affinity than PE (Schwalbe *et al.*, 1992). The rat SAP structure reported here contains PC in the ligand binding site rather than PE indicating that rat SAP is also a PC-binding protein. At present, this binding specificity distinguishes rat SAP from other more distinct CRP-like and SAP-like pentraxins, which exhibit high specificities for PC and PE respectively. However, the affinity of rat SAP for PC and PE has not been successfully measured.

Analysis of the PC-binding sites of rat SAP indicates that the position of PC is similar to the position of PE in human SAP. Figure 3.30 shows an α-carbon superposition of the SAP-PE complex structure with the rat SAP-PC complex structure. There are small differences in the key residue side-chain positions coordinating the calcium ions. The biggest difference is seen in the repositioning of the Asp58. Interestingly, the residues (Leu62, Tyr64 and Tyr74) forming the hydrophobic pocket do not show repositioning. It was thought that the residue Tyr74 would clash with the tri-methyl ammonium group of PC. However, it appears that the presence of the bulky tyrosine residues in rat SAP have forced the tri-methyl ammonium group of PC away from the protein surface (Figure 3.30). In addition, Glu66, which interacts with the amine group of PE via a water molecule,

is replaced in rat SAP with Asp66. This residue holds the nitrogen end of PC in place via a water molecule.

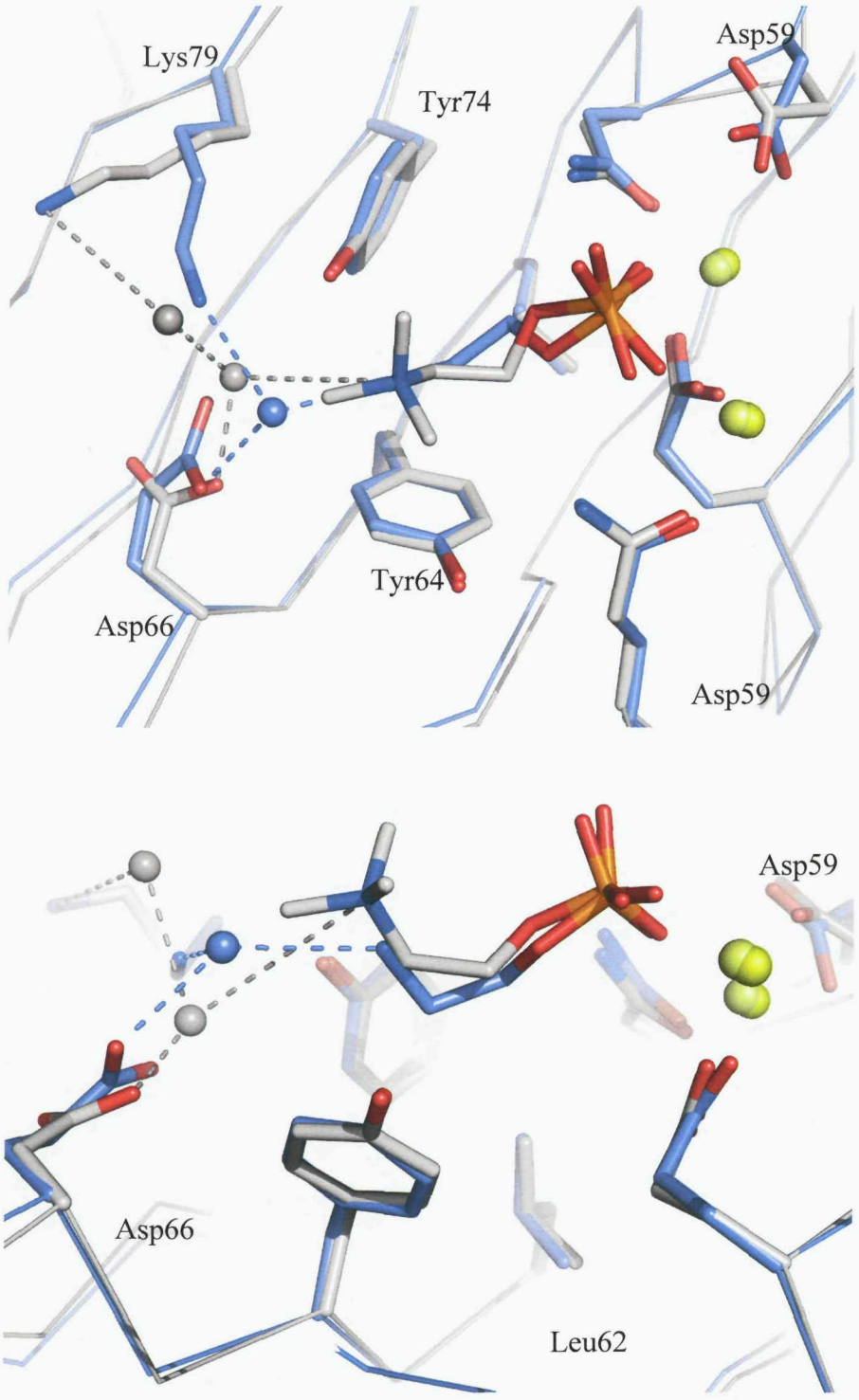

Figure 3.30 Superposition of the 2.2 Å rat SAP-PC complex (grey) with the 1.5 Å SAP-PE complex structures (blue). Calcium atoms are shown in yellow. Water molecules of the human SAP structure (blue) and rat SAP structure (grey) are shown. Rat SAP residues are labelled.

4.1 Introduction

Chapter 4

Human CRP in Complex with PE

C-reactive protein is a major acute phase serum protein in man and most higher order mammals. Since CRP was discovered in 1930 by Tillet and Francis, a wide variety of biological properties and functions have been assigned to the protein. Several of these biological properties ascribed to CRP resemble those of immunoglobulins. Like the immunoglobulins, CRP possesses the capacity to promote reactions of precipitation (Tillet & Francis, 1930), agglutination (Gal & Miltenyi, 1955), phagocytosis (Hokema *et al.*, 1962) and complement activation (Kaplan & Volanakis, 1974).

The first described reactivity of CRP (precipitation) was calcium-dependent binding to C-polysaccharide (CPS) of the cell wall of Streptococcus pneumonia (Tillet & Francis, 1930; Abernathy & Avery, 1941). Forty years later, Volanakis and Kaplan (1971) identified phosphocholine residues present on CPS as the major reactive group for the binding of CRP. It is now known that CRP also binds a variety of exogenous and autologous molecules containing phosphocholine with high affinity in a calcium dependent fashion (Pepys & Hirschfield, 2003). In addition, CRP also binds a wide variety of other ligands that do not contain PC, such as fibronectin (Robey *et al.*, 1984; DuClos *et al.*, 1987), snRNPs (Du Clos *et al.*, 1989; Pepys *et al.*, 1994), laminin (Swanson *et al.*, 1989) and polycations (Potempa *et al.*, 1981). Although there are no obvious structural features shared by these ligands, it has been suggested that CRP may function as a pattern recognition molecule and plays an important role in innate host defence (Black *et al.*, 2004).

Although the first CRP crystals were reported in 1947 by McCarty, for many years the only structural information about CRP came from imaging techniques such as electron microscopy. This changed rapidly as a result of the elucidation of the X-ray crystal structure of the related pentraxin human SAP (Emsley *et al.*, 1994). This structure provided a model for molecular replacement and led to the elucidation of the structure of human CRP (Shrive *et al.* 1996). The structure of human CRP revealed that like SAP, CRP consists of five identical protomers arranged as a cyclic pentamer. However, although this provided details of the overall structure of CRP, information about the ligand binding site remained incomplete as some of the

subunits were devoid of calcium. Further insight came from the elucidation of the X-ray crystal structure of CRP in complex with PC (Thomson *et al.*, 1999). The structure of CRP in complex with PC showed how PC is bound in a shallow pocket on each subunit, interacting with the two protein-bound calcium ions via a phosphate group, while the quaternary amine interacts with Glu81. This indicates that the human CRP binding site for PC recognises two structural features, a phosphate group and a quaternary amine. In addition, it was found that Phe66 was critical for CRP binding to PC (Agrawal *et al.*, 2002). These residues important for PC binding, Phe66 and Glu81, however are not conserved in SAP, which has been reported not to bind PC with as high an avidity as CRP (Cristner *et al.*, 1994). It has been proposed that the equivalent residue in SAP, the positively charged Lys79 would not favour an ionic interaction with the quaternary amine (Thomson *et al.*, 1999). Furthermore, Tyr74 of SAP would clash with the tri-methyl ammonium group of PC. Thus, it has been suggested that SAP is not likely to function as a major PC-binding protein in human serum (Christner *et al.*, 1994).

Studies have also shown that CRP binds to PE, albeit with much lower affinity than PC (Volanakis & Kaplan, 1971; Schwalbe *et al.*, 1992). Thus, the two pentraxins have complimentary specificities. This relationship suggests a complimentary and/or related function for the pentraxins.

The structure determination of human CRP in complex with PE may allow interpretation of the differences in specificity between human CRP and SAP with respect to PE and PC binding.

4.2 Methods and Results

4.2.1 Purification and Crystallisation of Human CRP

Human CRP was purified in the laboratory of Professor Mark Pepys, UCL, London as previously described by Hawkins *et al.* (1991). Attempts to co-crystallise human CRP with PE prior to the work presented in this report, had been unsuccessful. However, a crystal of the CRP-PE complex has been obtained by soaking a single crystal of a CRP-PC complex in a PE solution (personal communication Darren Thomson). Unfortunately, due to soaking only a low resolution dataset was collected. A higher resolution structure of the CRP-PE complex was therefore sought to enable a more detailed analysis of protein-ligand binding.

Over a two year period, various attempts to co-crystallise human CRP in the presence of PE were made using previously determined crystallisation conditions published by Thompson *et al.* 1999 (10 % MPD, 60 mM HEPES pH 7.6, 140 mM NaCl and 10 mM $CaCl_2$) and novel conditions. Crystallisation trials were performed using the hanging-drop vapour diffusion method in 4 µl hanging drops. These attempts produced a scatter of only poorly diffracting needle crystals.

In an attempt to slow down the process of crystallisation, varying concentrations of low melting agarose (Product code: HR8-092, Hampton Research) were used in the crystallisation trials. After three months, crystals of the CRP-PE complex were eventually obtained at room temperature in hanging drops containing 0.1 - 0.2 % agarose, 2 µl of the protein solution (23 mg/ml with a 10 fold molar excess of pH-adjusted PE) and 2 µl of reservoir solution (10 % MPD, 60 mM Tris pH 7.5, 140 mM NaCl and 10 mM $CaCl_2$). These crystals had an appearance of a pencil (Figure 4.1).

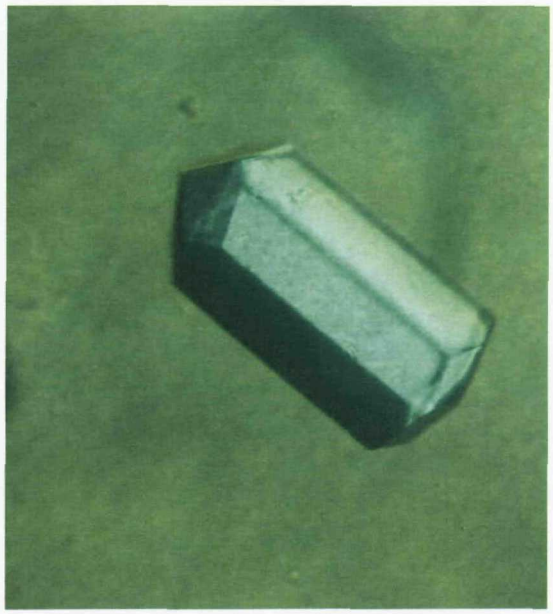

Figure 4.1 A Crystal of human CRP in complex with PE, grown in Tris buffer (10 % MPD, 60 mM Tris pH 8.2-8.5, 10 mM $CaCl_2$, 140 mM NaCl, 0.1 % agarose and 10 fold excess of PE).

4.2.2 Cryo-Crystallography, Data Collection and Data Processing from the CRP-PE Crystal

X-ray diffraction data from the human CRP-PE crystal were collected to 2.7 Å on the beamline ID 29 at the ESRF (France) on an ADSC Quantum-4 CCD detector (Figure 4.2). A data set of 190 1° oscillation frames was recorded with an exposure time of 5 seconds per frame and a crystal to detector distance of 399.96 mm.

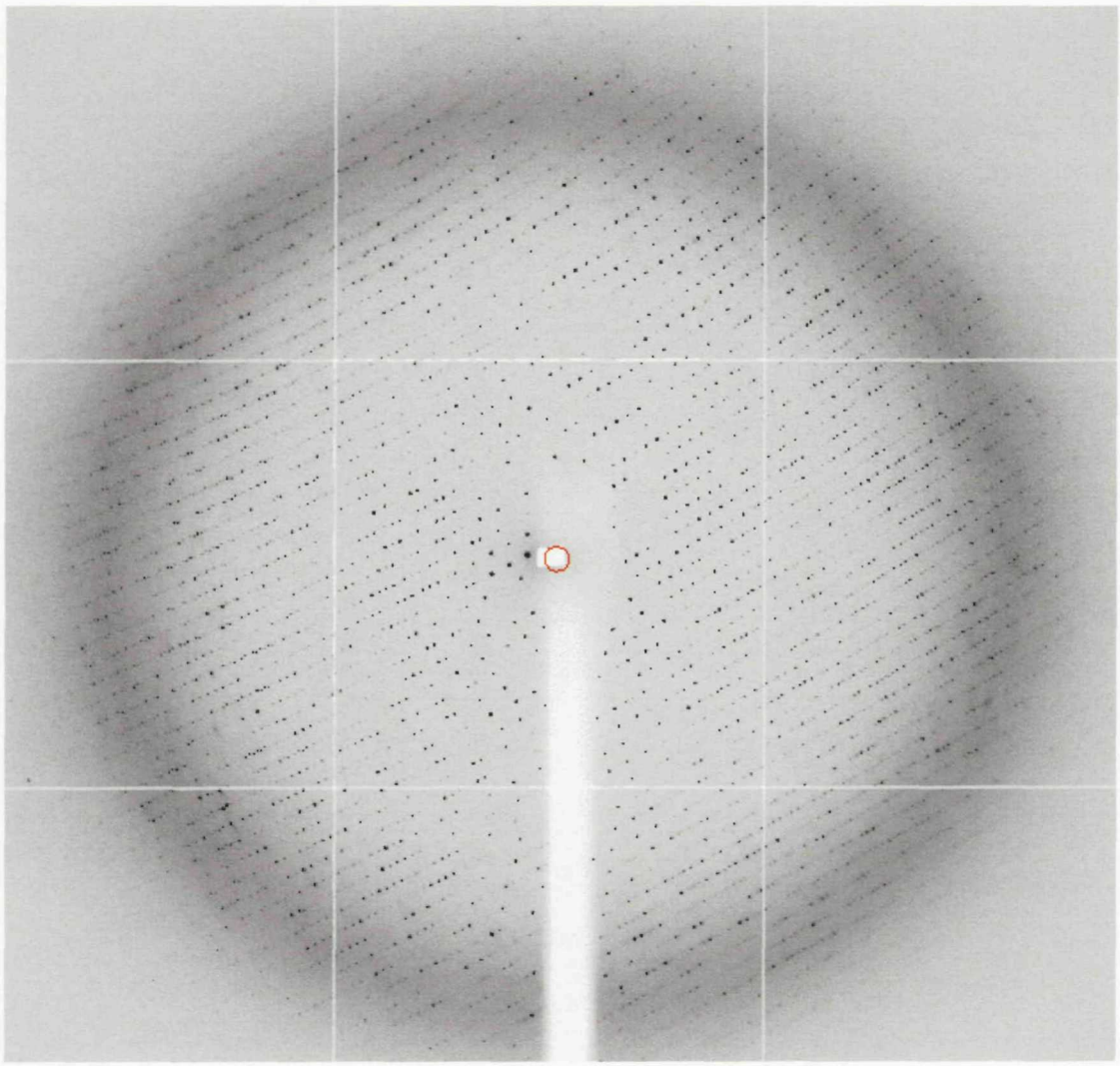

Figure 4.2 A 1° oscillation diffraction image collected from the human CRP-PE crystal at the ESRF (France).

Data processing of the raw data was carried out using MOSFLM. Auto-indexing of the 2.7 Å resolution data from the human CRP-PE crystal indicated that the crystal had unit cell dimensions of a = 278.4 Å, b = 278.4 Å, c = 92.1 Å, $\alpha = \beta = \gamma = 90°$

and that the crystal belonged to one of the following tetragonal space groups: P4, $P4_1$ $P4_2$, $P4_3$, P422, $P42_12$, $P4_122$, $P4_12_12$, $P4_222$, $P4_22_12$, $P4_322$ or $P4_32_12$ (Table 4.1).

Penalty	Lattice	a	b	c	α	β	γ	Possible space groups
55	mC	567.30	92.36	280.51	89.8	90.2	80.7	C2
54	mC	568.32	92.36	279.95	89.9	90.2	80.8	C2
5	tP	279.95	280.51	92.36	90.2	89.9	90.2	P4,$P4_1$,P42,$P4_3$,P422, $P42_12$,$P4_122$,$P4_12_12$, $P4_222$,$P4_22_12$,$P4_322$, $P4_32_12$
3	mC	395.59	397.02	92.36	90.2	90	89.9	C2
3	oC	395.59	397.02	92.36	90.2	90	89.9	C222,$C222_1$
3	oP	92.36	279.95	280.51	90.2	90.2	89.9	P222, $P222_1$, $P2_12_12$, $P2_12_12_1$
3	mP	92.36	280.51	279.95	90.2	89.9	90.2	P2,$P2_1$
2	mC	397.02	395.59	92.36	90	90.2	90.1	C2
2	mP	92.36	279.95	280.51	90.2	90.2	89.9	P2, $P2_1$
1	mP	279.95	92.36	280.51	90.2	90.2	89.9	P2, $P2_1$
0	aP	92.36	279.95	280.51	89.8	89.8	89.9	P1
0	aP	92.36	279.95	280.51	90.2	90.2	89.9	P1

Table 4.1 Penalty table generated by MOSFLM showing the possible unit cell dimensions and space groups.

As a result, diffraction data were processed and merged in the space group P4. These data were then inspected for systematic absences and additional symmetry present in the diffraction pattern using HKLVIEW. Examination of the 00*l* zone revealed absences in the reflections such that only reflections that fulfilled the conditions of $l = 4n$ were present (Figure 4.3). This indicated that a 4_1 or a 4_3 screw axis was present. The *hk*0 reflections were then inspected for diagonal symmetry which would be present if the space group of the crystal had 422 point group symmetry. However, diagonal symmetry was not observed (Figure 4.4). As it is not possible to distinguish between $P4_1$ and $P4_3$ at this stage, the diffraction data was reprocessed in $P4_1$ and $P4_3$.

Figure 4.3 Pseudo-precession camera image of the CRP-PE diffraction data generated using HKLVIEW in P4 (The 0*kl* plane). Systematic absences are observed along the 00*l* axis indicating a $P4_1$ or $P4_3$ space group.

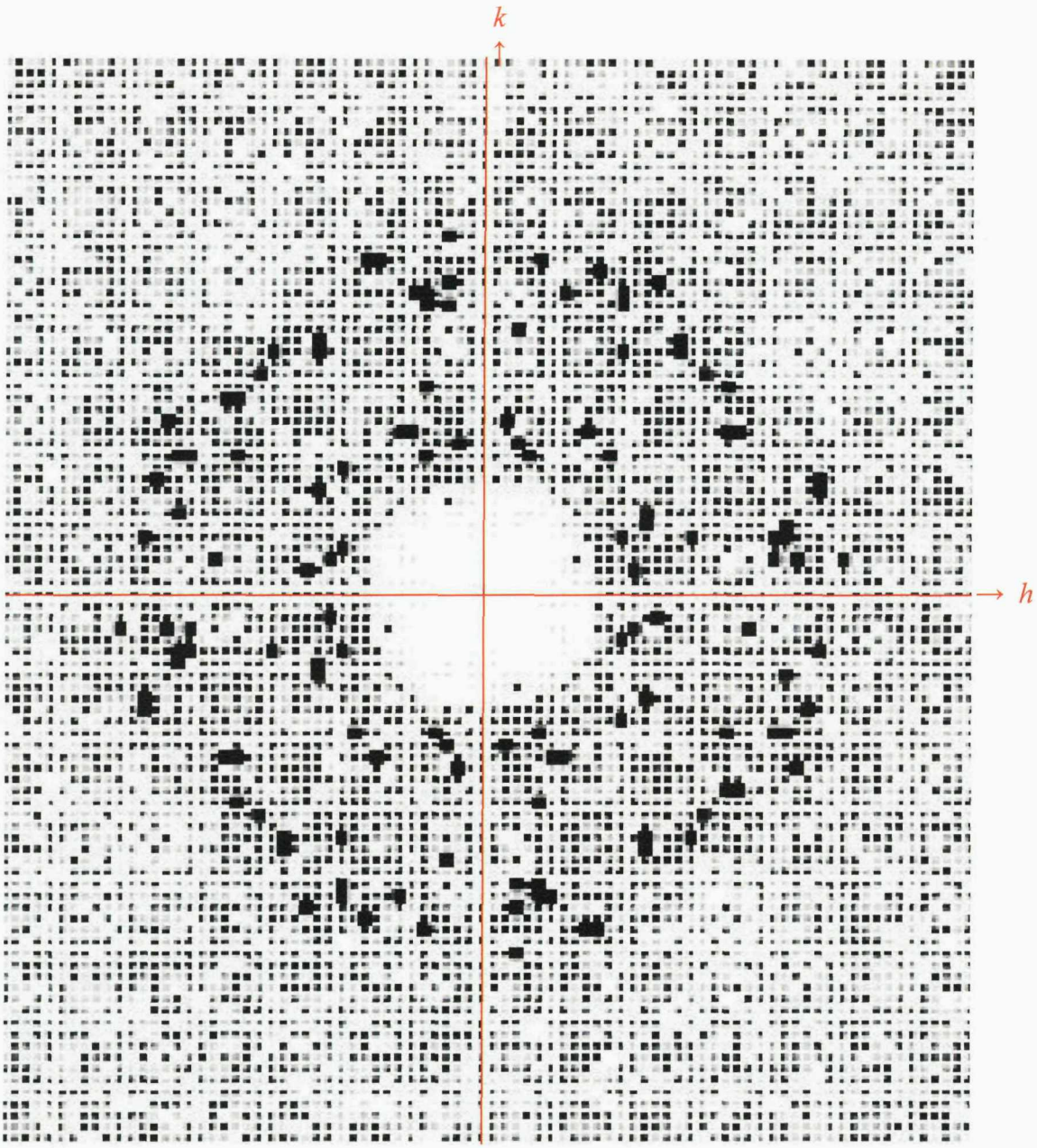

Figure 4.4 Pseudo-precession camera image of the CRP-PE diffraction data generated using HKLVIEW in P4 (The *hk*0 plane). Diagonal symmetry is not observed in the data, indicating that the point group is not 422.

The final processing statistics for the data (125 - 2.7 Å) processed in $P4_1$ and $P4_3$ gave an R-merge of 11.1 % (Table 4.2).

Space Group	$P4_1$ or $P4_3$
Unit Cell (Å) (°)	a = 278.44, b = 278.44, c = 92.11, $\alpha = \beta = \gamma = 90.0$
Resolution range (Å)	125 - 2.7 (2.85 - 2.7)
Measured reflections	1044545 (139700)
Unique Reflections	193026 (27836)
Multiplicity	5.4 (5.0)
Completeness (%)	99.5 (98.9)
R-merge (%)	11.1 (76.4)
(I)/sd(I)	12.2 (2.0)

Table 4.2 A summary of the data processing statistics for the human CRP-PE crystal. Figures in parentheses apply to data in the highest resolution shell.

4.2.3 Molecular replacement of Human CRP in Complex with PE

Numerous attempts to solve the structure of CRP-PE by molecular replacement using various programs and the pentamer & protomer coordinates from the previously published 2.5 Å resolution CRP structure (accession code 1b09; Thompson *et al.*, 1999) as a search model failed. Finally, the program Phaser (McCoy *et al.*, 2007) was used successfully.

Phaser uses likelihood functions to judge how well molecular replacement models agree with the observed diffraction data after they have been first rotated and then also translated. Fast-fourier-transform-based approximations are used to calculate sets of possible solutions, which are rescored with the full likelihood targets. By using a tree-search-with-pruning strategy, almost all solutions that would be found with a full six-dimensional search are found, but with a much lower computational cost. This strategy also allows effective searches for multiple copies, in crystals with more than one molecule in the asymmetric unit.

The solvent content of the unit cell for this data was estimated to be 68 % for four CRP pentamers, 60 % for five CRP pentamers or 52 % for six CRP pentamers in the asymmetric unit (Matthews, 1968). As most protein crystals have a solvent content of approximately 50 %, it seemed most likely that the asymmetric unit contained six CRP pentamers.

For each molecule to be placed, a rotation search is first carried out. A translation search is then carried out for each plausible orientation. All plausible rotation/translation solutions are checked for packing in the lattice and solutions that pack successfully are subjected to rigid body refinement. If more than one copy is present (in this case four copies), all plausible partial solutions are fixed in turn while carrying out rotation and translation searches for subsequent copies.

In molecular replacement trials with Phaser, the clearest indication of success comes from high values of the Z-score (number of standard deviations above the mean), computed by comparing the log-likelihood-gain (LLG) for the peak with LLG scores for a random sample of search points. For the molecular replacement studies with the CRP-PE data, Phaser gave a solution in the space group $P4_1$ with four CRP pentamers in the asymmetric unit with a log-likelihood gain of 3329 and a RFZ-score of 11.7 and TFZ-score of 61 (Table 4.3).

No of Molecules	RF-Z	TF-Z	LL-Gain
1	10.3	22.2	595
2	9.6	38.7	1439
3	10.4	49.6	2527
4	11.7	61	3229

Table 4.3 The molecular replacement partial and final solution found by Phaser.

In order to check the molecular replacement solution, the crystal packing was visualized using NUcheck (Feng *et al.*, 1998). The diagram demonstrated the feasibility of the present solution and confirmed the presence of four human CRP pentamers in the asymmetric unit (Figure 4.5). Therefore, it was decided to proceed with refinement.

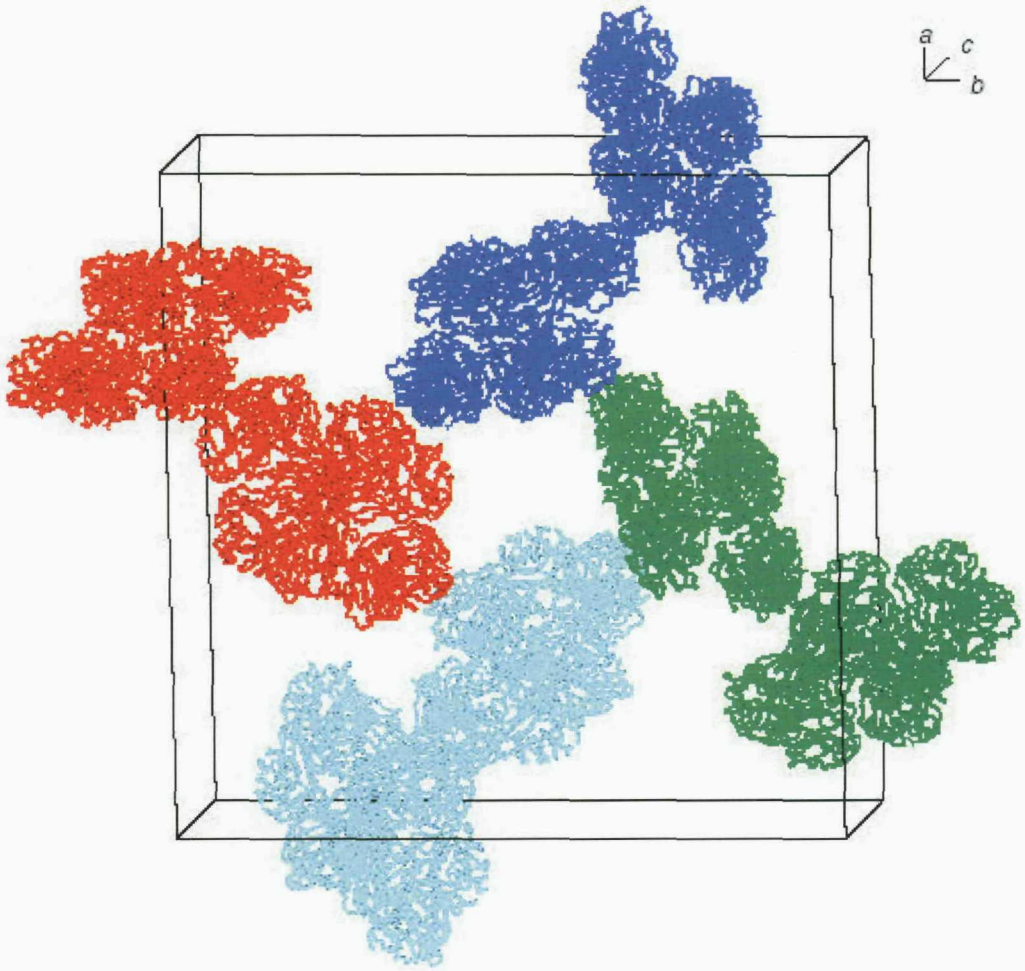

Figure 4.5 Crystal packing of human CRP in complex with PE (NUcheck, Feng *et al.*, 1998). Human CRP-PE crystallises in the primitive tetragonal space group $P4_1$ (a = 278.44 Å, b = 278.44 Å, c = 92.11 Å, $\alpha = \beta = \gamma = 90^{\circ}$ and contains four CRP pentamers in the asymmetric unit (shown in red). Symmetry related pentamers are shown in blue, green and turquoise.

4.2.4 Refinement and Model Building of Human CRP in Complex with PE at 2.7 Å

The model was refined using the Phenix package (Adams *et al.*, 2002). The Phenix refinement tools include Cartesian dynamics simulated annealing, a novel robust bulk solvent correction procedure including overall anisotropic scaling, maximum likelihood refinement, isotropic and anisotropic refinement of displacement parameters (Afonine *et al.*, 2005).

An R-free set was selected in thin resolution shells to minimise the bias due to non-crystallographic symmetry. The first round of refinement with full NCS restraints imposed reduced the R-factor from 42.6 to 25.9 % (R-free = 27.6 %). After the initial round of refinement, the resulting maps generated were analysed and manipulated using the graphics package COOT (Emsley & Cowtan, 2004). Analysis of the maps indicated well-defined F_o-F_c density for the forty calcium ions and twenty PE molecules at the binding sites. During model building, calcium ions were added and where possible side chains were fitted into the electron density. The second round of refinement reduced the R-factor and R-free to 24.42 % and 26.48 % respectively. Analysis of the maps revealed good F_o-F_c density for the twenty PE molecules, which were built into the structure (Figure 4.6 & Figure 4.7). The next refinement round reduced the R-factor and R-free to 23.35 % and 25.25 % respectively. During another round of model building, water molecules (194) were added to the structure and refined. The final R-factor with data to 2.7 Å was 23.1 % (R-free = 25.0 %). The refinement statistics for the model are shown in Table 4.4.

Resolution range (Å)	125 – 2.7
Number of reflections in the working set	183025
Number of reflections in the test set	9714
R-factor (%)	23.1
R-free (%)	25.0
Rms bond length deviation (Å)	0.005
Rms bond angle deviation (°)	0.64

Table 4.4 Refinement statistics for the human CRP structure in complex with PE.

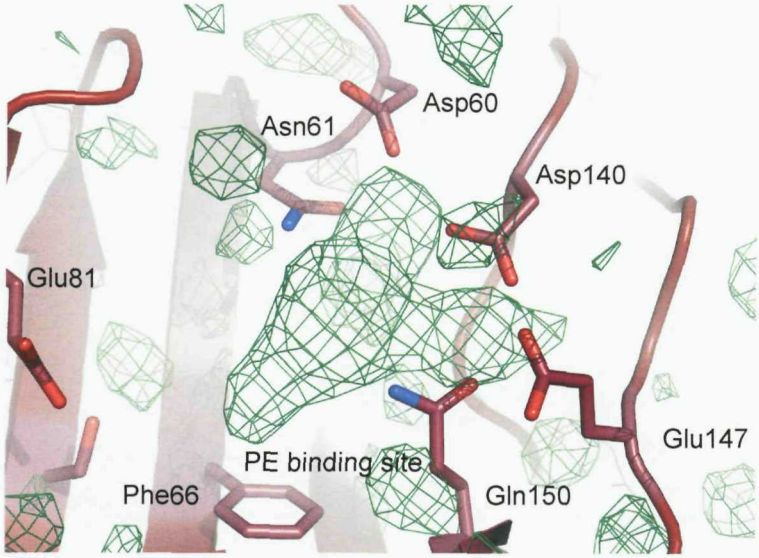

Figure 4.6 F_o-F_c electron density contoured at 2 σ (green) of the calcium binding site before the addition of two calcium atoms and a PE molecule. The amino acid residues (dark red) of CRP are also shown.

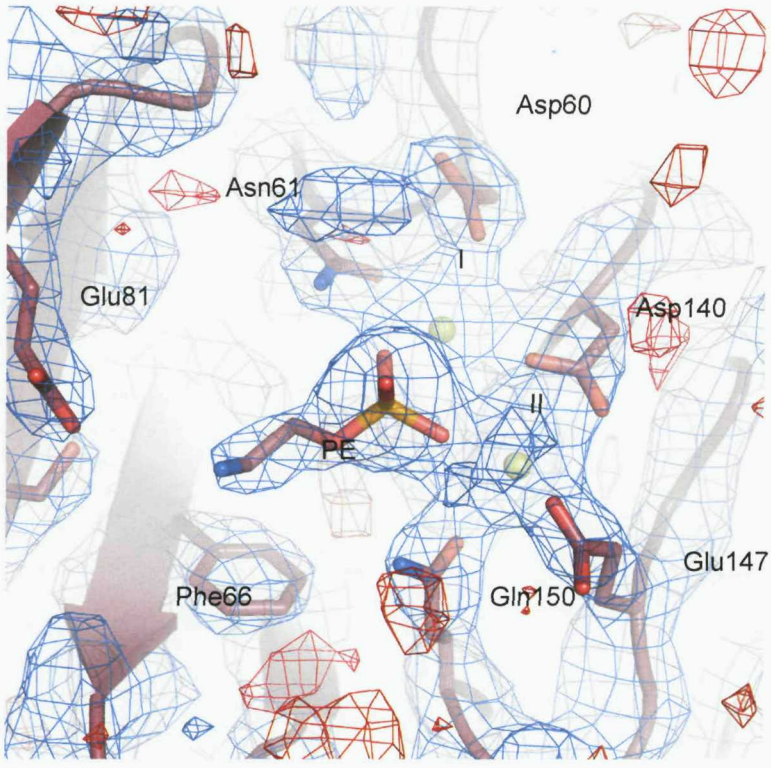

Figure 4.7 $2F_o$-F_c electron density contoured at 1.5 σ (blue) and negative F_o-F_c electron density contoured at -2 σ (red) of the fitted PE molecule and surrounding amino acids. Calcium atoms are shown as yellow spheres.

4.3 The Structure of CRP in Complex with PE

The structure of CRP in complex with PE at 2.7 Å shows good stereo-chemical properties with 87.7 % of residues in the most favoured regions of the Ramachandran plot, 12.3 % in the additional allowed regions and 0 % in the generously allowed and disallowed regions (Figure 4.8).

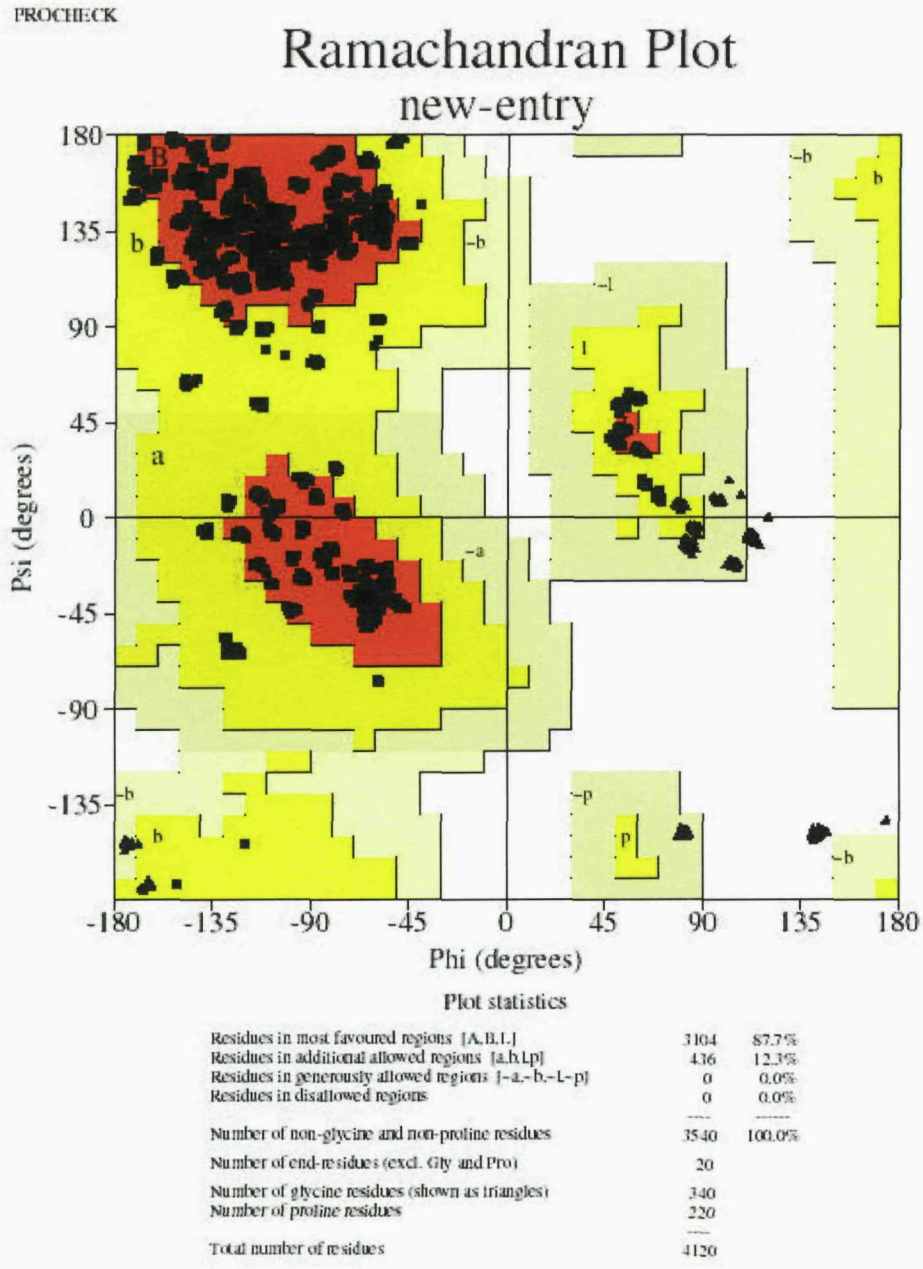

Figure 4.8 Ramachandran plot for the human CRP structure in complex with PE.

An alignment of the temperature factors for the twenty CRP subunits demonstrates a similar B-factor distribution across all subunits (Figure 4.9). The overall B-factor value was relatively high (51.4 $Å^2$), suggesting that the CRP-PE complex is highly flexible or disordered in the crystal. Several regions across the four pentamers have particularly high B-factor values. These regions are between residues 20–30 and 85-95, which have very little electron density surrounding these residues, making model building difficult. The residues 20-30 constitute to a flexible loop region at the surface of the protomer, while the residues 85-95 link strands G and H.

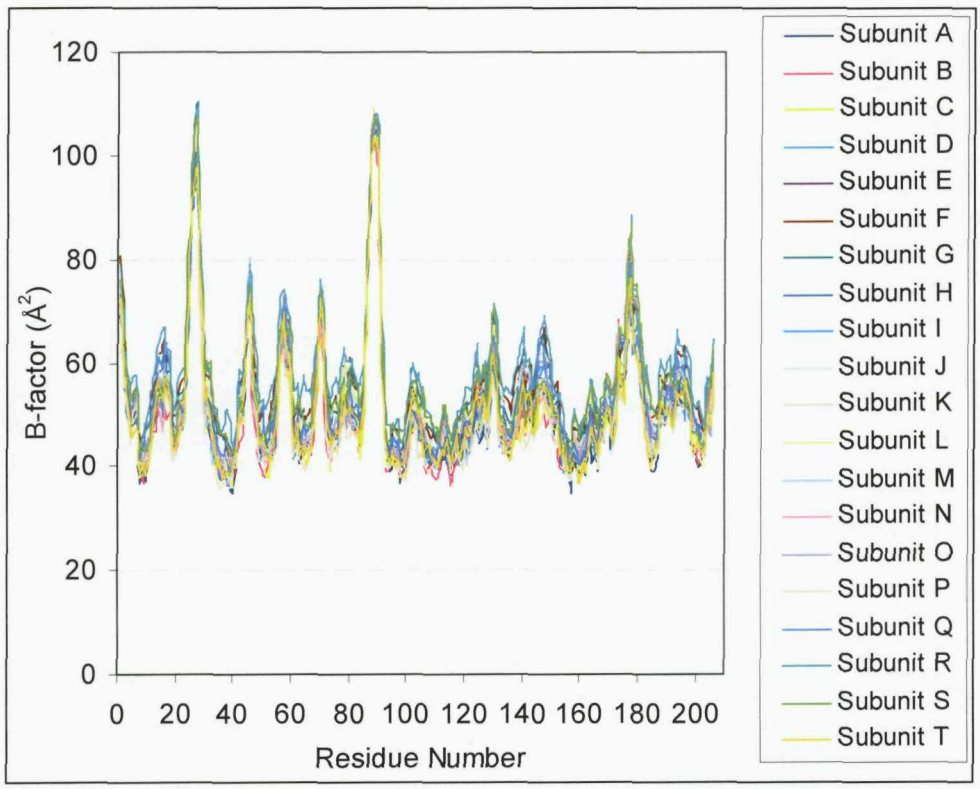

Figure 4.9 Comparison of the average isotropic B-factors for main chain atoms of the twenty CRP subunits.

A comparative alignment of the C_α atom positions between all twenty CRP protomers reveals a C_α rms fit of 0.029 Å (Figure 4.10). The regions in which the largest rms deviation is observed are residues 20-25 and 170-180. These regions have also high B-factor values.

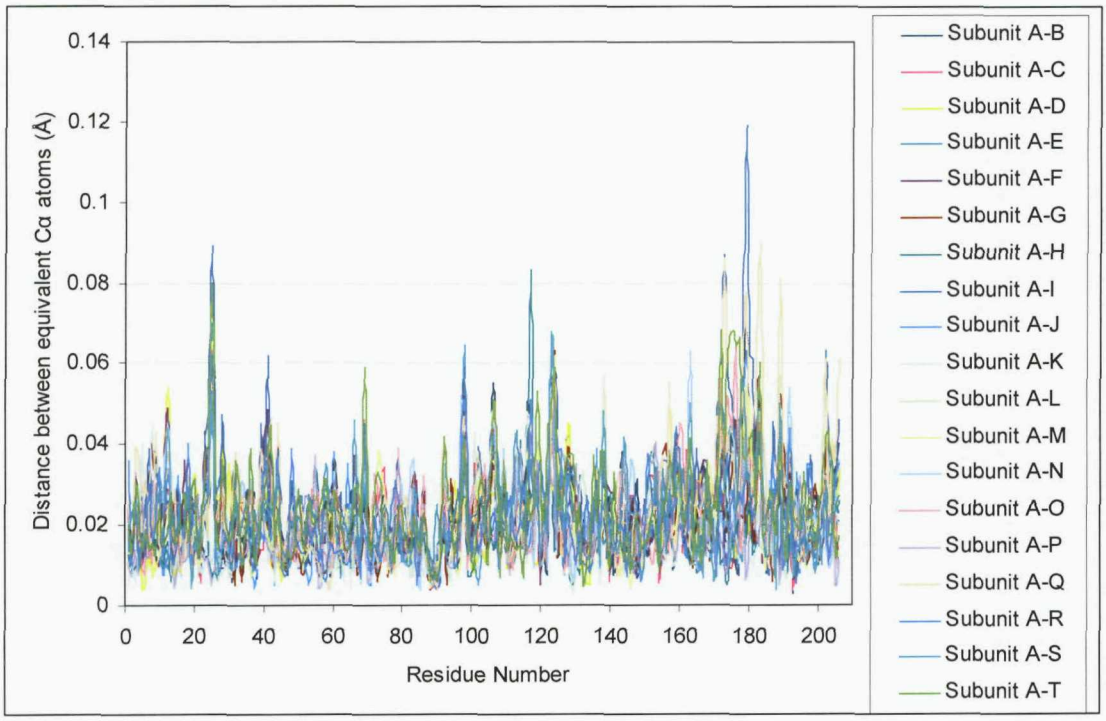

Figure 4.10 A comparison of the root mean squared C_α atom distances between all twenty human CRP protomers in the human CRP-PE complex.

4.4 Structural Comparison of Human CRP in Complex with PE and PC

The overall structure of the CRP-PE complex is similar to the previously described CRP-PC complex (Thompson *et al.*, 1999) with exception of the ligand position as shown by the α-carbon superposition (Figure 4.11).

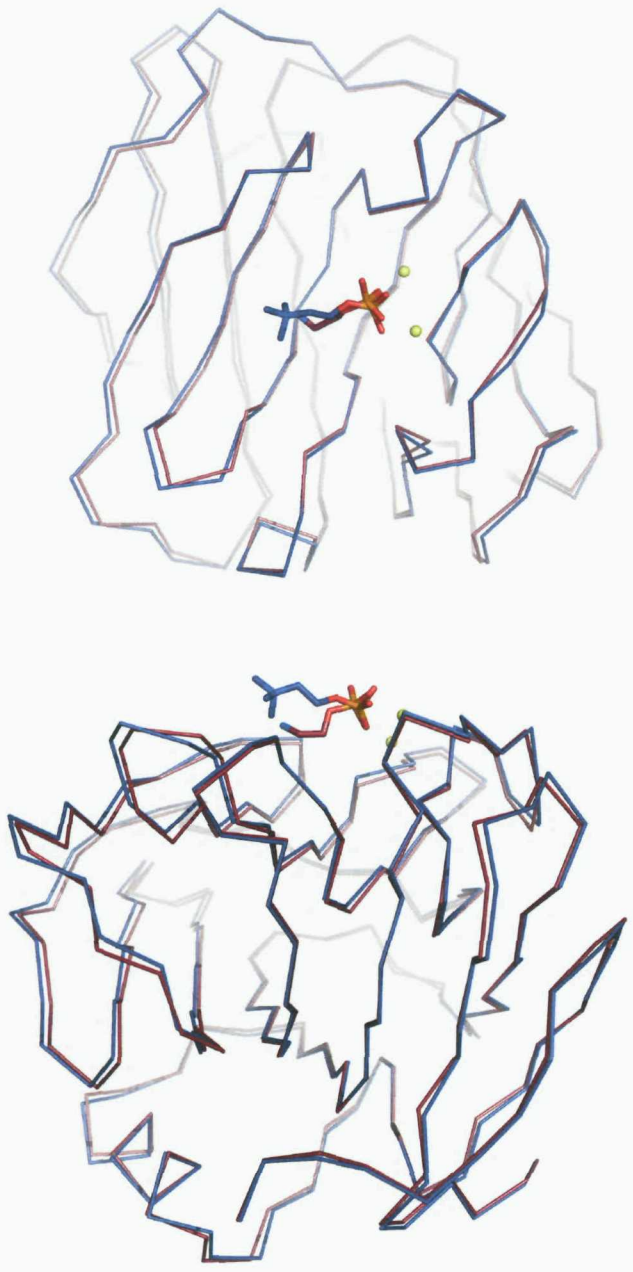

Figure 4.11 Superposition of the 2.5 Å CRP-PC complex (blue) with the 2.7 Å CRP-PE complex structure (dark red). PC is shown blue and PE in dark red. Calcium atoms are as yellow space filling spheres.

Superposition of the CRP-PE structure on human CRP-PC structure yielded an overall rms deviation of 0.41 Å. Plotting the main-chain rms deviation between the protomers taken from the CRP-PE complex and CRP-PC complex confirms the overall similarity of the two structures (Figure 4.12). Regions showing the largest main chain rms deviation are residues 70-75 and 85-95. Analysis of the dihedral angles for these regions in both structures indicates that there are no changes to the secondary structure of CRP in the CRP-PE complex when compared to that of the CRP-PC complex. This might reflect the high flexibility of these regions and suggests that these residues are able to adopt a number of different conformations.

Analysis of the average B-factor values for all five subunits between the structures of CRP-PE and CRP-PC reveals a strongly correlated distribution of B-factor values across the CRP protomers from the two structures (Figure 4.13).

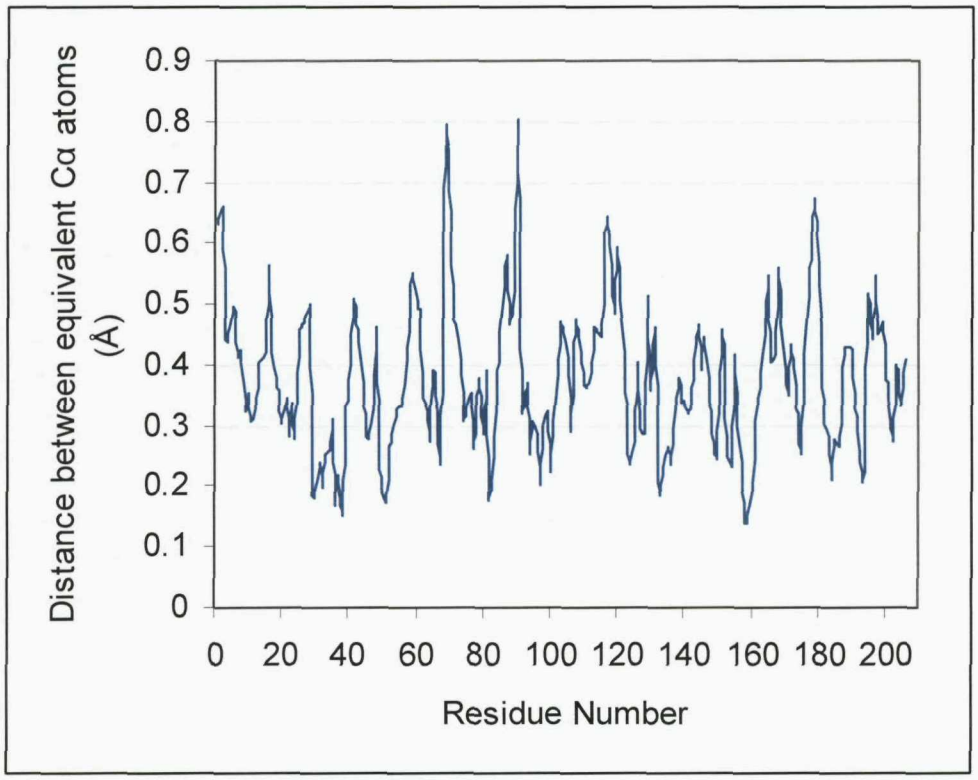

Figure 4.12 Average C_α distance between superimposed subunits of the human CRP-PE and human CRP-PC pentamers.

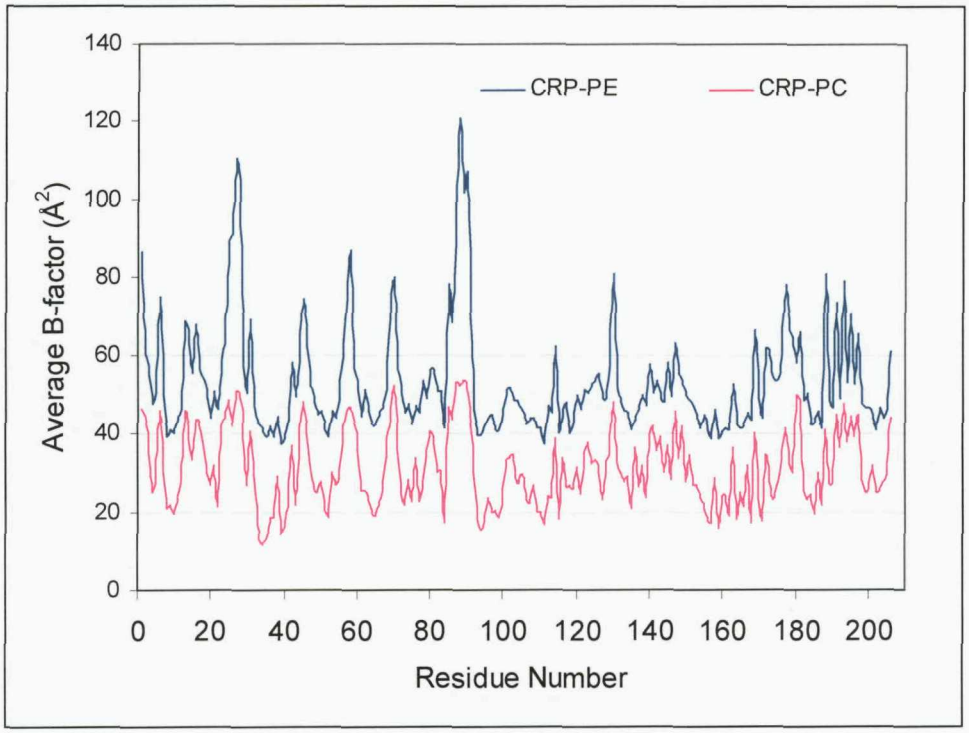

Figure 4.13 A comparison of average isotropic B-factor values for all residues between the human CRP subunits of the human CRP-PE complex (2.7 Å) and human CRP-PC complex (2.5 Å).

4.5 Discussion

This structural study of human CRP in complex with PE provides a full description of the structural basis of PE binding to CRP, a pentraxin traditionally defined by its binding affinity for PC. Characterisation of PE binding by CRP has not been done previously because of problems in obtaining suitable crystals for X-ray studies and because of its lower affinity. The affinity was measured using isothermal titration calorimetry (ITC), which is a technique used to determine the thermodynamic parameters of biochemical interactions. It can directly measure the binding affinity (K_a), enthalpy changes (ΔH), and binding stoichiometry (n) of the interaction between two molecules in solution. Comparative analysis of ITC binding data for CRP and SAP with respect to PE binding indicated that SAP was able to bind to PE with higher avidity than CRP (37 μM for PE with SAP and 41 μM for PE with CRP)(Kolstoe, 2005). However, this analysis of the binding affinities was done under slightly different conditions for the two pentraxins since SAP is insoluble in low salt concentrations. Thus, ITC studies were carried out for SAP in 200 mM calcium chloride, while for CRP in 5 mM calcium chloride. This could have an effect on the measured ligand values.

The X-ray crystal structure of the CRP-PE complex reported here revealed that the position of PE at the CRP binding site is reminiscent of the PC binding site in that both ligands share the coordination of the phosphate group with the calcium ions (Figure 4.14). The nitrogen end of PE is held in place by Glu81, which helps stabilise the ligand position. This is similar in the CRP-PC structure, where the distance between the quaternary nitrogen end of PC and the acidic side chain of Glu81 is 3.8 Å (Figure 4.15).

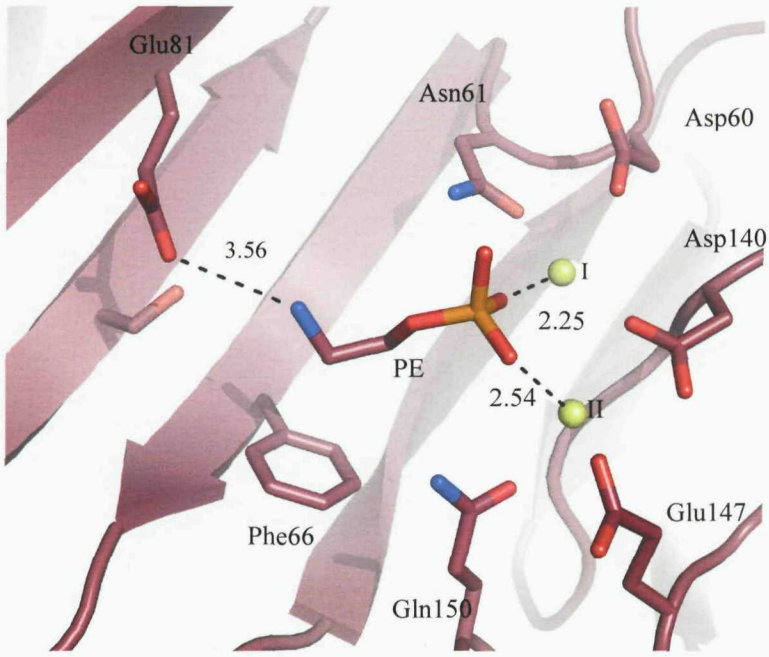

Figure 4.14 Coordination of PE in the CRP binding site. The phosphate group binds to the two calcium ions (yellow), while the nitrogen end of PE points toward the side chain of Glu81. Dashed line show distances in Å. Figure produced in Pymol.

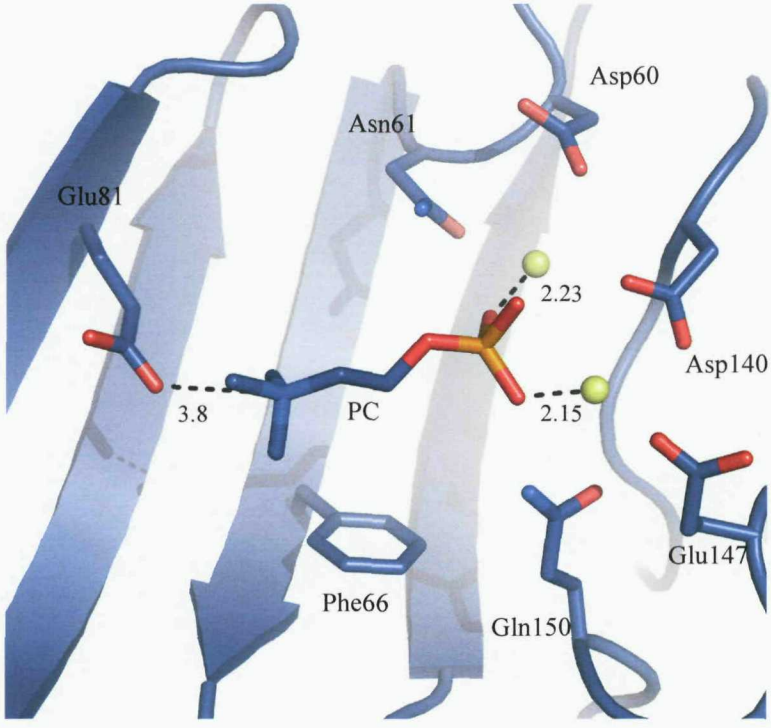

Figure 4.15 Coordination of PC in the CRP binding site. The phosphate group binds to the two calcium ions (yellow), while the quaternary nitrogen end of PC interacts with the side chain of Glu81. Dashed line show distances in Å. Figure produced using the published CRP structure (accession code: 1b09; Thompson *et al.*, 1999) in Pymol.

However, the nitrogen end of PE is positioned further downwards into the hydrophobic pocket in CRP in the CRP-PE structure (Figure 4.16), suggesting that PE fits the binding pocket of CRP far more efficiently. Interestingly, there seems to be a small difference in the geometry of the phosphate group at the calcium ions. This observation could possibly be explained by the polarising effect of the positive metal ions on the phosphate group. Ionic interactions do not represent the same geometric constraints as found in covalent bonds (McPhalen *et al.*, 1991) and therefore the optimum bond angle for this interaction is most likely to represent a compromise between the positions of the three lone pairs on the oxygen atoms (Kolstoe, 2005).

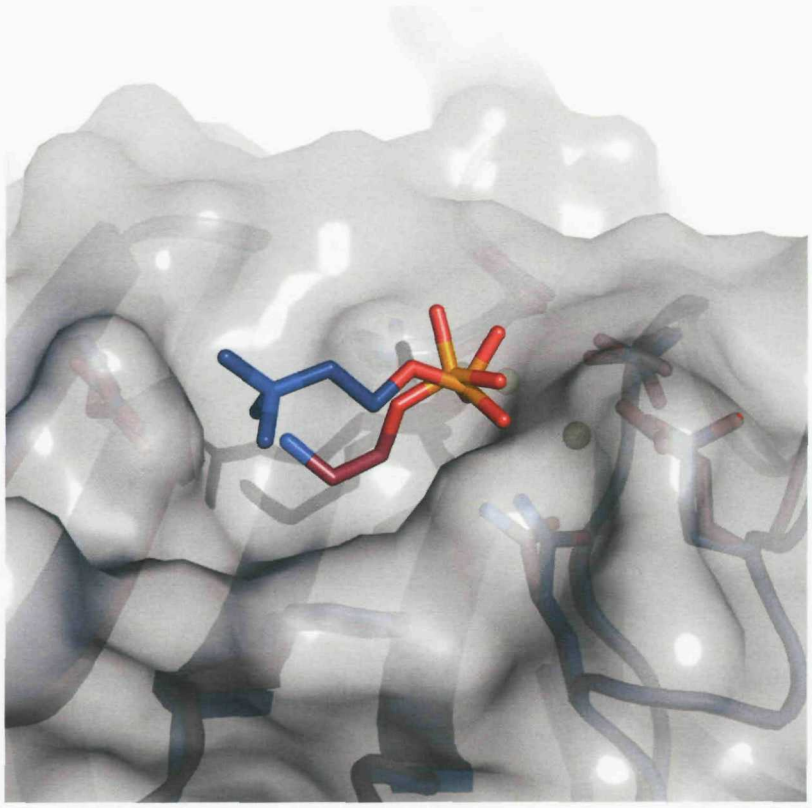

Figure 4.16 Superposition of the 2.5 Å CRP-PC complex (blue) with the 2.7 Å CRP-PE complex structure (red).

Examination of the ligand binding site of the CRP-PE complex structure and the CRP-PC structure shows that there is very little difference in the key residue side-chain positions (Figure 4.17).

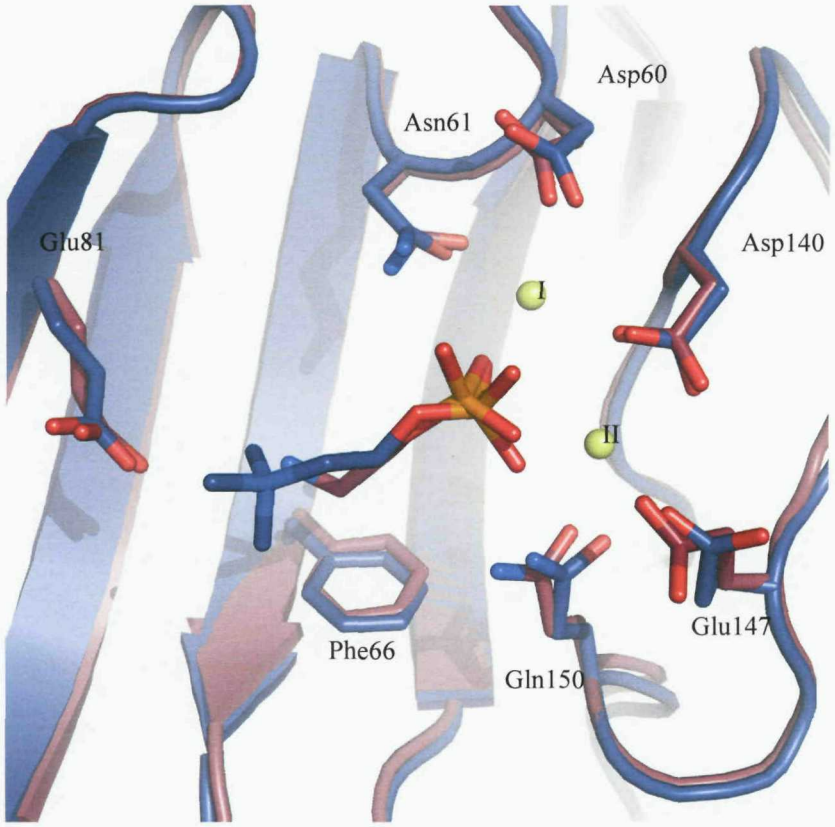

Figure 4.17 Superposition of the 2.5 Å CRP-PC complex (blue) with the 2.7 Å CRP-PE complex structure (red).

In SAP, the nitrogen end of PE is held in place by Glu66 via a water molecule, which helps stabilise the ligand position. The quaternary nitrogen end of PC however, has been suggested can not interact with the equivalent positively charged Lys79. In addition, Tyr74 of SAP would clash with the tri-methyl ammonium group of PC. When the structure of the CRP-PE complex is superimposed onto the structure of the SAP-PE complex, the PE molecule is shown to interact with the calcium ions in the same way (Figure 4.18). The position of the ligand is very similar. However, differences occur between residues Glu147 (CRP) and ASP 145 (SAP) and Asp60 (CRP) and Asp58 (SAP). These differences were also observed when superimposing the human CRP-PC structure onto the human SAP-PE structure.

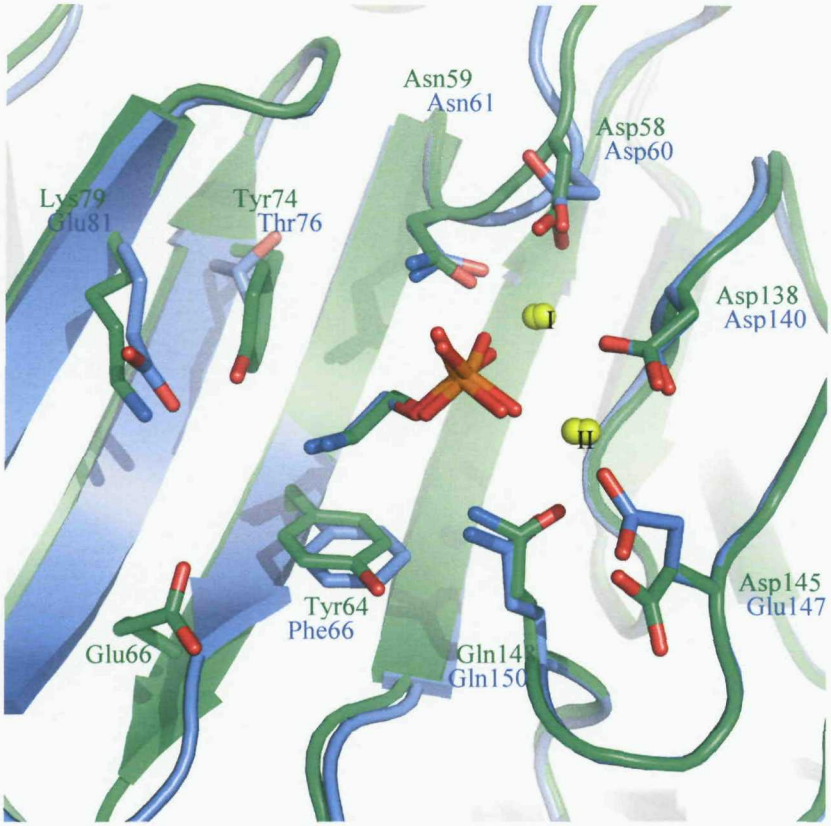

Figure 4.18 Superposition of the structures of the 1.5 Å SAP-PE complex (green) with the 2.7 Å CRP-PE complex (blue).

Chapter 5

Seeking a CRP-C1Q Complex

5.1 Introduction

Many studies now show that the activation of complement by CRP is a major contributor to the tissue damage occurring in stroke and myocardial infarction, the most common causes of death in developed countries. CRP, the classic acute phase protein is always increased after acute myocardial infarction and is found co-deposited with activated complement on myocardial cells within the infarcted area (Lagrand *et al.*, 1997). It has been proposed that CRP binds to ligands exposed in damaged tissue and can then activate complement and its pro-inflammatory actions (Griselli *et al.*, 1999; Thompson *et al.*, 1999; Nijmeijer *et al.*, 2003). Therefore, therapeutic inhibition of CRP is a promising new approach for tissue protection in cases of stroke as well as in acute myocardial infarction (Pepys *et al.*, 2006).

Although early investigations by Jiang *et al.* (1991) characterising the interaction between C1q and C-reactive protein indicate that the CRP binding site on C1q is located on the collagen-like region of C1q, more recent studies by McGrath *et al.* (2006) have established that the CRP binding site is localised on the globular head region (globular domain) rather than the collagen-like region of C1q. Mutagenesis studies to define the topology and structure of the C1q binding site on CRP suggest that the C1q binding site is located on the face of the CRP molecule carrying the α-helix, which is opposite the PC-binding site (Agrawal *et al.*, 1997). Subsequent analysis of the X-ray crystal structures of CRP by Shrive *et al.* (1996) and Thompson *et al.* (1999) have shown a deep cleft on the face opposite to the calcium site, which agrees with the results from the mutagenesis studies.

These studies, in particular the recent elucidation of the X-ray crystal structure of the globular head domain of C1q solved by Garboriaud *et al.* (2003) have led to a plausible three dimensional model of the C1q globular domain in complex with its physiological ligand, CRP. However, knowledge of the exact stoichiometry and the protein-protein interactions between CRP and C1q will eventually aid the development of small molecules capable of disrupting such protein-protein interactions. Therefore, the key objective is to obtain detailed structural information on the mode of interaction of these two proteins by X-ray crystallography.

5.2 Materials and Methods

5.2.1 Purification of Human C1q

Several methods for the isolation of C1q have been described, which utilize the physiological and/or biological properties of the molecule including: (1) affinity chromatography on IgG or immune aggregates (Assimeh *et al.*, 1974; Kolb, 1979), (2) precipitation procedures involving the use of DNA (Agnello *et al.*, 1970) or (3) low ionic strength buffers containing EDTA (Volanakis & Strout, 1972). However, the technique by Tenner *et al.* (1981) based on ion-exchange chromatography and gel filtration chromatography is highly selective, relatively simple to perform and yields fully active, immunoglobulin-free unaggregated C1q. This purification method was developed after it was noted that a large amounts of C1q co-eluted with Factor D from the cationic-exchange resin, Biorex 70 (Lesavre *et al.*, 1979). It is this purification procedure that has been adapted here to isolate C1q in large enough quantities for structural studies. This method utilises BPL paste from the Bio products Laboratory (BPL) as the starting material rather than plasma or serum. BPL paste is a fractionation product of pooled serum, from which Factor VIII, II, IX, X & anti-thrombin have already been extracted.

5.2.1.1 Preparation of BPL paste

BPL paste (100 g) was thawed and resuspended in 400 ml of starting buffer composed of 50 mM sodium phosphate, 82 mM NaCl, and 2 mM EDTA, pH 7.3. The suspension was homogenised using a cell homogeniser to aid resuspension and made up to 10 mM EDTA (by the addition of the appropriate amount of 200 mM EDTA stock solution, pH 7.2).

5.2.1.2 Ion-Exchange Chromatography of Human C1q

The prepared BPL paste (500 ml) was incubated with ~100 g of Biorex 70 beads (cationic exchanger) equilibrated with the starting buffer at 4 °C for 3 hours. After

the incubation period, the beads were washed with 1 litre of more of starting buffer until clear. The washed beads were packed into an Amersham XK50 column and connected to an Amersham Pharmacia Biotech Akta prime with UV absorbance detector and fraction collector attached. The column was further washed until the absorbance at 280 nm reached a baseline. The bound proteins including C1q were eluted with 100 % elution buffer (50 mM sodium phosphate, 500 mM NaCl, 2 mM EDTA, pH 7.3), while collecting 10 ml fractions. All fractions eluted from the Biorex 70 column were analysed by SDS-PAGE. Fractions containing C1q were pooled and concentrated to ~25 ml using 20 ml vivapins with a 100 kDa exclusion cut-off membrane.

5.2.1.3 Gel Filtration Chromatography of Human C1q

A Superose 6 gel filtration column (3 × 60 cm) was equilibrated with a high salt buffer (50 mM Tris, 500 mM NaCl, pH 7.3) at a flow rate of 2 ml/min. A concentrated sample (5 ml) was loaded into a 10 ml superloop and applied to the column at a flow rate of 2 ml/min. All peak fractions eluted from the gel filtration column were analysed by SDS-PAGE. The fractions containing C1q were pooled and concentrated down using vivaspins. The protein solution was buffer exchanged from 50 mM Tris pH 7.3 and 500 mM NaCl to 10 mM Tris pH 7.3, whilst carrying out the vivaspin concentration. The C1q concentration was calculated using the Beer-Lambert relationship with an extinction coefficient of 0.68. The purified protein was stored at 4 °C.

5.2.2 Purification of the C1q Globular Head Domain

It is known that the collagen-like region of C1q can be removed by digestion with bacterial collagenase, resulting in the liberation of the globular C1q head domain (Reid *et al.*, 1974; Knobel *et al.*, 1974). However, the procedure to purify the globular C1q head domain was not described until 1980 (Sasaki *et al.*, 1983). This isolation procedure was further developed by Garboriaud *et al.* (2003) producing large enough quantities to initiate structural studies. It is this experimental procedure that has been adapted here to prepare and purify the C1q globular head domain.

5.2.2.1 Enzymatic Digestion of C1q with Collagenase

Purified C1q (30 mg) was buffer exchanged into the collagenase buffer (50 mM Tris, 5 mM $CaCl_2$ and 250 mM NaCl, pH 7.5) using vivaspins as previously. An appropriate amount of collagenase (3 mg) (Sigma type III from *Clostridium histolyticum*) was added to the sample and incubated at 37 °C for 20 hours. Samples were taken at several time intervals for analysis by SDS-PAGE.

5.2.2.2 Ion-Exchange Chromatography of the Human C1q Globular Head Domain

After the incubation period, the sample was spun at 30 000 g for 20 min at 4 °C. The supernatant was buffer exchanged into the low salt MES buffer (50 mM MES and 25 mM NaCl, pH 6.5) using vivaspins with a cut-off of 30 kDa. To remove the collagenase, the buffer exchanged sample was applied to a 5 ml SP column (cationic-exchange resin from Amersham Biosciences) equilibrated with the low salt MES buffer. The column was washed with this buffer until the UV280nm baseline was achieved. The bound proteins (C1q and C1q globular head domain) were eluted with 100 % high salt MES buffer (50 mM MES and 500 mM NaCl, pH 6.5), while collecting 1 ml fractions. All fractions eluted from the SP column were analysed by SDS-PAGE. Fractions containing both C1q and C1q globular head domains were pooled and concentrated to ~1 ml using 2 ml vivapins with a 30 kDa exclusion cut-off membrane.

5.2.2.3 Gel Filtration Chromatography of the Human C1q Globular Head Domain

To separate undigested C1q from digested C1q (C1q globular head domain), a Superdex 200 gel filtration column (2 × 140 cm) was equilibrated with a high salt buffer (50 mM Tris, 500 mM NaCl, pH 7.3) at a flow rate of 1 ml/min. A concentrated sample (1 ml) was loaded into a 1 ml loop and applied to the column at a flow rate of 1 ml/min. All peak fractions eluted from the gel filtration column were analysed by SDS-PAGE. The fractions containing the globular head domain

of C1q were pooled and concentrated using vivaspins with a cut-off of 30 kDa. The protein solution was buffer exchanged from 50 mM Tris, 500 mM NaCl pH 7.3 to 10 mM Tris (pH 7.3), whilst carrying out the vivaspin concentration. The C1q globular head domain concentration was calculated using the Beer-Lambert relationship, with an extinction coefficient of 0.7. The pure protein was stored at 4 °C.

5.2.3 Protein-Protein Interactions

5.2.3.1 Analytical Gel Filtration Studies of Human C1q

Analytical gel filtration provides a very powerful and conceptually simple method to evaluate the strength of the interaction between CRP and C1q and to obtain a protein complex in solution as the elution position of a protein or of a protein complex depends on its Stokes radius (Horiike et al., 1983). In the simplest approach, the non-equilibrium small zone gel filtration method, a solution containing a protein and a ligand protein is applied in a small volume to the column and the material is resolved in the usual way. The elution positions of the protein and ligand protein in the mixture are compared with those of the protein and ligand protein when each is chromatographed individually on the same column. If a complex has formed between the protein and ligand, the complex will elute earlier than either protein alone. The use of a preformed complex can improve the probability of crystal formation and ordered growth as excess material is removed. More often then not, the protein-protein interaction is of low affinity and different ratios as well as different crystallisation conditions have to be screened.

5.2.3.1.1 Gel Filtration Studies with Human C1q and Human CRP

Highly pure human CRP was provided by Prof Mark Pepys. Separately 50 µl aliquots of C1q and CRP were mixed with buffer A (50 mM Tris, 500 mM NaCl, pH 7.3) and incubated at 20 °C for at least 30 min, prior to loading on to a

Superdex 200 column (bed volume, V_t, of 24 ml; Amersham Biosciences), which had been pre-equilibrated in buffer A. The column was run at 0.5 ml/min and 0.5 ml fractions were collected, while continuously monitoring with a UV detector at a wavelength of 280 nm. Proteins were precipitated from these fractions by acetone precipitation and analysed by SDS-PAGE.

C1q and CRP were mixed in buffer A in the absence or presence of the ligand PC (50 µl total volume) and incubated at 20 °C for at least 30 min, prior to loading on to a Superdex 200 column, which had been pre-equilibrated in buffer A containing the same ligand at the same concentration as the protein mixture. The column was run at 0.5 ml/min and 0.5 ml fractions were collected while continuously monitoring with a UV detector at a wavelength of 280 nm. Proteins were precipitated from these fractions by acetone precipitation and analysed by SDS-PAGE. This procedure was repeated with several different buffers: Buffer B (50 mM Tris, 140 mM NaCl, pH 7.3), Buffer C (50 mM Tris, 20 mM $CaCl_2$, 500 mM NaCl, pH 7.3). The same protocol was used for gel filtration studies with the C1q globular head domain and CRP.

5.2.3.2 Affinity Chromatography Binding Studies of Human C1q

Human CRP was loaded onto a column containing PC Sepharose resin, which had been pre-equilibrated with binding buffer (100 mM Tris, 140 mM NaCl, 2 mM $CaCl_2$, pH 8). The column was run at 0.5 ml/min, while continuously monitoring with a UV detector at a wavelength of 280 nm. When all unbound protein was washed away, purified intact C1q was loaded at 0.3 ml/min. After another washing step, bound CRP-C1q complexes were eluted from the resin with 5 mM PC. Fractions (0.5 ml) were collected and analysed by SDS-PAGE. The same protocol was used to prepare the CRP-C1q globular head domain complex.

5.2.4 Crystallisation Trials of Human C1q with Human CRP

5.2.4.1 Co-crystallisation of Human C1q with Human CRP

A sample containing a mixture of C1q and CRP/PC was mixed with an equal amount of structure screen solution on a cover slip. The cover slip was then placed

over a greased well containing one ml of the structure screen solution forming an enclosed system. This was repeated for the remaining 99 crystallisation conditions from structure screen 1 and 2 and for the Jena Biosciences screens 1-10.

5.2.4.2 Co-crystallisation of the Human C1q Globular Head Domain with Human CRP

A sample containing a mixture of C1q globular head domain and CRP/PC was mixed with an equal amount of structure screen solution on a cover slip. The cover slip was then placed over a greased well containing one ml of the structure screen solution forming an enclosed system. This was repeated for the remaining 99 crystallisation conditions from Structure screen 1 and 2 (Molecular Dimensions) and for the Jena Biosciences screens 1-10.

The following molar ratios have been tried:

1 C1q globular head domain : 6 CRP molecules
1 C1q globular head domain : 1 CRP molecule

5.3 Results

5.3.1 Preparation and Purification of Human C1q

5.3.1.1 Ion-Exchange Chromatography of Human C1q

After preparing the BPL paste, C1q was partially purified by ion-exchange chromatography using Biorex 70 resin. This first purification step is highly selective for C1q as very few proteins other than C1q bind to the cationic-exchange chromatography column. The chart trace is shown below (Figure 5.1).

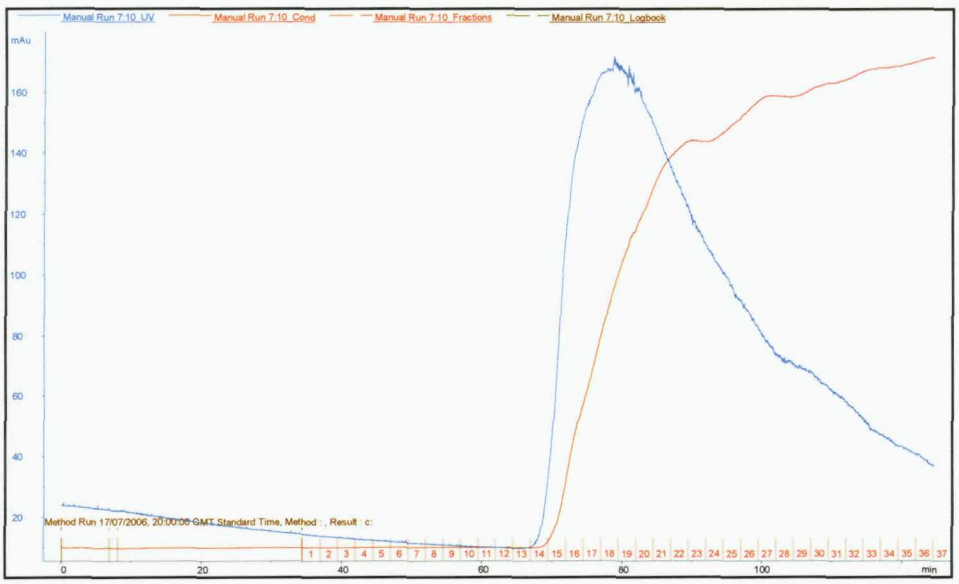

Figure 5.1 Ion-exchange chromatography on the Biorex 70 column from the BPL paste resuspension. Fractions (12 ml) were collected at a flow rate of 5 ml/min and analysed for absorbance at 280 nm (shown in blue) and NaCl concentration (shown in red).

Analysis of the fractions eluted from the Biorex 70 column by SDS-PAGE (Figure 5.2) revealed that C1q is present in fractions 14 - 26. These fractions containing C1q were pooled together and concentrated using vivaspins rather than the original ammonium sulphate precipitation step. This results in a higher yield of protein, although is slightly more time consuming.

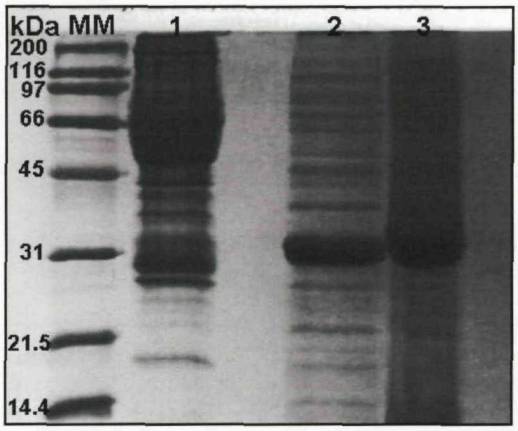

Figure 5.2 13 % Sodium dodecyl sulphate polyacrylamide gel electrophoresis of C1q purification after Biorex 70 cation-exchange chromatography. Protein bands were visualised by Coomasie brilliant blue staining. The flow through (Lane 1) does not appear to contain any C1q. Fraction 20 (Lane 2) and the concentrated elution peak (Lane 3) contains largely C1q with a variety of high and low molecular weight contaminants. Lane MM contains 10 µl of broad molecular weight range standards (Biorad)

5.3.1.2 Gel Filtration Chromatography of Human C1q

Following the partial purification of C1q by ion-exchange chromatography, a sample from the Biorex 70 concentrate was further purified by gel filtration chromatography using a Superose 6 column. The chromatogram from the Superpose 6 column is shown in figure 5.3.

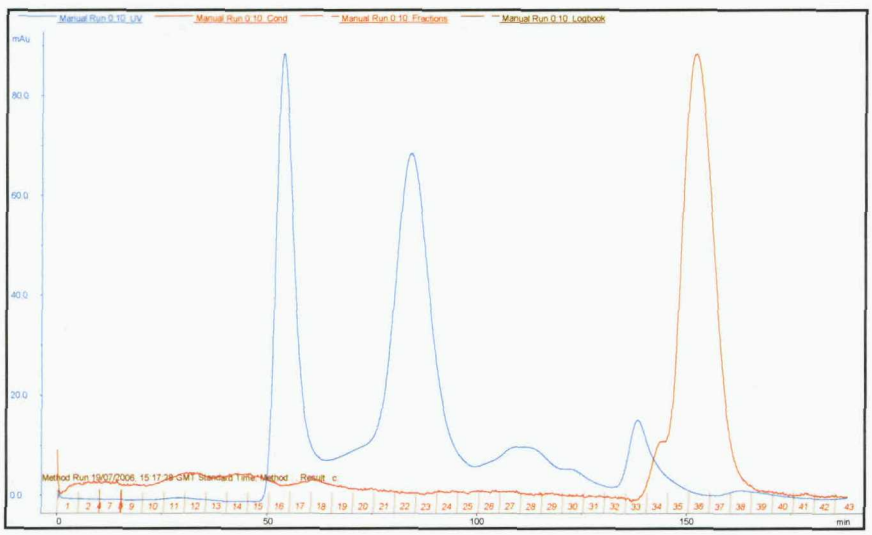

Figure 5.3 Gel filtration on a Superose 6 column of the Biorex concentrate eluent. Fractions (10 ml) were collected at a flow rate of 2 ml/min and analysed for absorbance at 280 nm (shown in blue) and NaCl concentration (shown in red).

This second step in the purification is highly reproducible with the same elution fractions being pooled every run. Analysis of the fractions from the gel filtration column by SDS-PAGE revealed that the second peak contains pure C1q. The first peak appears to contain aggregates and lipids (Figure 5.4). Mostly, several gel filtration runs are necessary due to the viscosity of the concentrated sample after ion- exchange chromatography.

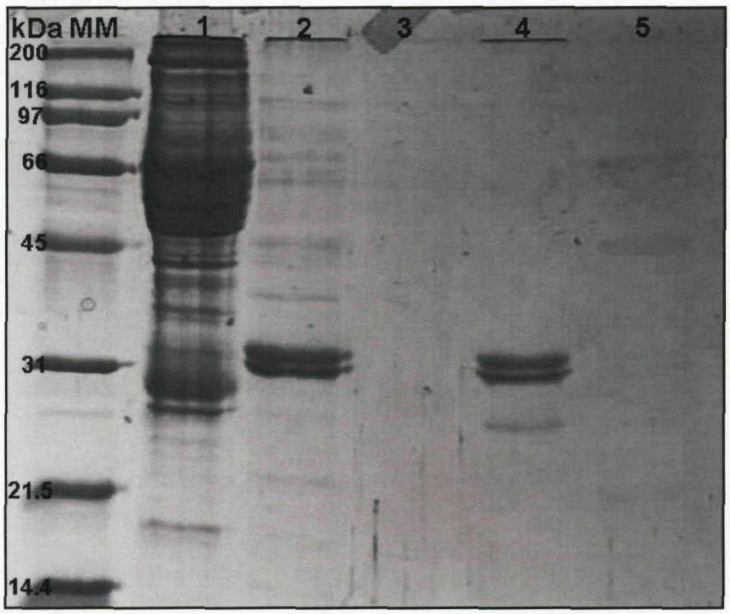

Figure 5.4 13 % Sodium dodecyl sulphate polyacrylamide gel electrophoresis of C1q purification after Superose 6. Protein bands were visualised by Coomasie brilliant blue staining. Fraction 20 from the Biorex 70 column (Lane 2) contains largely C1q with a variety of high and low molecular weight contaminants. Fraction 16 from the Superose 6 column (Lane 3) does not appear to stain by Comassie brilliant blue. Fraction 22 (Lane 4) corresponds to the second peak and contains C1q with one low molecular weight contaminant at ~26 kDa. Fraction 27 of the Superose 6 column (Lane 5) corresponds to peak 3 and contains low and high molecular weight contaminants. Lane MM contains 10 µl of broad molecular weight range standards (Biorad).

5.3.2 Preparation and Purification of the Human C1q Globular Head Domain

5.3.2.1 Enzymatic Digestion of Human C1q with Collagenase

Usually 3 mg of collagenase were added to about 20 - 30 mg of C1q. However, it appears that the best protein yield was achieved when the concentration of C1q was around 1.5 mg/ml. Although, the rate at which collagenase "digests" the

collagenase region of C1q did not seem to vary, it was always necessary to test the extent of digestion by SDS-PAGE prior to loading onto the next column as leaving the reaction for longer than required can be detrimental to the sample (Figure 5.5).

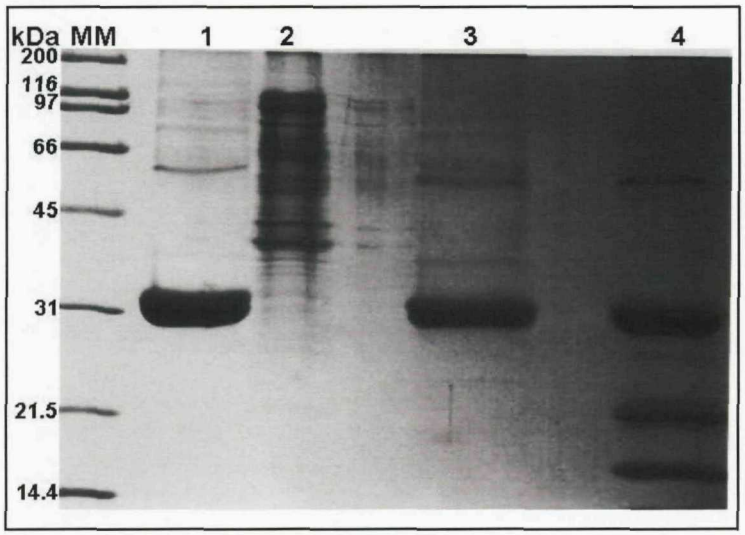

Figure 5.5 13 % Sodium dodecyl sulphate polyacrylamide gel electrophoresis of C1q after collagenase digestion. Protein bands were visualised by Coomasie brilliant blue staining. Fraction 22 (Lane 1) corresponds to the second peak on the Superose 6 trace and contains C1q with one high molecular weight contaminant at ~60 kDa. Lane 2 contains Collagenase. Lane 3 contains C1q after incubation at 37 °C without collagenase. Lane 4 contains C1q and C1q globular head domains after 20 hours incubation with collagenase.

5.3.2.2 Ion-Exchange Chromatography of the Human C1q Globular Head Domain

A second cationic-exchange column (SP) was used to remove the collagenase from the sample. Collagenase does not seem to bind to the column and a major protein peak elutes. The chromatogram from the ion-exchange column is shown in figure 5.6.

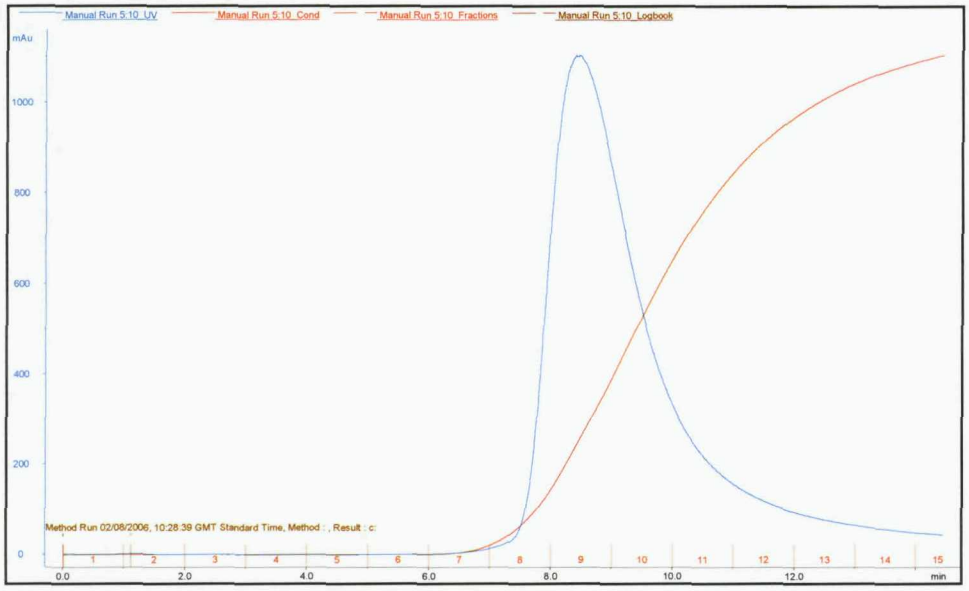

Figure 5.6 Ion-exchange chromatography on a SP column of the collagenenase digest of C1q. The chart trace of the IEX elution profile. Fractions (1 ml) were collected at a flow rate of 2 ml/min and analysed for absorbance at 280 nm (shown in blue) and NaCl concentration (shown in red).

Analysis of the eluted fractions by SDS-PAGE showed that 85 % of C1q was converted to C1q globular head domains and about 15 % of C1q remained intact (Figure 5.7).

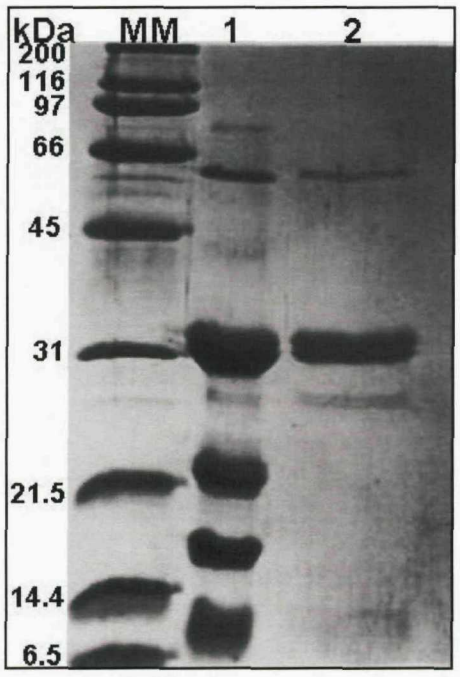

Figure 5.7 13 % Sodium dodecyl sulphate polyacrylamide gel electrophoresis of C1q after cationic-exchange chromatography on a SP column. Protein bands were visualised by Coomasie brilliant blue staining. Lane 1 contains C1q and C1q globular head domains after 20 hours incubation with collagenase.

5.3.2.3 Gel Filtration Chromatography of the Human C1q Globular Head Domain

A second gel filtration chromatography column (Superdex 200) was used in order to separate remaining intact C1q from C1q globular head domains. The chart trace is shown below (Figure 5.8).

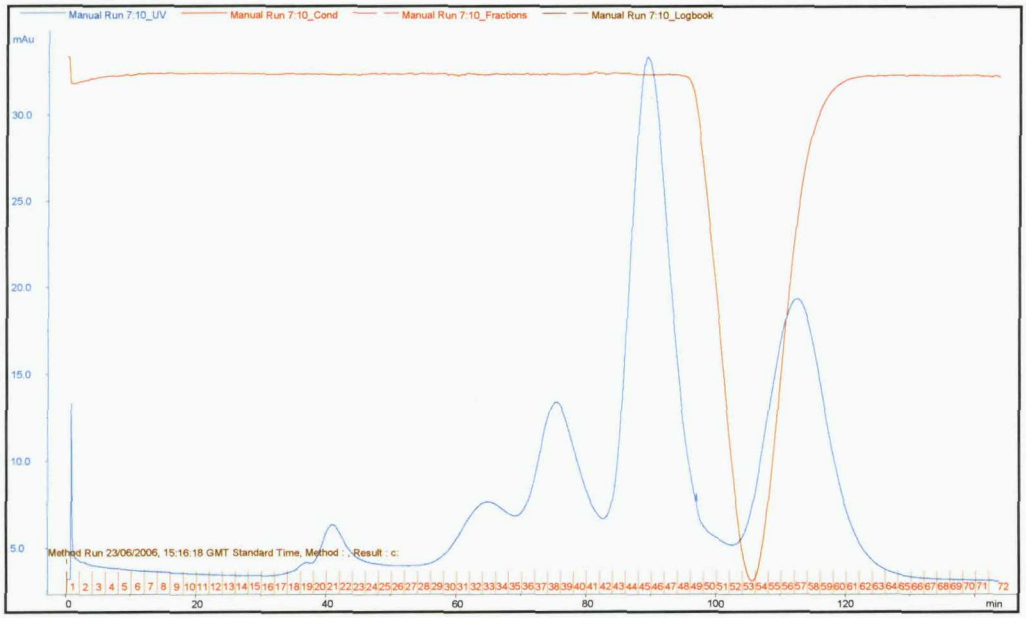

Figure 5.8 Gel filtration on a Superdex 200 column of the ion-exchange concentrate. Fractions (2 ml) were collected at a flow rate of 1 ml/min and analysed for absorbance at 280 nm (shown in blue) and NaCl concentration (shown in red).

Analysis of the eluted fractions by SDS-PAGE revealed that C1q was present in fractions 30-40, while the C1q head domains were in fractions 42-49 (Figure 5.9).

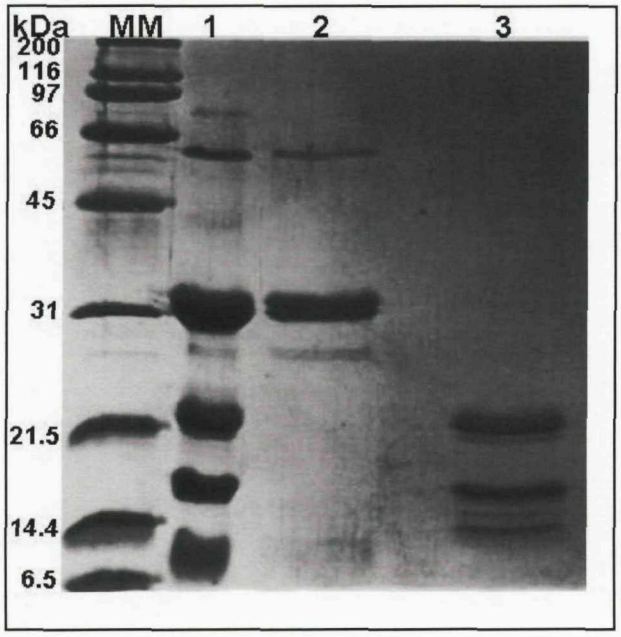

Figure 5.9 13 % Sodium dodecyl sulphate polyacrylamide gel electrophoresis of C1q after cationic-exchange chromatography on a SP column. Protein bands were visualised by Coomasie brilliant blue staining. Lane 1 contains C1q and C1q globular head domains after 20 hours incubation with collagenase. Lane 2 corresponds to the second peak of the Superose 6 column and contains C1q with one high molecular weight contaminant at ~60 kDa. Lane 3 contains C1q globular head domains after gel filtration on a Superdex 200 column. Digestion was not always complete.

The fractions containing C1q globular head domains were pooled together and concentrated down to 10 mg/ml. The final protein is >99 % pure and yields are typically 10 mg for 100 g of BPL paste. Freezing appears to be detrimental to the sample. Therefore the pure protein sample was stored at 4 °C.

5.3.3 Mass Spectrometry of the Human C1q Globular Head Domain

Mass spectra were obtained for the C1q globular head domains. Analysis of mass spectrometry yielded two major peaks with mass values of about 14707.00 Da and 16739.00 Da and a very small third peak with a mass value of 17670.00 Da. Mass spectra are shown below (Figure 5.10 & 5.11).

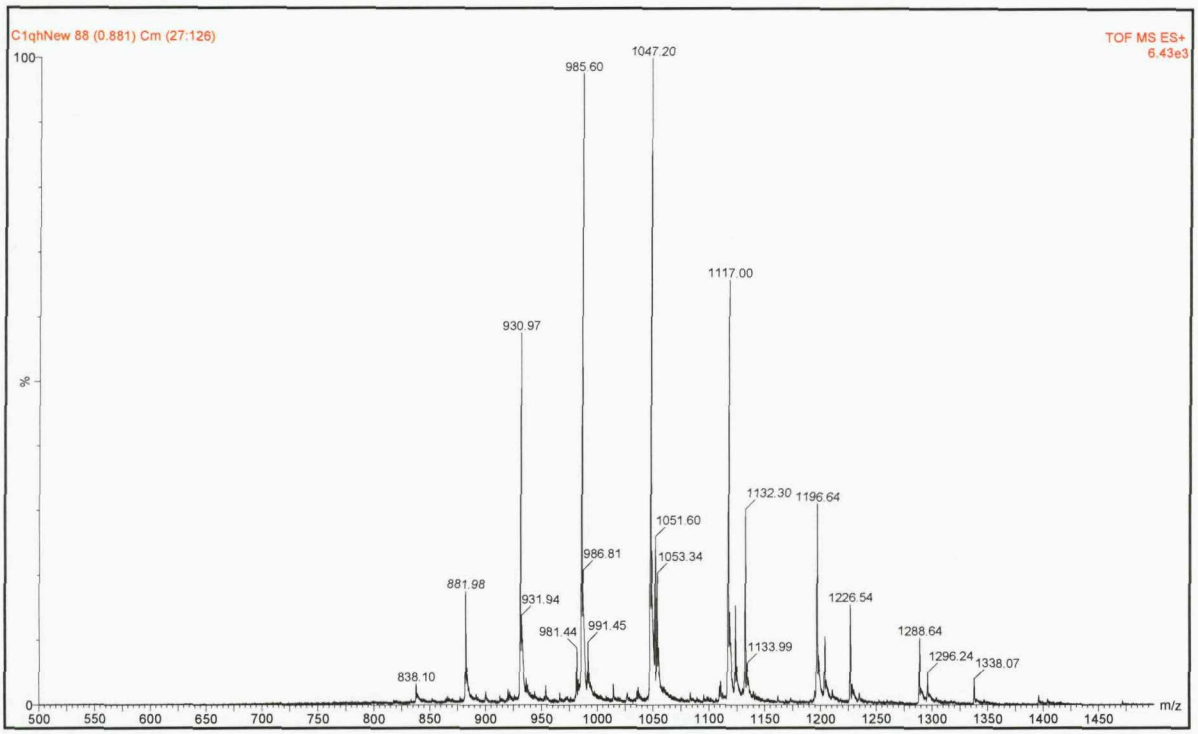

Figure 5.10 Mass spectrometry trace of C1q globular head domains.

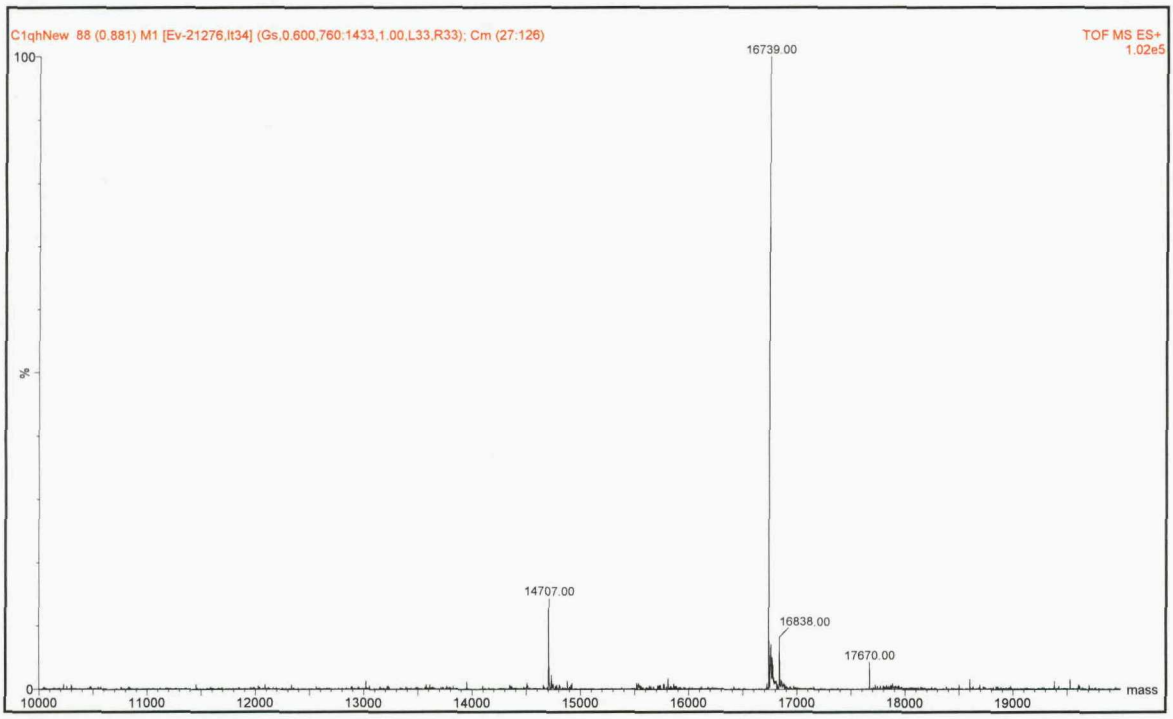

Figure 5.11 Mass spectrum of C1q globular head domains.

5.3.4 Analytical Gel Filtration Studies of Human C1q

When CRP was applied to a gel filtration column, it was eluted as a single peak (Figure 5.12), corresponding to a molecular mass of 115 kDa. When a similar quantity of C1q was applied to the column, it was eluted as a single peak (Figure 5.13), corresponding to a molecular weight of 460 kDa.

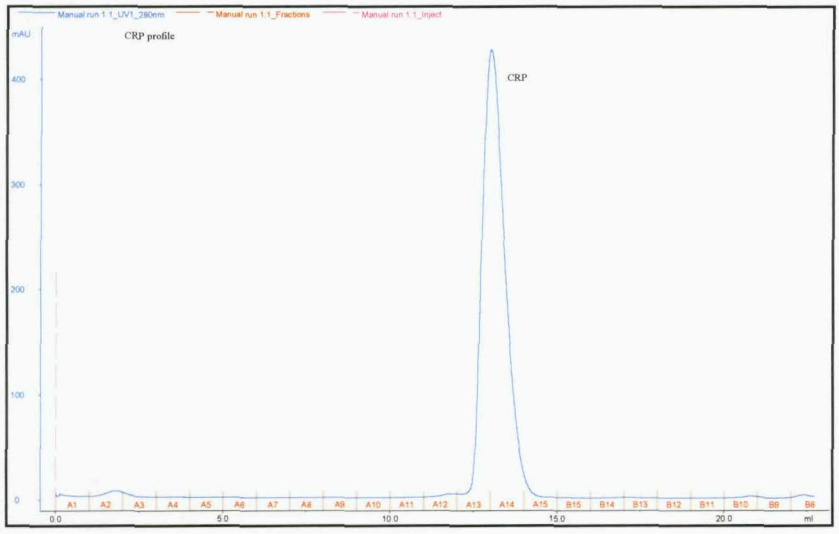

Figure 5.12 Analytical gel filtration chromatography of pure human CRP. The sample was analysed on a Superdex 200 column using 50 mM Tris pH 7.3 and 0.5 M NaCl as the buffer. Fractions (1 ml) were collected at a flow rate of 0.3 ml/min and analysed for absorbance at 280 nm (shown in blue). Human CRP is retained as a single peak at min with an estimated molecular mass of 115 kDa compared with standard proteins (results not shown).

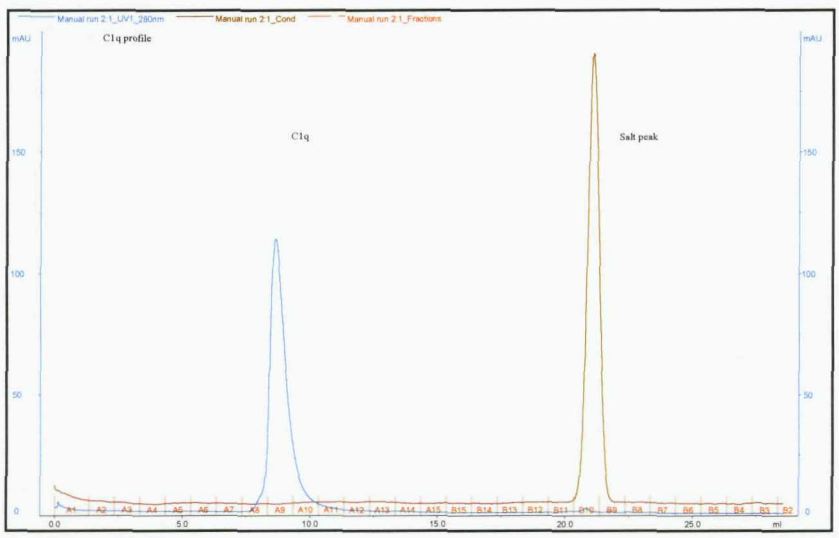

Figure 5.13 Analytical gel filtration chromatography of pure human C1q. The sample was analysed on a Superdex 200 column using 50 mM Tris pH 7.3 and 0.5 M NaCl as the buffer. Human C1q is retained as a single peak at 8 ml with an

estimated molecular mass of 460 kDa compared with standard proteins (results not shown). Fractions (1 ml) were collected at a flow rate of 0.3 ml/min and analysed for absorbance at 280 nm (shown in blue) and NaCl concentration (shown in light brown).

When a mixture of CRP and C1q was applied to the column (in buffer A), two peaks were observed (Figure 5.14 & 5.15). The elution volume of each peak corresponded exactly with the same elution volume as seen with CRP and C1q alone. The first peak (Peak 1) contained C1q, while the second peak contained CRP as shown by SDS-PAGE analysis of the precipitated fractions.

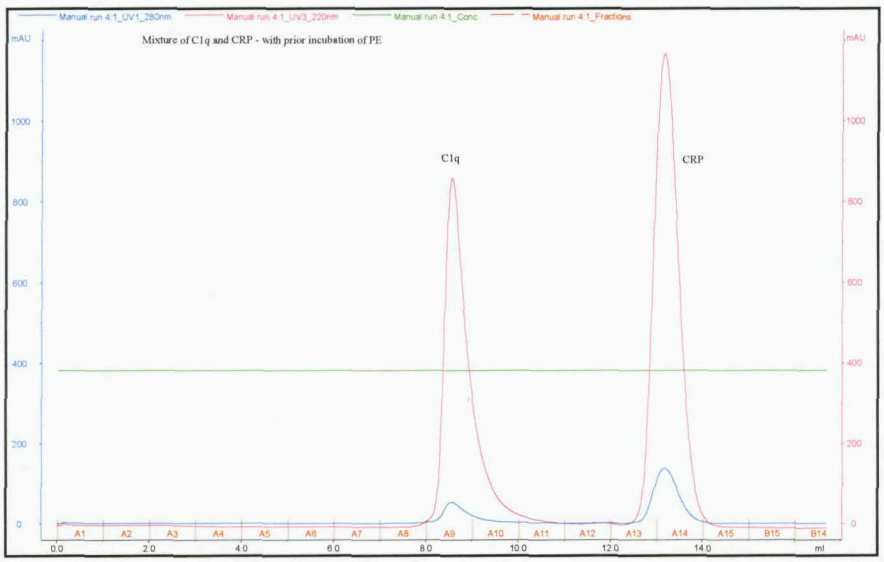

Figure 5.14 Analytical gel filtration chromatography of a mixture of pure human CRP and human C1q. The mixture was analysed on a Superdex 200 column in a buffer of 50 mM Tris pH 7.3 and 0.5 M NaCl at a flow rate of 0.3 ml/min. Fractions (1 ml) were collected and analysed for absorbance at 280 nm (shown in blue) and 220 nm (shown in pink). Two peaks where observed. The elution volume of each peak corresponded exactly with the same elution volume as seen with CRP and C1q alone. The first peak (Peak 1) contained C1q, while the second peak contained CRP as shown by SDS-PAGE analysis of the precipitated fractions.

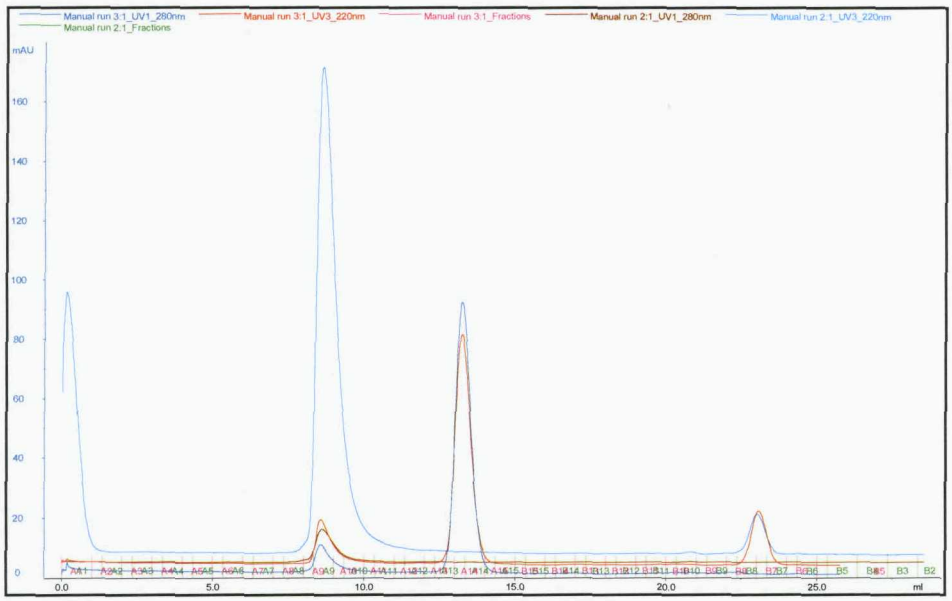

Figure 5.15 Comparison of gel filtration profiles of human CRP, human C1q and the mixture. Absorbance at 280 nm (shown in blue) corresponds to mixture of CRP and C1q, while absorbance at 280 nm (shown in light brown corresponds to C1q alone. Abs at 220 shown in red) corresponds to the mixture of CRP and C1q, while abs at 220 nm (shown in cyan) corresponds to C1q alone. A peak at a higher molecular weight or a shift of the C1q peak indicating the formation of a complex was not observed.

5.3.5 Affinity Chromatography Studies of Human C1q

To obtain CRP–C1q complexes in solution, an affinity chromatography experiment using PC Sepharose beads was designed. After applying both CRP and C1q to the PC affinity column, elution of the protein-protein complex was achieved by PC rather than EDTA addition. Two different sized peaks were observed (Figure 5.16).

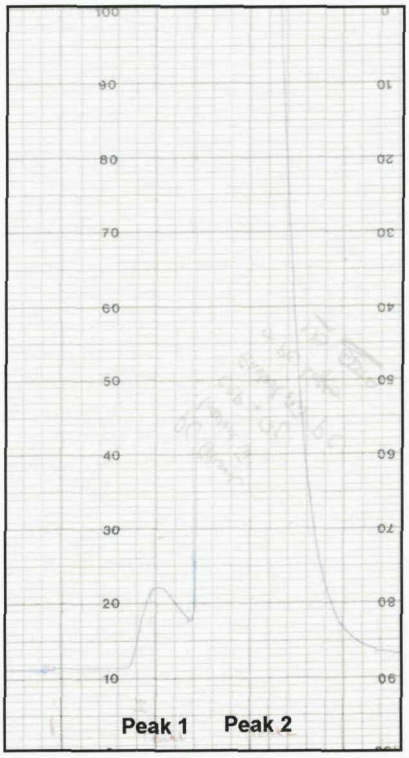

Figure 5.16 Affinity chromatography on a PC column with human CRP and C1q. Human CRP was loaded onto a column containing PC Sepharose resin, pre-equilibrated with binding buffer (100 mM Tris, 140 mM NaCl, 2 mM $CaCl_2$, pH 8). The column was run at 0.5 ml/min, while continuously monitoring with a UV detector at a wavelength of 280 nm. Following loading of C1q, the bound complex was eluted using PC. Two peaks were observed indicating the formation of a complex.

SDS-PAGE analysis of fractions from the smaller peak revealed the presence of both CRP and C1q (Figure 5.17). Visual inspection of the bands suggested that both proteins were present in approximately equal amounts, which suggests that a complex containing one molecule of CRP and one molecule of C1q had been isolated. SDS-PAGE analysis of the fractions of the larger peak revealed also the presence of both proteins. However, there was a large excess of CRP, despite an excess of C1q being loaded.

Figure 5.17 13 % Sodium dodecyl sulphate polyacrylamide gel electrophoresis after affinity chromatography on a PC Sepharose column. Protein bands were visualised by Coomasie brilliant blue staining. Lane 1 contains CRP alone. Lane 2 corresponds to the second peak of the affinity chromatography column and contains a large excess of CRP. Lane 3 contains C1q alone. Lane 4 corresponds to the first peak of the affinity chromatography column and contains an equal amount of C1q and CRP, which suggests that a protein complex was formed.

Loading of C1q onto the PC Sepharose column separately gave no indication for non-specific binding of C1q to the beads.

5.3.6 Co-crystallisation of Human CRP with Human C1q

No crystals have been observed.

5.3.7 Co-crystallisation of Human CRP with the Human C1q Globular Head Domain

Two different crystal forms were grown from a CRP-C1q globular head domain mixture in a similar crystallisation condition.

Crystals of the form I (Figure 5.18) were grown upon equilibration of the protein mixture (6 CRP: 1 C1q globular head domain) against reservoir buffer containing 18 % PEG 4000, 150 mM Tris pH 7.0, 100 mM $MgCl_2$. These crystals appeared after 3 weeks with dimensions of 200 × 100 × 100 μm.

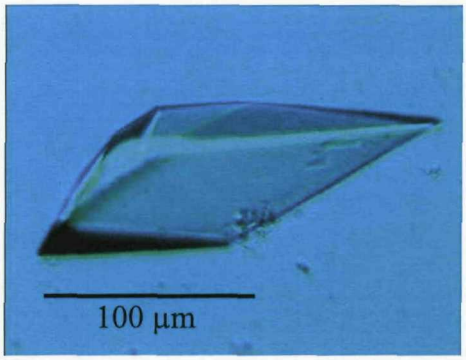

Figure 5.18 Crystals of crystal form I were grown by the hanging-drop method from a ratio of 1 C1q head domain : 6 CRP molecules.

Crystals of the crystal form II (Figure 5.19) were grown in 30 % PEG 4000, 100 mM Tris pH 8.0, 100 mM Na Acetate from a CRP-C1q globular head domain mixture (1:1). These crystals appeared after 2 weeks with dimensions of 150 × 100 × 100 µm.

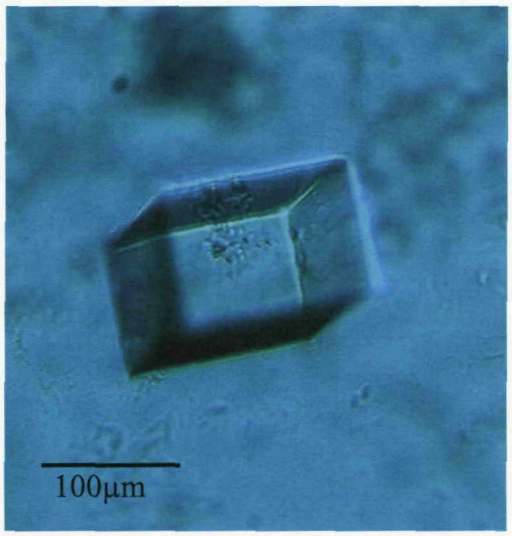

Figure 5.19 Crystals of crystal form II were grown by the hanging-drop method from a ratio of 1 C1q globular head domain : 1 CRP molecule.

5.3.8 Data Collection of the two Crystal Forms

5.3.8.1 Crystal Form I

5.3.8.1.1 Data Collection and Processing from Crystal Form I

X-ray diffraction data from crystal form I were collected to 3.5 Å on the beamline ID 29 at the ESRF in Grenoble on an ADSC Quantum-4 CCD detector. A data set was collected under cryogenic temperatures using oscillation angles of 1 degree and an exposure time of 6 seconds (Figure 5.20). The crystal to detector distance was 456.62 mm.

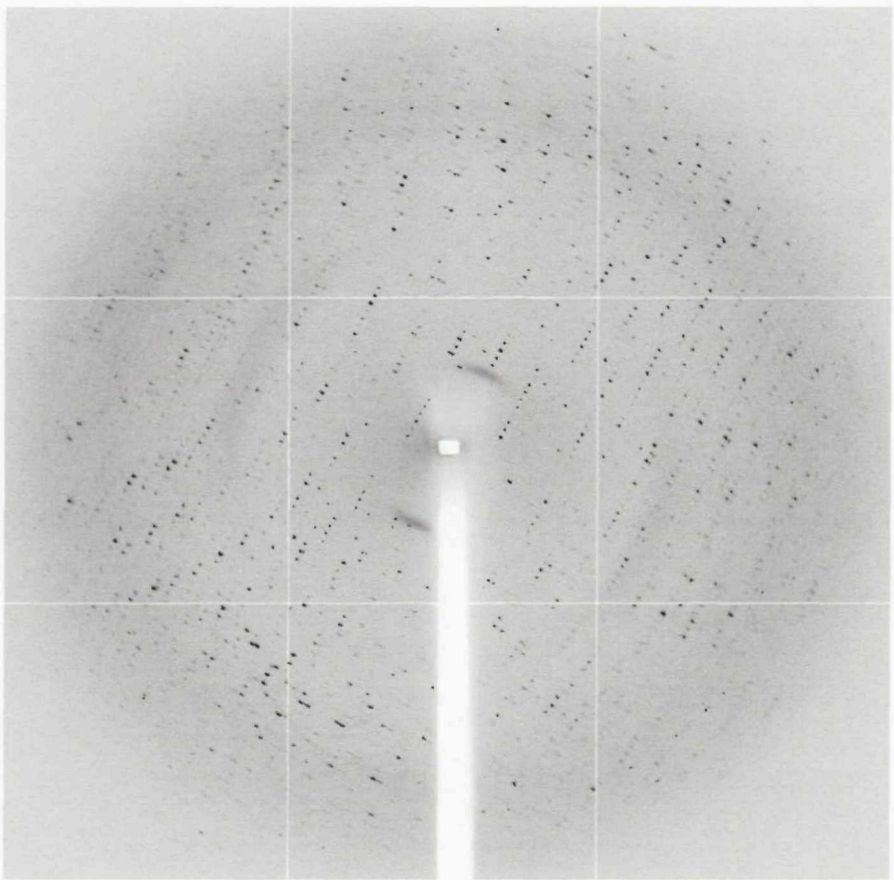

Figure 5.20 A 1° oscillation diffraction image collected from crystal form I at the ESRF (France).

The data were processed using MOSFLM and the CCP4 suite of programs. Initial unit cell dimension determination suggested unit cell of dimensions a = 78.67 Å, b

= 95.66 Å, c = 159.17 Å, α = 79.3, β = 76.7° and γ = 69.8° implying a triclinic space group (Table 5.1).

Penalty	Lattice	a	b	c	α	β	γ	Possible space groups
106	mP	78.78	95.83	160.52	90.8	105.2	110.4	P2, $P2_1$
97	mC	143.70	100.64	159.14	90.1	104.5	101.9	C2
46	mC	108.04	78.78	169.72	91.1.8	115.0	86.2	C2
14	aP	78.67	95.66	160.51	90.9	105.2	110.2	P1
0	aP	78.67	95.66	159.18	79.3	76.7	69.8	P1

Table 5.1 Penalty table generated by MOSFLM. This table shows the possible unit cell dimensions and space groups for the data collected from crystal form I.

As a result, the data were processed, merged and reduced in the space group P1 as previously described. Table 5.2 gives the final processing statistics of the data collected from crystal form I.

Space Group	P1
Unit cell dimensions (Å) (°)	a = 78.81, b = 95.77, c = 159.08 α = 79.1, β = 77.15, γ = 69.22
Resolution range (Å)	88.73 – 3.5 (3.69 - 3.5)
Measured reflections	97791 (14587)
Unique Reflections	50203 (7358)
Multiplicity	1.9 (2.0)
Completeness (%)	94.5 (94.4)
R-merge (%)	18 (49.8)
(I)/σ(I)	6.3 (2.4)

Table 5.2 A summary of the data processing statistics of the crystal form I. Figures in parentheses apply to the highest resolution shell.

5.3.8.1.2 Molecular Replacement of Crystal Form I

Initial phases for crystal form I were determined by molecular replacement with the program MOLREP. Both the hetero-trimer from the crystal structure of the globular head domain of human C1q (accession code 1PK6; Garboriaud et al., 2003) and the

homo-pentamer from the crystal structure of human CRP (accession code; Thompson et al., 1999) were used as search models. The solvent content of the unit cell was estimated to be 47 % for four CRP pentamers in the asymmetric unit and 60 % for three pentamers in the asymmetric unit (Matthews, 1968). It seemed most likely that the asymmetric unit contained four CRP pentamers.

The cross rotation search was performed using reflections within the resolution range 51.45 to 4.58 Å and yielded 20 significant solutions when a single CRP pentamer was used as a search model (Table 5.3). These twenty solutions corresponded to the five orientations of the four CRP pentamers within the target asymmetric unit as implied by the solvent calculations. No solutions were found when a single heterotrimeric C1q globular head domain was used as a search model.

Peak no.	α (°)	β (°)	γ (°)	Rf/σ
1	48.68	64.95	136.44	10.76
2	138.22	26.50	242.50	10.57
3	224.46	135.77	124.77	10.39
4	91.60	149.42	334.99	10.38
5	85.27	82.36	305.62	10.36
6	221.82	68.74	150.99	10.21
7	288.95	141.31	355.10	10.04
8	264.61	76.85	317.93	9.70
9	113.13	63.32	271.65	9.32
10	307.32	13.80	255.11	9.29
11	286.73	168.62	172.30	9.22
12	279.42	100.06	345.90	9.08
13	50.22	94.47	107.23	9.07
14	79.99	122.48	296.23	8.81
15	34.57	130.82	108.07	8.75
16	195.25	51.46	195.11	8.62
17	239.09	104.88	257.76	8.61
18	252.27	36.93	331.30	8.59
19	78.96	30.55	116.82	8.23
20	346.99	136.50	49.24	7.89
21	323.99	79.68	293.44	4.51
22	323.83	78.29	291.69	4.47
23	112.38	144.67	137.91	4.38

Table 5.3 Cross-rotation function peaks found by MOLREP for the data from crystal form I using 1b09 as the search model.

The position of each CRP pentamer molecule within the asymmetric unit was determined following a translation search calculated in space group P1. The search gave a solution in P1 with four CRP pentamers in the asymmetric unit with a R-factor of 50.3 %.

In order to check the suggested molecular replacement solution, the crystal packing was visualized using Pymol (Delano, 2002). The diagram confirmed the feasibility of the present solution and confirmed the presence of four CRP pentamers in the asymmetric unit (Figure 5.21).

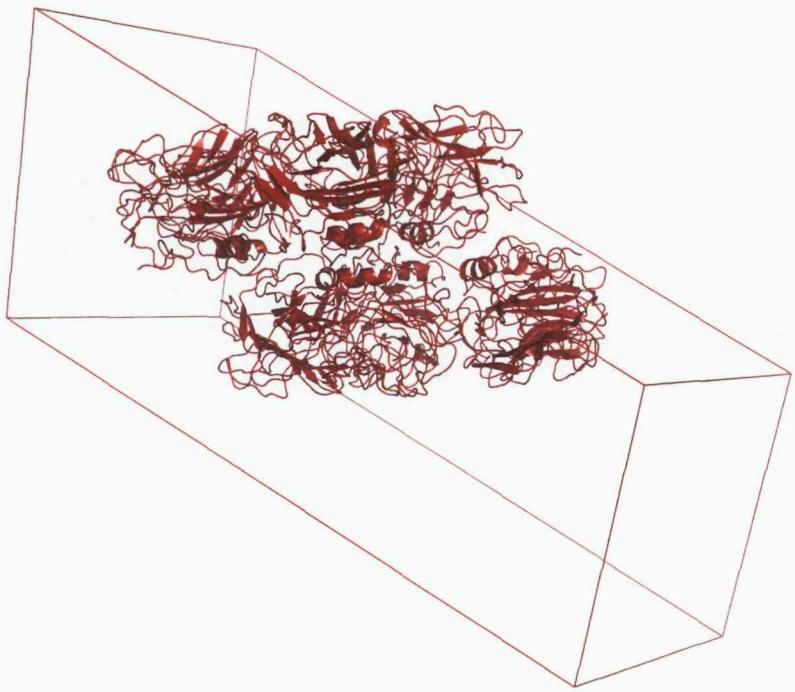

Figure 5.21 Crystal packing of crystal form I (produced in Pymol). The crystal form I belonged to the triclinic space group P1 (a = 78.81 Å, b = 95.77 Å, c = 159.08 Å, α = 79.1°, β = 77.15°, γ = 69.22°) and contained four CRP pentamers in the asymmetric unit. Only two pentamers are shown for clarity.

5.3.8.2 Crystal Form II

5.3.8.2.1 Data Collection and Processing from Crystal Form II

X-ray diffraction data from crystal form II were collected to 1.6 Å on the beamline ID 14-3 at the ESRF in Grenoble on an ADSC Quantum-4 CCD detector. The data were collected under cryogenic temperatures using oscillation angles of 1 degree and an exposure time of 5 seconds (Figure 5.22). The crystal to detector distance was 150 mm.

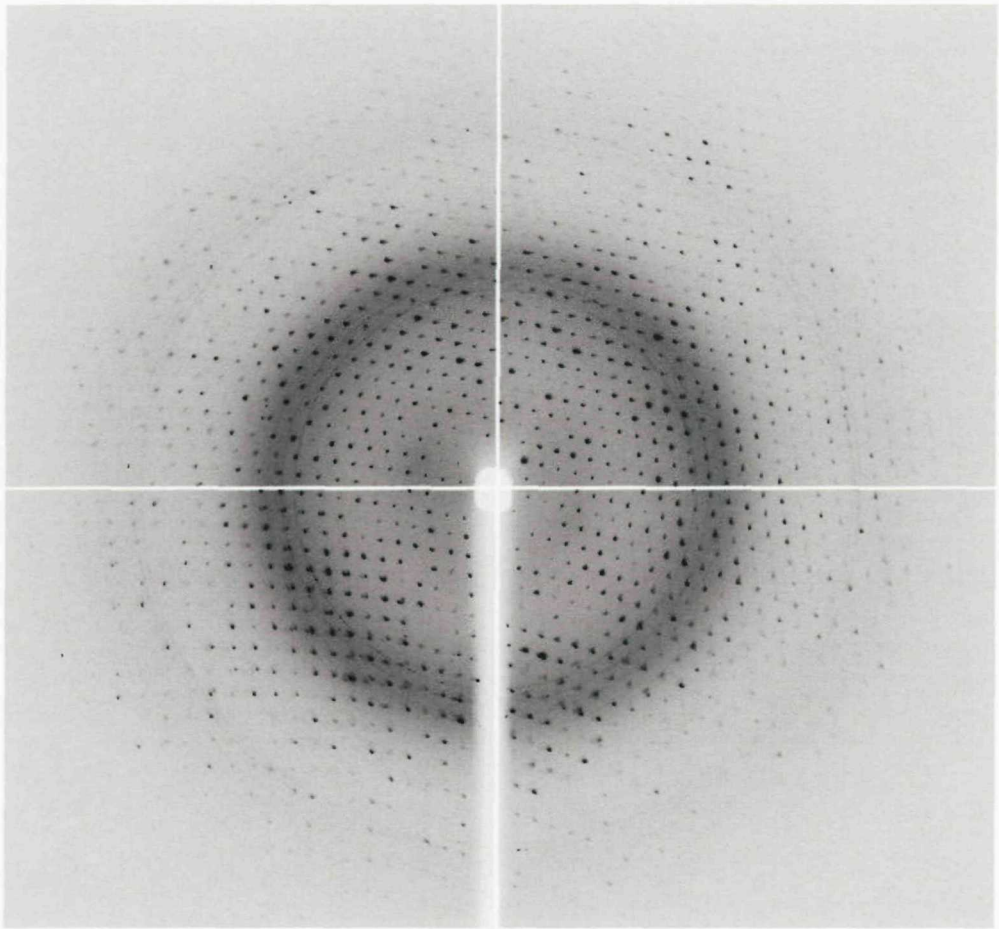

Figure 5.22 A 1° oscillation diffraction image collected from crystal form II at the ESRF (France).

The data were processed using MOSFLM and the CCP4 suite of programs. Initial unit cell dimension determination suggested a unit cell dimensions of a = 80.37 Å,

b = 52.20 Å, c = 83.34 Å, α, γ = 90°, β = 94° implying C centred symmetry (Table 5.4).

Penalty	Lattice	a	b	C	α	β	γ	Possible space groups
70	mC	52.20	83.34	48.06	93.2	123.3	90.3	P2, $P2_1$
62	mC	47.78	88.24	83.34	88.5	93.6	84.3	C2
50	mC	80.37	52.20	83.83	90.3	94	90.4	C2
23	aP	47.78	48.06	83.34	86.8	93.6	114.0	P1
5	mC	80.37	52.20	83.34	90.3	94	90.4	C2
0	aP	47.78	48.06	83.34	86.8	86.4	66	P1

Table 5.4 Penalty table generated by MOSFLM. This table shows the possible unit cell dimensions and space groups for the data collected from crystal form II.

As a result, the data were processed, merged and reduced in the space group C2 as previously described. Table 5.5 gives the final processing statistics of the data collected from crystal form II.

Space Group	C2
Unit cell dimensions (Å) (°)	a = 80.86, b = 52.58, c = 83.69 α = γ = 90.0, β = 93.48
Resolution range (Å)	44.06 – 1.6 (1.69 - 1.6)
Measured reflections	161761 (16566)
Unique Reflections	44113 (5265)
Multiplicity	3.7 (3.1)
Completeness (%)	95.1 (78.4)
R-merge (%)	10 (30.2)
(I)/σ(I)	8.3 (2.4)

Table 5.5 A summary of the data processing statistics of the crystal form II. Figures in parentheses apply to the highest resolution shell.

5.3.8.2.2 Molecular Replacement of Crystal Form II

Initial phases for crystal form II were determined by molecular replacement with the program MOLREP as previously described. The solvent content of the unit cell

was estimated to be 38 % for a single heterotrimeric C1q globular head domain in the asymmetric unit (Matthews, 1968).

The cross rotation search was performed using reflections within the resolution range 44.06 - 1.75 Å and yielded 3 significant solutions when the C1q globular head domain was used as a search model (Table 5.6). These three solutions corresponded to the three orientations of the heterotrimeric C1q globular head domain within the target asymmetric unit as implied by the solvent calculations. When a single CRP pentamer or protomer was used, no solutions were found.

Peak no.	α (°)	β (°)	γ (°)	Rf/σ
1	111.73	0.00	68.53	18.86
2	0.00	62.22	152.69	9.31
3	151.60	62.64	1.52	9.03
4	203.89	82.76	156.39	3.73
5	24.92	61.10	155.97	3.70

Table 5.6 Cross-rotation function peaks found by MOLREP for the data from crystal form II using 1PK6 as the search model.

The position of a single C1q globular head domain within the asymmetric unit was determined following a translation search calculated in space group C2. The highest peak from the cross rotation function ($\alpha = 111.73°$, $\beta = 0.00°$, $\gamma = 68.53°$) yielded a translation peak of 27.55 σ (R-factor = 40.4 %). The position of the first molecule corresponded to fractional co-ordinate shifts of X = 0.073, Y = 0.0 and Z = 0.235 (Table 5.7).

Peak no.	X	Y	Z	Rf/σ	Rfac
1	0.073	0	0.235	27.55	40.4
2	0.424	0	0.267	12.27	56.0
3	0.424	0	0.264	11.33	56.4
4	0.485	0	0.244	2.66	59.7
5	0.203	0	0.200	3.03	59.6

Table 5.7 The five highest translation function peaks calculated in space group C2 using the cross rotation function solutions.

In order to check the suggested molecular replacement solution, the crystal packing was visualized using NUcheck (Feng *et al.*, 1998). The diagram confirmed the feasibility of the present solution and confirmed the presence of a single hetero-

trimeric C1q globular domain in the asymmetric unit (Figure 5.23). Therefore, it was decided to proceed with the refinement process using this solution as the model.

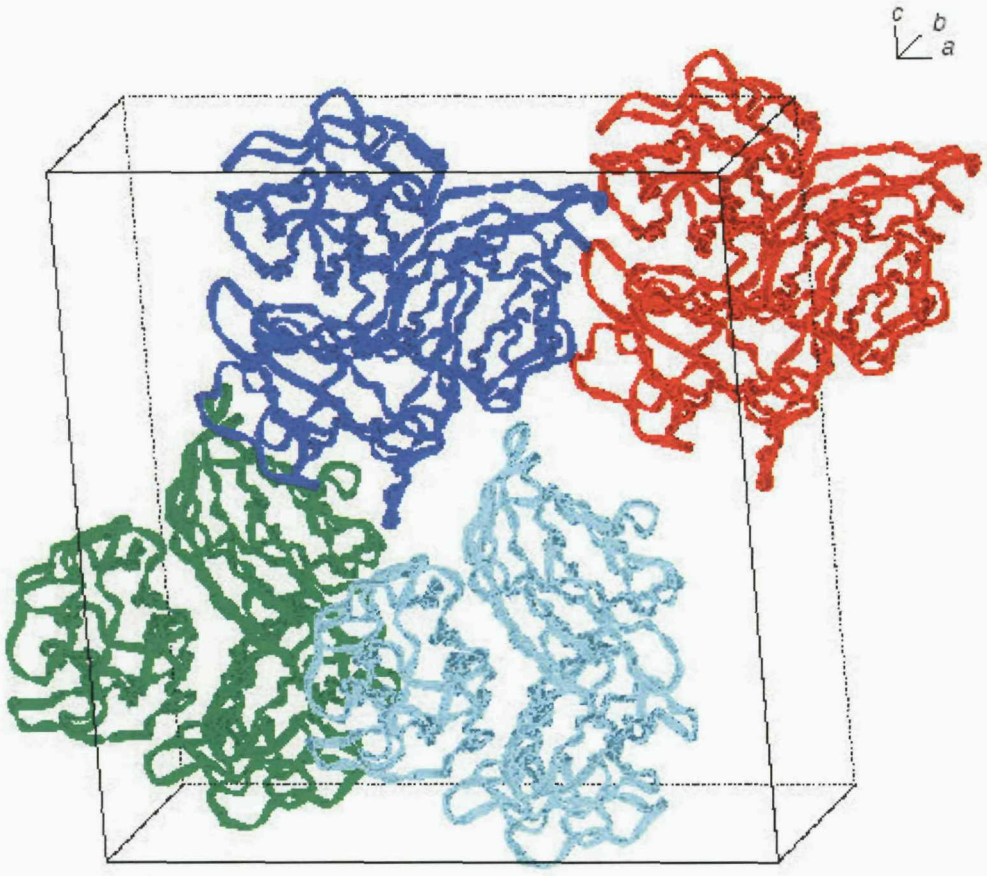

Figure 5.23 Crystal packing of crystal form II (NUcheck, Feng *et al.*, 1998). The crystal form II belonged to the monoclinic space group C2 (a = 80.86 Å, b = 52.58 Å, c = 83.69 Å, $\alpha = \gamma = 90°$, $\beta = 93.48°$) and contained one C1q globular head domain in the asymmetric unit (shown in red). Symmetry related pentamers are shown in blue, green and turquoise.

5.3.8.2.3 Refinement and Model Building of the C1q Globular Head Domain at 1.6 Å

The model was refined using the Phenix software suite. The first round of refinement reduced the R-factor from 40.4 to 24.3 % (R-free = 26.2 %). The maps were analysed and manipulated using the graphics package COOT. Analysis of the maps indicated well-defined F_o-F_c density for one calcium ion at the binding sites. During a round of model building, one calcium ion was added and side chains were modelled and refined (Figure 5.24). Residues modelled as alanines in the search model (GlnA90, ArgA92, GlnA160, ThrB92, GlnB93, ArgB108, ArgB109, ArgB163, GlnB165, LysC89) were substituted where density was present (Figure 5.25).

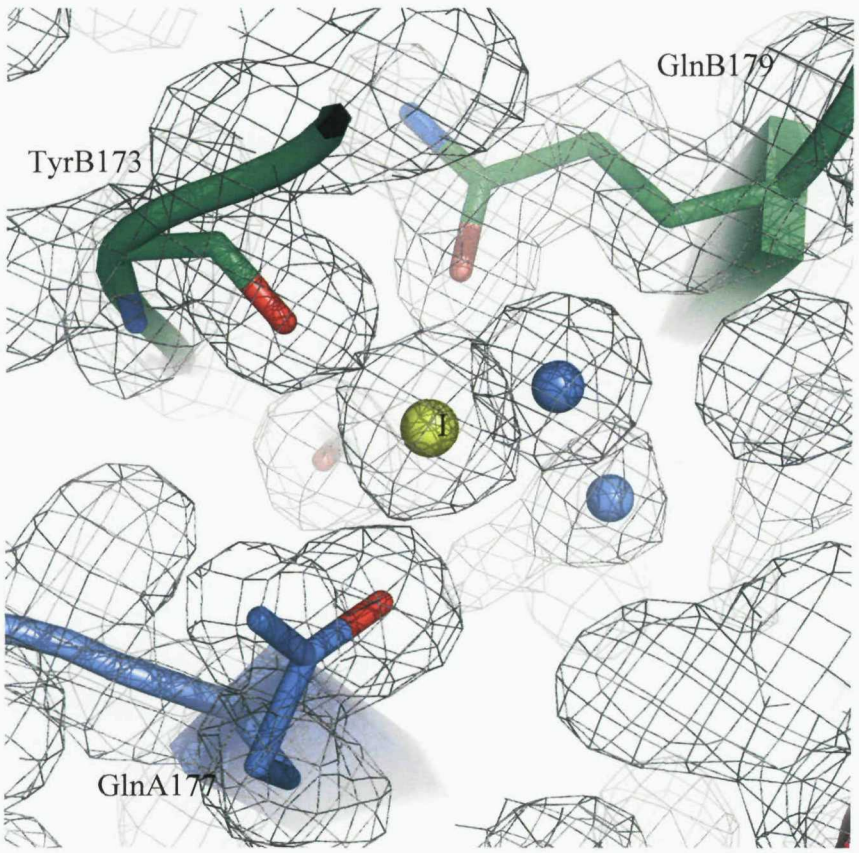

Figure 5.24 $2F_o$-F_c electron density contoured at 1.5 σ (grey) of the calcium-binding site. The calcium ion (I) is shown as a yellow sphere. The surrounding amino acids (TyrB173, GlnB179 and GlnA177) are shown as sticks and the two water molecules bound as blue spheres.

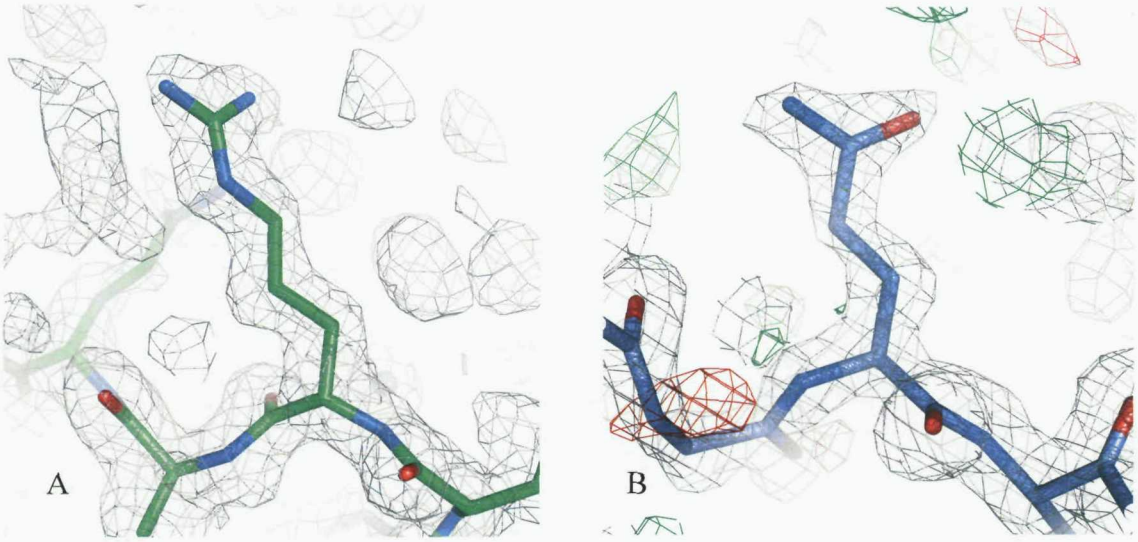

Figure 5.25 $2F_o$-F_c electron density contoured at 1.5 σ for residues of the C1q globular head domain. Diagram A (left) shows electron density for residue ArgB163, while diagram B (right) shows electron density for residue GlnA160.

Once all the side chains had been substituted and refined, the R-factor was reduced to 20.2 % and the R-free to 22.7 %. 257 water molecules were added to the structure and refined. The final R-factor for this structure was 19.5 % (R-free = 21.8 %). The refinement statistics for the model are shown in table 5.8.

Resolution range (Å)	29.82 – 1.6
Number of reflections in the working set	41868
Number of reflections in the test set	2235
R-factor (%)	19.5
R-free (%)	21.8
Rms bond length deviation (Å)	0.015
Rms bond angle deviation (°)	1.710

Table 5.8 Refinement statistics for the heterotrimeric C1q globular head domain structure.

5.3.8.2.4 The Structure of the Human C1q Globular Head Domain

The overall structure of the C1q globular head domain is similar to the previously published structure by Garboriaud *et al.* (2003) (Figure 5.26).

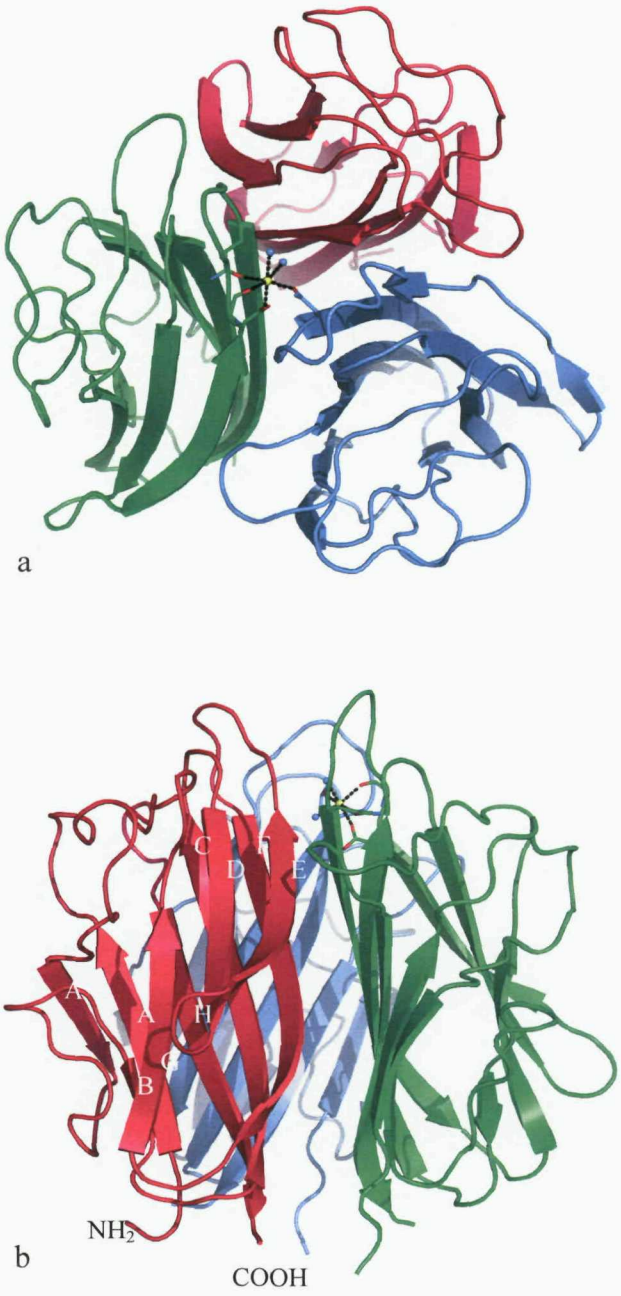

Figure 5.26 Structure of the heterotrimeric C1q globular head domain. Cartoon representation of the heterotrimer seen from the top (a) and side (b). Modules A, B and C are shown in blue, green and red respectively. Beta strands are labelled according to TNF nomenclature and the calcium ion is represented as a yellow sphere. The N- and C-terminal ends are shown for module C.

The refined model has an overall B-factor value of 13.6 $Å^2$ and shows good stereochemistry with 86.3 % of residues in the most favoured regions of the Ramachandran plot, 13.1 % in the additional allowed region and 0.3 % in the disallowed regions (Figure 5.27). The disallowed residues consisted of Thr147 from chain A, located on a loop between strands C and D and Lys170 from chain C, located on a loop between E and F (Figure 5.26). Similar conformations have been observed for these residues in the published C1q globular head domain structure (Gaboriaud *et al.*, 2003).

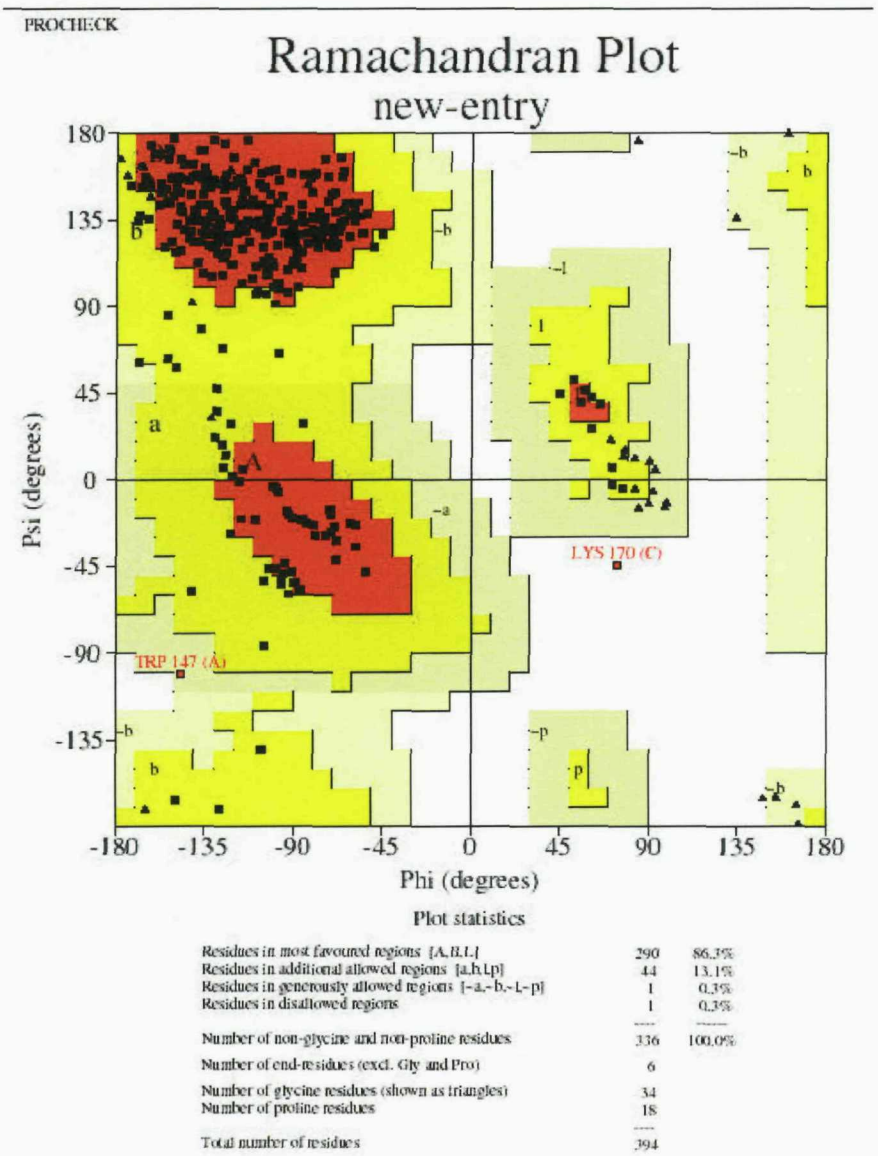

Figure 5.27 Ramachandran plot for the C1q globular head domain structure.

5.3.8.2.5 Structural Comparison with the published the Human C1q Globular Head Domain Structure by Garboriaud *et al.*

As expected, a structural comparison of the C1q globular head domain structure with that of the originally solved human C1q globular head domain structure (1PK6, Garboriaud *et al.*, 2003) confirms the overall similarity of the two structures (Figure 5.28). Small structural differences in the human C1q globular head domain occur in module B in the loop region (105-111 and 160-164). These loop regions are on the outer surface of the heterotrimer.

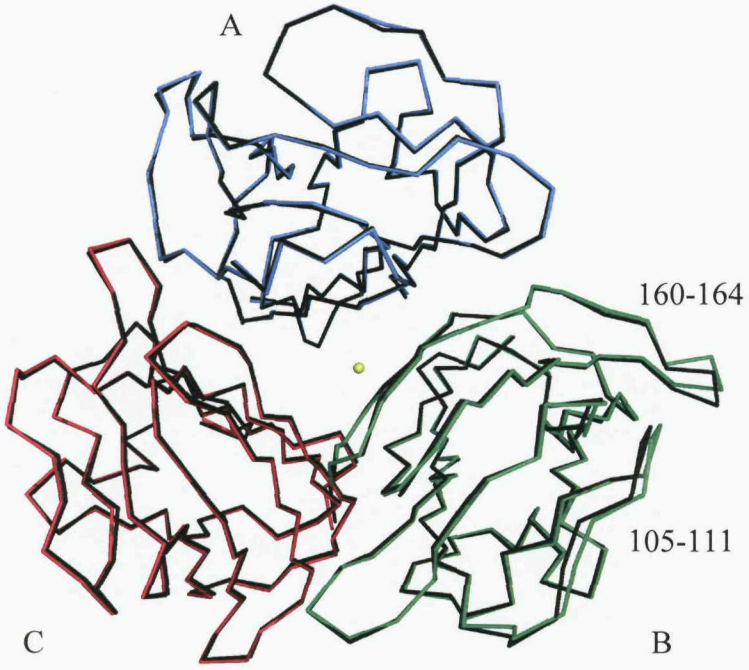

Figure 5.28 Superposition of the 1.6 Å C1q globular head domain structure (blue, red and green) with the previously published 1.9 Å C1q globular head domain structure (black). The calcium ion is shown as a yellow sphere. The residue regions showing structural differences are shown.

5.4 Discussion

The preparation of single, well diffracting protein crystals is required for any protein structure analysis by X-ray crystallography. Crystallization of a protein-protein complex is seldom simple. Often the affinity and size as well as the physical properties of the complex such as surface charge distribution, shape, size, and flexibility limit the crystallisation of a protein-protein complex. However, advances in molecular cloning techniques have been made, which allow structural biologists to over-express isolated domains of target proteins. Domains, in which high affinity interactions are maximised and non-interacting, flexible portions are removed or stabilised can be selected and often readily crystallise as a protein-protein complex. Unfortunately, this technique could not be applied in this case due to the unavailability of recombinant C1q. However, the size of C1q was modified by collagenase digestion. This reduced the size of the C1q molecule from 460 kDa to approximately 45 kDa due to the liberation of individual C1q globular head domains. It is important to note, that this modification in itself might have hindered crystal formation due to homogeneity problems caused by the non-specific enzymatic digestion with collagenase.

Analytical gel filtration studies were used initially to give an indication for conditions that promote crystallisation. This, however, proved unsuccessful in this case suggesting that the affinity is very weak. Therefore, crystallisation of the protein-protein complex was attempted by simply combining the proteins prior to crystallisation. This yielded crystals. These crystals, however, contained only the individual proteins rather then the protein-protein complex.

The determination of the 1.6 Å C1q globular head domain structure described in this report provides confirmation of the published structure and that the preparation and purification of the C1q globular head domain was successful. We concluded from this that the preparation of the C1q globular head domain was possibly not a problem for crystallisation of the protein-protein complex.

In an attempt to prepare the protein-protein complex prior to crystallisation, an affinity experiment was designed using PC-Sepharose beads. This experiment was

based on the aggregation hypothesis and ligand binding to PC that has been proposed to be necessary for CRP to bind and activate C1q. The experiment clearly showed that CRP does interact with C1q. However, crystals of the complex suitable for X-ray diffraction were not obtained.

A possible explanation for not obtaining crystals of the protein-protein complex might be due to some preparations being contaminated with an unknown protein. This might have hindered crystallisation. As other projects proved more successful, further attempts were not undertaken.

Chapter 6

Summary and Conclusion

6.1 Summary and Conclusions

This thesis describes crystallographic studies that explore the ligand binding properties of the short pentraxins, SAP and CRP. Problems, limitations and future developments are discussed.

Since the determination of the X-ray crystal structure of SAP in 1994 (Emsley *et al.*, 1994), a number of small molecule ligands including PE (Emsley *et al.*, 1994), MOβDG (Emsley *et al.*, 1994, Thompson et al., 2002), dAMP (Hohenester *et al.*, 1997), N-Acetyl-D-proline (Purvis, 2002) and N-Acetal-L-proline (Kolstoe, 2005) have been identified and characterised (Table 6.1). These crystal structures as well as *in vitro* binding studies have consistently demonstrated the importance of the electrostatic interaction between the calcium ions located on the B face of SAP and a carboxylate or phosphate group from the ligand.

The crystal structures of PE and MM described in chapter 1 bind in the previously characterised calcium binding site, with PE coordinating the calcium ions through its phosphate group and MM showing similarities to the binding of MOβDG by coordinating the calcium ions through its carboxylate group and by orienting its methyl group downwards into the hydrophobic pocket. Despite MM not being the most ideal SAP ligand as shown by isothermal calorimetry studies, it represents a promising candidate for an *in vivo* ligand because the second carboxylate group encourages the design of branched MM analogues. Analysis of these two structures reiterates the importance of the electrostatic interaction between the two positive calcium ions and a negatively charged group on the ligand along with the hydrophobic pocket.

Chapter 2 describes the X-ray crystal structure of rat SAP in complex with PC. This is the first rat pentraxin structure to be determined. Interestingly, this mammalian SAP structure reported here contains in the calcium binding site a PC molecule, a ligand traditionally defined as CRP- specific. This PC binding specificity is not shared by human SAP. This observation points to a major difference in the binding properties of rat SAP and human SAP. It suggests that rat SAP may be able to bind PC- as well as PE- containing residues. Therefore, classifying SAP and CRP from

different species based on their calcium dependent binding specificity for agarose (PE) and PC, respectively, appears to be inadequate because SAPs and CRPs from the rat as well as other non-human species overlap in their ligand binding specificities.

Table 6.1 SAP-ligand complexes

Ligand	Resolution (Å)	Space group	Unit cell (a,b,c, β)	Solvent content (%)	R-factor/ R-free (%)	Reference
Human SAP						
Acetate	2.0	$P2_1$	68.9,99.3,96.7 95.9	52	17.9	Emsley *et al.*, 1994
PE	2.9	$P2_1$	67,103.4,102.4 95.7		20	Emsley *et al.*, 1994
PE	1.88	$P2_1$	67.4,104.9,102.7 95.8	57	20.1/ 25.6	Pye, 2000
dAMP (decamer)	2.8	$P4_12_12$	190,190,119.7	71	23.2/ 25.2	Hohenester *et al.*, 1997
MOβDG	2.9	$P2_1$	69.1,99.3,96.75 95.8		19.7	Emsley *et al.*, 1994
MOβDG pentamer	2.2	$P2_1$	95.8,70.5,103.4 96.8	55	18.6/ 22.4	Thompson *et al.*,2002
MOβDG decamer	2.6	$P2_1$	118.6,109.1,120.8 95.2	60	21.9/ 24.5	Thompson *et al.*, 2002
GABA	2.7	$P6_1$	110.5,110.5,213	58	22.3/ 27.1	Pye, 2000
N-Acetyl-D-Pro	2.4	$P2_1$	96.1,70.8,103.6 95.8	55	19.6/ 21.6	Purvis, 2002
N-Acetyl-L-Pro	1.55	$P2_1$	94.9,69.8,102.4 97	56	16/ 20	Kolstoe, 2005
O-Phospho-L-Thr	1.8	$P2_1$	94.8,69.4,102 97	56	17.9/ 22.4	Kolstoe, 2005
CPHPC	2.55	$P2_1$	96.1,70.9,103.7 96.8	55	21.5/ 24.0	Purvis,2002
CPHPC decamer	3.2	$P4_32_12$	230.9,230.9,281.4	83	23.0/ 23.6	Purvis,2002
CPHPC	1.6	C2	154.3,108.1,120.3 138.4	63	21.32/ 22.66	Jenvey, 2006
MM	1.6	$P2_1$	94.75,69.7,102.3 96.9		17.7/ 20.6	Chapter 2
Rat SAP						
PC	2.2	$P2_1$	95.3, 144.7,95.5 108.6	54	20.7/ 25	Chapter 3

There are also major differences between species with respect to baseline plasma concentration, behaviour as acute phase protein and capacity to activate complement (Table 6.2).

Table 6.2 Comparisons between pentraxins from different species

Species	**Human**	**Rat**	**Rabbit**	**Mouse**	**Guinea pig**	**Human**	**Rat**	**Mouse**	**Guinea pig**
Protein	**CRP**	**CRP**	**CRP**	**CRP**	**CRP**	**SAP**	**SAP**	**SAP**	**SAP**
Acute phase protein	Yes	no	Yes	No	no	no	no	yes	no
Normal & Increased Serum Conc.	0.8mg/l 300-500mg/l	300-500mg/l 2fold	0.8mg/l 300mg/l	Trace 1-2 mg/l		30mg/l	20-50mg/l	60mg/l 200-500mg/ml	25mg/l 2-3fold rise
Aa's	206	211	205	206	206	204	208	204	204
Mw	23	24	22.9			23.5 kDa	24.5kDa		
Disulphide bonds	C36-C97	C36-C97 C208-C209	C36-C97	C36-C97	C36-C97	C36-C95	C36-C95	C36-C95	C36-C95
Glycosylation	No	Asn 128	-	unknown	unknown	Asn 32	Asn32	unknown	unknown
PI exp	7.9	3.8				5.5	4.2	4.6	
Ligand specificity	PC high PE low PnC, C1q Modified LDL	PC=PE?	PC Modified LDL	PC		PE high, MOβDG, dAMP, DNA, LPS, GAGs,Histones, Amyloid fibrils	PC		
Complement activation	Yes	no	Unknown	unknown	unknown	yes (binding)	Unknown	unknown	unknown
Calcium coordinating amino acids	(I):Asp60, Asn61, Glu138, Asp140, Gln139 (II):Glu138, Asp140, Glu147, Gln150					(I): Asp58, Asn59, Glu136, Asp138, Gln137, ligand (II): Glu136,Asp138Gln148 , ligand, H2O (2)	(I): Asp58, Asn59,Glu136, Asp138, Gln137 ligand (II): Glu136, Asp138,Gln148, ligand, H2O (2)		

Chapter 3 CRP provides a full description of the structural basis of PE binding to CRP, a pentraxin defined by its binding affinity for PC. The only other ligands co-crystallised with CRP are PC and bis (PC)-H (Table 6.3). These three ligands share the coordination of the phosphate group of the ligand with the calcium ions from the protein. Crystallisation of CRP-ligand complexes has been attempted with ligands containing carboxylate groups such as MOβDG. However, these attempts proved unsuccessful in the growth of crystals (unpublished data). It has been suggested that in the case of MOβDG, the interaction between the side chains of SAP Lys79 and MOβDG cannot be satisfied by CRP Glu81, and van der Waals contacts to MOβDG provided by SAP Trp74 are not available from CRP Thr76 (Thompson *et al.*, 1999). These residue differences appear to be responsible for the failure of CRP to bind the carboxylate group containing ligands such as MOβDG.

Table 6.3 Summary of CRP-ligand complexes

Ligand	Resolution (Å)	Space group	Unit cell (a,b,c, β)	Solvent content (%)	R-factor/ R-free (%)	Reference
Human CRP						
PC	2.5	$P4_12_12$	193.4,193.9,134.4	76	19.6/ 24.2	Thompson *et al.*, 1999
Bis(PC)-H (decamer)	2.3	$P2_12_12_1$	96,158.2,165.390		19.02/ 19.74	Jenvey, 2006; Pepys *et al.*, 2006
PE	2.7	$P4_1$	278.4,278.4,92.190	68	23.1/ 25	Chapter 4
Rat CRP						
Preliminary X-ray analysis	3	Tetra-gonal	163.8,163.8,125.2	-	unsolved	Hopkins *et al.*, 1994

To answer the question what is a CRP and what is an SAP, the crystal structures of the ligand complexes, the sequences and the ligand binding specificities were examined (Figure 6.1). The alignment of the CRP sequence with that of the SAP sequences from different species in figure 1 highlights one particular residue (Asp108), which seems to occur exclusively in CRP and not in SAP. This

residue, however, does not appear to influence PC or PE binding. One of the other possible ways to delineate CRP from SAP could be the 22° rotation of the subunits in CRP towards the five fold axis (Figure 6.2). The delineation in the sequence and the rotation may allow prediction of the probable quaternary structures of pentraxins from diverse species.

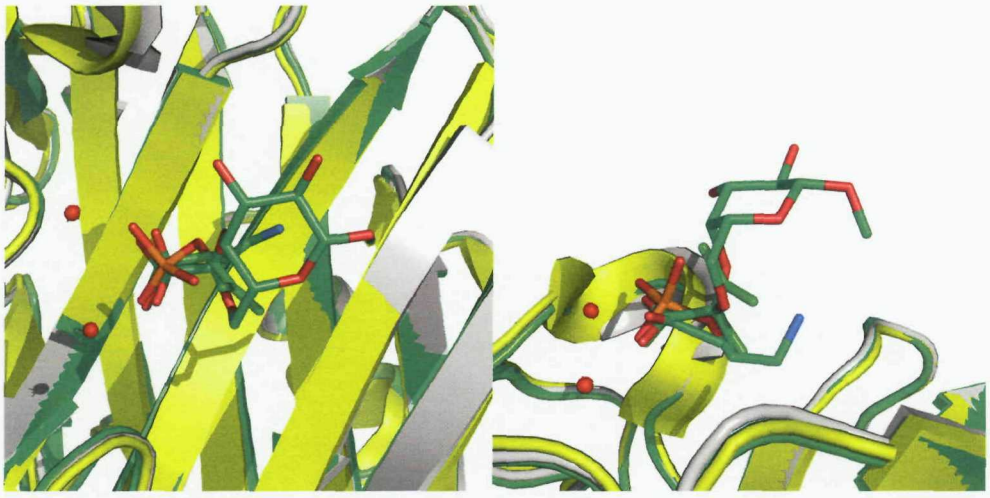

Figure 6.1 Cartoon overlay of SAP protomers from different X-ray crystal structures showing different ligands in the active site

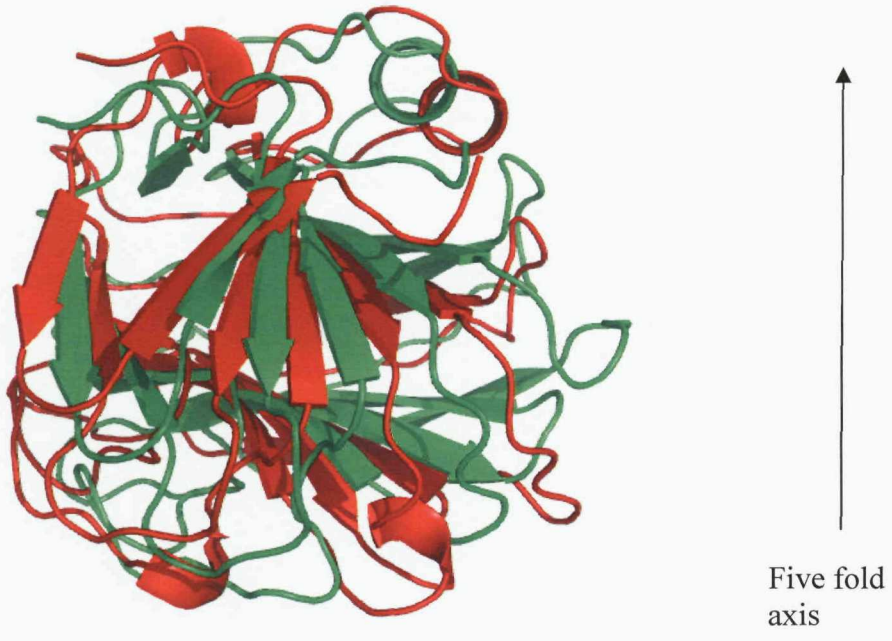

Figure 6.2 Cartoon overlay of a SAP protomer (green) and a CRP protomer (red) indicating the orientation of the protomers with respect to the five fold axis of the pentamers.

Rat CRP exhibits calcium-dependent binding specificity towards PC similar to that in the human CRP, although it can also bind PE. In addition, majority of the residues in the vicinity of the pentraxin ligand binding site are conserved. In contrast, to human CRP, rat CRP is glycosylated, can not activate rat complement and has an extra disulphide bridge at the C-terminus. Due to the lack of structural data, molecular model building was used to determine whether rat CRP has the same rotation of the subunits as human CRP (Figure 6.3 & 6.4). Although the conservation of the inter-protomer contacts such as salt bridges are insufficient to predict the exact protomer relationship in each of the two pentraxins (Shrive *et al.*, 1996), it is indicative of similar protomer orientation within the cyclic aggregates. In conclusion, the combined evidence suggests that although rat CRP displays some SAP characteristics, rat CRP has been correctly designated as a CRP-like protein.

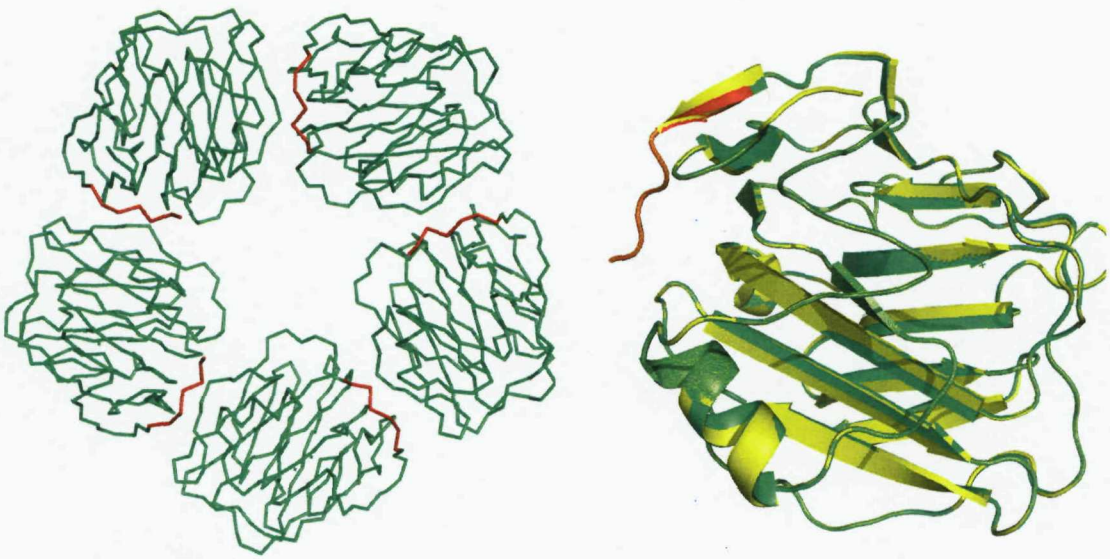

Figure 6.3 A proposed model of the rat CRP structure (left), 7 residues are shown in red. The seven additional residues in the rat CRP sequence are not shown. Cartoon overlay of a human CRP protomer with the rat CRP protomer model.

The majority of the suggested functions of the pentraxins CRP and SAP are based on their pattern recognition properties for common pathogen-associated molecular patterns (PAMPs). These PAMPs include LPS from the gram-negative cell wall, peptidoglycan and lipotechoic acids from the gram-positive cell wall, the sugar mannose (a terminal sugar common in microbial glycolipids and glycoproteins but rare in those of humans), double-stranded and single-stranded

RNA from viruses, and glucans from fungal cell walls. Since both CRP and SAP have been shown to be capable to bind specifically to conserved portions of these PAMP's and to use these for the benefit of the host, the pentraxins have been assigned the term pattern recognition molecule.

The final results chapter describes an attempt to gain knowledge of the exact stoichiometry and the protein-protein interactions between CRP and C1q. A plausible three-dimensional model of the C1q globular domain in complex with its physiological ligand, CRP, has been proposed by Gaboriaud *et al.*, 2003 (Figure 6.5), however, two possible recognition modes (via head group; via stalk region) of C1q are still debated.

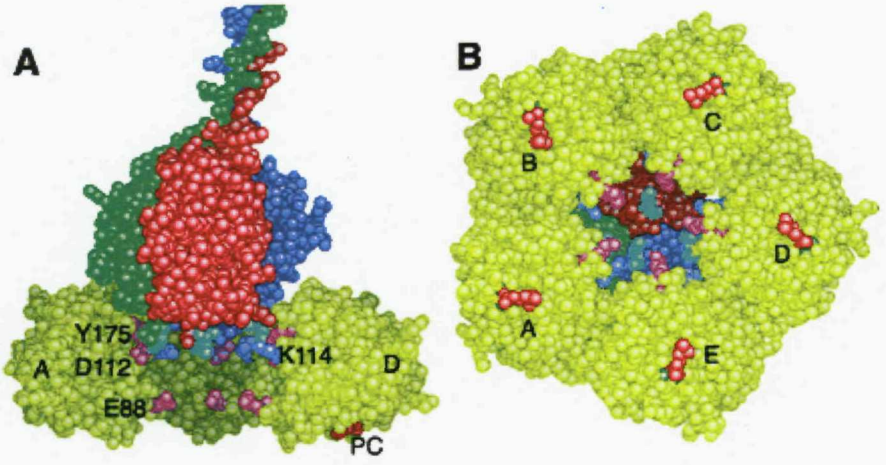

Figure 6.5 A plausible model of the CRP-C1q globular domain complex *A*, side view. Subunits B and C of CRP have been omitted for clarity. *B*, perpendicular bottom view. Colour coding for the C1q subunits (A, B, and C are shown in *blue, green*, and *red*, respectively). The top of the C1q head shows lysines (A173, A200, A201, C170) and Tyr^{B175} in *light blue.* CRP protomers are designated by A-E as described by Shrive *et al.*, .1996 The phosphocholine (*PC*) ligand is in *red*, and the nearby Ca^{2+} ion is in *green*. CRP mutations (Agrawal et al., 2001) are coloured as follows: Mutations impairing complement activation (Glu-88, Asp-112, Tyr-175) are *magenta*, and mutations enhancing complement activation (Lys-114) are *blue*. Figure and amended text taken from Gaboriaud *et al.*, 2003).

Purification of C1q has been achieved by ion-exchange and gel filtration chromatography from BPL paste. Crystallisation trials have been performed, however no crystals have been obtained that contain the protein-protein complex. There are a number of possible explanations for not obtaining crystals of the protein-protein complex: contamination with unknown proteins, selection of incorrect protein ratios, weak affinity, unhomogenous protein. Each of these could have a deleterious effect on the nucleation and crystallisation of this protein-protein complex.

Purification of C1q has been achieved by ion-exchange and gel filtration chromatography from BPL paste. Crystallisation trials have been performed, however no crystals have been obtained that contain the protein-protein complex. There are a number of possible explanations for not obtaining crystals of the protein-protein complex: contamination with unknown proteins, selection of incorrect protein ratios, weak affinity, unhomogenous protein. Each of these could have a deleterious effect on the nucleation and crystallisation of this protein-protein complex.

Chapter 7

References

References

Ablij, H. & Meinders, A. 2002, "C-reactive protein: history and revival", *Eur.J.Intern.Med.*, vol. 13, no. 7, p. 412.

Adams, P. D., Grosse-Kunstleve, R. W., Hung, L. W., Ioerger, T. R., McCoy, A. J., Moriarty, N. W., Read, R. J., Sacchettini, J. C., Sauter, N. K., & Terwilliger, T. C. 2002, "PHENIX: building new software for automated crystallographic structure determination", *Acta Crystallogr.D.Biol.Crystallogr.*, vol. 58, no. Pt 11, pp. 1948-1954.

Afonine, P. V., Grosse-Kunstleve, R. W., & Adams, P. D. 2005, "A robust bulk-solvent correction and anisotropic scaling procedure", *Acta Crystallogr.D Biol.Crystallogr.*, vol. 61, no. Pt 7, pp. 850-855.

Agnello, V., Winchester, R. J., & Kunkel, H. G. 1970, "Precipitin reactions of the C1q component of complement with aggregated gamma-globulin and immune complexes in gel diffusion", *Immunology*, vol. 19, no. 6, pp. 909-919.

Agrawal, A., Shrive, A. K., Greenhough, T. J., & Volanakis, J. E. 2001, "Topology and structure of the C1q-binding site on C-reactive protein", *J.Immunol.*, vol. 166, no. 6, pp. 3998-4004.

Agrawal, A., Simpson, M. J., Black, S., Carey, M. P., & Samols, D. 2002, "A C-reactive protein mutant that does not bind to phosphocholine and pneumococcal C-polysaccharide", *J.Immunol.*, vol. 169, no. 6, pp. 3217-3222.

Agrawal, A. & Volanakis, J. E. 1994, "Probing the C1q-binding site on human C-reactive protein by site-directed mutagenesis", *J.Immunol.*, vol. 152, no. 11, pp. 5404-5410.

Agrawal, A., Xu, Y., Ansardi, D., Macon, K. J., & Volanakis, J. E. 1992, "Probing the phosphocholine-binding site of human C-reactive protein by site-directed mutagenesis", *J.Biol.Chem.*, vol. 267, no. 35, pp. 25353-25358.

Alles, V. V., Bottazzi, B., Peri, G., Golay, J., Introna, M., & Mantovani, A. 1994, "Inducible expression of PTX3, a new member of the pentraxin family, in human mononuclear phagocytes", *Blood*, vol. 84, no. 10, pp. 3483-3493.

Anderson, J. K, Stroud R. M. & Volanakis, J. E. 1978, "Studies on the binding specificity of human C-reactive protein for phosphorylcholine", *Fed. Proc.* 37, p. 1495.

Andersen, O., Vilsgaard, R. K., Juul, S., I, Jonson, G., Holm, N. E., & Svehag, S. E. 1997, "Serum amyloid P component binds to influenza A virus haemagglutinin and inhibits the virus infection in vitro", *Scand.J.Immunol.*, vol. 46, no. 4, pp. 331-337.

Antzutkin, O. N., Balbach, J. J., Leapman, R. D., Rizzo, N. W., Reed, J., & Tycko, R. 2000, "Multiple quantum solid-state NMR indicates a parallel, not

antiparallel, organization of beta-sheets in Alzheimer's beta-amyloid fibrils", *Proc.Natl.Acad.Sci.U.S.A*, vol. 97, no. 24, pp. 13045-13050.

Arlaud, G. J., Gaboriaud, C., Thielens, N. M., & Rossi, V. 2002, "Structural biology of C1", *Biochem.Soc.Trans.*, vol. 30, no. Pt 6, pp. 1001-1006.

Arlaud, G. J., Gaboriaud, C., Thielens, N. M., Rossi, V., Bersch, B., Hernandez, J. F., & Fontecilla-Camps, J. C. 2001, "Structural biology of C1: dissection of a complex molecular machinery", *Immunol.Rev.*, vol. 180, pp. 136-145.

Assimeh, S. N., Bing, D. H., & Painter, R. H. 1974, "A simple method for the isolation of the subcomponents of the first component of complement by affinity chromatography", *J.Immunol.*, vol. 113, no. 1, pp. 225-234.

Balbach, J. J., Ishii, Y., Antzutkin, O. N., Leapman, R. D., Rizzo, N. W., Dyda, F., Reed, J., & Tycko, R. 2000, "Amyloid fibril formation by A beta 16-22, a seven-residue fragment of the Alzheimer's beta-amyloid peptide, and structural characterization by solid state NMR", *Biochemistry*, vol. 39, no. 45, pp. 13748-13759.

Balbach, J. J., Petkova, A. T., Oyler, N. A., Antzutkin, O. N., Gordon, D. J., Meredith, S. C., & Tycko, R. 2002, "Supramolecular structure in full-length Alzheimer's beta-amyloid fibrils: evidence for a parallel beta-sheet organization from solid-state nuclear magnetic resonance", *Biophys.J.*, vol. 83, no. 2, pp. 1205-1216.

Baltz, M. L., Caspi, D., Evans, D. J., Rowe, I. F., Hind, C. R., & Pepys, M. B. 1986, "Circulating serum amyloid P component is the precursor of amyloid P component in tissue amyloid deposits", *Clin.Exp.Immunol.*, vol. 66, no. 3, pp. 691-700.

Baltz, M. L., de Beer, F. C., Feinstein, A., Munn, E. A., Milstein, C. P., Fletcher, T. C., March, J. F., Taylor, J., Bruton, C., Clamp, J. R., Davies, A. J., & Pepys, M. B. 1982, "Phylogenetic aspects of C-reactive protein and related proteins", *Ann.N.Y.Acad.Sci.*, vol. 389, pp. 49-75.

Baltz, M. L., Gomer, K., Davies, A. J., Evans, D. J., Klaus, G. G., & Pepys, M. B. 1980, "Differences in the acute phase responses of serum amyloid P-component (SAP) and C3 to injections of casein or bovine serum albumin in amyloid-susceptible and -resistant mouse strains", *Clin.Exp.Immunol.*, vol. 39, no. 2, pp. 355-360.

Bang, R., Marnell, L., Mold, C., Stein, M. P., Clos, K. T., Chivington-Buck, C., & Clos, T. W. 2005, "Analysis of binding sites in human C-reactive protein for Fc{gamma}RI, Fc{gamma}RIIA, and C1q by site-directed mutagenesis", *J.Biol.Chem.*, vol. 280, no. 26, pp. 25095-25102.

Becker, J. W. & Reeke, G. N., Jr. 1985, "Three-dimensional structure of beta 2-microglobulin", *Proc.Natl.Acad.Sci.U.S.A*, vol. 82, no. 12, pp. 4225-4229.

Benzinger, T. L., Gregory, D. M., Burkoth, T. S., Miller-Auer, H., Lynn, D. G., Botto, R. E., & Meredith, S. C. 1998, "Propagating structure of Alzheimer's beta-

amyloid(10-35) is parallel beta-sheet with residues in exact register", *Proc.Natl.Acad.Sci.U.S.A*, vol. 95, no. 23, pp. 13407-13412.

Bhakdi, S., Torzewski, M., Klouche, M., & Hemmes, M. 1999, "Complement and atherogenesis: binding of CRP to degraded, nonoxidized LDL enhances complement activation", *Arterioscler.Thromb.Vasc.Biol.*, vol. 19, no. 10, pp. 2348-2354.

Bharadwaj, D., Stein, M. P., Volzer, M., Mold, C., & Du Clos, T. W. 1999, "The major receptor for C-reactive protein on leukocytes is fcgamma receptor II", *J.Exp.Med.*, vol. 190, no. 4, pp. 585-590.

Bickerstaff, M. C., Botto, M., Hutchinson, W. L., Herbert, J., Tennent, G. A., Bybee, A., Mitchell, D. A., Cook, H. T., Butler, P. J., Walport, M. J., & Pepys, M. B. 1999, "Serum amyloid P component controls chromatin degradation and prevents antinuclear autoimmunity", *Nat.Med.*, vol. 5, no. 6, pp. 694-697.

Black, S., Agrawal, A., & Samols, D. 2003, "The phosphocholine and the polycation-binding sites on rabbit C-reactive protein are structurally and functionally distinct", *Mol.Immunol.*, vol. 39, no. 16, pp. 1045-1054.

Black, S., Kushner, I., & Samols, D. 2004, "C-reactive Protein", *J.Biol.Chem.*, vol. 279, no. 47, pp. 48487-48490.

Bladen, H. A., Nylen, M. U., & Glenner, G. G. 1966, "The ultrastructure of human amyloid as revealed by the negative staining technique", *J.Ultrastruct.Res.*, vol. 14, no. 5, pp. 449-459.

Blake, C. & Serpell, L. 1996, "Synchrotron X-ray studies suggest that the core of the transthyretin amyloid fibril is a continuous beta-sheet helix", *Structure.*, vol. 4, no. 8, pp. 989-998.

Blake, C. C., Geisow, M. J., Oatley, S. J., Rerat, B., & Rerat, C. 1978, "Structure of prealbumin: secondary, tertiary and quaternary interactions determined by Fourier refinement at 1.8 A", *J.Mol.Biol.*, vol. 121, no. 3, pp. 339-356.

Bodman-Smith, K. B., Melendez, A. J., Campbell, I., Harrison, P. T., Allen, J. M., & Raynes, J. G. 2002, "C-reactive protein-mediated phagocytosis and phospholipase D signalling through the high-affinity receptor for immunoglobulin G (FcgammaRI)", *Immunology*, vol. 107, no. 2, pp. 252-260.

Bodmer, B. & Siboo, R. 1977, "Isolation of mouse C-reactive protein from liver and serum", *J.Immunol.*, vol. 118, no. 3, pp. 1086-1089.

Bokisch, V. A., Muller-Eberhard, H. J., & Cochrane, C. G. 1969, "Isolation of a fragment (C3a) of the third component of human complement containing anaphylatoxin and chemotactic activity and description of an anaphylatoxin inactivator of human serum", *J.Exp.Med.*, vol. 129, no. 5, pp. 1109-1130.

Booth, D. R., Sunde, M., Bellotti, V., Robinson, C. V., Hutchinson, W. L., Fraser, P. E., Hawkins, P. N., Dobson, C. M., Radford, S. E., Blake, C. C., & Pepys, M. B. 1997, "Instability, unfolding and aggregation of human lysozyme

variants underlying amyloid fibrillogenesis", *Nature*, vol. 385, no. 6619, pp. 787-793.

Botto, M., Dell'Agnola, C., Bygrave, A. E., Thompson, E. M., Cook, H. T., Petry, F., Loos, M., Pandolfi, P. P., & Walport, M. J. 1998, "Homozygous C1q deficiency causes glomerulonephritis associated with multiple apoptotic bodies", *Nat.Genet.*, vol. 19, no. 1, pp. 56-59.

Botto, M., Hawkins, P. N., Bickerstaff, M. C., Herbert, J., Bygrave, A. E., McBride, A., Hutchinson, W. L., Tennent, G. A., Walport, M. J., & Pepys, M. B. 1997, "Amyloid deposition is delayed in mice with targeted deletion of the serum amyloid P component gene", *Nat.Med.*, vol. 3, no. 8, pp. 855-859.

Breathnach, S. M., Kofler, H., Sepp, N., Ashworth, J., Woodrow, D., Pepys, M. B., & Hintner, H. 1989, "Serum amyloid P component binds to cell nuclei in vitro and to in vivo deposits of extracellular chromatin in systemic lupus erythematosus", *J.Exp.Med.*, vol. 170, no. 4, pp. 1433-1438.

Bricogne, G. 1997 "Bayesian statistical viewpoint on structure determination: basic concepts and examples", *Methods Enzymol.*, vol. 276, pp. 361–423.

Bristow, C. L. & Boackle, R. J. 1986, "Evidence for the binding of human serum amyloid P component to Clq and Fab gamma", *Mol.Immunol.*, vol. 23, no. 10, pp. 1045-1052.

Brundish, D. E. & Baddiley, J. 1968, "Pneumococcal C-substance, a ribitol teichoic acid containing choline phosphate", *Biochem.J.*, vol. 110, no. 3, pp. 573-582.

Brunger, A. T., Adams, P. D., Clore, G. M., DeLano, W. L., Gros, P., Grosse-Kunstleve, R. W., Jiang, J. S., Kuszewski, J., Nilges, M., Pannu, N. S., Read, R. J., Rice, L. M., Simonson, T., & Warren, G. L. 1998, "Crystallography & NMR system: A new software suite for macromolecular structure determination", *Acta Crystallogr.D.Biol.Crystallogr.*, vol. 54, no. Pt 5, pp. 905-921.

Brunger, A. T., Adams, P. D., & Rice, L. M. 1998, "Recent developments for the efficient crystallographic refinement of macromolecular structures", *Curr.Opin.Struct.Biol.*, vol. 8, no. 5, pp. 606-611.

Brunger, A. T., Krukowski, A., & Erickson, J. W. 1990, "Slow-cooling protocols for crystallographic refinement by simulated annealing", *Acta Crystallogr.A*, vol. 46 (Pt 7), pp. 585-593.

Brünger A. T. 1992, "Free *R* value: a novel statistical quantity for assessing the accuracy of crystal structures", *Nature*, vol. 355, pp. 472–475.

Brünger, A. T., Adams, P. D., Clore, G. M., DeLano, W. L., Gros, P., Grosse-Kunstleve, R. W., Jiang, J.-S., Kuszewski, J., Nilges, M., Pannu, N. S., Read, R. J., Rice, L. M., Simonson, T. & Warren, G. L. 1998, "Crystallography & NMR

system: A new software suite for macromolecular structure determination", *Acta Cryst.*, D54, pp. 905-921.

Butler, P. J., Tennent, G. A., & Pepys, M. B. 1990, "Pentraxin-chromatin interactions: serum amyloid P component specifically displaces H1-type histones and solubilizes native long chromatin", *J.Exp.Med.*, vol. 172, no. 1, pp. 13-18.

Carroll, M. C. 2004, "The complement system in regulation of adaptive immunity", *Nat.Immunol.*, vol. 5, no. 10, pp. 981-986.

Casciola-Rosen, L. A., Miller, D. K., Anhalt, G. J., & Rosen, A. 1994, "Specific cleavage of the 70-kDa protein component of the U1 small nuclear ribonucleoprotein is a characteristic biochemical feature of apoptotic cell death", *J.Biol.Chem.*, vol. 269, no. 49, pp. 30757-30760.

CATHCART, E. S., COMERFORD, F. R., & COHEN, A. S. 1965, "IMMUNOLOGIC STUDIES ON A PROTEIN EXTRACTED FROM HUMAN SECONDARY AMYLOID", *N.Engl.J.Med.*, vol. 273, pp. 143-146.

Chakraborti, T., Mandal, A., Mandal, M., Das, S., & Chakraborti, S. 2000, "Complement activation in heart diseases. Role of oxidants", *Cell Signal.*, vol. 12, no. 9-10, pp. 607-617.

Chang, M. K., Binder, C. J., Torzewski, M., & Witztum, J. L. 2002, "C-reactive protein binds to both oxidized LDL and apoptotic cells through recognition of a common ligand: Phosphorylcholine of oxidized phospholipids", *Proc.Natl.Acad.Sci.U.S.A*, vol. 99, no. 20, pp. 13043-13048.

Chiti, F., Webster, P., Taddei, N., Clark, A., Stefani, M., Ramponi, G., & Dobson, C. M. 1999, "Designing conditions for in vitro formation of amyloid protofilaments and fibrils", *Proc.Natl.Acad.Sci.U.S.A*, vol. 96, no. 7, pp. 3590-3594.

Christner, R. B. & Mortensen, R. F. 1994, "Binding of human serum amyloid P-component to phosphocholine", *Arch.Biochem.Biophys.*, vol. 314, no. 2, pp. 337-343.

Clapp, B. R., Hirschfield, G. M., Storry, C., Gallimore, J. R., Stidwill, R. P., Singer, M., Deanfield, J. E., MacAllister, R. J., Pepys, M. B., Vallance, P., & Hingorani, A. D. 2005, "Inflammation and endothelial function: direct vascular effects of human C-reactive protein on nitric oxide bioavailability", *Circulation*, vol. 111, no. 12, pp. 1530-1536.

Coe, J. E. 1977, "A sex-limited serum protein of Syrian hamsters: definition of female protein and regulation by testosterone", *Proc.Natl.Acad.Sci.U.S.A*, vol. 74, no. 2, pp. 730-733.

Coe, J. E., Margossian, S. S., Slayter, H. S., & Sogn, J. A. 1981, "Hamster female protein. A new Pentraxin structurally and functionally similar to C-reactive protein and amyloid P component", *J.Exp.Med.*, vol. 153, no. 4, pp. 977-991.

Coe, J. E. & Ross, M. J. 1985, "Hamster female protein, a sex-limited pentraxin, is a constituent of Syrian hamster amyloid", *J.Clin.Invest*, vol. 76, no. 1, pp. 66-74.

Coe, J. E. & Ross, M. J. 1990, "Amyloidosis and female protein in the Syrian hamster. Concurrent regulation by sex hormones", *J.Exp.Med.*, vol. 171, no. 4, pp. 1257-1267.

Collaborative Computing Project Number 4, "The CCP4 suite: programs for protein crystallography", Acta Crystallog. sect. *D* 50 (1994), pp. 760–763.

Coria, F., Castano, E., Prelli, F., Larrondo-Lillo, M., van, D. S., Shelanski, M. L., & Frangione, B. 1988, "Isolation and characterization of amyloid P component from Alzheimer's disease and other types of cerebral amyloidosis", *Lab Invest*, vol. 58, no. 4, pp. 454-458.

Crowther, R.A. 1972. In: Rossmann M.G. (Ed.). The Molecular Replacement Method. Gordon and Breach, New York, pp. 173–178.

Damaschun, G., Damaschun, H., Gast, K., & Zirwer, D. 1999, "Proteins can adopt totally different folded conformations", *J.Mol.Biol.*, vol. 291, no. 3, pp. 715-725.

Danesh, J., Wheeler, J. G., Hirschfield, G. M., Eda, S., Eiriksdottir, G., Rumley, A., Lowe, G. D., Pepys, M. B., & Gudnason, V. 2004, "C-reactive protein and other circulating markers of inflammation in the prediction of coronary heart disease", *N.Engl.J.Med.*, vol. 350, no. 14, pp. 1387-1397.

de Beer, F. C., Baltz, M. L., Munn, E. A., Feinstein, A., Taylor, J., Bruton, C., Clamp, J. R., & Pepys, M. B. 1982a, "Isolation and characterization of C-reactive protein and serum amyloid P component in the rat", *Immunology*, vol. 45, no. 1, pp. 55-70.

de Beer, F. C., Hind, C. R., Fox, K. M., Allan, R. M., Maseri, A., & Pepys, M. B. 1982b, "Measurement of serum C-reactive protein concentration in myocardial ischaemia and infarction", *Br.Heart J.*, vol. 47, no. 3, pp. 239-243.

de Beer, F. C., Shine, B., & Pepys, M. B. 1982, "Radiometric ligand binding assay for C-reactive protein. Complexed C-reactive protein is not detectable in acute phase serum", *Clin.Exp.Immunol.*, vol. 50, no. 1, pp. 231-237.

de Haas, C. J., van der Tol, M. E., van Kessel, K. P., Verhoef, J., & van Strijp, J. A. 1998, "A synthetic lipopolysaccharide-binding peptide based on amino acids 27-39 of serum amyloid P component inhibits lipopolysaccharide-induced responses in human blood", *J.Immunol.*, vol. 161, no. 7, pp. 3607-3615.

de Haas, C. J., van Leeuwen, E. M., van, B. T., Verhoef, J., van Kessel, K. P., & van Strijp, J. A. 2000, "Serum amyloid P component bound to gram-negative bacteria prevents lipopolysaccharide-mediated classical pathway complement activation", *Infect.Immun.*, vol. 68, no. 4, pp. 1753-1759.

DeLano, W. L. 2002, "The PyMOL molecular graphics system", DeLano Scientific, San Carlos, CA.
DeLucas, L. J., Greenhough, T. J., Rule, S. A., Myles, D. A., Babu, Y. S., Volanakis, J. E., & Bugg, C. E. 1987, "Preliminary X-ray study of crystals of human C-reactive protein", *J.Mol.Biol.*, vol. 196, no. 3, pp. 741-742.

Dobson, C. M. 1999, "Protein misfolding, evolution and disease", *Trends Biochem.Sci.*, vol. 24, no. 9, pp. 329-332.

Dobson, C. M. 2004, "Principles of protein folding, misfolding and aggregation", *Semin.Cell Dev.Biol.*, vol. 15, no. 1, pp. 3-16.

Dowton, S. B. & Holden, S. N. 1991, "C-reactive protein (CRP) of the Syrian hamster", *Biochemistry*, vol. 30, no. 39, pp. 9531-9538.

Du Clos, T. W. 1989, "C-reactive protein reacts with the U1 small nuclear ribonucleoprotein", *J.Immunol.*, vol. 143, no. 8, pp. 2553-2559.

Du Clos, T. W., Zlock, L. T., & Rubin, R. L. 1988, "Analysis of the binding of C-reactive protein to histones and chromatin", *J.Immunol.*, vol. 141, no. 12, pp. 4266-4270.

Dubrey, S. W., Cha, K., Skinner, M., LaValley, M., & Falk, R. H. 1997, "Familial and primary (AL) cardiac amyloidosis: echocardiographically similar diseases with distinctly different clinical outcomes", *Heart*, vol. 78, no. 1, pp. 74-82.

Eanes, E. D. & Glenner, G. G. 1968, "X-ray diffraction studies on amyloid filaments", *J.Histochem.Cytochem.*, vol. 16, no. 11, pp. 673-677.

Ember, J. A., Sanderson, S. D., Taylor, S. M., Kawahara, M., & Hugli, T. E. 1992, "Biologic activity of synthetic analogues of C5a anaphylatoxin", *J.Immunol.*, vol. 148, no. 10, pp. 3165-3173.

Emsley, J., White, H. E., O'Hara, B. P., Oliva, G., Srinivasan, N., Tickle, I. J., Blundell, T. L., Pepys, M. B., & Wood, S. P. 1994, "Structure of pentameric human serum amyloid P component", *Nature*, vol. 367, no. 6461, pp. 338-345.

Emsley, P. & Cowtan, K. 2004, "Coot: model-building tools for molecular graphics", *Acta Crystallogr.D.Biol.Crystallogr.*, vol. 60, no. Pt 12 Pt 1, pp. 2126-2132.

Entman, M. L., Michael, L., Rossen, R. D., Dreyer, W. J., Anderson, D. C., Taylor, A. A., & Smith, C. W. 1991, "Inflammation in the course of early myocardial ischemia", *FASEB J.*, vol. 5, no. 11, pp. 2529-2537.

Epstein, S. E., Zhou, Y. F., & Zhu, J. 1999, "Infection and atherosclerosis: emerging mechanistic paradigms", *Circulation*, vol. 100, no. 4, p. e20-e28.

Familian, A., Zwart, B., Huisman, H. G., Rensink, I., Roem, D., Hordijk, P. L., Aarden, L. A., & Hack, C. E. 2001, "Chromatin-independent binding of serum

amyloid P component to apoptotic cells", *J.Immunol.*, vol. 167, no. 2, pp. 647-654.

Fan, J. & Watanabe, T. 2003, "Inflammatory reactions in the pathogenesis of atherosclerosis", *J.Atheroscler.Thromb.*, vol. 10, no. 2, pp. 63-71.

Feng Z,. Westbrook J., Berman H.M. 1998, "NUcheck", Rutgers University, New Brunswick, NJ. Report No.: NDB-407.

Fishelson, Z., Attali, G., & Mevorach, D. 2001, "Complement and apoptosis", *Mol.Immunol.*, vol. 38, no. 2-3, pp. 207-219.

Fourcade, O., Simon, M. F., Viode, C., Rugani, N., Leballe, F., Ragab, A., Fournie, B., Sarda, L., & Chap, H. 1995, "Secretory phospholipase A2 generates the novel lipid mediator lysophosphatidic acid in membrane microvesicles shed from activated cells", *Cell*, vol. 80, no. 6, pp. 919-927.

Fraser, P. E., Nguyen, J. T., Surewicz, W. K., & Kirschner, D. A. 1991, "pH-dependent structural transitions of Alzheimer amyloid peptides", *Biophys.J.*, vol. 60, no. 5, pp. 1190-1201.

French, G. S. & Wilson, K. S. 1978, *Acta. Cryst.*, A34, pp. 517-534.

Fu, T. & Borensztajn, J. 2002, "Macrophage uptake of low-density lipoprotein bound to aggregated C-reactive protein: possible mechanism of foam-cell formation in atherosclerotic lesions", *Biochem.J.*, vol. 366, no. Pt 1, pp. 195-201.

Fujita, T., Matsushita, M., & Endo, Y. 2004, "The lectin-complement pathway--its role in innate immunity and evolution", *Immunol.Rev.*, vol. 198, pp. 185-202.

Gaboriaud, C., Juanhuix, J., Gruez, A., Lacroix, M., Darnault, C., Pignol, D., Verger, D., Fontecilla-Camps, J. C., & Arlaud, G. J. 2003, "The crystal structure of the globular head of complement protein C1q provides a basis for its versatile recognition properties", *J.Biol.Chem.*, vol. 278, no. 47, pp. 46974-46982.

GAL, K. & MILTENYI, M. 1955, "Haemagglutination test for the demonstration of C-reactive protein", *Acta Microbiol.Acad.Sci.Hung.*, vol. 3, no. 1-2, pp. 41-51.

Gal, P., Barna, L., Kocsis, A., & Zavodszky, P. 2007, "Serine proteases of the classical and lectin pathways: similarities and differences", *Immunobiology*, vol. 212, no. 4-5, pp. 267-277.

Ganrot, P. O. & Kindmark, C. O. 1969, "A simple two-step procedure for isolation of C-reactive protein", *Biochim.Biophys.Acta*, vol. 194, no. 2, pp. 443-448.

Garcia de, F. P. & Dahlback, B. 1994, "Interaction between serum amyloid P component and C4b-binding protein associated with inhibition of factor I-mediated C4b degradation", *J.Immunol.*, vol. 152, no. 5, pp. 2430-2437.

Garcia de, F. P., Hardig, Y., & Dahlback, B. 1995, "Serum amyloid P component binding to C4b-binding protein", *J.Biol.Chem.*, vol. 270, no. 45, pp. 26950-26955.

Garlanda, C., Bottazzi, B., Bastone, A., & Mantovani, A. 2005, "Pentraxins at the crossroads between innate immunity, inflammation, matrix deposition, and female fertility", *Annu.Rev.Immunol.*, vol. 23, pp. 337-366.

Garman, E. 1999b, "Cool data: quantity AND quality", *Acta Crystallogr.D.Biol.Crystallogr.*, vol. 55, no. Pt 10, pp. 1641-1653.

Garman, E. 1999a, "Cool data: quantity AND quality", *Acta Crystallogr.D.Biol.Crystallogr.*, vol. 55, no. Pt 10, pp. 1641-1653.

Garman, E. F. 1996, "Modern methods for rapid x-ray diffraction data collection from crystals of macromolecules", *Methods Mol.Biol.*, vol. 56, pp. 87-126.

Gershov, D., Kim, S., Brot, N., & Elkon, K. B. 2000, "C-Reactive protein binds to apoptotic cells, protects the cells from assembly of the terminal complement components, and sustains an antiinflammatory innate immune response: implications for systemic autoimmunity", *J.Exp.Med.*, vol. 192, no. 9, pp. 1353-1364.

Gill, R., Kemp, J. A., Sabin, C., & Pepys, M. B. 2004, "Human C-reactive protein increases cerebral infarct size after middle cerebral artery occlusion in adult rats", *J.Cereb.Blood Flow Metab*, vol. 24, no. 11, pp. 1214-1218.

Gitlin, J. D., Gitlin, J. I., & Gitlin, D. 1977, "Localizing of C-reactive protein in synovium of patients with rheumatoid arthritis", *Arthritis Rheum.*, vol. 20, no. 8, pp. 1491-1499.

Glaser, K. B., Mobilio, D., Chang, J. Y., & Senko, N. 1993, "Phospholipase A2 enzymes: regulation and inhibition", *Trends Pharmacol.Sci.*, vol. 14, no. 3, pp. 92-98.

Glenner, G. G. 1980, "Amyloid deposits and amyloidosis. The beta-fibrilloses (first of two parts)", *N.Engl.J.Med.*, vol. 302, no. 23, pp. 1283-1292.

Goldberger, G., Bing, D. H., Sipe, J. D., Rits, M., & Colten, H. R. 1987, "Transcriptional regulation of genes encoding the acute-phase proteins CRP, SAA, and C3", *J.Immunol.*, vol. 138, no. 11, pp. 3967-3971.

Goodman, A. R., Cardozo, T., Abagyan, R., Altmeyer, A., Wisniewski, H. G., & Vilcek, J. 1996, "Long pentraxins: an emerging group of proteins with diverse functions", *Cytokine Growth Factor Rev.*, vol. 7, no. 2, pp. 191-202.

Goodman, H. J., Wechalekar, A. D., & Hawkins, P. N. 2005, "Amyloidosis, not myeloma", *Br.J.Haematol.*, vol. 129, no. 1, pp. 158-159.

Griselli, M., Herbert, J., Hutchinson, W. L., Taylor, K. M., Sohail, M., Krausz, T., & Pepys, M. B. 1999, "C-reactive protein and complement are important

mediators of tissue damage in acute myocardial infarction", *J.Exp.Med.*, vol. 190, no. 12, pp. 1733-1740.

Hack, C. E., Wolbink, G. J., Schalkwijk, C., Speijer, H., Hermens, W. T., & van den, B. H. 1997, "A role for secretory phospholipase A2 and C-reactive protein in the removal of injured cells", *Immunol.Today*, vol. 18, no. 3, pp. 111-115.

Hammarstrom, P., Jiang, X., Hurshman, A. R., Powers, E. T., & Kelly, J. W. 2002, "Sequence-dependent denaturation energetics: A major determinant in amyloid disease diversity", *Proc.Natl.Acad.Sci.U.S.A*, vol. 99 Suppl 4, pp. 16427-16432.

Harnett, W. & Harnett, M. M. 1999, "Phosphorylcholine: friend or foe of the immune system?", *Immunol.Today*, vol. 20, no. 3, pp. 125-129.

Harper, J. D. & Lansbury, P. T., Jr. 1997, "Models of amyloid seeding in Alzheimer's disease and scrapie: mechanistic truths and physiological consequences of the time-dependent solubility of amyloid proteins", *Annu.Rev.Biochem.*, vol. 66, pp. 385-407.

Hattori, Y., Matsumura, M., & Kasai, K. 2003, "Vascular smooth muscle cell activation by C-reactive protein", *Cardiovasc.Res.*, vol. 58, no. 1, pp. 186-195.

Haunstetter, A. & Izumo, S. 1998, "Apoptosis: basic mechanisms and implications for cardiovascular disease", *Circ.Res.*, vol. 82, no. 11, pp. 1111-1129.

Haupt, H. & Heimburger, N. 1972, "[Human serum proteins with high affinity for carboxymethylcellulose. I. Isolation of lysozyme, C1q and 2 hitherto unknown -globulins]", *Hoppe Seylers.Z.Physiol Chem.*, vol. 353, no. 7, pp. 1125-1132.

Haverkate, F., Thompson, S. G., Pyke, S. D., Gallimore, J. R., & Pepys, M. B. 1997, "Production of C-reactive protein and risk of coronary events in stable and unstable angina. European Concerted Action on Thrombosis and Disabilities Angina Pectoris Study Group", *Lancet*, vol. 349, no. 9050, pp. 462-466.

Hawkins, P. N. 1988, "Amyloidosis", *Blood Rev.*, vol. 2, no. 4, pp. 270-280.

Hawkins, P. N., Lavender, J. P., & Pepys, M. B. 1990, "Evaluation of systemic amyloidosis by scintigraphy with 123I-labeled serum amyloid P component", *N.Engl.J.Med.*, vol. 323, no. 8, pp. 508-513.

Hawkins, P. N. & Pepys, M. B. 1995, "Imaging amyloidosis with radiolabelled SAP", *Eur.J.Nucl.Med.*, vol. 22, no. 7, pp. 595-599.

Hawkins, P. N., Tennent, G. A., Woo, P., & Pepys, M. B. 1991, "Studies in vivo and in vitro of serum amyloid P component in normals and in a patient with AA amyloidosis", *Clin.Exp.Immunol.*, vol. 84, no. 2, pp. 308-316.

Hawkins, P. N., Wootton, R., & Pepys, M. B. 1990, "Metabolic studies of radioiodinated serum amyloid P component in normal subjects and patients with systemic amyloidosis", *J.Clin.Invest*, vol. 86, no. 6, pp. 1862-1869.

Heaton, R. J.; Raynes, J. G.; Johnston, D. S. 1999, "A study of the denaturation of human C-reactive protein in the presence of calcium ions and glycero-phosphorylcholine ", Thermochimica Acta, vol. 334(1-2), pp. 97-106.

Hevonoja, T., Pentikainen, M. O., Hyvonen, M. T., Kovanen, P. T., & la-Korpela, M. 2000, "Structure of low density lipoprotein (LDL) particles: basis for understanding molecular changes in modified LDL", *Biochim.Biophys.Acta*, vol. 1488, no. 3, pp. 189-210.

Hicks, P. S., Saunero-Nava, L., Du Clos, T. W., & Mold, C. 1992, "Serum amyloid P component binds to histones and activates the classical complement pathway", *J.Immunol.*, vol. 149, no. 11, pp. 3689-3694.

Hind, C. R., Collins, P. M., Baltz, M. L., & Pepys, M. B. 1985, "Human serum amyloid P component, a circulating lectin with specificity for the cyclic 4,6-pyruvate acetal of galactose. Interactions with various bacteria", *Biochem.J.*, vol. 225, no. 1, pp. 107-111.

Hind, C. R., Collins, P. M., Caspi, D., Baltz, M. L., & Pepys, M. B. 1984a, "Specific chemical dissociation of fibrillar and non-fibrillar components of amyloid deposits", *Lancet*, vol. 2, no. 8399, pp. 376-378.

Hind, C. R., Collins, P. M., Renn, D., Cook, R. B., Caspi, D., Baltz, M. L., & Pepys, M. B. 1984b, "Binding specificity of serum amyloid P component for the pyruvate acetal of galactose", *J.Exp.Med.*, vol. 159, no. 4, pp. 1058-1069.

Hirschfield, G. M. 2004, "Amyloidosis: a clinico-pathophysiological synopsis", *Semin.Cell Dev.Biol.*, vol. 15, no. 1, pp. 39-44.

Hirschfield, G. M., Gallimore, J. R., Kahan, M. C., Hutchinson, W. L., Sabin, C. A., Benson, G. M., Dhillon, A. P., Tennent, G. A., & Pepys, M. B. 2005, "Transgenic human C-reactive protein is not proatherogenic in apolipoprotein E-deficient mice", *Proc.Natl.Acad.Sci.U.S.A*, vol. 102, no. 23, pp. 8309-8314.

Hirschfield, G. M., Herbert, J., Kahan, M. C., & Pepys, M. B. 2003, "Human C-reactive protein does not protect against acute lipopolysaccharide challenge in mice", *J.Immunol.*, vol. 171, no. 11, pp. 6046-6051.

Hirschfield, G. M. & Pepys, M. B. 2003, "C-reactive protein and cardiovascular disease: new insights from an old molecule", *QJM.*, vol. 96, no. 11, pp. 793-807.

Hitsumoto, Y., Okada, M., & Makino, H. 1999, "Inhibition of human and mouse complement-dependent hemolytic activity by mouse fibronectin", *Immunopharmacology*, vol. 42, no. 1-3, pp. 203-208.

Hohenester, E., Hutchinson, W. L., Pepys, M. B., & Wood, S. P. 1997, "Crystal structure of a decameric complex of human serum amyloid P component with bound dAMP", *J.Mol.Biol.*, vol. 269, no. 4, pp. 570-578.

HOKAMA, Y., COLEMAN, M. K., & RILEY, R. F. 1962, "In vitro effects of C-reactive protein on phagocytosis", *J.Bacteriol.*, vol. 83, pp. 1017-1024.

Hokama, Y., Tam, R., Hirano, W., & Kimura, L. 1974, "Significance of C-reactive protein binding by lecithin: a simplified procedure for CRP isolation", *Clin.Chim.Acta*, vol. 50, no. 1, pp. 53-62.

Hopkins, M., Flanagan, P. A., Bailey, S., Glover, I. D., Myles, D. A., & Greenhough, T. J. 1994, "Crystallization and preliminary X-ray analysis of C-reactive protein from rat", *J.Mol.Biol.*, vol. 235, no. 2, pp. 767-771.

Horiike, K., Tojo, H., Yamano, T., & Nozaki, M. 1983, "Interpretation of the stokes radius of macromolecules determined by gel filtration chromatography", *J.Biochem.(Tokyo)*, vol. 93, no. 1, pp. 99-106.

Hugli, T. E. 1978, "Chemical aspects of the serum anaphylatoxins", *Contemp.Top.Mol.Immunol.*, vol. 7, pp. 181-214.

Hugli, T. E. & Muller-Eberhard, H. J. 1978, "Anaphylatoxins: C3a and C5a", *Adv.Immunol.*, vol. 26, pp. 1-53.

Hundt, M., Zielinska-Skowronek, M., & Schmidt, R. E. 2001, "Lack of specific receptors for C-reactive protein on white blood cells", *Eur.J.Immunol.*, vol. 31, no. 12, pp. 3475-3483.

Jakob, W. 1971, "Spontaneous amyloidosis of mammals", *Vet.Pathol.*, vol. 8, no. 4, pp. 292-306.

Janson, J., Ashley, R. H., Harrison, D., McIntyre, S., & Butler, P. C. 1999, "The mechanism of islet amyloid polypeptide toxicity is membrane disruption by intermediate-sized toxic amyloid particles", *Diabetes*, vol. 48, no. 3, pp. 491-498.

Jarrett, J. T. & Lansbury, P. T., Jr. 1993, "Seeding "one-dimensional crystallization" of amyloid: a pathogenic mechanism in Alzheimer's disease and scrapie?", *Cell*, vol. 73, no. 6, pp. 1055-1058.

Jenvey, C. M. 2006, "Structure led drug design for the pentraxins", PhD thesis, University of Southampton.

Jewell, W. S., Marnell, L. L., Rokeach, L. A., & Du Clos, T. W. 1993, "C-reactive protein (CRP) binding to the Sm-D protein of snRNPS. Identification of a short polypeptide binding region", *Mol.Immunol.*, vol. 30, no. 8, pp. 701-708.

Jiang, H. X., Siegel, J. N., & Gewurz, H. 1991, "Binding and complement activation by C-reactive protein via the collagen-like region of C1q and inhibition of these reactions by monoclonal antibodies to C-reactive protein and C1q", *J.Immunol.*, vol. 146, no. 7, pp. 2324-2330.

Kabsch, W. 1988, "Evaluation of single crystal X-ray diffraction data from a position sensitive detector", *J. Appl. Crystallogr.*, vol. 21, pp. 916–924.

Kaplan, M. H. & Volanakis, J. E. 1974, "Interaction of C-reactive protein complexes with the complement system. I. Consumption of human complement associated with the reaction of C-reactive protein with pneumococcal C-polysaccharide and with the choline phosphatides, lecithin and sphingomyelin", *J.Immunol.*, vol. 112, no. 6, pp. 2135-2147.

Kinoshita, C. M., Gewurz, A. T., Siegel, J. N., Ying, S. C., Hugli, T. E., Coe, J. E., Gupta, R. K., Huckman, R., & Gewurz, H. 1992, "A protease-sensitive site in the proposed Ca(2+)-binding region of human serum amyloid P component and other pentraxins", *Protein Sci.*, vol. 1, no. 6, pp. 700-709.

Kinoshita, C. M., Ying, S. C., Hugli, T. E., Siegel, J. N., Potempa, L. A., Jiang, H., Houghten, R. A., & Gewurz, H. 1989, "Elucidation of a protease-sensitive site involved in the binding of calcium to C-reactive protein", *Biochemistry*, vol. 28, no. 25, pp. 9840-9848.

Kirschner, D. A., Inouye, H., Duffy, L. K., Sinclair, A., Lind, M., & Selkoe, D. J. 1987, "Synthetic peptide homologous to beta protein from Alzheimer disease forms amyloid-like fibrils in vitro", *Proc.Natl.Acad.Sci.U.S.A*, vol. 84, no. 19, pp. 6953-6957.

Kishore, U., Gaboriaud, C., Waters, P., Shrive, A. K., Greenhough, T. J., Reid, K. B., Sim, R. B., & Arlaud, G. J. 2004, "C1q and tumor necrosis factor superfamily: modularity and versatility", *Trends Immunol.*, vol. 25, no. 10, pp. 551-561.

Kishore, U., Gupta, S. K., Perdikoulis, M. V., Kojouharova, M. S., Urban, B. C., & Reid, K. B. 2003, "Modular organization of the carboxyl-terminal, globular head region of human C1q A, B, and C chains", *J.Immunol.*, vol. 171, no. 2, pp. 812-820.

Kishore, U., Kojouharova, M. S., & Reid, K. B. 2002, "Recent progress in the understanding of the structure-function relationships of the globular head regions of C1q", *Immunobiology*, vol. 205, no. 4-5, pp. 355-364.

Kishore, U. & Reid, K. B. 2000, "C1q: structure, function, and receptors", *Immunopharmacology*, vol. 49, no. 1-2, pp. 159-170.

Kleywegt, G. J. & Jones, T. A. 1996, "xdlMAPMAN and xdlDATA", *Acta Crystallogr.D.Biol.Crystallogr.*, vol. 52, no. Pt 4, pp. 826-828.

Knobel, H. R., Heusser, C., Rodrick, M. L., & Isliker, H. 1974, "Enzymatic digestion of the first component of human complement (C1q)", *J.Immunol.*, vol. 112, no. 6, pp. 2094-2101.

Koenig, W., Sund, M., Frohlich, M., Fischer, H. G., Lowel, H., Doring, A., Hutchinson, W. L., & Pepys, M. B. 1999, "C-Reactive protein, a sensitive marker of inflammation, predicts future risk of coronary heart disease in initially healthy

middle-aged men: results from the MONICA (Monitoring Trends and Determinants in Cardiovascular Disease) Augsburg Cohort Study, 1984 to 1992", *Circulation*, vol. 99, no. 2, pp. 237-242.

Kojouharova, M. S., Tsacheva, I. G., Tchorbadjieva, M. I., Reid, K. B., & Kishore, U. 2003, "Localization of ligand-binding sites on human C1q globular head region using recombinant globular head fragments and single-chain antibodies", *Biochim.Biophys.Acta*, vol. 1652, no. 1, pp. 64-74.

Kolb, W. P., Kolb, L. M., & Podack, E. R. 1979a, "C1q: isolation from human serum in high yield by affinity chromatography and development of a highly sensitive hemolytic assay", *J.Immunol.*, vol. 122, no. 5, pp. 2103-2111.

Kolb, W. P., Kolb, L. M., & Podack, E. R. 1979b, "C1q: isolation from human serum in high yield by affinity chromatography and development of a highly sensitive hemolytic assay", *J.Immunol.*, vol. 122, no. 5, pp. 2103-2111.

Kolstoe, E. S. 2005, "Ligand binding to pentraxins", PhD thesis, University of Southampton.

Kovacs, A., Tornvall, P., Nilsson, R., Tegner, J., Hamsten, A., & Bjorkegren, J. 2007, "Human C-reactive protein slows atherosclerosis development in a mouse model with human-like hypercholesterolemia", *Proc.Natl.Acad.Sci.U.S.A*, vol. 104, no. 34, pp. 13768-13773.

Kuller, L. H., Tracy, R. P., Shaten, J., & Meilahn, E. N. 1996, "Relation of C-reactive protein and coronary heart disease in the MRFIT nested case-control study. Multiple Risk Factor Intervention Trial", *Am.J.Epidemiol.*, vol. 144, no. 6, pp. 537-547.

Kushner, I. 1982, "The phenomenon of the acute phase response", *Ann.N.Y.Acad.Sci.*, vol. 389, pp. 39-48.

Kushner, I. & Feldmann, G. 1978, "Control of the acute phase response. Demonstration of C-reactive protein synthesis and secretion by hepatocytes during acute inflammation in the rabbit", *J.Exp.Med.*, vol. 148, no. 2, pp. 466-477.

KUSHNER, I. & KAPLAN, M. H. 1961, "Studies of acute phase protein. I. An immunohistochemical method for the localization of Cx-reactive protein in rabbits. Association with necrosis in local inflammatory lesions", *J.Exp.Med.*, vol. 114, pp. 961-974.

Lafuente, N., Azcutia, V., Matesanz, N., Cercas, E., Rodriguez-Manas, L., Sanchez-Ferrer, C. F., & Peiro, C. 2005, "Evidence for sodium azide as an artifact mediating the modulation of inducible nitric oxide synthase by C-reactive protein", *J.Cardiovasc.Pharmacol.*, vol. 45, no. 3, pp. 193-196.

Lagrand, W. K., Niessen, H. W., Wolbink, G. J., Jaspars, L. H., Visser, C. A., Verheugt, F. W., Meijer, C. J., & Hack, C. E. 1997, "C-reactive protein colocalizes with complement in human hearts during acute myocardial infarction", *Circulation*, vol. 95, no. 1, pp. 97-103.

Lansbury, P. T., Jr., Costa, P. R., Griffiths, J. M., Simon, E. J., Auger, M., Halverson, K. J., Kocisko, D. A., Hendsch, Z. S., Ashburn, T. T., Spencer, R. G., & . 1995, "Structural model for the beta-amyloid fibril based on interstrand alignment of an antiparallel-sheet comprising a C-terminal peptide", *Nat.Struct.Biol.*, vol. 2, no. 11, pp. 990-998.

Law, S. K., Lichtenberg, N. A., & Levine, R. P. 1979, "Evidence for an ester linkage between the labile binding site of C3b and receptive surfaces", *J.Immunol.*, vol. 123, no. 3, pp. 1388-1394.

Lee, G. W., Lee, T. H., & Vilcek, J. 1993, "TSG-14, a tumor necrosis factor- and IL-1-inducible protein, is a novel member of the pentaxin family of acute phase proteins", *J.Immunol.*, vol. 150, no. 5, pp. 1804-1812.

Lesavre, P. & Leibowitch, J. 1979, "[Progress in the knowledge of complement. I. Structure, activation and control of the complement system]", *Nouv.Presse Med.*, vol. 8, no. 29, pp. 2385-2387.

Libby, P. 2002a, "Atherosclerosis: the new view", *Sci.Am.*, vol. 286, no. 5, pp. 46-55.

Libby, P. 2002b, "Inflammation in atherosclerosis", *Nature*, vol. 420, no. 6917, pp. 868-874.

Libby, P., Ridker, P. M., & Maseri, A. 2002, "Inflammation and atherosclerosis", *Circulation*, vol. 105, no. 9, pp. 1135-1143.

Liuzzo, G., Biasucci, L. M., Gallimore, J. R., Grillo, R. L., Rebuzzi, A. G., Pepys, M. B., & Maseri, A. 1994, "The prognostic value of C-reactive protein and serum amyloid a protein in severe unstable angina", *N.Engl.J.Med.*, vol. 331, no. 7, pp. 417-424.

Lorenzo, A. & Yankner, B. A. 1994, "Beta-amyloid neurotoxicity requires fibril formation and is inhibited by congo red", *Proc.Natl.Acad.Sci.U.S.A*, vol. 91, no. 25, pp. 12243-12247.

Lusis, A. J. 2000, "Atherosclerosis", *Nature*, vol. 407, no. 6801, pp. 233-241.

Lutz, H. U., Fumia, S., Schurtenberger, C., & Alaia, V. 2007, "Opinion paper: Stimulation of complement amplification or activation of the alternative pathway of complement?", *Mol.Immunol.*, vol. 44, no. 16, pp. 3862-3865.

Lysenko, E., Richards, J. C., Cox, A. D., Stewart, A., Martin, A., Kapoor, M., & Weiser, J. N. 2000, "The position of phosphorylcholine on the lipopolysaccharide of Haemophilus influenzae affects binding and sensitivity to C-reactive protein-mediated killing", *Mol.Microbiol.*, vol. 35, no. 1, pp. 234-245.

Macintyre, S. S., Kushner, I., & Samols, D. 1985, "Secretion of C-reactive protein becomes more efficient during the course of the acute phase response", *J.Biol.Chem.*, vol. 260, no. 7, pp. 4169-4173.

Maclellan, W. R. & Schneider, M. D. 1997, "Death by design. Programmed cell death in cardiovascular biology and disease", *Circ.Res.*, vol. 81, no. 2, pp. 137-144.

Manolov, D. E., Rocker, C., Hombach, V., Nienhaus, G. U., & Torzewski, J. 2004, "Ultrasensitive confocal fluorescence microscopy of C-reactive protein interacting with FcgammaRIIa", *Arterioscler.Thromb.Vasc.Biol.*, vol. 24, no. 12, pp. 2372-2377.

Mantovani, A., Garlanda, C., & Bottazzi, B. 2003, "Pentraxin 3, a non-redundant soluble pattern recognition receptor involved in innate immunity", *Vaccine*, vol. 21 Suppl 2, p. S43-S47.

Marnell, L. L., Mold, C., Volzer, M. A., Burlingame, R. W., & Du Clos, T. W. 1995, "C-reactive protein binds to Fc gamma RI in transfected COS cells", *J.Immunol.*, vol. 155, no. 4, pp. 2185-2193.

Martin, S. J., Reutelingsperger, C. P., McGahon, A. J., Rader, J. A., van Schie, R. C., LaFace, D. M., & Green, D. R. 1995, "Early redistribution of plasma membrane phosphatidylserine is a general feature of apoptosis regardless of the initiating stimulus: inhibition by overexpression of Bcl-2 and Abl", *J.Exp.Med.*, vol. 182, no. 5, pp. 1545-1556.

Matthews, B. W. 1968, "Solvent content of protein crystals", *J.Mol.Biol.*, vol. 33, no. 2, pp. 491-497.

McCarty M. 1947, "The occurrence during acute infections of a protein not normally present in the blood IV Crystallization of C-reactive protein". Journal of Experimental Medicine, vol. 85, pp. 491-498.
McGrath, F. D., Brouwer, M. C., Arlaud, G. J., Daha, M. R., Hack, C. E., & Roos, A. 2006, "Evidence that complement protein C1q interacts with C-reactive protein through its globular head region", *J.Immunol.*, vol. 176, no. 5, pp. 2950-2957.

McPhalen, C. A., Strynadka, N. C., & James, M. N. 1991, "Calcium-binding sites in proteins: a structural perspective", *Adv.Protein Chem.*, vol. 42, pp. 77-144.

McPherson, A. 2004, "Introduction to protein crystallization", *Methods*, vol. 34, no. 3, pp. 254-265.

Mitchell, E., Kuhn, P., & Garman, E. 1999, "Demystifying the synchrotron trip: a first time user's guide", *Structure.*, vol. 7, no. 5, p. R111-R121.

Mold, C., Baca, R., & Du Clos, T. W. 2002, "Serum amyloid P component and C-reactive protein opsonize apoptotic cells for phagocytosis through Fcgamma receptors", *J.Autoimmun.*, vol. 19, no. 3, pp. 147-154.

Mold, C., Gewurz, H., & Du Clos, T. W. 1999, "Regulation of complement activation by C-reactive protein", *Immunopharmacology*, vol. 42, no. 1-3, pp. 23-30.

Morozova-Roche, L. A., Zurdo, J., Spencer, A., Noppe, W., Receveur, V., Archer, D. B., Joniau, M., & Dobson, C. M. 2000, "Amyloid fibril formation and seeding by wild-type human lysozyme and its disease-related mutational variants", *J.Struct.Biol.*, vol. 130, no. 2-3, pp. 339-351.

Mullane, K. M. & Smith, C. W., 1990, "The role of leukocyte in ischemic damage, reperfusion injury and repair of the myocardium", In: H.M. Piper, Editor, *Pathophysiology of Severe Ischemic Myocardial Injury*, Kluwer, Dordrecht, The Netherlands, pp. 239–267.

Murshudov, G. N. 1997, "Refinement of macromolecular structures by the maximum-likelihood method", *Acta Crystallogr. D Biol. Crystallogr.*, vol 53, pp. 240–255.

Murshudov, G. N., Vagin, A. A., & Dodson, E. J. 1997, "Refinement of macromolecular structures by the maximum-likelihood method", *Acta Crystallogr.D.Biol.Crystallogr.*, vol. 53, no. Pt 3, pp. 240-255.

Myles, D. A., Bailey, S., Rule, S. A., Jones, G. R., & Greenhough, T. J. 1990a, "Preliminary crystallographic study of C-reactive protein from Limulus polyphemus", *J.Mol.Biol.*, vol. 213, no. 2, pp. 223-225.

Myles, D. A., Rule, S. A., DeLucas, L. J., Babu, Y. S., Xu, Y., Volanakis, J. E., Bugg, C. E., Bailey, S., & Greenhough, T. J. 1990b, "Rotation function studies of human C-reactive protein", *J.Mol.Biol.*, vol. 216, no. 3, pp. 491-496.

Nagpurkar, A. & Mookerjea, S. 1981, "A novel phosphorylcholine-binding protein from rat serum and its effect on heparin-lipoprotein complex formation in the presence of calcium", *J.Biol.Chem.*, vol. 256, no. 14, pp. 7440-7446.

Narkates, A. J. & Volanakis, J. E. 1982, "C-reactive protein binding specificities: artificial and natural phospholipid bilayers", *Ann.N.Y.Acad.Sci.*, vol. 389, pp. 172-182.

Navaza, J. 1993, "On the computation of the fast rotation function", *Acta Crystallogr.D.Biol.Crystallogr.*, vol. 49, no. Pt 6, pp. 588-591.

Navaza, L. 1994. "AMoRe: an automated package for molecular replacement", *Acta Crystallogr. A50*, pp. 157-163.

Nelson, R., Sawaya, M. R., Balbirnie, M., Madsen, A. O., Riekel, C., Grothe, R., & Eisenberg, D. 2005, "Structure of the cross-beta spine of amyloid-like fibrils", *Nature*, vol. 435, no. 7043, pp. 773-778.

Nguyen, N. Y., Suzuki, A., Boykins, R. A., & Liu, T. Y. 1986a, "The amino acid sequence of Limulus C-reactive protein. Evidence of polymorphism", *J.Biol.Chem.*, vol. 261, no. 22, pp. 10456-10465.

Nguyen, N. Y., Suzuki, A., Cheng, S. M., Zon, G., & Liu, T. Y. 1986b, "Isolation and characterization of Limulus C-reactive protein genes", *J.Biol.Chem.*, vol. 261, no. 22, pp. 10450-10455.

Nijmeijer, R., Lagrand, W. K., Baidoshvili, A., Lubbers, Y. T., Hermens, W. T., Meijer, C. J., Visser, C. A., Hack, C. E., & Niessen, H. W. 2002, "Secretory type II phospholipase A(2) binds to ischemic myocardium during myocardial infarction in humans", *Cardiovasc.Res.*, vol. 53, no. 1, pp. 138-146.

Nijmeijer, R., Lagrand, W. K., Lubbers, Y. T., Visser, C. A., Meijer, C. J., Niessen, H. W., & Hack, C. E. 2003a, "C-reactive protein activates complement in infarcted human myocardium", *Am.J.Pathol.*, vol. 163, no. 1, pp. 269-275.

Nijmeijer, R., Lagrand, W. K., Visser, C. A., Meijer, C. J., Niessen, H. W., & Hack, C. E. 2001, "CRP, a major culprit in complement-mediated tissue damage in acute myocardial infarction?", *Int.Immunopharmacol.*, vol. 1, no. 3, pp. 403-414.

Nijmeijer, R., Willemsen, M., Meijer, C. J., Visser, C. A., Verheijen, R. H., Gottlieb, R. A., Hack, C. E., & Niessen, H. W. 2003b, "Type II secretory phospholipase A2 binds to ischemic flip-flopped cardiomyocytes and subsequently induces cell death", *Am.J.Physiol Heart Circ.Physiol*, vol. 285, no. 5, p. H2218-H2224.

Nilsberth, C., Westlind-Danielsson, A., Eckman, C. B., Condron, M. M., Axelman, K., Forsell, C., Stenh, C., Luthman, J., Teplow, D. B., Younkin, S. G., Naslund, J., & Lannfelt, L. 2001, "The 'Arctic' APP mutation (E693G) causes Alzheimer's disease by enhanced Abeta protofibril formation", *Nat.Neurosci.*, vol. 4, no. 9, pp. 887-893.

Noursadeghi, M., Bickerstaff, M. C., Gallimore, J. R., Herbert, J., Cohen, J., & Pepys, M. B. 2000, "Role of serum amyloid P component in bacterial infection: protection of the host or protection of the pathogen", *Proc.Natl.Acad.Sci.U.S.A*, vol. 97, no. 26, pp. 14584-14589.

Nunomura, W., Takakuwa, Y., & Higashi, T. 1994, "Changes in serum concentration and mRNA level of rat C-reactive protein", *Biochim.Biophys.Acta*, vol. 1227, no. 1-2, pp. 74-78.

Oliveira, E. B., Gotschlich, E. C., & Liu, T. Y. 1980, "Comparative studies on the binding properties of human and rabbit C-reactive proteins", *J.Immunol.*, vol. 124, no. 3, pp. 1396-1402.

Osmand, A. P., Gerwurz, H., & Friedenson, B. 1977, "Partial amino-acid sequences of human and rabbit C-reactive proteins: homology with immunoglobulins and histocompatibility antigens", *Proc.Natl.Acad.Sci.U.S.A*, vol. 74, no. 3, pp. 1214-1218.

Osmand, A. P., Friedenson, B., Gewurz, H., Painter, R. H., Hofmann, T., & Shelton, E. 1977, "Characterization of C-reactive protein and the complement

subcomponent C1t as homologous proteins displaying cyclic pentameric symmetry (pentraxins)", *Proc.Natl.Acad.Sci.U.S.A*, vol. 74, no. 2, pp. 739-743.

Otwinowski, Z. 1993, "DENZO", *in*, Proc. of the CCP4 Study Weekend, 56, 62, Science and Engineering Research Council, Daresbury Laboratory.

Pasceri, V., Cheng, J. S., Willerson, J. T., & Yeh, E. T. 2001, "Modulation of C-reactive protein-mediated monocyte chemoattractant protein-1 induction in human endothelial cells by anti-atherosclerosis drugs", *Circulation*, vol. 103, no. 21, pp. 2531-2534.

Pasceri, V., Willerson, J. T., & Yeh, E. T. 2000, "Direct proinflammatory effect of C-reactive protein on human endothelial cells", *Circulation*, vol. 102, no. 18, pp. 2165-2168.

Paul, A., Ko, K. W., Li, L., Yechoor, V., McCrory, M. A., Szalai, A. J., & Chan, L. 2004, "C-reactive protein accelerates the progression of atherosclerosis in apolipoprotein E-deficient mice", *Circulation*, vol. 109, no. 5, pp. 647-655.

Pepys, J. & Longbottom, J. L. 1971, "Antigenic and C-substance activities of related glycopeptides from fungal, parasitic and vegetable sources", *Int.Arch.Allergy Appl.Immunol.*, vol. 41, no. 1, pp. 219-221.

Pepys, M. B. 1988, "Amyloidosis: some recent developments", *Q.J.Med.*, vol. 67, no. 252, pp. 283-298.

Pepys, M. B. 2001, "Pathogenesis, diagnosis and treatment of systemic amyloidosis", *Philos.Trans.R.Soc.Lond B Biol.Sci.*, vol. 356, no. 1406, pp. 203-210.

Pepys, M. B. 2006, "Amyloidosis", *Annu.Rev.Med.*, vol. 57, pp. 223-241.

Pepys, M. B., Baltz, M., Gomer, K., Davies, A. J., & Doenhoff, M. 1979a, "Serum amyloid P-component is an acute-phase reactant in the mouse", *Nature*, vol. 278, no. 5701, pp. 259-261.

Pepys, M. B. & Baltz, M. L. 1983, "Acute phase proteins with special reference to C-reactive protein and related proteins (pentaxins) and serum amyloid A protein", *Adv.Immunol.*, vol. 34, pp. 141-212.

Pepys, M. B., Baltz, M. L., de Beer, F. C., Dyck, R. F., Holford, S., Breathnach, S. M., Black, M. M., Tribe, C. R., Evans, D. J., & Feinstein, A. 1982, "Biology of serum amyloid P component", *Ann.N.Y.Acad.Sci.*, vol. 389, pp. 286-298.

Pepys, M. B., Booth, S. E., Tennent, G. A., Butler, P. J., & Williams, D. G. 1994a, "Binding of pentraxins to different nuclear structures: C-reactive protein binds to small nuclear ribonucleoprotein particles, serum amyloid P component binds to chromatin and nucleoli", *Clin.Exp.Immunol.*, vol. 97, no. 1, pp. 152-157.

Pepys, M. B. & Butler, P. J. 1987, "Serum amyloid P component is the major calcium-dependent specific DNA binding protein of the serum", *Biochem.Biophys.Res.Commun.*, vol. 148, no. 1, pp. 308-313.

Pepys, M. B. & Dash, A. C. 1977, "Isolation of amyloid P component (protein AP) from normal serum as a calcium-dependent binding protein", *Lancet*, vol. 1, no. 8020, pp. 1029-1031.

Pepys, M. B., Dash, A. C., Fletcher, T. C., Richardson, N., Munn, E. A., & Feinstein, A. 1978, "Analogues in other mammals and in fish of human plasma proteins, C-reactive protein and amyloid P component", *Nature*, vol. 273, no. 5658, pp. 168-170.

Pepys, M. B., Dyck, R. F., de Beer, F. C., Skinner, M., & Cohen, A. S. 1979b, "Binding of serum amyloid P-component (SAP) by amyloid fibrils", *Clin.Exp.Immunol.*, vol. 38, no. 2, pp. 284-293.

Pepys, M. B., Hawkins, P. N., Booth, D. R., Vigushin, D. M., Tennent, G. A., Soutar, A. K., Totty, N., Nguyen, O., Blake, C. C., Terry, C. J., & . 1993, "Human lysozyme gene mutations cause hereditary systemic amyloidosis", *Nature*, vol. 362, no. 6420, pp. 553-557.

Pepys, M. B. & Hawkins, P. N. 2003, "Amyloidosis". In D. A. Warrell, T. M. Cox, J. D. Firth, & E. J. Benz Jr. (Eds.), *Oxford textbook of medicine* (pp. 162–173). Oxford: Oxford University Press.

Pepys, M. B., Hawkins, P. N., Kahan, M. C., Tennent, G. A., Gallimore, J. R., Graham, D., Sabin, C. A., Zychlinsky, A., & de, D. J. 2005, "Proinflammatory effects of bacterial recombinant human C-reactive protein are caused by contamination with bacterial products, not by C-reactive protein itself", *Circ.Res.*, vol. 97, no. 11, pp. e97-103.

Pepys, M. B., Herbert, J., Hutchinson, W. L., Tennent, G. A., Lachmann, H. J., Gallimore, J. R., Lovat, L. B., Bartfai, T., Alanine, A., Hertel, C., Hoffmann, T., Jakob-Roetne, R., Norcross, R. D., Kemp, J. A., Yamamura, K., Suzuki, M., Taylor, G. W., Murray, S., Thompson, D., Purvis, A., Kolstoe, S., Wood, S. P., & Hawkins, P. N. 2002, "Targeted pharmacological depletion of serum amyloid P component for treatment of human amyloidosis", *Nature*, vol. 417, no. 6886, pp. 254-259.

Pepys, M. B. & Hirschfield, G. M. 2003, "C-reactive protein: a critical update", *J.Clin.Invest*, vol. 111, no. 12, pp. 1805-1812.

Pepys, M. B., Hirschfield, G. M., Tennent, G. A., Gallimore, J. R., Kahan, M. C., Bellotti, V., Hawkins, P. N., Myers, R. M., Smith, M. D., Polara, A., Cobb, A. J., Ley, S. V., Aquilina, J. A., Robinson, C. V., Sharif, I., Gray, G. A., Sabin, C. A., Jenvey, M. C., Kolstoe, S. E., Thompson, D., & Wood, S. P. 2006a, "Targeting C-reactive protein for the treatment of cardiovascular disease", *Nature*, vol. 440, no. 7088, pp. 1217-1221.

Pepys, M. B., Hirschfield, G. M., Tennent, G. A., Gallimore, J. R., Kahan, M. C., Bellotti, V., Hawkins, P. N., Myers, R. M., Smith, M. D., Polara, A., Cobb, A. J., Ley, S. V., Aquilina, J. A., Robinson, C. V., Sharif, I., Gray, G. A., Sabin, C. A., Jenvey, M. C., Kolstoe, S. E., Thompson, D., & Wood, S. P. 2006b, "Targeting C-reactive protein for the treatment of cardiovascular disease", *Nature*, vol. 440, no. 7088, pp. 1217-1221.

Pepys, M. B., Rademacher, T. W., matayakul-Chantler, S., Williams, P., Noble, G. E., Hutchinson, W. L., Hawkins, P. N., Nelson, S. R., Gallimore, J. R., Herbert, J., & . 1994b, "Human serum amyloid P component is an invariant constituent of amyloid deposits and has a uniquely homogeneous glycostructure", *Proc.Natl.Acad.Sci.U.S.A*, vol. 91, no. 12, pp. 5602-5606.

Pepys, M. B., Rowe, I. F., & Baltz, M. L. 1985, "C-reactive protein: binding to lipids and lipoproteins", *Int.Rev.Exp.Pathol.*, vol. 27, pp. 83-111.

Petkova, A. T., Baldus, M., Belenky, M., Hong, M., Griffin, R. G., & Herzfeld, J. 2003, "Backbone and side chain assignment strategies for multiply labeled membrane peptides and proteins in the solid state", *J.Magn Reson.*, vol. 160, no. 1, pp. 1-12.

Pietila, K., Harmoinen, A., Hermens, W., Simoons, M. L., Van de, W. F., & Verstraete, M. 1993, "Serum C-reactive protein and infarct size in myocardial infarct patients with a closed versus an open infarct-related coronary artery after thrombolytic therapy", *Eur.Heart J.*, vol. 14, no. 7, pp. 915-919.

Pietila, K. O., Harmoinen, A. P., Jokiniitty, J., & Pasternack, A. I. 1996, "Serum C-reactive protein concentration in acute myocardial infarction and its relationship to mortality during 24 months of follow-up in patients under thrombolytic treatment", *Eur.Heart J.*, vol. 17, no. 9, pp. 1345-1349.

Pinteric, L., Assimeh, S. N., Kells, D. I., & Painter, R. H. 1976, "The ultrastructure of C1t, a subcomponent of the first component of complement: an E.M. and ultracentrifuge study", *J.Immunol.*, vol. 117, no. 1, pp. 79-83.

Pober, J. S., Doukas, J., Hughes, C. C., Savage, C. O., Munro, J. M., & Cotran, R. S. 1990, "The potential roles of vascular endothelium in immune reactions", *Hum.Immunol.*, vol. 28, no. 2, pp. 258-262.

Pontet, M., D'Asnieres, M., Gache, D., Escaig, J., & Engler, R. 1981, "A new pentraxin (serum amyloid P-component) in the rat: evidence for two quaternary structures and effect of ligands on self-association", *Biochim.Biophys.Acta*, vol. 671, no. 2, pp. 202-210.

Potempa, L. A., Maldonado, B. A., Laurent, P., Zemel, E. S., & Gewurz, H. 1983, "Antigenic, electrophoretic and binding alterations of human C-reactive protein modified selectively in the absence of calcium", *Mol.Immunol.*, vol. 20, no. 11, pp. 1165-1175.

PUCHTLER, H. & SWEAT, F. 1962, "Amidoblack as a stain for hemoglobin", *Arch.Pathol.*, vol. 73, pp. 245-249.

Purvis, A. 2002, "Amyloid recognition by amyloid P component", PhD thesis, University of Southampton.

Pye, V. 1999, "Structural studies of human serum amyloid P component", PhD thesis, University of London.

Radaev, S. & Sun, P. D. 2002, "Crystallization of protein-protein complexes", *J. Appl. Cryst.*, vol. 35, pp. 674-676.

Radaev, S. & Sun, P. 2002, "Recognition of immunoglobulins by Fcgamma receptors", *Mol.Immunol.*, vol. 38, no. 14, pp. 1073-1083.

Ramadan, M. A., Shrive, A. K., Holden, D., Myles, D. A., Volanakis, J. E., DeLucas, L. J., & Greenhough, T. J. 2002, "The three-dimensional structure of calcium-depleted human C-reactive protein from perfectly twinned crystals", *Acta Crystallogr.D.Biol.Crystallogr.*, vol. 58, no. Pt 6 Pt 2, pp. 992-1001.

Rassouli, M., Sambasivam, H., Azadi, P., Dell, A., Morris, H. R., Nagpurkar, A., Mookerjea, S., & Murray, R. K. 1992, "Derivation of the amino acid sequence of rat C-reactive protein from cDNA cloning with additional studies on the nature of its dimeric component", *J.Biol.Chem.*, vol. 267, no. 5, pp. 2947-2954.

Read, R. J. 2001, "Pushing the boundaries of molecular replacement with maximum likelihood", *Acta Cryst.*, D57, pp. 1373-1382.

Reid, K. B. 1983, "Proteins involved in the activation and control of the two pathways of human complement", *Biochem.Soc.Trans.*, vol. 11, no. 1, pp. 1-12.

Reid, K. B. & Thompson, R. A. 1983, "Characterization of a non-functional form of C1q found in patients with a genetically linked deficiency of C1q activity", *Mol.Immunol.*, vol. 20, no. 10, pp. 1117-1125.

Reid, K. B. & Turner, M. W. 1994, "Mammalian lectins in activation and clearance mechanisms involving the complement system", *Springer Semin.Immunopathol.*, vol. 15, no. 4, pp. 307-326.

Reifenberg, K., Lehr, H. A., Baskal, D., Wiese, E., Schaefer, S. C., Black, S., Samols, D., Torzewski, M., Lackner, K. J., Husmann, M., Blettner, M., & Bhakdi, S. 2005, "Role of C-reactive protein in atherogenesis: can the apolipoprotein E knockout mouse provide the answer?", *Arterioscler.Thromb.Vasc.Biol.*, vol. 25, no. 8, pp. 1641-1646.

Reixach, N., Deechongkit, S., Jiang, X., Kelly, J. W., & Buxbaum, J. N. 2004, "Tissue damage in the amyloidoses: Transthyretin monomers and nonnative oligomers are the major cytotoxic species in tissue culture", *Proc.Natl.Acad.Sci.U.S.A*, vol. 101, no. 9, pp. 2817-2822.

Rhodes, Gale. *Crystallography Made Crystal Clear.* San Diego: Academic Press, 1993

Richards, R. L., Gewurz, H., Osmand, A. P., & Alving, C. R. 1977, "Interactions of C-reactive protein and complement with liposomes", *Proc.Natl.Acad.Sci.U.S.A*, vol. 74, no. 12, pp. 5672-5676.

Ridker, P. M. 1997, "Fibrinolytic and inflammatory markers for arterial occlusion: the evolving epidemiology of thrombosis and hemostasis", *Thromb.Haemost.*, vol. 78, no. 1, pp. 53-59.

Riek, R., Hornemann, S., Wider, G., Billeter, M., Glockshuber, R., & Wuthrich, K. 1996, "NMR structure of the mouse prion protein domain PrP(121-321)", *Nature*, vol. 382, no. 6587, pp. 180-182.

Ritter, C., Maddelein, M. L., Siemer, A. B., Luhrs, T., Ernst, M., Meier, B. H., Saupe, S. J., & Riek, R. 2005, "Correlation of structural elements and infectivity of the HET-s prion", *Nature*, vol. 435, no. 7043, pp. 844-848.

Robey, F. A., Jones, K. D., Tanaka, T., & Liu, T. Y. 1984, "Binding of C-reactive protein to chromatin and nucleosome core particles. A possible physiological role of C-reactive protein", *J.Biol.Chem.*, vol. 259, no. 11, pp. 7311-7316.

Robey, F. A. & Liu, T. Y. 1981, "Limulin: a C-reactive protein from Limulus polyphemus", *J.Biol.Chem.*, vol. 256, no. 2, pp. 969-975.

Ross, R. 1999, "Atherosclerosis--an inflammatory disease", *N.Engl.J.Med.*, vol. 340, no. 2, pp. 115-126.

Roumenina, L., Bureeva, S., Kantardjiev, A., Karlinsky, D., ndia-Pravdivy, J. E., Sim, R., Kaplun, A., Popov, M., Kishore, U., & Atanasov, B. 2007, "Complement C1q-target proteins recognition is inhibited by electric moment effectors", *J.Mol.Recognit.*

Roumenina, L. T., Kantardjiev, A. A., Atanasov, B. P., Waters, P., Gadjeva, M., Reid, K. B., Mantovani, A., Kishore, U., & Kojouharova, M. S. 2005, "Role of Ca2+ in the electrostatic stability and the functional activity of the globular domain of human C1q", *Biochemistry*, vol. 44, no. 43, pp. 14097-14109.

Roux, K. H., Kilpatrick, J. M., Volanakis, J. E., & Kearney, J. F. 1983, "Localization of the phosphocholine-binding sites on C-reactive protein by immunoelectron microscopy", *J.Immunol.*, vol. 131, no. 5, pp. 2411-2415.

Rowe, I. F., Soutar, A. K., Trayner, I. M., Thompson, G. R., & Pepys, M. B. 1984, "Circulating human C-reactive protein binds very low density lipoproteins", *Clin.Exp.Immunol.*, vol. 58, no. 1, pp. 237-244.

Rowe, I. F., Walker, L. N., Bowyer, D. E., Soutar, A. K., Smith, L. C., & Pepys, M. B. 1985, "Immunohistochemical studies of C-reactive protein and apolipoprotein B in inflammatory and arterial lesions", *J.Pathol.*, vol. 145, no. 3, pp. 241-249.

Rubio, N., Sharp, P. M., Rits, M., Zahedi, K., & Whitehead, A. S. 1993, "Structure, expression, and evolution of guinea pig serum amyloid P component and C-reactive protein", *J.Biochem.(Tokyo)*, vol. 113, no. 3, pp. 277-284.

Rudnick, C. M. & Dowton, S. B. 1993, "Serum amyloid P (female protein) of the Syrian hamster. Gene structure and expression", *J.Biol.Chem.*, vol. 268, no. 29, pp. 21760-21769.

Russel, A. & Cambillau, C. 1991, "Turbo Frodo", Silicon Graphics Geometry, Partners Directory, Silicon Graphics, Mountain View, CA.

Saeland, E., van, R. A., Hendriksen, K., Vile-Weekhout, H., Rijkers, G. T., Sanders, L. A., & van de Winkel, J. G. 2001, "Human C-reactive protein does not bind to FcgammaRIIa on phagocytic cells", *J.Clin.Invest*, vol. 107, no. 5, pp. 641-643.

Sambasivam, H., Rassouli, M., Murray, R. K., Nagpurkar, A., Mookerjea, S., Azadi, P., Dell, A., & Morris, H. R. 1993, "Studies on the carbohydrate moiety and on the biosynthesis of rat C-reactive protein", *J.Biol.Chem.*, vol. 268, no. 14, pp. 10007-10016.

Sasaki, T. & Yonemasu, K. 1983, "Chemical studies on the isolated collagen-like and globular fragment of complement component C1q. Comparative studies on bovine and human C1q", *Biochim.Biophys.Acta*, vol. 742, no. 1, pp. 122-128.

Schuler, B., Rachel, R., & Seckler, R. 1999, "Formation of fibrous aggregates from a non-native intermediate: the isolated P22 tailspike beta-helix domain", *J.Biol.Chem.*, vol. 274, no. 26, pp. 18589-18596.

Schwalbe, R. A., Dahlback, B., Coe, J. E., & Nelsestuen, G. L. 1992, "Pentraxin family of proteins interact specifically with phosphorylcholine and/or phosphorylethanolamine", *Biochemistry*, vol. 31, no. 20, pp. 4907-4915.

Selkoe, D. J. 2003, "Folding proteins in fatal ways", *Nature*, vol. 426, no. 6968, pp. 900-904.

Sellar, G. C., Blake, D. J., & Reid, K. B. 1991, "Characterization and organization of the genes encoding the A-, B- and C-chains of human complement subcomponent C1q. The complete derived amino acid sequence of human C1q", *Biochem.J.*, vol. 274 (Pt 2), pp. 481-490.

Serino, L. & Virji, M. 2000, "Phosphorylcholine decoration of lipopolysaccharide differentiates commensal Neisseriae from pathogenic strains: identification of licA-type genes in commensal Neisseriae", *Mol.Microbiol.*, vol. 35, no. 6, pp. 1550-1559.

Serpell, L. C., Sunde, M., Benson, M. D., Tennent, G. A., Pepys, M. B., & Fraser, P. E. 2000, "The protofilament substructure of amyloid fibrils", *J.Mol.Biol.*, vol. 300, no. 5, pp. 1033-1039.

Sheldrick, G. M. & Schneider, T. R. 1997, *Methods in Enzymology*, vol. 277, pp. 319-343.

Shine, B., de Beer, F. C., & Pepys, M. B. 1981, "Solid phase radioimmunoassays for human C-reactive protein", *Clin.Chim.Acta*, vol. 117, no. 1, pp. 13-23.

Shirahama, T. & Cohen, A. S. 1967, "High-resolution electron microscopic analysis of the amyloid fibril", *J.Cell Biol.*, vol. 33, no. 3, pp. 679-708.

Shrive, A. K., Cheetham, G. M., Holden, D., Myles, D. A., Turnell, W. G., Volanakis, J. E., Pepys, M. B., Bloomer, A. C., & Greenhough, T. J. 1996b, "Three dimensional structure of human C-reactive protein", *Nat.Struct.Biol.*, vol. 3, no. 4, pp. 346-354.

Shrive, A. K., Cheetham, G. M., Holden, D., Myles, D. A., Turnell, W. G., Volanakis, J. E., Pepys, M. B., Bloomer, A. C., & Greenhough, T. J. 1996a, "Three dimensional structure of human C-reactive protein", *Nat.Struct.Biol.*, vol. 3, no. 4, pp. 346-354.

Shrive, A. K., Holden, D., Myles, D. A., & Greenhough, T. J. 1996c, "Structure solution of C-reactive proteins: molecular replacement with a twist", *Acta Crystallogr.D.Biol.Crystallogr.*, vol. 52, no. Pt 6, pp. 1049-1057.

Shrive, A. K., Metcalfe, A. M., Cartwright, J. R., & Greenhough, T. J. 1999, "C-reactive protein and SAP-like pentraxin are both present in Limulus polyphemus haemolymph: crystal structure of Limulus SAP", *J.Mol.Biol.*, vol. 290, no. 5, pp. 997-1008.

Siboo, R. & Kulisek, E. 1978, "A fluorescent immunoassay for the quantification of C-reactive protein", *J.Immunol.Methods*, vol. 23, no. 1-2, pp. 59-67.

Siegel, J., Rent, R., & Gewurz, H. 1974, "Interactions of C-reactive protein with the complement system. I. Protamine-induced consumption of complement in acute phase sera", *J.Exp.Med.*, vol. 140, no. 3, pp. 631-647.

Sim, R. B. & Tsiftsoglou, S. A. 2004, "Proteases of the complement system", *Biochem.Soc.Trans.*, vol. 32, no. Pt 1, pp. 21-27.

Simmons, L. K., May, P. C., Tomaselli, K. J., Rydel, R. E., Fuson, K. S., Brigham, E. F., Wright, S., Lieberburg, I., Becker, G. W., Brems, D. N., & . 1994, "Secondary structure of amyloid beta peptide correlates with neurotoxic activity in vitro", *Mol.Pharmacol.*, vol. 45, no. 3, pp. 373-379.

Sivia, D.S., 1996, "Data Analysis: A Bayesian Tutorial", Oxford University Press, Oxford.

Snel, F. W., Niewold, T. A., Baltz, M. L., Hol, P. R., Van Ederen, A. M., Pepys, M. B., & Gruys, E. 1989, "Experimental amyloidosis in the hamster: correlation between hamster female protein levels and amyloid deposition", *Clin.Exp.Immunol.*, vol. 76, no. 2, pp. 296-300.

Sorensen, I. J., Nielsen, E. H., Andersen, O., Danielsen, B., & Svehag, S. E. 1996, "Binding of complement proteins C1q and C4bp to serum amyloid P component (SAP) in solid contra liquid phase", *Scand.J.Immunol.*, vol. 44, no. 4, pp. 401-407.

Sun, H., Koike, T., Ichikawa, T., Hatakeyama, K., Shiomi, M., Zhang, B., Kitajima, S., Morimoto, M., Watanabe, T., Asada, Y., Chen, Y. E., & Fan, J. 2005, "C-reactive protein in atherosclerotic lesions: its origin and pathophysiological significance", *Am.J.Pathol.*, vol. 167, no. 4, pp. 1139-1148.

Sunde, M. & Blake, C. 1997, "The structure of amyloid fibrils by electron microscopy and X-ray diffraction", *Adv.Protein Chem.*, vol. 50, pp. 123-159.

Sunde, M., Serpell, L. C., Bartlam, M., Fraser, P. E., Pepys, M. B., & Blake, C. C. 1997, "Common core structure of amyloid fibrils by synchrotron X-ray diffraction", *J.Mol.Biol.*, vol. 273, no. 3, pp. 729-739.

Szalai, A. J., Briles, D. E., & Volanakis, J. E. 1995, "Human C-reactive protein is protective against fatal Streptococcus pneumoniae infection in transgenic mice", *J.Immunol.*, vol. 155, no. 5, pp. 2557-2563.

Szalai, A. J., VanCott, J. L., McGhee, J. R., Volanakis, J. E., & Benjamin, W. H., Jr. 2000, "Human C-reactive protein is protective against fatal Salmonella enterica serovar typhimurium infection in transgenic mice", *Infect.Immun.*, vol. 68, no. 10, pp. 5652-5656.

Taskinen, S., Hyvonen, M., Kovanen, P. T., Meri, S., & Pentikainen, M. O. 2005, "C-reactive protein binds to the 3beta-OH group of cholesterol in LDL particles", *Biochem.Biophys.Res.Commun.*, vol. 329, no. 4, pp. 1208-1216.

Taskinen, S., Kovanen, P. T., Jarva, H., Meri, S., & Pentikainen, M. O. 2002, "Binding of C-reactive protein to modified low-density-lipoprotein particles: identification of cholesterol as a novel ligand for C-reactive protein", *Biochem.J.*, vol. 367, no. Pt 2, pp. 403-412.

Taylor, J. A., Bruton, C. J., Anderson, J. K., Mole, J. E., de Beer, F. C., Baltz, M. L., & Pepys, M. B. 1984, "Amino acid sequence homology between rat and human C-reactive protein", *Biochem.J.*, vol. 221, no. 3, pp. 903-906.

Taylor, K. E., Giddings, J. C., & van den Berg, C. W. 2005, "C-reactive protein-induced in vitro endothelial cell activation is an artefact caused by azide and lipopolysaccharide", *Arterioscler.Thromb.Vasc.Biol.*, vol. 25, no. 6, pp. 1225-1230.

Tennent, G. A., Baltz, M. L., Osborn, G. D., Butler, P. J., Noble, G. E., Hawkins, P. N., & Pepys, M. B. 1993a, "Studies of the structure and binding properties of hamster female protein", *Immunology*, vol. 80, no. 4, pp. 645-651.

Tennent, G. A., Butler, P. J., Hutton, T., Woolfitt, A. R., Harvey, D. J., Rademacher, T. W., & Pepys, M. B. 1993b, "Molecular characterization of Limulus polyphemus C-reactive protein. I. Subunit composition", *Eur.J.Biochem.*, vol. 214, no. 1, pp. 91-97.

Tennent, G. A., Lovat, L. B., & Pepys, M. B. 1995, "Serum amyloid P component prevents proteolysis of the amyloid fibrils of Alzheimer disease and systemic amyloidosis", *Proc.Natl.Acad.Sci.U.S.A*, vol. 92, no. 10, pp. 4299-4303.

Tenner, A. J., Lesavre, P. H., & Cooper, N. R. 1981, "Purification and radiolabeling of human C1q", *J.Immunol.*, vol. 127, no. 2, pp. 648-653.

Terry, C. J., Damas, A. M., Oliveira, P., Saraiva, M. J., Alves, I. L., Costa, P. P., Matias, P. M., Sakaki, Y., & Blake, C. C. 1993, "Structure of Met30 variant of transthyretin and its amyloidogenic implications", *EMBO J.*, vol. 12, no. 2, pp. 735-741.

Tharia, H. A., Shrive, A. K., Mills, J. D., Arme, C., Williams, G. T., & Greenhough, T. J. 2002, "Complete cDNA sequence of SAP-like pentraxin from Limulus polyphemus: implications for pentraxin evolution", *J.Mol.Biol.*, vol. 316, no. 3, pp. 583-597.

Thompson, A. J. & Barrow, C. J. 2002, "Protein conformational misfolding and amyloid formation: characteristics of a new class of disorders that include Alzheimer's and Prion diseases", *Curr.Med.Chem.*, vol. 9, no. 19, pp. 1751-1762.

Thompson, D., Pepys, M. B., Tickle, I., & Wood, S. 2002, "The structures of crystalline complexes of human serum amyloid P component with its carbohydrate ligand, the cyclic pyruvate acetal of galactose", *J.Mol.Biol.*, vol. 320, no. 5, pp. 1081-1086.

Thompson, D., Pepys, M. B., & Wood, S. P. 1999, "The physiological structure of human C-reactive protein and its complex with phosphocholine", *Structure.*, vol. 7, no. 2, pp. 169-177.

Thompson, S. G., Kienast, J., Pyke, S. D., Haverkate, F., & van de Loo, J. C. 1995, "Hemostatic factors and the risk of myocardial infarction or sudden death in patients with angina pectoris. European Concerted Action on Thrombosis and Disabilities Angina Pectoris Study Group", *N.Engl.J.Med.*, vol. 332, no. 10, pp. 635-641.

Tillett, W. S., & T. Francis, JR. 1930, "Serological reactions in pneumonia with a non-protein fraction of pneumococcus", *J. Exp. Med.*, vol. 52, pp. 561-571.

Togashi, S., Lim, S. K., Kawano, H., Ito, S., Ishihara, T., Okada, Y., Nakano, S., Kinoshita, T., Horie, K., Episkopou, V., Gottesman, M. E., Costantini, F., Shimada, K., & Maeda, S. 1997, "Serum amyloid P component enhances induction of murine amyloidosis", *Lab Invest*, vol. 77, no. 5, pp. 525-531.

Torzewski, J., Bowyer, D. E., Waltenberger, J., & Fitzsimmons, C. 1997a, "Processes in atherogenesis: complement activation", *Atherosclerosis*, vol. 132, no. 2, pp. 131-138.

Torzewski, J., Torzewski, M., Bowyer, D. E., Frohlich, M., Koenig, W., Waltenberger, J., Fitzsimmons, C., & Hombach, V. 1998, "C-reactive protein frequently colocalizes with the terminal complement complex in the intima of

early atherosclerotic lesions of human coronary arteries", *Arterioscler.Thromb.Vasc.Biol.*, vol. 18, no. 9, pp. 1386-1392.

Torzewski, M., Rist, C., Mortensen, R. F., Zwaka, T. P., Bienek, M., Waltenberger, J., Koenig, W., Schmitz, G., Hombach, V., & Torzewski, J. 2000, "C-reactive protein in the arterial intima: role of C-reactive protein receptor-dependent monocyte recruitment in atherogenesis", *Arterioscler.Thromb.Vasc.Biol.*, vol. 20, no. 9, pp. 2094-2099.

Torzewski, M., Torzewski, J., Bowyer, D. E., Waltenberger, J., Fitzsimmons, C., Hombach, V., & Gabbert, H. E. 1997b, "Immunohistochemical colocalization of the terminal complex of human complement and smooth muscle cell alpha-actin in early atherosclerotic lesions", *Arterioscler.Thromb.Vasc.Biol.*, vol. 17, no. 11, pp. 2448-2452.

Trion, A., de Maat, M. P., Jukema, J. W., van der, L. A., Maas, M. C., Offerman, E. H., Havekes, L. M., Szalai, A. J., Princen, H. M., & Emeis, J. J. 2005, "No effect of C-reactive protein on early atherosclerosis development in apolipoprotein E*3-leiden/human C-reactive protein transgenic mice", *Arterioscler.Thromb.Vasc.Biol.*, vol. 25, no. 8, pp. 1635-1640.

Ueda, S., Ikeda, U., Yamamoto, K., Takahashi, M., Nishinaga, M., Nago, N., & Shimada, K. 1996, "C-reactive protein as a predictor of cardiac rupture after acute myocardial infarction", *Am.Heart J.*, vol. 131, no. 5, pp. 857-860.

Vagin, A. & Teplyakov, A. 1997, *J. Appl. Cryst., vol.* 30, pp. 1022–1025.

Vagin, A. & Teplyakov, A. 1998, "A translation-function approach for heavy-atom location in macromolecular crystallography", *Acta Crystallogr.D.Biol.Crystallogr.*, vol. 54, no. Pt 3, pp. 400-402.

van Aalten, D. M., Bywater, R., Findlay, J. B., Hendlich, M., Hooft, R. W., & Vriend, G. 1996, "PRODRG, a program for generating molecular topologies and unique molecular descriptors from coordinates of small molecules", *J.Comput.Aided Mol.Des*, vol. 10, no. 3, pp. 255-262.

Venugopal, S. K., Devaraj, S., & Jialal, I. 2003, "C-reactive protein decreases prostacyclin release from human aortic endothelial cells", *Circulation*, vol. 108, no. 14, pp. 1676-1678.

Venugopal, S. K., Devaraj, S., Yuhanna, I., Shaul, P., & Jialal, I. 2002, "Demonstration that C-reactive protein decreases eNOS expression and bioactivity in human aortic endothelial cells", *Circulation*, vol. 106, no. 12, pp. 1439-1441.

Verdone, G., Corazza, A., Viglino, P., Pettirossi, F., Giorgetti, S., Mangione, P., Andreola, A., Stoppini, M., Bellotti, V., & Esposito, G. 2002, "The solution structure of human beta2-microglobulin reveals the prodromes of its amyloid transition", *Protein Sci.*, vol. 11, no. 3, pp. 487-499.

Verma, S., Wang, C. H., Li, S. H., Dumont, A. S., Fedak, P. W., Badiwala, M. V., Dhillon, B., Weisel, R. D., Li, R. K., Mickle, D. A., & Stewart, D. J. 2002, "A self-fulfilling prophecy: C-reactive protein attenuates nitric oxide production and inhibits angiogenesis", *Circulation*, vol. 106, no. 8, pp. 913-919.

Vigushin, D. M., Pepys, M. B., & Hawkins, P. N. 1993, "Metabolic and scintigraphic studies of radioiodinated human C-reactive protein in health and disease", *J.Clin.Invest*, vol. 91, no. 4, pp. 1351-1357.

Villiers, C. L., Arlaud, G. J., Painter, R. H., & Colomb, M. G. 1980, "Calcium binding properties of the C1 subcomponents C1q, C1r and C1s", *FEBS Lett.*, vol. 117, no. 1, pp. 289-294.

Volanakis, J. E. 2001, "Human C-reactive protein: expression, structure, and function", *Mol.Immunol.*, vol. 38, no. 2-3, pp. 189-197.

Volanakis, J. E. & Kaplan, M. H. 1971, "Specificity of C-reactive protein for choline phosphate residues of pneumococcal C-polysaccharide", *Proc.Soc.Exp.Biol.Med.*, vol. 136, no. 2, pp. 612-614.

Volanakis, J. E. & Stroud, R. M. 1972, "Rabbit C1q: purification, functional and structural studies", *J.Immunol.Methods*, vol. 2, no. 1, pp. 25-34.

Volanakis, J. E. & Wirtz, K. W. 1979, "Interaction of C-reactive protein with artificial phosphatidylcholine bilayers", *Nature*, vol. 281, no. 5727, pp. 155-157.

Walport, M. J. 2001a, "Complement. First of two parts", *N.Engl.J.Med.*, vol. 344, no. 14, pp. 1058-1066.

Walport, M. J. 2001b, "Complement. Second of two parts", *N.Engl.J.Med.*, vol. 344, no. 15, pp. 1140-1144.

Wang, C. H., Li, S. H., Weisel, R. D., Fedak, P. W., Dumont, A. S., Szmitko, P., Li, R. K., Mickle, D. A., & Verma, S. 2003, "C-reactive protein upregulates angiotensin type 1 receptors in vascular smooth muscle", *Circulation*, vol. 107, no. 13, pp. 1783-1790.

Weiser, J. N., Pan, N., McGowan, K. L., Musher, D., Martin, A., & Richards, J. 1998, "Phosphorylcholine on the lipopolysaccharide of Haemophilus influenzae contributes to persistence in the respiratory tract and sensitivity to serum killing mediated by C-reactive protein", *J.Exp.Med.*, vol. 187, no. 4, pp. 631-640.

Weiser, J. N., Shchepetov, M., & Chong, S. T. 1997, "Decoration of lipopolysaccharide with phosphorylcholine: a phase-variable characteristic of Haemophilus influenzae", *Infect.Immun.*, vol. 65, no. 3, pp. 943-950.

Woo, P., Korenberg, J. R., & Whitehead, A. S. 1985, "Characterization of genomic and complementary DNA sequence of human C-reactive protein, and comparison with the complementary DNA sequence of serum amyloid P component", *J.Biol.Chem.*, vol. 260, no. 24, pp. 13384-13388.

Wood, S. P., Oliva, G., O'Hara, B. P., White, H. E., Blundell, T. L., Perkins, S. J., Sardharwalla, I., & Pepys, M. B. 1988, "A pentameric form of human serum amyloid P component. Crystallization, X-ray diffraction and neutron scattering studies", *J.Mol.Biol.*, vol. 202, no. 1, pp. 169-173.

Wooh, J. W., Kidd, R. D., Martin, J. L., & Kobe, B. 2003, "Comparison of three commercial sparse-matrix crystallization screens", *Acta Crystallogr.D.Biol.Crystallogr.*, vol. 59, no. Pt 4, pp. 769-772.

Xia, D. & Samols, D. 1997, "Transgenic mice expressing rabbit C-reactive protein are resistant to endotoxemia", *Proc.Natl.Acad.Sci.U.S.A*, vol. 94, no. 6, pp. 2575-2580.

Zachowski, A. 1993, "Phospholipids in animal eukaryotic membranes: transverse asymmetry and movement", *Biochem.J.*, vol. 294 (Pt 1), pp. 1-14.

Zhao, Z. Q. & Vinten-Johansen, J. 2002, "Myocardial apoptosis and ischemic preconditioning", *Cardiovasc.Res.*, vol. 55, no. 3, pp. 438-455.

Zwaka, T. P., Hombach, V., & Torzewski, J. 2001, "C-reactive protein-mediated low density lipoprotein uptake by macrophages: implications for atherosclerosis", *Circulation*, vol. 103, no. 9, pp. 1194-1197.

http://www.cuemol.org
http://www.povray.org